

Assessment of Real-World Running With Lab-Validated Algorithms Based on Foot-Worn Inertial Sensors

Présentée le 13 mai 2020

à la Faculté des sciences et techniques de l'ingénieur
Laboratoire de mesure et d'analyse des mouvements
Programme doctoral en génie électrique

pour l'obtention du grade de Docteur ès Sciences

par

Mathieu Pascal FALBRIARD

Acceptée sur proposition du jury

Prof. D. Atienza Alonso, président du jury
Prof. K. Aminian, directeur de thèse
Prof. Y. Pitsiladis, rapporteur
Prof. H. Schwameder, rapporteur
Dr J. Skaloud, rapporteur

Do not go gentle into that good night,
Old age should burn and rave at close of day;
Rage, rage against the dying of the light.

Though wise men at their end know dark is right,
Because their words had forked no lightning they
Do not go gentle into that good night.

Good men, the last wave by, crying how bright
Their frail deeds might have danced in a green bay,
Rage, rage against the dying of the light.

Wild men who caught and sang the sun in flight,
And learn, too late, they grieved it on its way,
Do not go gentle into that good night.

Grave men, near death, who see with blinding sight
Blind eyes could blaze like meteors and be gay,
Rage, rage against the dying of the light.

And you, my father, there on the sad height,
Curse, bless, me now with your fierce tears, I pray.
Do not go gentle into that good night.
Rage, rage against the dying of the light.

— Dylan Thomas

Abstract

Following the cultural revolution of the late 1960s, the number of elite and recreational runners rose consistently, reaching approximately 7.9 million road races participants in 2018. Today, running is everywhere. City parks, forests, mountain trails, and athletic tracks are now the playground of numerous running enthusiasts, whatever their ages, gender, and social background. With such heterogeneity in the runners' profiles, the motives to maintain a running habit vary from psychological, social, and physical objectives to performance-oriented goals. Although the health benefits of running are well-recognized in the scientific literature, its regular practice also presents risks of injuries. To study the underlying mechanisms associated with injuries or improvements in performances, scientists have investigated the kinematics and the kinetics characteristics of the running gait. Habitually, this quest requires the use of precise monitoring instruments only accessible in well-equipped research laboratories. However, over the past two decades, the advent of wearable sensors shifted the analysis of running into real-world settings, where runners encounter different environments, outside, in the wild. It is in this setting that the current thesis situates itself.

This thesis presents a new wearable system for the objective assessment of the running gait in real-world conditions. The proposed method uses foot-worn inertial sensors and lab-validated algorithms to provide a reliable analysis of the spatiotemporal parameters of running. The system can operate outdoors and over extended periods while providing a quasi-real-time evaluation of each step. Further, with its automatic detection of the sensor location and calibration, the proposed method is easy-to-use and accessible to non-initiated users. For the technical validation of the proposed system, the spatiotemporal metrics were compared with gold-standard reference systems. Temporal events and gait phases were validated in-lab against a reference force plate integrated into a treadmill, and the results of a novel orientation-drift correction model compared to a state-of-the-art motion capture system. Three overground speed estimation methods were evaluated in real-world conditions and compared to a Global Navigation Satellite System device. Finally, these methods were tested in different settings, such as a marathon race, a mountain ultra-marathon, and a 400-m hurdling competition. These tests provided valuable insight into the limitations of the proposed system and suggested several improvements for its use in real-world conditions.

Overall, this thesis presents a new device for researchers to assess the running gait outside of the laboratories. It aims to augment the resolution of running analysis by handling the technical challenges associated with inertial sensors and providing fast and reliable biomechanical metrics. As such, the system could contribute to extending the knowledge about

Abstract

the mechanical adaptations experienced in real-world environments and long-term running. Moreover, the potential of such an instrument for in-field performance evaluation was tested in this thesis and showed promising results. Hence, such an assessment of the running gait during training and competitions could help athletes and coaches monitor the training load and improvement in performances. Finally, with the advents in the miniaturization of wearable sensors, the proposed methods could be used in various running-related applications, such as shoe-fitting, rugby, soccer, and other sports where running is a critical component.

Keywords: running, inertial sensors, wearable, foot, spatiotemporal parameters, orientation drift correction, speed, validation, marathon, trail running, hurdling, real-world running

Résumé

Suite à la révolution culturelle de la fin des années 1960, le nombre de coureurs professionnels et amateurs n'a cessé d'augmenter, avoisinant les 7.9 millions de participants à des courses sur route en 2018. Aujourd'hui, la course à pied est partout. Les parcs, les forêts, les chemins de montagne et les pistes d'athlétisme sont le terrain de jeu d'une multitude de coureurs, indépendamment de leur âge, genre ou statut social. Avec une telle hétérogénéité de profils, les motivations conduisant à une pratique régulière peuvent être diverses ; psychologiques, sociales, physiologiques ou dans un but de performance. Bien que les bénéfices de la course à pied sur la santé soient reconnus par la littérature scientifique, une pratique régulière peut présenter des risques de blessures. Afin de mieux comprendre les mécanismes sous-jacents associés à ces blessures ou à une amélioration des performances, les scientifiques ont étudié la cinématique et la cinétique des différents mouvements générés en course à pied. Habituellement, cette quête requiert l'utilisation d'appareils de mesure avancés et rarement accessibles en dehors des laboratoires scientifiques. Toutefois, les progrès réalisés dans le domaine des capteurs portés ont transposé l'analyse de la foulée hors des laboratoires, dans des conditions réelles qui requièrent une adaptation constante du coureur en fonction de son environnement.

Cette thèse présente un nouveau système porté capable de fournir une évaluation objective des paramètres biomécaniques de course. Les méthodes proposées utilisent des capteurs inertiels placés sur le pied et des algorithmes validés en laboratoire. Le système a été conçu pour une utilisation en conditions réelles, sur de longues périodes et dans le but de fournir une évaluation quasi-instantanée de chaque pas. En outre, étant capable de détecter automatiquement son emplacement et de se calibrer en fonction celui-ci, le système proposé est facile d'utilisation et accessible aux utilisateurs non-initiés. La validation technique a été effectuée de manière contrôlée et par comparaison à des systèmes de référence précis. Les paramètres temporels de course ont été comparés aux mesures d'une plateforme de force intégrée dans un tapis roulant. La méthode d'estimation de l'orientation du pied basée sur un modèle biomécanique du pied a quant à elle été comparée à un système optique de capture du mouvement. De plus, trois méthodes d'estimation de la vitesse de course ont été proposées et comparées à un système de positionnement par satellites. Enfin, les méthodes développées ont été testées dans différentes situations : lors d'un marathon, d'un ultra-marathon de montagne ainsi que lors d'une compétition de 400 mètres haies.

En conclusion, ma thèse propose un nouveau système de capteurs portés permettant aux chercheurs d'évaluer la foulée en course à pied en dehors des traditionnels laboratoires de

Abstract

mesure. Le système a pour objectif d'augmenter la résolution de l'analyse de course en résolvant les défis techniques associés aux capteurs inertiels et en fournissant une évaluation fiable et rapide des paramètres biomécaniques. Ainsi, le système pourra contribuer à étendre les connaissances sur les adaptations mécaniques nécessaires lors d'une course hors laboratoire, dans différents environnements et sur une durée prolongée. De plus, les tests réalisés lors de ma thèse ont démontré le potentiel d'une telle technologie dans le suivi des performances. Le système pourrait ainsi permettre aux athlètes et aux entraîneurs de quantifier la charge d'entraînement ainsi que d'éventuelles améliorations. Enfin, grâce à la miniaturisation continue des capteurs, les méthodes proposées dans ma thèse pourraient également servir à d'autres applications, telles que le choix et la personnalisation des chaussures ou l'analyse d'autres sports, tels que le rugby et le football.

Mot clés : course à pied, capteurs inertiels, capteurs portés, pied, paramètres spatiotemporels, correction de la dérive des capteurs, vitesse, validation, marathon, course de montagne, 400 mètres haies, conditions réelles de course

Acknowledgements

Learning the sweet science of metrology at the Laboratory of Movement Analysis and Measurement (LMAM) has been an exciting and fulfilling adventure, which I largely owe to the kind and professional guidance of Prof. Aminian. Under Kamiar's supervision, I had the opportunity to participate in several projects, and the freedom to set the direction of my research; a luxury I sincerely enjoyed. I consider myself lucky to have had such a great supervisor, and I genuinely thank him for his support and disponibility throughout my thesis.

Over the past four and a half years, I also had the pleasure to exchange about science (and life in general) with the other members of LMAM: Pritish Chakravarty (my office mate), Mahdi Hamidi Rad, Salil Apte, Dr. Anisoara Ionescu, Gaëlle Prigent, Dr. Mina Baniasad, Abolfazl Soltani, Arash Atrsaei, Dr. Lena Carcreff, Yasaman Izadmehr, Dr. Matteo Mancuso, Dr. Benedikt Fasel, Dr. Christopher Moufawad El Achkar, Dr. Wei Zhang, Francine Eglese (or Francesca), and Pascal Morel. By filling the coffee breaks with cakes and sweets from your home countries, you shared a bit of your story and made these moments remarkable.

If innovative research projects are essential for an exciting Ph.D. experience, the people you meet during these projects are the ones who make every day's work particularly enjoyable. During the RunUp and WattsUp projects, I had the chance to collaborate with Dr. Frederic Meyer and Prof. Grégoire Millet from the University of Lausanne. Most of the work presented in this thesis originated from our regular meetings, and I thank them for sharing with me their expertise in running biomechanics and human physiology. I can honestly say that the many measurement sessions carried with Dr. Meyer have been amongst the funniest moments of my Ph.D. I also want to thank Dr. Maurice Mohr for his contribution to the hurdling study and for inviting me to co-chair a session (and discover the local micro-breweries) at the ISB/ASB 2019 conference in Calgary, Canada.

Starting with my master thesis and continuing through my Ph.D., I had the pleasure to see some of my work being transferred into a commercialized product at GaitUp. Discovering the challenging world of startups and trying to match the company's reality with my research has been a genuinely motivating objective. Dr. Farzin Dadashi, Rebekka Anker, Madeline Trousseau, Stephane Lovejoy, Cléo Moulin, Manuel Reynaert, Sakura Nussbaum, and everybody at GaitUp, thank you for your kind welcome and for making my baby-foot skills somewhat better. I want to address a special thanks to Dr. Benoît Mariani for offering me the opportunity to start a Ph.D. position at LMAM and for supporting my candidacy; I learned a great deal about research and industry working with Benoît and hope that the future will bring new openings for collaborations.

Acknowledgements

In addition to the studies on running biomechanics, I also took part in a two-year project that aimed to design a new prosthetic foot for developing countries. The Agilis project, a collaboration between four EPFL laboratories and the International Committee of the Red Cross (ICRC), has been a particularly rich experience, both scientifically and personally. Hence, I would like to thank everybody who I had the opportunity to work with on this project and address a special acknowledgment to Grégory Huot, Mathieu Janier, Dr. Rajasundar Chandran, and Michael Rechsteiner.

I would also like to thank the president (Prof. D. Atienza Alonso) and jury (Prof. Y. Pitsiladis, Prof. H. Schwameder, and Dr. J. Skaloud) of this thesis for accepting to review and evaluate the content of my research. I sincerely appreciate the extent of the comments and believe that their recommendations improved the content of this document. Moreover, the research projects presented here would not have been possible without the financial contribution from the Swiss Commission for Technology and Innovation (CTI) and the Swiss Innovation Agency (Innosuisse) and without the volunteers who participated in the different measurement protocols.

I conclude this chapter with a word to my teammates at LUC Rugby, friends, and family. Your company and support have been phenomenal, and I can't emphasize enough how central your presence has been in accomplishing this thesis. Your attention, often involving some sort of food or drinks, made the intense working periods more relaxed and comfortable. Lastly, I would like to thank my parents, brother, and sister for their unconditional and loving support. Without them, none of this would have been possible. Some say a man can only be blessed with so much; you proved them wrong!

Vendlincourt, May 6, 2020

M. E

Contents

Abstract (English/Français)	i
Acknowledgements	v
List of Figures	xi
List of Tables	xiii
I Introduction and Background	1
1 Introduction	3
1.1 Run, Forrest, Run!	3
1.2 Running analysis: a brief history	4
1.3 Benefits and risks of running	8
1.4 Running demographics	9
1.5 The assessment of running	10
1.5.1 Temporal events and gait phases	11
1.5.2 Kinetics of running	14
1.5.3 Foot kinematics	17
1.6 The objectives of this thesis	20
1.7 Thesis overview	22
2 State of the Art in Running Assessment	25
2.1 Overview	25
2.2 Reference measurement systems	25
2.2.1 Force plates	25
2.2.2 Optical motion tracking systems	27
2.2.3 Video cameras and visual assessment	29
2.3 Inertial sensors in running	30
2.3.1 Temporal analysis of the running gait	32
2.3.2 Foot strike patterns and rear-foot eversion	35
2.3.3 Stride length and speed	37
2.3.4 Impacts and ground reaction forces	39
2.3.5 Overall conclusions	40
	vii

II Algorithms Development and Validation	43
3 Accurate Estimation of Running Temporal Parameters	45
3.1 Introduction	46
3.2 Methods	47
3.2.1 Measurement protocol	47
3.2.2 Wearable device and temporal features estimation	47
3.2.3 Reference system and temporal features	49
3.2.4 Statistical analysis and error estimation	51
3.3 Results	52
3.3.1 Temporal events detection	52
3.3.2 Inner-stride phases estimation	55
3.4 Discussion	57
3.5 Conclusions	58
3.A Additional Results	60
3.A.1 Introduction	60
3.A.2 Material and Methods	61
3.A.3 Results	64
3.A.4 Discussion	65
4 Drift-Free Foot Orientation Estimation in Running Using Wearable IMU	67
4.1 Introduction	68
4.2 Materials and Methods	69
4.2.1 Protocol	69
4.2.2 Wearable systems	69
4.2.3 Reference system	75
4.2.4 Validated angles	77
4.2.5 Statistical analysis and error computation	78
4.3 Results	78
4.4 Discussions	82
4.5 Conclusions	84
4.A Additional Results	85
4.A.1 Introduction	85
4.A.2 Methods	86
4.A.3 Results	87
4.A.4 Discussion	88
5 Running Speed Estimation Using Shoe-Worn Inertial Sensors	91
5.1 Introduction	92
5.2 Methods	93
5.2.1 Protocol and instrumentation	93
5.2.2 Estimation of reference GNSS speed	94
5.2.3 Speed estimation based on direct integration of foot acceleration	94

5.2.4	Development of a linear model for speed prediction	97
5.2.5	Personalized model	101
5.2.6	Statistical analysis	103
5.3	Results	103
5.3.1	Direct speed estimation	103
5.3.2	Linear model	105
5.3.3	Personalization	109
5.4	Discussion	111
5.5	Conclusion	114
III	Real-World Applications	117
6	Gait Changes, Foot Strike Pattern and Stiffness During Marathon Running	119
6.1	Introduction	120
6.2	Material and Methods	121
6.2.1	Protocol	121
6.2.2	Data processing	122
6.2.3	Statistical analysis	123
6.3	Results	123
6.4	Discussion	127
6.5	Conclusions	129
7	Gait Parameters and Vertical Speed During a Mountain Ultra-Marathon	131
7.1	Introduction	132
7.2	Methods	133
7.2.1	Participants	133
7.2.2	Design	133
7.2.3	Methodology	134
7.2.4	Statistical Analysis	136
7.3	Results	136
7.4	Discussion	137
7.5	Conclusion	138
8	Hurdle Clearance Detection and Spatiotemporal Analysis in Hurdling	139
8.1	Introduction	140
8.2	Materials and Methods	141
8.2.1	Protocol	141
8.2.2	Instrumentation	141
8.2.3	Data processing	141
8.2.4	Hurdle Clearance Detection	143
8.2.5	Data Analysis	149
8.3	Results	150
8.4	Discussion	155

Contents

8.5	Conclusions	156
IV	Conclusions	159
9	General Discussion	161
9.1	Main contributions	161
9.1.1	Part II – Algorithms development and validation	162
9.1.2	Part III – Real-world applications	163
9.2	The proposed system in the industry	166
9.3	Limitations	167
9.4	Future developments	169
9.4.1	Integration of other sensor data	170
9.4.2	Modeling the running power	170
9.4.3	Relevance in other applications	171
	Bibliography	173
	Appendix	205
	Curriculum Vitae	217

List of Figures

1.1	Greek vase paintings of distance running and sprinting	5
1.2	Early systems of E. J. Marey used for walking and running gait analysis	7
1.3	Number and gender of running races participants between 2001 and 2018	10
1.4	Temporal events and gait phases of a running cycle	12
1.5	Temporal parameters as a function of the running speed	13
1.6	Vertical ground reaction force observed for two landing techniques	15
1.7	Subtalar joint and most common angles used to assess pronation	19
1.8	Outline of the thesis	23
2.1	Schematic representation of an instrumented treadmill	26
2.2	Configuration of markers used for motion capture	29
2.3	Validation of temporal events detection	34
2.4	IMU-based methods to discriminate rearfoot, midfoot, and toe strikers	36
2.5	IMU-based eversion range and optical motion capture system	37
3.1	Representation of the technical and functional frames	48
3.2	Features used on the kinematic signals recorded by the sensors	53
3.3	Initial contact and terminal contact inter-trials bias	53
3.4	Bland-Altman plot of the ground contact time estimation errors	55
3.5	The tree structure of the classification steps	62
4.1	The two-segments model of the foot during the stance phase	71
4.2	Configuration of markers on the shoe	76
4.3	Comparison of the pitch angle measured from different measurement systems	79
4.4	Boxplot of the biases and precision for the foot pitch activation angle	80
4.5	Bland-Altman plot of the activation pitch angle	80
4.6	Agreement between foot strike index, foot strike angle, and visual classification	88
5.1	Elevation and speed of the running circuit and sensors configuration	94
5.2	Pre-processing steps applied to the GNSS measurements of speed	95
5.3	Processing steps applied on the IMU measurements	96
5.4	Schematic representation of the data set organization	99
5.5	Bland-Altman plot of the direct speed estimation method and GNSS	104
5.6	Relation between the ground incline and direct speed estimation method	104

List of Figures

5.7	MSE of the forward step-wise selection process	105
5.8	Bland-Altman plot of the speed estimation using the linear model	108
5.9	Speed estimation results of the linear model (CDF and instantaneous speed) . .	108
5.10	Evolution of the RMSE error during the personalization of the speed model . .	110
5.11	Bland-Altman plot of the proposed personalized model	110
6.1	Evolution of the temporal parameters during a marathon	125
6.2	Evolution of running speed, duty factor, and stride length during the marathon	125
6.3	Evolution of the stiffness during the marathon	126
6.4	Evolution of foot strike angle during the marathon	126
7.1	Average vertical speed of the first five mountain passes	134
7.2	Correlation between vertical speed and stride height	136
7.3	Correlation between vertical speed and stride frequency	137
8.1	Participant clearing a hurdle with shoe-mounted IMUs and magnets on a hurdle	142
8.2	Description of the technical, functional, and global frames.	143
8.3	Flow chart of the proposed hurdle clearance detection method	144
8.4	Block diagram of the magnets and magnetometer based detection method . . .	145
8.5	A sequence of temporal events for the leading and trailing leg	147
8.6	Flow chart of the orientation based detection method	148
8.7	Detection results obtained by MAG, TEMP, and ORIENT methods	151
8.8	Speed, contact time, step frequency, and flight phase during the race	153
8.9	Example of feedback instantly extracted using the proposed method	154
9.1	WT Innovation World Cup award	166

List of Tables

3.1	Summary of the features used to detect initial and terminal contact	50
3.2	List of time differences for all the initial and terminal contact candidates	54
3.3	Duration differences for contact time estimation in the validation set	56
3.4	Flight phase, swing phase, and step time duration estimations errors	56
3.5	List of the features extracted for the accelerometer and angular velocity norm .	63
3.6	Results from the feature selection process	64
3.7	Accuracy, specificity, sensitivity, and precision of the classifiers	64
3.8	F1-score of the different classifiers at different running speeds	64
4.1	Analysis of the IMU-based pitch and roll angles estimation errors	81
4.2	Performance of the foot strike pattern assessment methods	87
4.3	Performance of pronation assessment methods	87
5.1	Features extracted for each stride on the IMU measurements	98
5.2	Features automatically selected by the forward stepwise selection algorithm . .	106
5.3	Performance statistics of the linear model for two sets of features	107
5.4	Performance statistics of the personalized model	109
6.1	Biomechanical parameters for the two identical sections (5-10 vs. 25-30 km) . .	124
7.1	Description of the population studied	133
7.2	Characteristics of the portions of the mountain passes	135
8.1	Features and sensors configurations required to detect hurdle clearance	146
8.2	Hurdle clearance and leading leg detection results	152
8.3	Contact time, flight time, step frequency, and speed between the hurdles	154

Introduction and Background Part I

1 Introduction

1.1 Run, Forrest, Run!

“Every morning in Africa, a gazelle wakes up. It knows it must outrun the fastest lion or it will be killed. Every morning in Africa, a lion wakes up. It knows it must run faster than the slowest gazelle, or it will starve. It does not matter whether you are a lion or a gazelle. When the sun comes up, you better be running.” – Unknown

The past few decades have seen the rapid development of biomechanics studies and the quest to unveil the underlying principles of human locomotion. The reason why locomotion became the cornerstone of human movement analysis inevitably finds its root in its prominence in Humans life and its requirements in metabolic energy. In the human and animal kingdom, energy is the currency that dictates how each metabolism operates, and we, humans, evolved into an incredibly efficient mechanism, optimizing the metabolic cost of locomotion by switching between different types of gait (Alexander McN., 1989); walking, running, and sprinting are the direct consequences of this adaptation. Although these types of gait differ in function, the broad scientific literature on walking constituted a well-founded knowledge basis for the early running studies. The scientific analysis of running is, somehow, the logical continuation of walking studies. Walking and running are cyclic by nature; they consist of a repetition of movements coordinated to generate the forward motion of the body segments. Although the two methods share similarities, running is distinguished from walking by higher over-ground speed and by the presence of a period when both feet are off the ground (i.e., the aerial phase), whereas walking is a succession of single and double support phases. Moreover, higher impacts and ground reaction forces, decreased stance phase, increased swing phase, more ample range of motion of the lower limbs, and greater eccentric muscle contraction have been observed for running (Dugan & Bhat, 2005; Keith R Williams, 1985). Consequently, running is more complex to measure, and technological advancements in laboratory instrumentation were required for biomechanical studies to emerge.

Back in early 1970, academics were disputing whether the mechanics of running was a valid topic of scientific study. It is the explosive growth of running in the late 1960s that raised the

interest of scientists, supported by more influential lobbies, attractive market opportunities, and an increasing incidence of running injuries to study (P. R. Cavanagh, 1990). Today, running is pursued by millions of recreational runners worldwide (Scheerder et al., 2015) and is studied for its own sake.

Running can take many forms, and several of its branches have also rapidly developed in the past decades. Competitive marathon running is an excellent example of this evolution. Marathon used to be reserved for well-trained individuals, and finishing a marathon was gratifyingly rare. Today, marathons attract both athletes and recreational runners. Surely recreational runners attain the end of the 42 kilometers slower than the well-trained individuals, but they nonetheless reach the finish line. Mountains races also captured the interest of new adepts. These events, often referred to as trail running, offer a different running experience. Surrounded by nature, participants are running at different altitudes and shifting from uphill walking to down-hill running many times within the course of a race. As for marathons, trail running also has its extremes, the so-called “ultra-trail” events. These races can be up to 330 km long and take approximately a week for the slowest participants to complete. Furthermore, running also occurs in many other disciplines; the obvious ones, such as track and field events, and the less obvious ones, such as rugby and soccer. Track and field disciplines are at the origin of today’s modern running, with several Olympic games events actually being variations of running. Sprinting, for instance, is the fastest form of running and hurdling is a form of running with obstacles that an athlete must clear in order to complete the race.

After all, running stands at the root of most sports activities. It is, therefore, crucial to carefully appreciate its underlying mechanisms and provide a safe environment for anyone who seeks either health benefits, competition rewards, or wishes to enjoy a pleasant and relaxing run.

1.2 Running analysis: a brief history

Before diving into the current state-of-the-art of running studies, it seems essential, or at the very least interesting, to understand how running became a valid and recognized topic of research. Therefore, this section aims to provide an overview of the history of running studies but does not have the pretentiousness to cover all the significant discoveries which led to today’s knowledge. Instead, an exhaustive list of key findings is discussed in chronological order. The content of this section was inspired, for the most part, by (P. R. Cavanagh, 1990; Heinrich, 2009).

Before any instrumentation was available, detailed observations and paintings were efficient ways to characterize movements; hence the first attempts toward an analysis of running were based on the description of its kinematics. The instantaneous postures illustrated on the vase paintings from the age of classical Greece (the fifth century B.C.) suggest that the artists at the time recognized the mechanical differences between long-distance running and sprinting as various body posture and ranges of movement are depicted on these works of art (Figure 1.1). Moreover, in his quest to describe the movements of humans and animals, the brilliant mind of

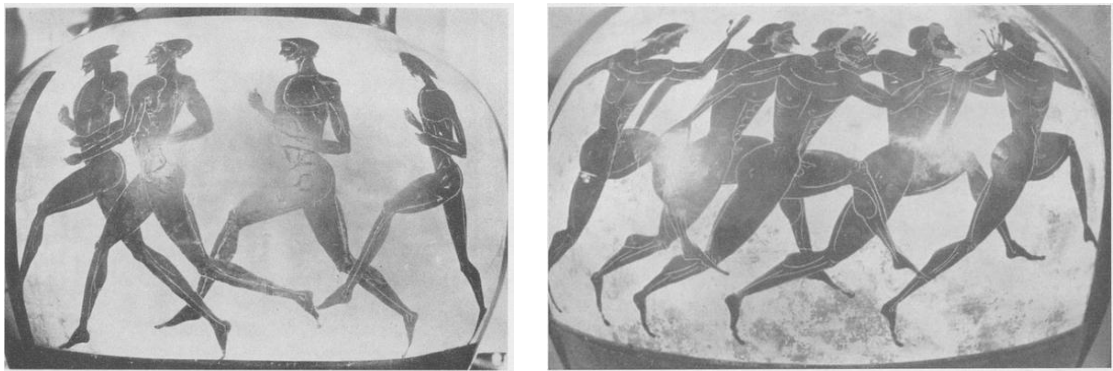


Figure 1.1 – Greek vase paintings of distance running (left) and sprinting (right). Source (Gardiner, 2002).

Aristotle (384-355 B.C.) scrutinized the different types of gait and reflected on the relationship of structure and function. For instance, he observed that flexion of the knee joint is necessary to minimize the vertical motion and sustain progression. He also understood the concept of forces, anticipating Newton's third law, as he wrote: "... the forces of that which causes movement and of that which remains still must be made equal... For as the pusher pushes, so the pusher is pushed."

With the decline of the Grecian and Roman society, came a rather fruitless period for locomotion analysis. Renaissance was a revival for the Aristotelian concepts of motion, and no one individual better embodies the relation between Science and Art than Leonardo da Vinci (1452-1519). He described and illustrated the principles of motion that were intended to help students of painting with accurate representations of a variety of human locomotion activities and demonstrated remarkable insight into the mechanics of running, meticulously analyzing its patterns under different conditions and going as far as speculating about the distribution of the weight under the foot during grade running: "He who runs down a slope has his axis on his heels; he who runs uphill has it on the toes of the feet; a man running on the level ground has it first on his heels and then on the toes of his feet (Keele, 1983)."

With the 17th-Century and its scientific revolution, arose one of the most important, if not the most significant, contribution to mechanics; Isaac Newton's (1642-1727) laws of motion. At the time, Newton and other scientists were trying to formulate the underlying mechanical rules to explain natural phenomena, and their rich heritage is still vividly used by biomechanists today. A contemporary of Newton, Giovanni Borelli (1608-1679) was among the first to describe the animal and human musculoskeletal system in terms of structural engineering. In his classical volume, *De Motu Animalium* ("Animal motion"), Borelli associated animals to machines and used a mechanical approach to prove his theories. With propositions such as the "compass gait," his work is considered as the starting point of biomechanical studies of locomotion.

A thoughtful and meticulous capacity to observe and describe movements was still the best instrument available then. An excellent example of such work is the study published in 1836

by the brothers Wilhelm and Eduard Weber, *Mechanik der menschlichen Gehwerkzeuge* ("The mechanics of human locomotion"). The Webers are best remembered for their suggestion that the lower limbs can act as a pendulum. As an attempt to explain the underlying principles of the human gait and without any sophisticated instrumentation, they proposed several postulates on running, separating their remarks according to the speed. For instance, they noticed that the duration of a stride is shorter in running than in walking, but the length of the stride is greater. They also commented on the smaller vertical oscillation of the trunk during running compared to walking. More importantly than the observations, they listed almost 150 hypotheses and hence established an agenda for future research. However, these needed appropriate measurement systems to be tested.

It is only a few years later that the field of instrumentation experienced one of its most significant advancements, and they all originated from the creativity and genius mind of Etienne Jules Marey (1830-1904). Marey was a pioneer in metrology, the automatic recording of the timing of events, and used his ingenuity to study human locomotion. One of the most famous inventions of Marey is the device that combined shoes instrumented with air chambers, a primitive head-worn accelerometer, and a pneumatic recording system (Figure 1.2, left). This device also included an onboard chart-recorder with a rotating drum to allow the running experiments to be carried outside the laboratory. With such an experimental arrangement Marey was able to record the swing and stance phases of locomotion. In a quest to estimate the exact length of stride, he undertook the construction of the most advanced facility ever dedicated to the study of locomotion called the Physiological Station (Figure 1.2, right). This outdoor laboratory included a 500-m circular track equipped with a variety of instruments; a telegraph wire ran all around the track, and posts equipped with a mechanism able to break the circuit when the runner came alongside were placed at regular intervals (50 meters). Besides, Marey also devised the first force platform and set a calibration method to account for non-linearities. He was also the first to synchronize photographic and force measurements. His understanding of running biomechanics at the time was astonishing; remarkably, he suggested that storage and reutilization of elastic energy was a process that operated to conserve metabolic energy. However, and somewhat surprisingly, Marey achieved more recognition as a pioneer of cinema, due to his inventions in photographic devices, than as an early biomechanist. In the same period, another scientist was constructing ingenious devices. Vierordt (1881) was using ink-spraying nozzles attached to the body to simultaneously track the position of the different body parts and realized that there were considerable variations in the gait phases of normal locomotion.

Later, it is to Braune and Fisher that we owe one of the major advances in the modern mathematical approach to the study of biomechanics. The content of their study of locomotion, published in *Der Gang des Menschen* (Braune & Fischer, 1895-1904/1987), was monumental in both the scope and vision. The authors reported their use of electrical discharge tubes attached to the subject and how time-consuming and fatiguing the experiments were (often from ten to twelve hours of continuous activity). The measurements had to be carried at night as there were no other means of darkening the room where they captured the position of the

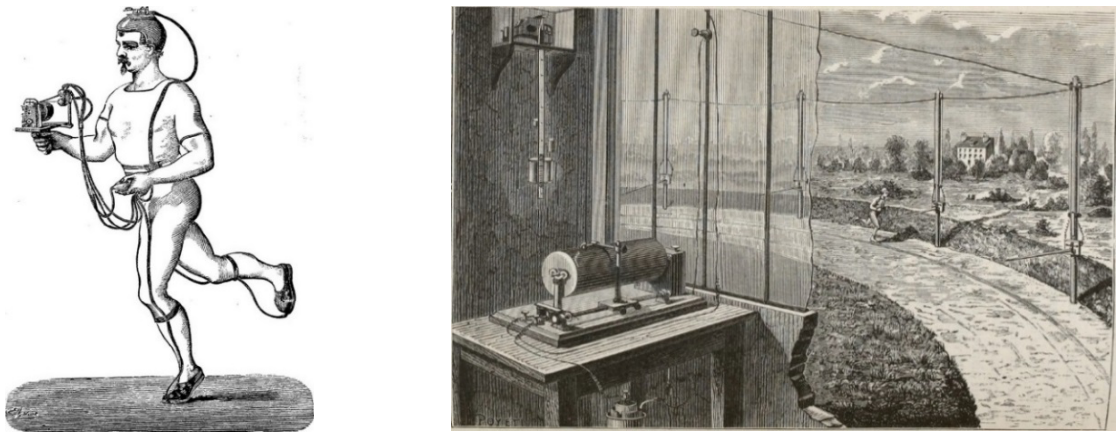


Figure 1.2 – (Left) A pneumatic recording system connected to instrumented shoes with air chambers and an early accelerometer placed on the head. (Right) the Physiological Station of E. J. Marey used for his work on walking and running gait analysis. Source (Marey, 1873; Bénabou, 2009).

Geissler tubes on photographic plates. They then digitized the film plates using a precision optical system, calculated the three-dimensional coordinates of the landmarks, and built graphical and physical models of the subject. From these data, they were able to calculate resultant forces and moments at the joints of a 12-segment rigid body model. With minor changes, the techniques used by biomechanists today are nearly the same as the one proposed by Braune and Fischer.

The photographic work of Eadweard Muybridge (1830-1894) also had an impact on the visual perception of the running gait. He produced over 20'000 photographs of humans and animals in motion. As the photographs were of good-quality, scientists and artists were able to appreciate the sequential images of various movements in more detail. For instance, Muybridge is said to have shown in 1872 that all the foot of a trotting horse concurrently left the ground.

The trends and discoveries of the twentieth century were predominantly orientated towards muscle mechanic and energy expenditure. A. V. Hill, a Nobel prize winner, was drawn toward the study of running as an experiment of maximal muscular effort. His research led to the definition of a velocity curve for sprint running, the evaluation of the external work during uphill running, discussions about the efficiency of running, and formulations about the effect of air resistance at different running speeds. He was one of the first scientists to combine a physiological and mechanical approach in the study of running. Benefitting from Hill's work, W. Fenn proposed a segment-by-segment calculation method of kinetic and potential energy to estimate the cost of sprint running. However, Fenn was also conducting significant experiments on isolated muscles, with the "Fenn effect" defined as the additional heat of shortening in an active muscle.

Today, the tremendous progress in new technologies, sensors miniaturization, wireless connectivity, computing facilities, intelligent system, and data analytics has once again shaken

the field of running biomechanics. As for Marey's inventions, new tools often provide answers to previously asked questions.

1.3 Benefits and risks of running

There is incontrovertible evidence that regular physical activity provides numerous health benefits (Warburton et al., 2006), and running does not act as an exception in that regard. Several cohort studies have investigated all-cause mortality and other health outcomes among runners compared with non-runners. For instance, these studies found that running can reduce the risk of premature death by 25%–40% (D. chul Lee et al., 2017), reduce the risks of cancer-related mortality by 30%–50% (Chakravarty et al., 2008; Schnohr et al., 2013), increase bone mineral density (Brown & Josse, 2002), decrease blood pressure (Swain & Franklin, 2006), lower depressive symptomatology and improve the emotional well-being (Galper et al., 2006). Running also promotes other healthy behaviors such as maintaining normal body weight, not smoking, and consuming light-to-moderate amounts of alcohol (D. chul Lee et al., 2017). For many, running provides the opportunity to enjoy the natural environment, and it helps to escape from worry and anxiety (Shipway & Holloway, 2010). In contrast, some studies revealed that using running to cope with stress can result in negative addiction and that some runners experience withdrawal when they are unable to run (Leedy, 2000; Morgan, 1979).

Similarly, running can also lead to injuries that diminish pleasure in exercise and lead to temporary or even permanent discontinuation of running. Extensive research suggested that the incidence of running-related injuries ranges from 6.8 to 59 injuries per 1000 hours of exposure (Lopes et al., 2012). Therefore, investigating the behaviors leading to higher risks of running-related injuries is a continuing concern within the field of biomechanics. Although runners sometimes endure traumatic injuries (e.g., sprains, muscle injuries, skin lesions), running injuries usually differ from the acute sports traumatism caused by an excessive load on a structure and resulting in a fracture or a tear of the tissues (e.g., ACL injuries, bone fractures). Running-related injuries tend to appear gradually as the lower-limbs absorb small to moderate impacts repetitively; hence, most of these injuries are soft tissue injuries. Several systematic reviews identified medial tibial stress syndrome, Achilles tendinopathy, plantar fasciitis, and patellofemoral syndrome as some of the most frequent running-related musculoskeletal injuries (Benca et al., 2020; Lopes et al., 2012; Van Gent et al., 2007). The lower limbs, especially to the knee, are the most affected by running-induced injuries, with an incidence of lower-leg injuries ranging from 9.0% to 32.2%, from 5.7% to 39.3% for the foot, and 3.4% to 38.1% for the upper leg (Van Gent et al., 2007). Identifying the origin of running-related injuries is a laborious task due to the multifactorial nature of these injuries. Nevertheless, several intrinsic and extrinsic factors, such as the weekly mileage, the history of previous injuries, malalignment of the leg, footwear, and training errors (e.g., training too often, too fast, or too long), have been associated with higher injury risks (Phillips et al., 2015; Van Der Worp et al., 2015).

In addition to its association with running economy and performances, a poor running technique can also lead to injuries (Folland et al., 2017; S. C. Winter et al., 2020). Assessing an individual's running mechanics remains a central component of injury prevention, as specific biomechanical faults enhance the risk of injury (Bredeweg et al., 2013; Noehren et al., 2013). Therefore, providing feedback on the running movements could help to keep the runners safe. For instance, research showed that most runners were able to reduce lower extremity loadings associated with stress fractures when real-time visual feedback was provided (Crowell et al., 2010). Unfortunately, today, state-of-the-art analysis of running remains confined in well-equipped laboratories and thus hardly accessible to most runners. Democratizing such analysis by making it affordable and easy-to-use, such as with wearable sensors, could significantly improve our understanding of running-related injuries and prevent injuries.

1.4 Running demographics

Before the cultural revolution of the 1960s and 1970s, recreational running was considered as an atypical and rather strange physical activity. For many, it was a waste of energy and was reserved for competitive athletes practicing through university and extracurricular programs. However, this cultural revolution changed the public's perception and gave rise to what is now referred to as the running boom (Scheerder et al., 2015), transforming running into a recreational activity attracting huge masses of runners and joggers. With a growing number of adepts, business companies started to identify new and promising marketing opportunities, therefore also contributing to the promotion of running.

Although the ensuing decades saw impressive growth in the number of elite and non-elite runners training in public spaces and registering to marathons, running was still merely practiced by men. At the time, misconceptions about women's capacity to run long distances were preventing a large portion of the population from running. It remained so until the period called the second wave of running when women started to take part in running activities actively (Lynch & Hoch, 2010; Scheerder et al., 2015). Hence, since 2000, the number of runners and running events increased steadily (Figure 1.3).

A recent analysis of more than 70 thousand events from 1986 to 2018 suggests that, for the first time in history, there are more female than male runners. In 2018, over the 7.9 million participants in road races, 50.14% were females (Andersen, 2019). Although a small decrease occurred since the peak of 2016 (9.1 million), running gave rise to the expansion of other disciplines within its scope (e.g., trail running, ultra-marathons, Ironman). Moreover, the recent decrease in marathon finishing times embodies the current shift in motivations observed in participants; a growing portion opts for a psychological, health and socially focused approach rather than an achievement-based focus (Andersen, 2019; Scheerder et al., 2015). Consequently, running event organizers have expanded or abolished the time limits of their races and have introduced new race distances, like 15km, 10km, 5km, and even 1km (Van bottenburg et al., 2010). Moreover, participants in road races have never been older. The

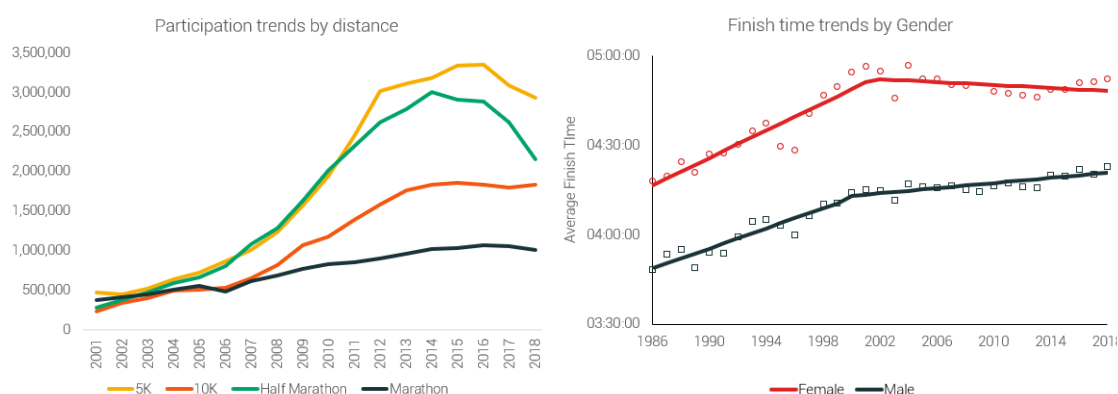


Figure 1.3 – (Left) Trends in the number of participants in running races of different distances between 2001 and 2018. (Right) Evolution of the average finish time in marathons for females and males (Andersen, 2019).

average age increased from 35.2 in 1986 to 39.3 years old in 2018. The most significant increase was observed in short distance races, with the average age of 5K runners rising from 32 to 40 years old (+25%).

As mentioned above, these demographics changes are accompanied by changes in running motives. Some of the most frequently reported reasons to take part in running activities are (1) psychological motives (e.g., maintaining or enhancing self-esteem, coping with negative emotions and stress), (2) social motives (e.g., feeling part of a group, recognition, and approval), (3) physical motives (e.g., health and weight loss), and (4) performance motives (e.g., competition, ambition) (Andersen, 2019; Shipway & Holloway, 2010).

1.5 The assessment of running

The analysis of the running gait is usually categorized based on the nature of the research question. Kinematics studies aim to assess the motion of the body-segments separately, or as a whole. It includes the description of the translational movements (e.g., the position, the speed, the acceleration) and rotations (e.g., orientation angles, angular velocity) in space, and do so independently of their causes (i.e., the forces). The position and orientation of the lower limbs during running have been of great interest for researchers, and the foot, as the only body-segment interacting with the ground, received particular attention. For instance, the orientation of the foot in the sagittal and frontal planes gave rise to a large number of publications on topics like the foot strike patterns (Daoud et al., 2012; Hatala et al., 2013), and pronation/supination (Benno Nigg et al., 2019). Also, a variety of upper-limb movements (Hinrichs, 2016; Hinrichs et al., 2016) have been thoughtfully documented, such as the description of the joint angles (Keith R Williams, 1985), the sagittal plane trunk posture (Teng & Powers, 2014a, 2014b) and the rotation and oscillation of the pelvis (Schache et al., 1999). Kinetics studies the cause of movement and examine the external or internal loads

acting on the body structure. Generally, these studies aim to quantify the forces and their moments acting on specific bones and joints. Of particular concern are the consequences on the health of the runners and the effectiveness of external interventions (e.g., footwear, insoles, feedbacks). For instance, studies have shown that relatively low levels of impact forces are at a reduced risk of incurring overuse running injuries (Hreljac, 2004). Physiological studies, such as oxygen uptake, describe how the human organism consumes metabolic energy to sustain the running movement. The influence of the running condition (e.g., speed, slope), environment (e.g., altitude, terrain), and other interventions (e.g., training programs, diet) are usually at the center of these researches. Studies occasionally also combine the kinematic and kinetic aspects of running and investigate their relation from a physiological standpoint, such as to examine the biomechanical factors associated with running economy (Moore, 2016). Central to the entire discipline is the quest to improve the running performances. Finally, spatio-temporal studies deal with the analysis of spatial and temporal parameters within the different phases of the running gait. With the running gait subdivided in cycles, these studies use a discrete approach in the resolution of their research questions. The duration of the stance phase (i.e., contact time), of the phase of flight, the running cadence, and the stride length are all examples of variables considered in spatio-temporal studies (Dugan & Bhat, 2005; Novacheck, 1998).

The subsequent sections introduce the fundamental components of running biomechanics and present the terminology for the rest of this thesis. The review starts with a description of the temporal events and gait phases that compose the running cycles and discusses the effects and causes associated with variations in these parameters. Finally, the most common kinematic and kinetic features are reviewed.

1.5.1 Temporal events and gait phases

The running gait is comprised of a succession of cycles called strides as the basic units of measurement in gait analysis (Novacheck, 1998). A cycle is comprised of two steps, and the inverse function of the duration of a stride and a step are defined as the stride and step frequency (or cadence), respectively. Moreover, one stride can be divided into two stages: the aerial and terrestrial phases. The terrestrial phase is generally referred to as the stance phase and the aerial phase as the flight phase (or phase of float). As shown in Figure 1.4 and later discussed in this section, each period can further be subdivided into sub-phases. The study of those phases, as well as the different methods and instrumentation required to assess them, is often denoted as the temporal analysis of the running gait.

In running, two events must be detected on each leg in order to extract the main temporal features of a stride: the initial contact (or touchdown) and terminal contact (or take-off) events. Initial contact occurs when the foot first initiates contact with the ground during landing and terminal contact when the toes lose contact at the end of the pushing phase. The mid-point between initial and terminal contact is known as the mid-stance event. Initial

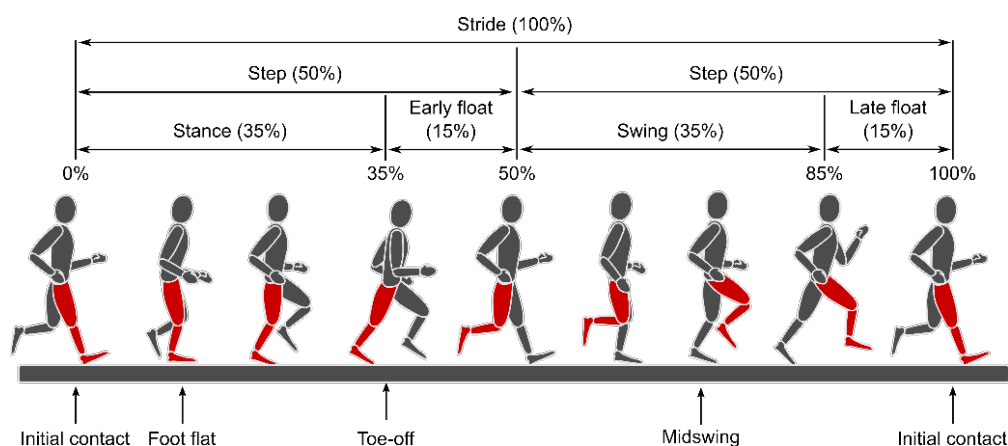


Figure 1.4 – Temporal events and gait phases of a running cycle (or stride). The temporal events are depicted according to the leg highlighted in red, and the percentages are approximations reported during jogging.

contact marks the start of the stance phase, which is often divided into two sub-phases: (1) the weight acceptance phase (or braking phase) where the subject absorbs the landing forces and supports the vertical collapse of the center-of-mass (CoM), and (2) the pushing phase (or push-off) where a forward acceleration is generated to propel the body mass forward (Hamner et al., 2010). With terminal contact and the end of the stance phase starts the swing phase. The term “contact time” is often encountered in the literature as it refers to the duration of the stance phase. This phase lasts until the following initial contact event of the same foot and has its mid-point defined as the midswing event. Moreover, as the swing phase period starts for one leg, the contralateral leg approaches the end of its swing phase, leading to a period where none of the foot is in contact with the ground, the flight phase. By definition, the flight phase starts with terminal contact of ipsilateral leg and ends with initial contact of the contralateral leg. Hence one swing phase is composed of a period of flight (“early float” in Figure 1.4), the stance phase of the contralateral leg, and a second flight phase (“late float” in Figure 1.4).

As the early inventions of Etienne Jules Marey (section 1.2) illustrate, the absolute and relative duration of the abovementioned gait phases has been of interest for more than a century. How these phases changes as the running speed increases has received particular attention. For instance, a considerable amount of literature has shown that stride frequency increases almost linearly for slow to moderate speed and non-linearly for fast running (Luhtanen & Komi, 1978; Ari Nummela et al., 2007; Keith R Williams, 1985) (Figure 1.5, left). However, the method used to augment the velocity through a change in the stride frequency and stride length varies among individuals (Ari Nummela et al., 2007; Van Oeveren et al., 2019; Weyand et al., 2000). Also, it is well recognized that the absolute contact time and flight time decrease as the running speed increases (Luhtanen & Komi, 1978; Nilsson et al., 1985; Ari Nummela et al., 2007; Keith R Williams, 1985) (Figure 1.5, right). The change in contact time with speed is non-linear in that decreases are greater at slower speeds than at faster speeds. Interestingly, their relative time, often expressed in percent of a gait cycle, is responding otherwise to an

increase in velocity; runners spend proportionally more time in the flight phase than in the stance phase as velocity augments (Dugan & Bhat, 2005; Nilsson et al., 1985). For example, the observations in (K.R. Williams, 2008), for one individual, showed that contact time during a step decreased from 80% at 3.6 m/s to 66% at 6 m/s, and flight time increasing from 20% to 34%. Moreover, a recent study was able to predict the running speed of an individual based on a personalized model with contact time as the only input (De Ruiter et al., 2016).

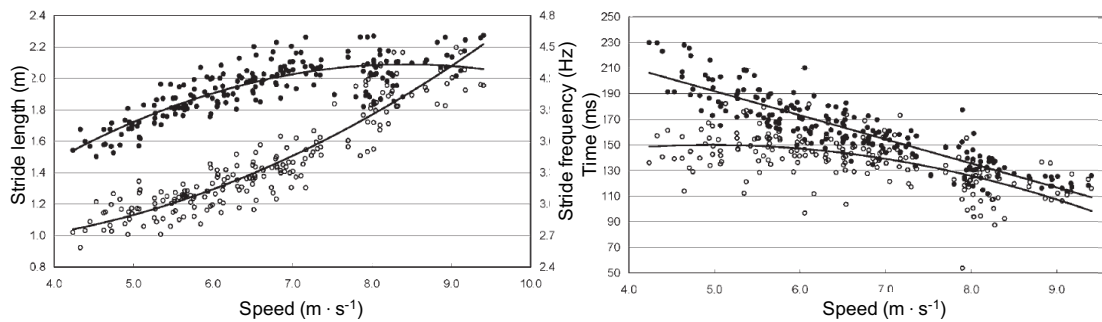


Figure 1.5 – (Left) Stride frequency (open circles) and stride length (black dots) as a function of the running speed. (Right) Flight time (open circles) and contact time (black dots) as a function of the running speed. Source (Ari Nummela, Keränen, & Mikkelsen, 2007).

Other studies have investigated how these temporal parameters were affected by the appearance of fatigue (Bates & Haven, 1974; Elliot & Ackland, 1981; Joseph Mizrahi et al., 2000; Jean Benoît Morin et al., 2011; S. Winter et al., 2017). Fatigue can diminish coordination and efficiency in the movements, thereby affecting the running performance. A common problem in fatigue studies is that running speed also changes during a prolonged run, and it can be challenging to identify the changes due to fatigue and those due to the altered velocity. In a study (Elliott & Roberts, 1980) where the speed was controlled, the authors reported trends towards an increase in stride frequency, an increase in contact time, and a decrease in flight time.

Tightly linked with the notion of fatigue is the notion of running economy and running efficiency. In distance running, small improvements in energy expenditure can lead to substantial progress in performance. Consequently, researchers have tried to relate these physiological improvements with the temporal parameters of gait (P. E. Martin et al., 2008; Moore, 2016). For instance, runners seem to naturally select the most economical (or nearly optimal) stride frequency (or stride length). The studies supporting this self-optimization theory often used precise manipulations of both cadence and stride length to extrapolate the most economical stride frequency mathematically. Interestingly, the difference between preferred and mathematically optimal stride frequencies is greater for novice (8%) than for trained runners (3%) (de Ruiter et al., 2014). However, there is little agreement yet regarding the association of contact time and flight time with the cost of running.

Overall, the analysis of the aforementioned gait phases plays a fundamental role in the assessment of running. Stance, swing, and flight phases constitute the framework within which

other kinetic and kinematic features are studied. For these studies, it is therefore imperative to accurately and precisely detect the events of initial contact and terminal contact. In the literature, the majority of studies have used force plates, contact mats, or high-speed cameras as reference measurement systems (Van Hooren et al. 2019; (Peter R. Cavanagh and Lafortune 1980; Munro, Miller, and Fuglevand 1987; J. Hamill et al. 1983). Although force plates are accepted as state-of-the-art systems for temporal events detection in running, they suffer from several limitations; the detection timing of the initial and terminal contact events on the vertical ground reaction force depends on the filtering method, and the detection threshold used (BM Nigg 1983). Moreover, their lack of portability and their setup complexity restrict their use for in-laboratory experiments, which is a major drawback given the in-field nature of the running activity.

1.5.2 Kinetics of running

Kinetics studies examine the external or internal loads acting on the musculoskeletal structure. For it is within the period of ground contact that the body interacts with the earth, a vast portion of the scientific literature focused on the stance phase, and specifically on the assessment of the ground reaction forces (GRF). These forces are generally measured using floor-integrated force plates or instrumented treadmills. Although the instrumented treadmills allow for continuous monitoring of the GRF, they can be affected by the noise induced by the vibrations of the treadmill. While a recent review suggested that the mechanics of running are mostly comparable between motorized treadmill and overground running, they also observed considerable differences for sagittal plane kinematics (Van Hooren et al., 2019).

The GRFs have been a subject of research in many biomechanical studies and the shape of the force-time curves investigated under various conditions (Peter R. Cavanagh & Lafortune, 1980; J. Hamill et al., 1983; Munro et al., 1987). Because it approximates the loading on the lower extremities required for the support of the body mass, the vertical GRF received particular attention. Moreover, the magnitude of the vertical GRF is usually higher than in the anteroposterior and mediolateral directions. The magnitude of the vertical GRF can vary considerably among individuals running at the same speed (4.5 m/s), ranging from approximately 2 to 3 times the body weight, according to (Peter R. Cavanagh & Lafortune, 1980). Also, increases in the running velocity have been associated with increased peak force amplitudes (Weyand et al., 2010). The terminology used to describe the vertical force-time curve has varied among studies, but a naming convention (BM Nigg, 1983) is now predominant; the initial peak referred to as the impact peak, occurs within 10% of the stance phase, and the second peak referred to as the active peak, over the latter 60-75% of stance (Figure 1.6). Interestingly, one study has shown that during uphill and downhill running, as the angle of the hill changes from a steep downhill to a steep uphill: normal (i.e., perpendicular to the ground surface) impact peaks decrease and normal active peaks do not change (Gottschall & Kram, 2005). Also, it is important to note that the shape of the ground reaction force patterns depends primarily on the running style (i.e., the foot strike pattern). For midfoot and forefoot

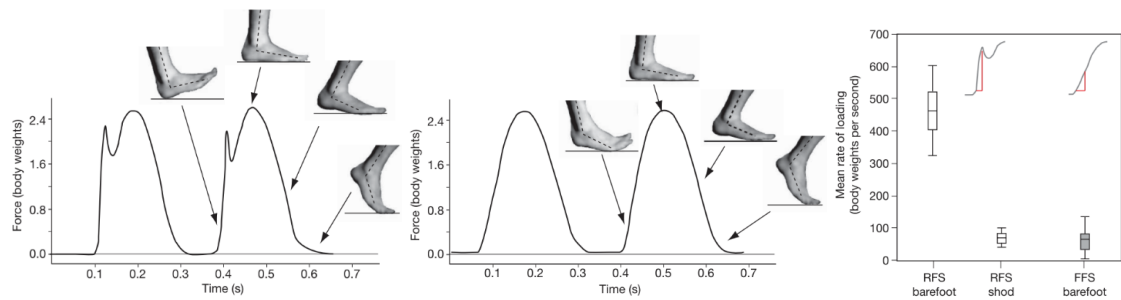


Figure 1.6 – Vertical ground reaction force observed for two landing techniques: (Left) rear-foot strike and (Middle) forefoot strike. (Right) Differences in loading rate between barefoot rearfoot strikers (RFS), shod RFS, and barefoot forefoot strikers (FFS). Source (Lieberman et al., 2010).

strikers (see section 1.5.3), the impact peak is typically attenuated or absent (P. R. Cavanagh, 1990; Lieberman et al., 2010; Payne, 1983; Keith R Williams, 1985) (Figure 1.6, middle).

The loading rate best characterizes these differences in the shape of the early vertical GRF between populations and is often expressed in bodyweight per second to facilitate the comparison of across runners. In addition to the landing technique (Figure 1.6, right), the loading rate also depends on the running speed (Munro et al., 1987). Despite its association with the notion of impact and shock, a systematic understanding of how this feature contributes to injuries is still missing. For instance, several studies have investigated the association between the loading rate and the history of lower-limb stress fractures but found conflicting results (Zadpoor & Nikooyan, 2011). Some researchers used a different approach toward the assessment of the landing impact; they examined how it propagates across the body and suggested that the primary mechanisms for attenuation may differ according to the footfall patterns (Gruber et al., 2014).

The GRF in the anteroposterior direction is often related to the notions of braking and propulsion. In the initial phase, the anteroposterior GRF opposes forward motion, hence the forward speed of the runner is slowed down (i.e., the braking phase). In the second phase, its direction is consistent with the movement, hence the forward speed increases (i.e., propulsion phase). Although extensive research has been carried out to explain the interindividual variations, no evidence of a regular pattern has emerged. However, the anteroposterior GRF was shown to be relevant for the understanding of sprint mechanics and is commonly used in the estimation of the running power (Rabita et al., 2015). In comparison, it was proven more difficult to find relevant patterns in the mediolateral GRF.

The point of application of the GRFs known as the center of pressure (CoP), is located below the foot. The trajectory of the CoP has been proposed to classify the landing technique across runners; the strike index (Peter R. Cavanagh & Lafortune, 1980). This index aims to divide the shoe midsole into three equal parts, record the position of the CoP at the time of initial contact, and use that position to define whether an individual first contact was made in the rear one

third (rear-foot strike), in the middle third (mid-foot strike) or the front third (fore-foot strike) of the shoe. Researchers also used the mediolateral trajectory of the CoP to assess the inward and outward rotation of the foot during the stance phase and the timing of such mechanisms (De Cock et al., 2005, 2008). Similarly, existing research recognizes that the initial contact with the ground for most runners occurs on the lateral border of the foot (P. R. Cavanagh, 1990). A more descriptive metric than the CoP is the distribution of the plantar pressure. For instance, plantar pressure distribution was proposed to examine the association between the structure and the function of the foot (Hillstrom et al., 2013), to classify runner according to the function of their foot (De Cock et al., 2006), to compare the mechanics of overground and treadmill running (Hong et al., 2012) or investigate the pressure patterns and their associations with running-related injuries (Mann et al., 2016).

Attempts to describe the interdependency of mechanical parameters and examine the relationship between the motion of the center of mass (CoM) and the GRF resulted in a variety of models. Arguably the most common one, the spring-mass model, simplify the whole body mass with a point mass on top of a single spring (Blickhan, 1989; McMahon & Cheng, 1990). The motion of the point mass is assumed to be linear vertical and downward during the first half of the stance phase and upward during the second half. So if the displacement of the CoM, the active peak force, and the mass of a subject are known, the vertical and leg stiffness can determine based on this model and using Hooke's law (Farley & González, 1996; Marlène Giandolini et al., 2014; Pappas et al., 2014). Inversely, this model can also be used to predict the vertical ground reaction force (Geyer et al., 2006), running economy (Dalleau et al., 1998), stride length, and other features (Bullimore & Burn, 2007). This model was designed for level running, yet one study suggested that it could be generalized by adding a damper in parallel with the spring for downhill running, and a motor for uphill running (Dewolf et al., 2016). However, the spring-mass model does not account for the asymmetric force-time curve of the vertical GRF and fail to predict its high-frequency components, such as the impact force peak.

Consequently, more sophisticated models have been proposed to solve this issue. These are generally referred to as the multi-body mass-spring-damper models (Clark et al., 2017; J. Mizrahi & Susak, 1982; Nedergaard et al., 2018). Whereas these complex models tend to predict the GRF more accurately than the simpler spring-mass model, the additional parameters required for these models need to be estimated, hence are a potential source of error, and makes them increasingly difficult to understand their physical meaning.

Another commonly used model to calculate the mechanics of the lower limbs is the so-called inverse dynamic method. This method estimates the net joint forces and moments at each joint of the lower limbs using inputs such as the GRF, the center of pressure, the segments parameters (e.g., mass, length), and the segments kinematics. The early work of Braune and Fischer (section 1.2) laid the foundation of this indirect measurement method, which has, since then, been used in a consequent amount of running researches to examine the relationship between technique and internal load (Mei et al., 2019; Van Hulle et al., 2020). This method emphasizes the cause and effect relationship between kinetics and kinematics, and

the importance of considering both approaches in the analysis of the running gait.

Muscle activity timing and relative intensity have also been widely documented for running, and it constitutes a field of research by itself. These metrics are commonly obtained through electromyography and surface or fine wire needle electrodes. However, muscle activity can not be measured with inertial sensors. Thus, its review is not included in this thesis.

1.5.3 Foot kinematics

Investigating the whole-body kinematics is a continuing concern in the field of running biomechanics. Although a considerable amount of literature investigated the motion of the upper limbs and trunk segment, the majority of studies focused on lower extremities. Nevertheless, it is important to note the significance of the existing literature regarding the oscillation of the CoM. This characterization directly relates to the spring-mass model previously discussed (section 1.5.2). For instance, studies have demonstrated that the vertical oscillation of the CoM decreases with running speed and was reported from 10.9 to 6.7 cm for speeds between 3.9 and 9.3 m/s (Luhtanen & Komi, 1978). Also, low vertical oscillations were shown to be beneficial for running expenditure (Moore, 2016); from a mechanic standpoint, the amount of work required to support the CoM during the stance phase increases as the CoM vertical displacement also increases. Besides, scientists scrutinized numerous other upper-segment kinematic features such as the trunk angle in the sagittal plane (Teng & Powers, 2014a, 2014b), and the role of the arm swing movement (Arellano & Kram, 2014).

Regarding the lower limbs, the kinematics of the knee and hip have been thoughtfully described. In particular, the continuous changes in the thigh and knee angles have been reported under various running conditions (e.g., speed, footwear, landing technique) (Keith R Williams, 1985), and many studies have investigated the position of the lower leg at initial contact; it has been proposed that the orientation of the lower-limb segments could affect the changes in the horizontal running speed observed during the braking phase of support (Peter R. Cavanagh et al., 1977).

As the only segment interacting directly with the ground, the movement of the foot received particular attention. Also, in this thesis, the main focus is on the movement of the foot due to the comfort and simplicity that shoes offer in the placement of motion sensors, and in the relevance of foot biomechanics to analyze gait. Therefore, the remaining of the current section reviews the kinematic features of the foot only. The pose of the foot (i.e., position and orientation) have been particularly scrutinized throughout the last decades. Two key concepts have been at the center of many discussions: the foot strike patterns and the inward and outward rolling motion of the foot during the stance phase.

The sagittal plane orientation of the foot at initial contact is usually classified into one of three classes, the so-called foot strike patterns: a rear-foot strike (RFS) occurs when the heel lands first; a midfoot strike (MFS) when the heel and ball of the foot land nearly simultaneously;

and a fore-foot strike (FFS) when the ball of the foot initiate contact first after which the heel follows shortly. As introduced above, in most research, this characterization of the landing phase was performed through the measurement of the strike index (section 1.5.2). Recently, the footstrike angle (FSA), defined as the sagittal plane angle between the foot and the ground surface at initial contact, was shown to be an acceptable alternative to the strike index (Altman & Davis, 2012). The authors of the same study also proposed the following classification limits based on the FSA: rearfoot strike $> 8^\circ$, midfoot strike between -1.6° and 8° , and forefoot strike $< 1.6^\circ$.

Most recreational runners use an RFS at slow and moderate running speeds. Studies have analyzed the distribution of the foot strike patterns of a large number of participants in a competitive distance race and found that over 80% of individuals were rear-foot strikers, approximately 20% were midfoot strikers, and roughly 1% were forefoot strikers (Hasegawa et al., 2007; Larson et al., 2011). In sprinting, however, nearly all individuals use an FFS (Mero et al., 1992). A cluster analysis of 102 recreational runners suggest that three distinct and approximately equally sized groups of strike angle adaptations exist as the velocity increases: (1) small/negative FAS throughout; (2) large positive FSA at low velocities (≤ 4 m/s) transitioning to a smaller FSA at higher velocities (≥ 5 m/s); (3) large positive FSA throughout (Forrester & Townend, 2015). Nevertheless, speed is not the only factor affecting the foot strike angle. Two studies observed that a high percentage of marathon participants switched from an FFS or MSF to an RFS as the distance increased and that the more elite performers were less likely to heel-strike (Bovalino et al., 2020; Larson et al., 2011). Such observations suggest that fatigue can alter the preferred landing technique, which in turn depends on the running experience.

From a mechanical perspective, the Achilles tendon and the plantar arch are the anatomical springs that contribute most to the energy storage and restitution process of each step; together, they retain roughly 50% of the potential and kinetic energy lost during stance phase (Alexander, 1991). Since these anatomical springs are most activated using FFS and MFS (Perl et al., 2012), it seems theoretically sound that experienced runners, and faster runners tend to prefer an FFS or MFS landing technique. Though the connection between the foot-strike patterns and running-related injuries is still today widely debated among researchers, evidence shows that individuals running barefoot tend to avoid RFS landing instinctively and that the rear-foot strikers experience a higher loading rate than the mid-foot and forefoot strikers (Lieberman et al., 2010) (Figure 1.6). Hence, researchers addressed footwear cushioning as an injury prevention strategy making RFS acceptable (Kulmala et al., 2018; Ryan et al., 2014; Sun et al., 2020). A recent review on the topic concluded that 1) increasing the forefoot bending stiffness of running at the optimal range can benefit performance-related variables; 2) softer midsoles can reduce impact forces and loading rates; 3) thicker midsoles can provide remarkable cushioning effects and attenuate shock during impacts but may decrease plantar sensations at touchdown; 4) minimalist shoes would improve running performance (Sun et al., 2020).

Although the foot strike pattern describes the pose of the foot in the sagittal plane, another

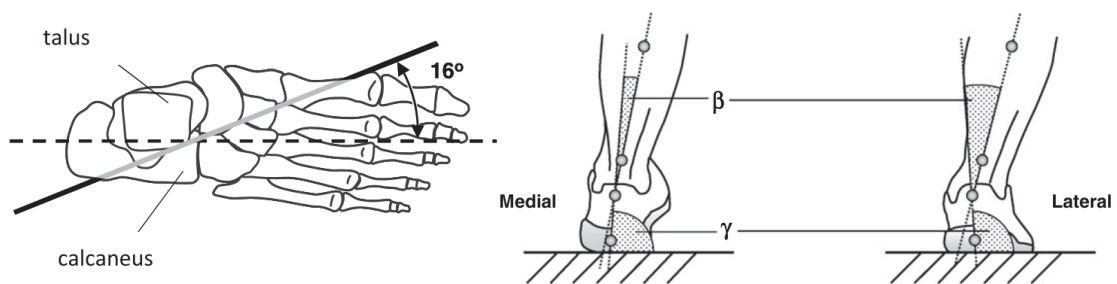


Figure 1.7 – (Left) The subtalar joint axis indicated by the solid black line and the longitudinal axis by the dashed black line. (Right) Two most common alternatives to pronation quantified in the literature: β the Achilles tendon angle and γ the rear-foot eversion. Source (Nigg, Behling, & Hamill, 2019).

term focuses on the rolling motion of the foot during the stance phase: the pronation and supination movement. Pronation is defined as the inward rotation of the rear foot about the subtalar joint axis, and supination as the outward rotation of the rear foot about the subtalar joint axis (Benno Nigg et al., 2019) (Figure 1.7, left). At initial contact, the foot is supinated or locked, to better absorb the landing impact. Then, during the first 40-50% of the stance phase, the foot pronates or unlocks to offer more stability in support. Finally, the foot supinates again throughout the pushing phase (i.e., rigidifies) to help propel the runner forward (Ferber & Macdonald, 2015).

The assessment of pronation is complicated, if not impossible; measurement systems cannot directly access to the subtalar joint axis. Nevertheless, scientists have described pronation-like variables to study this rolling motion of the foot. The rear-foot eversion angle was defined as the angle between the talus and the ground (Figure 1.7, right) (Areblad et al., 1990); it corresponds to the inward rotation of the foot around the longitudinal axis of the foot. In comparison, the inversion angle refers to the outward rotation of the foot. Instead of describing the rotation based on the rear-foot, the Achilles tendon angle refers to the motion of the shank (Reinschmidt et al., 1997). Unfortunately, existing studies have used these surrogate variables (and many more) interchangeably with the term pronation, making it difficult to generalize the findings on that matter. This might explain why inconsistent results have been reported on the association between pronation and injuries (Behling et al., 2019).

Pronation and supination are natural protective mechanisms with which the foot accommodates to uneven surfaces. However, the terms “over-pronation” and “hyper-pronation” have been used many times in the literature. These terms refer to the potentially excessive motion of the foot, but a clinical definition is missing (Benno Nigg et al., 2019). One reason that drove researchers to examine pronation is the internal rotation that it induces to the tibia, which in turn may create problems at the knee (Van Der Worp et al., 2015).

Recent research suggested to abandon the “impact” and “pronation” paradigms due to a lack of biomechanical and epidemiological evidence and instead shift to new paradigms, such as

“Muscle tuning,” “preferred movement path,” and “habitual motion path” (B. M. Nigg et al., 2017; Trudeau et al., 2019). These studies suggest that each individual possesses a “habitual” motion path that the body naturally adopts as a consequence of the optimal path of least resistance of their joints and that any intervention affecting this path is inappropriate and potentially harmful.

Finally, stride length refers to the distance covered from initial contact of one foot to the next contact of the same foot. In comparison, step length is the distance between successive footstrikes of each leg. This parameter has often been reported in the literature, for its direct association with speed and stride frequency (Figure 1.5, left); if one knows the duration of a stride and the distance covered during that stride, one can estimate the velocity. Speed is a crucial element of running analysis; it affects the temporal parameters, the kinetic components, and the kinematic features of the running. The relation between stride length, stride frequency, and speed has been widely documented and suggest that each individual uses a different strategy to generate speed (Elliott & Blanksby, 1979; Högberg, 1952; Mercer et al., 2002).

1.6 The objectives of this thesis

The current chapter introduced running as a human locomotion method, its underlying mechanisms, and its journey into becoming one of the most popular physical activities worldwide. The main temporal, kinetic, and kinematic properties of running were briefly introduced to recognize the significance of gait assessment for injury prevention or performance analysis. This chapter also emphasized on the real-world nature of running and described the protective role of the foot in adapting to uneven surfaces.

While running is mostly an outdoor activity, paradoxically, most of today’s knowledge on running mechanics was uncovered from the confines of fully instrumented laboratories and not from its natural environment. These laboratories are generally equipped with state-of-the-art measurement systems but suffer, nonetheless, from several limitations. For instance, the limited volume that these systems can capture often restrain the analysis to treadmill running. Long-term measurements are generally not possible due to the consequent amount of data that needs to be stored. Consequently, continuous assessment of the running gait is impossible and must instead be carried periodically. Lastly, the cost and complexity of data processing restrict their use to research and elite athletes.

Nevertheless, the recent improvements and miniaturization efforts in sensor technologies and the progress of information and communication technologies have moved the assessment of running from the controlled in-lab environments towards real-world conditions using body-worn systems. But, only a few of the existing wearables devices have been validated against reference systems, making the outcomes of the studies that employed these body-worn systems somewhat hard to evaluate. Hence, the lack of accurate portable systems and the proliferation of real-world research increased the need for acutely validated wearable methods

(i.e., sensors and algorithms).

Considering the above, Chapter 2 of this thesis is dedicated to the review of the state-of-the-art of running assessment methods and challenges facing the recent shift from in-lab to in-fields studies that wearable technologies induced. Chapter 2 also discusses the limitations of wearable sensors and the potentially negative effects that non-validated devices could have on the reputation of these systems.

The configuration of inertial sensors can vary from one to several devices on each of the body segments. Nonetheless, attempts to reduce the configuration to a minimum should always be considered, in order to make the system more accessible and more convenient for the users. As introduced in this chapter, the foot has an essential role in absorbing the landing impact and protects the other limbs from uneven surfaces by an intricate mechanism of rotations. It is, therefore, a prime location for sensing technologies to monitor. Besides, the sensors can be fixed on the shoe without direct contact with the skin, making the system more comfortable for the runners. Therefore, by focusing on foot-worn sensors the main objectives of this thesis were to design and validate new algorithms for running gait analysis to:

1. Assess the temporal parameters of running (Chapter 3)
2. Measure the orientation of the foot by reducing the orientation drift (Chapter 4)
3. Estimate the running speed using three different approaches (Chapter 5)

The mandatory stage of any new instrumentation consists of validating its measurements with an appropriate reference system and carefully report the results. Although this affirmation may seem trivial, it is unfortunately frequent to come across running studies based on instruments or methods of inappropriately reported, or merely inexistent, evaluation of the error. The terminology is also regularly misemployed with fundamental concepts such as accuracy, bias (systematic error), and precision (random error) being incorrectly interchanged (Walther & Moore, 2005). This issue is particularly recurrent for studies using body-worn inertial sensors. Researchers rushed towards wearable sensors technology and sometimes forgot to question the reliability of these tools. The same observation holds for commercialized devices. Knowing the accuracy and precision of a measurement system is at the core of all scientific research. For instance, if a 5% difference between two types of populations is observed for a given metric, but the random error of the measurement system is unknown, how can anyone advocate whether the difference is significant or purely due to the random error of the system?

Hence, in Chapter 3 and Chapter 4, the performance of the proposed wearable system was validated for several kinematic features and the results compared to reference laboratory equipment (ground truth). Moreover, the effect of the running speed and foot orientation on the temporal detection bias (Chapter 3) is also discussed. Surprisingly, no drift correction model was specifically designed for running; most studies assessed the orientation of the foot using methods derived from walking analysis without considering the kinematic differences

between the two types of locomotion. Hence, Chapter 4 proposes and evaluates a new drift-correction method to assess the foot orientation in running. This method is based on a two-segment model of the foot and suits to the different foot strike patterns observed in running. Using the methods introduced in previous chapters, Chapter 5 presents the limitations of the direct integration of foot acceleration in estimating the overground running speed and proposes a linear model approach to estimate the instantaneous overground running speed accurately. The system was validated against the reference measurements obtained from a body-worn GNSS system. Finally, the accuracy of running speed estimation was further improved based on a personalization process and sporadic access to GNSS measurements (Chapter 5).

Wearable systems are meant for real-world conditions, outside, in the wild. It seemed, therefore, essential to test the practical limitation of the system developed in-lab and propose adaptations when needed. The limitations that can be ignored during the technical validation can become major restrictions outside the labs. For instance, during a 30 seconds trial, the running cadence remains approximately the same and needs only to be estimated once with a simple frequency-domain analysis. When running a marathon, however, the cadence is continuously changing, and new methods must be implemented to cope with these real-world requirements.

Three applications were used to show the usefulness, robustness, and efficiency of the proposed running analysis system in real-world conditions: marathon running (Chapter 6), trail running (Chapter 7), and hurdling (Chapter 8). With each of these applications, new challenges occurred, either associated with the configuration of the sensors, the environment of the measurements, or atypical kinematic patterns (e.g., jumping over a hurdle). Chapter 6-8 address these challenges and propose several solutions to improve the robustness of the system. Such improvements include a sliding window estimation of the running cadence, the automatic detection of hurdle crossings, and a recurrent re-assessment of the misalignment between the sensor frame and the functional frame of the foot.

1.7 Thesis overview

This thesis is comprised of four parts. Part I, Introduction and background, includes the present introducing chapter and Chapter 2, State of the art in running assessment. Part II, Algorithms development and Validation, includes Chapters 3 to 5 for temporal parameters, foot orientation, and running speed estimation. Part III is dedicated to the applications of the developed methods in marathons (Chapter 6), extreme mountain ultra-marathons (Chapter 7), and hurdling (Chapter 8) settings. Finally, Part IV includes the last chapter (Chapter 9), which offers a general discussion about the main contributions of the current thesis.

The organization of the thesis is shown in Figure 1.8 and briefly described in the following paragraphs. Note that, in Figure 1.8, shorter versions of the chapters' names have been preferred for the sake of graphical clarity. Also, throughout this thesis, the pronoun "we" is

preferred when referring to a study with multiple authors. Hence, my contributions to these studies (Chapter 3 - 8) are listed in a footnote below the abstract of each chapter.

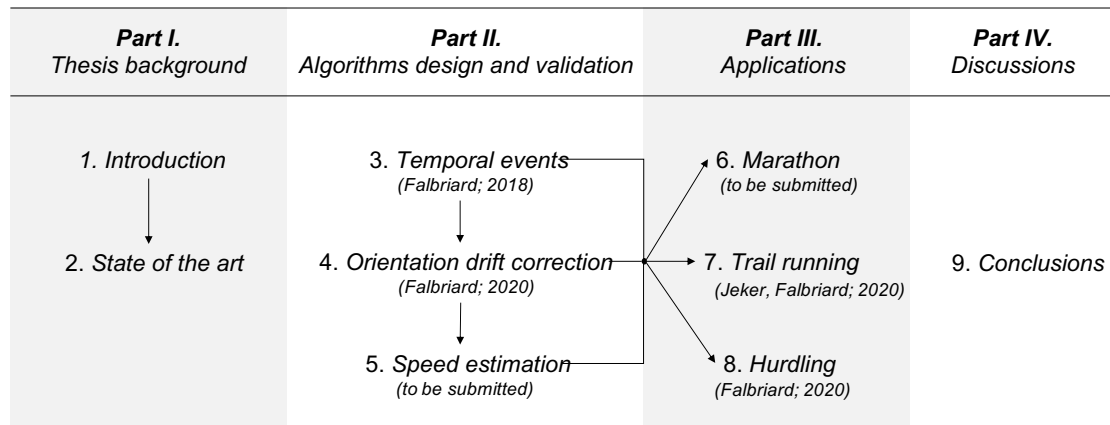


Figure 1.8 – Outline of the thesis, including four Parts and 9 Chapters. Chapters 3,4, 5, 7, and 8 are based on published or submitted papers, as shown in brackets.

Chapter 1 – (current chapter) introduces running as the main topic of the current thesis. An overview of the running biomechanics and analysis principles used in scientific studies is proposed with a historical perspective, from ancient Greece to the present knowledge. The health benefits and most common injuries associated with regular running are also introduced. Finally, this chapter briefly describes how running became one of the most popular sports around the globe.

Chapter 2 – presents an overview of the current state-of-the-art in running assessment. The instrumentation recognized as reference systems and the present state-of-the-art of wearable technologies in running is introduced, with a primary focus on inertial sensors.

Chapter 3 – assess the performance of different kinematic features measured by foot-worn inertial sensors for detecting running-gait temporal events to estimate inner-stride phases duration. The results from the IMU-based system are compared with the reference detection of a force plate and the errors presented in terms of accuracy and precision. Moreover, this chapter also discusses the effect of the running speed on the performance of the system. Finally, a new method based on a decision tree structure for automatic IMU-to-segment assignment is described as additional results.

Chapter 4 - introduces a new method to estimate and correct the orientation drift measured from foot-worn inertial sensors. The step-by-step description of a modified strapdown integration method that decreases the orientation drift is provided. This method is further compensated by estimation of the joint center acceleration of a two-segment model of the foot. The performance of the system was validated against an optical motion-tracking system during level treadmill running. Moreover, the agreement between the visual determination of the foot strike patterns and the foot strike angles obtained from a motion tracking system is discussed as additional results.

Chapter 5 – proposes and evaluates three different methods to predict the instantaneous overground running speed based on foot-worn inertial sensors; the first method involves the direct measurement of speed, the second a linear modelization of the speed, and the third a personalized modelization based on sporadic inputs from a GNSS system. The performances of a personalized and non-personalized model are compared, and the benefits of averaging the predictions over several steps are discussed. Compared to the previous chapters, the measurements of this study were obtained in a real-world environment at various running speeds and slopes.

Chapter 6 – presents the capacity of the system to analyze the running spatiotemporal parameters in a marathon setting. The results suggest that a significant change in the spatiotemporal parameters occurs around the 25th km and remains consistent until the end of the race. This chapter also emphasizes the different time-resolutions that the system can provide, from stepwise estimations to statistics over several kilometers.

Chapter 7 – investigates the effects of altitude and distance on the uphill vertical speed and cadence during an extreme mountain ultra-marathon. This study was included in the current thesis for two main reasons; first, the IMUs were placed inside a sock worn around the ankle, therefore, testing the limits of the algorithms presented in chapter 3. Second, the setting of the race was unusual as it comprised bouts of resting, walking, and running in inclined and declined terrains of different types (e.g., rocks, concrete roads, grass).

Chapter 8 – tests the algorithms in a track and field event with obstacles within the race; 400 meters hurdling. In particular, it determines whether: (1) shoe-worn magnetic and inertial sensors can be used to detect hurdle clearance and identify the leading leg in 400-m hurdles, and (2) to provide an analysis of the hurdlers' spatiotemporal parameters in the intervals defined by the hurdles' position.

Chapter 9 – provides a general discussion about the contribution of the current thesis, the limitations of the proposed system, and the future outcomes. It also presents the commercialized product, which has been developed based on the algorithms presented in this thesis.

2 State of the Art in Running Assessment

2.1 Overview

Scientific-grade running assessment is commonly performed inside research labs equipped with state-of-the-art measurement systems. However, as the size and price of wearable devices decreased, researchers started to monitor running in real-world conditions with, sometimes, poor reliability in the measurements. Today, when designing new measurement protocols, scientists need to evaluate the trade-off between the accuracy of the lab instruments and the convenience of wearable sensors to select the right instrumentation. Running biomechanists often refer to the laboratory equipment as “reference systems” or “state-of-the-art measurement system.” Such terminology emphasizes the distinction between reliable and accurate in-lab systems and supposedly less accurate ambulatory monitoring devices.

This chapter introduces the common in-lab measurement systems and reviews the state-of-the-art of inertial sensing technology in running. Since the present thesis proposes novel algorithms based on foot-worn inertial measurement units (IMU), this review focuses primarily on accelerometers and gyroscope sensors: discussing their configuration, monitoring capacities, and limitations. Also, the signals obtained from inertial sensors are not intuitively clear and require advanced algorithms to qualify and quantify the running gait objectively. Hence, these algorithms are the actual added-value of the existing systems and need to be carefully reported. Since the number of running studies based on inertial sensors is long and rapidly increasing, this chapter provides an overview of the latest developments.

2.2 Reference measurement systems

2.2.1 Force plates

Force plates are typically used to measure the ground reaction forces applied to the body during the period of stance. These systems are generally comprised of three-dimensional force transducers located in each corner of a rigid plate, measuring the force based on piezoelectric

Chapter 2. State of the Art in Running Assessment

or strain-gauge sensors (P. R. Cavanagh, 1990). Hence, a force platform can retrieve the ground reaction force in three dimensions: the anteroposterior, the mediolateral, and the vertical direction. Besides, several relevant parameters, such as the loading rate, the impact forces, and the center of pressure trajectory are derived from these three-dimensional ground reaction forces (section 1.5.2). In running studies, force plates are often set to record with a sampling frequency between 200 to 4800 Hz (Butler et al., 2006; Lieberman et al., 2010), and are recognized as the reference system in the assessment of the stance phase kinetics (Higginson, 2009).

Because of their relatively small size (between 0.6 to 0.9 m in the running direction), runners tend to adapt their stride length to make sure that their foot contacts with the ground within the area of the ground integrated force plate. This issue is known as “targeting” (Challis, 2001). Hiding the force plate from the runner by camouflaging its location offers a reliable solution, but it also leads to a high number of footstrike partially, or entirely, out of the force-sensing surface. To cope with this issue, researchers started using instrumented treadmills. These treadmills have a force plate directly integrated under the rotating belt (Figure 2.1), which makes them appropriate for continuous monitoring of the gait cycles (Belli et al., 2001; Dierick et al., 2004). Most of the running studies on instrumented treadmills were performed with the treadmill leveled. However, efforts were made to assess the kinetics of gait on inclined treadmills (Gottschall & Kram, 2005; Iversen & McMahon, 1992).

Unfortunately, treadmills also have their own limitations. A recent review suggested that the mechanics of running are mostly comparable between motorized treadmill and overground running, but also noted that differences are observed in sagittal plane kinematics (Van Hooren et al., 2019). Moreover, when running on a treadmill at a constant speed, intra-stride variations of the belt speed between 5% to 15% are observed. These intra-stride variations strongly

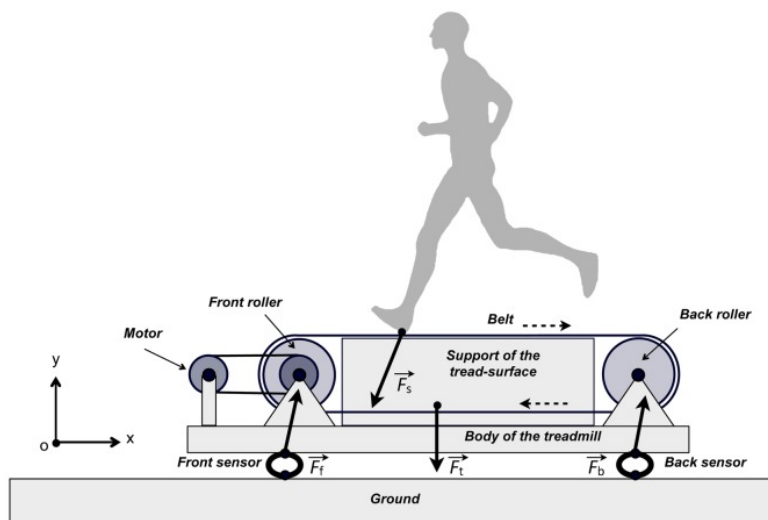


Figure 2.1 – Schematic representation of an instrumented treadmill. Source (Willems & Gosseye, 2013).

depend on the quality of the treadmill; some treadmills can minimize that effect (Willems & Gosseye, 2013). More importantly, the measurements tend to be noisier when obtained with an instrumented treadmill than with a force plate integrated into the ground. This artifact is partially due to the resonant frequency of the treadmill and the vibrations induced by the motor. It is recommended, when possible, to characterize the dynamics of the instrumented treadmill and apply corrective procedures when possible (Garofolini et al., 2019). Although a recent study proposed a new force-plate-treadmill-wobbling-mass model to compensate for these interfering oscillations, the most commonly used processing methods used to reduce the noise are numerical filters. Since the characteristics of the noise depend on the treadmill, different filtering methods have been reported in the literature. For instance, some studies have used lowpass filters with cutoff frequency at 30 Hz (Weyand et al., 2010), or 50 Hz (Fellin et al., 2010), or 100 Hz (Lieberman et al., 2015).

These differences in the pre-processing of the force signal can make the comparison of the results between studies complicated. This is especially true in the context of temporal events detection. The signal of the vertical ground reaction force is commonly used to detect the moments of initial and terminal contact. When the foot initiates contact with the ground, the vertical force suddenly increases. Since the vertical ground reaction force is roughly null within the preceding flight phase, such an abrupt change is easily detected with a threshold. The inverse situation also allows the detection of the terminal contact event. However, the filtering method will affect the slope of the force profile around initial contact; thus, the timing of the threshold-crossing event will change accordingly. Also, many thresholds have been used in the literature. Some studies used absolute thresholds, 0 -150 N (Cronin & Rumpf, 2014; Leitch et al., 2011; Nummela et al., 2007), others used thresholds relative to the subject's body weight, at 3-20% of the body weight (Cronin & Rumpf, 2014), and others relative to the maximum vertical force, e.g. 1% (K. R. Williams & Cavanagh, 1987). In some cases, two different thresholds were used for initial and terminal contact (Kiselyov & Muallem, 2008).

The threshold and the filtering method have an even greater influence on the estimation of the gait phases. When lowering the threshold, for instance, the event of initial contact is detected earlier and terminal contact later. Hence, the error in contact time corresponds to the sum of both errors. As showed in (Falbriard et al., 2018) that a difference in thresholds as low as 30 N could change the contact time by more than 10 ms. Even though force plates are recognized as reference systems for temporal analysis, the data processing method also influences the detection results. Hence it is recommended to keep these limits in mind when discussing the temporal analysis observations.

2.2.2 Optical motion tracking systems

Motion capture technologies are used to monitor the position and orientation of body segments in space. These systems provide reliable estimations of the running kinematics and have been widely used for in-lab measurements. Motion capture devices can be categorized

into two main categories: optical systems and electromagnetic systems. The latter has rarely been used in running, probably because the receiver coils worn by the subject are less comfortable than the markers in camera-based systems and the magnetic field is distorted due to the presence of iron in the ground.

Hence, optical motion capture is considered as the gold standard for the quantification of the motion of body segments during running. These camera-based devices track the position of markers attached to the subjects and compute their 3D coordinates with submillimeter-accuracy (Eichelberger et al., 2016). There are two types of markers; passive markers reflecting the ambient or infrared light, and active markers emitting light. Though active markers have been used in a few running studies (McGrath et al., 2012), the majority of the commercialized optoelectronic systems are based on passive markers (e.g., VICON, Qualisys, BTS SportLab). In general, passive markers are smaller and less hindering the subject.

The number of markers and their position on the body segments depends on the application (Figure 2.2). For instance, studies meant to quantify the lower and upper limbs opted for a full-body configuration of markers (Folland et al., 2017; Maurer et al., 2012), while other studies interested in a specific segment preferred customized settings (Koska et al., 2018; Smith et al., 2015). Some predefined marker settings have been proposed for gait analysis (Davis et al., 1991), and manufacturers of motion capture systems have even implemented their automatic analysis in their devices (e.g., Plugin gait of VICON systems). The predefined models allow for faster processing of the coordinates data but often require precise and somewhat compelling placement of the reflective markers on anatomical landmarks. In comparison, custom configurations can be relatively time-consuming during the labeling stage and require particular attention in the calculation of the different coordinate frames.

The volume that can be captured depends on the number of cameras, which in turn depends on the environment of the study (van der Kruk & Reijne, 2018). The cameras are usually organized along the perimeter of the laboratory to observe the scene from different angles. Their position is fixed at the calibration stage and must remain untouched throughout the measurements; hence, the cameras are typically set around a treadmill (Folland et al., 2017; Maurer et al., 2012), or on the side of a running lane (Kugler & Janshen, 2010; Zrenner et al., 2018). Moreover, the complexity of the camera setting defines whether the markers can be tracked continuously, or if temporary occlusion occurs. Occlusion is a typical limitation of these systems, and it can be resolved through interpolation and filtering methods. There is a lack, however, of consensus on which filtering method should be preferred. Different methods have been reported in the running literature. For instance, Eslami et al. (Eslami et al., 2007) used a low-pass zero-phase shift fourth-order Butterworth filter with a cut-off frequency at 12 Hz, while Lieberman et al. (Lieberman et al., 2015) preferred a cut-off frequency at 6 Hz, and other groups proposed more sophisticated methods based on machine learning approaches (Kucherenko et al., 2018).

The main objective of any markers' configuration is to allow for an accurate representation of

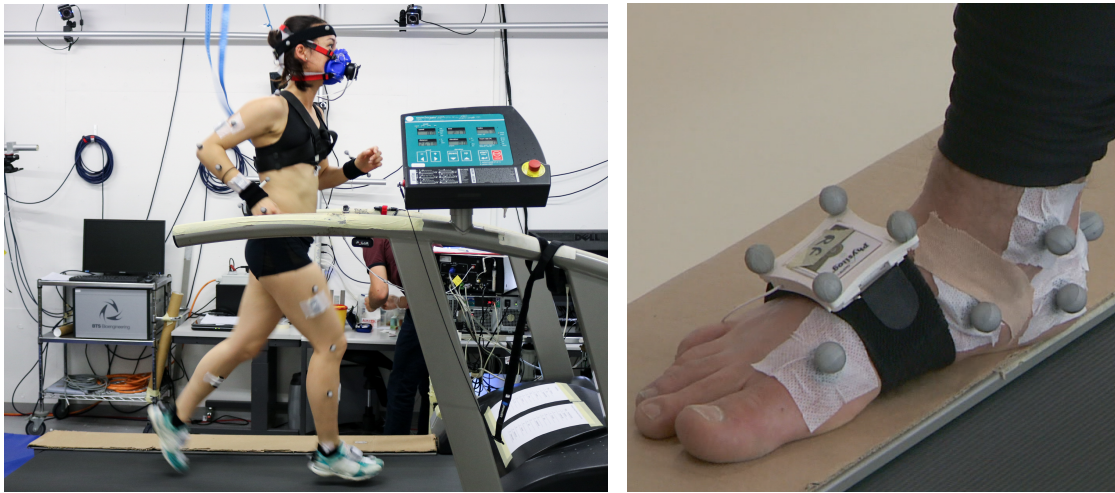


Figure 2.2 – (Left) Full-body configuration of markers during treadmill running. (Right) Configuration of markers focused on the foot segment.

the underlying bone structure. However, soft tissue artifacts can have a large amplitude during highly dynamics movement (Bélaïse et al., 2016). The issue of soft tissue artifact designates the relative motion between the skin markers and the underlying bones. The artifacts can be in the order of a few centimeters depending on the activity and the marker placement (Peters et al., 2010). In running, the main displacements were shown to occur for the skin markers placed on the distal shank and anterior thigh (Dumas et al., 2014).

Apart from the typical kinematic measurement, such as the knee angle, the oscillation of the center-of-mass, the foot strike angle, or the velocity of several body segments, motion cameras have also been used for temporal events detection in running. These techniques are particularly useful in circumstances where a force plate is not available. Several event detection methods have been proposed and some were compared with a force plate as a gold standard (King et al., 2019; Milner & Paquette, 2015). Handsaker et al. (Handsaker et al., 2016) investigated the accuracy of four kinematics-based algorithms to estimate the timing of initial contact over a range of running speeds and footstrike types. The authors recommended using the first vertical acceleration of a marker placed on the posterior aspect of the calcaneus to identify initial contact, and the vertical jerk peak of a marker placed on the distal end of the hallux to identify toe-off. The precision was in the range of twenty milliseconds.

2.2.3 Video cameras and visual assessment

Even if the optical motion capture technology presented in section 2.2.2 is considered the gold standard for kinematic assessment, they are rather time-consuming in their setup and post-processing stages. In some conditions (e.g. foot movement), there is no need for such a bulky setup, and simple video cameras can provide sufficient precision. Generally, the cameras are set up to record one of the three anatomical planes: the frontal, sagittal, or transverse

plane. Since the continuous assessment of any parameter would require to label each frame manually, video cameras were mainly used in running studies to examine discrete variables. For instance, Di Michele and Merni (Di Michele & Merni, 2014) used a high-speed camera (300 Hz) placed perpendicular to the running direction to determine the foot strike patterns on a 400-m outdoor athletic track. Video cameras were also used to assess the foot strike patterns in other real-world conditions, such as marathons (Hasegawa et al., 2007; Kasmer et al., 2013; Larson et al., 2011). Similarly, some studies attempted to examine the inversion and eversion of the foot (Muñoz-Jimenez et al., 2015) and, in some rare cases, estimate the contact time (Ammann et al., 2016).

Video cameras are often part of the whole instrumentation even when a state-of-the-art motion tracking system is available. In these situations, their role is more to provide visual assessment when needed. For instance, to check that the foot landed entirely on a ground integrated force plate, or ensure post-measurements that a specific marker was correctly placed on an anatomical landmark.

2.3 Inertial sensors in running

Inertial sensors or Inertial Measurement Units (IMUs) typically comprise accelerometers and gyroscope. The recent advances in Micro-Electro-Mechanical Systems (MEMS) have made these sensors smaller, power-efficient, and relatively inexpensive; thus, ideal for non-intrusive wearable technology in sports. In an IMU, accelerometers measure both dynamic and static acceleration (e.g., Earth gravitation acceleration) in an inertial frame of reference; and record a null acceleration in free-fall. Gyroscopes derive the angular velocity of a rotating body using the effect of the Coriolis force. The inertial sensor requires careful calibration to deduce their offset and sensitivity. Different procedures have been proposed to estimate these parameters, some simple and well-adapted to real-world applications (Ferraris et al., 1995), others more sophisticated (Aggarwal et al., 2008).

Although the calibration improves the accuracy of the measurement, their results are not error-free. For instance, the majority of modern inertial sensors measure in three directions by combining three uniaxial sensors perpendicular to each other. Misalignment of the three uniaxial sensors can lead to a phenomenon known as cross-talk. Although this issue has been considerably reduced with MEMS technology, cross-talk occurs when uniaxial sensors measure physical phenomena perpendicular to its axis. As for the offset and sensitivity, several methods have been proposed to reset the orthogonality of the axes (Bonnet et al., 2009; Gietzelt et al., 2013).

Like most electronics devices, sensors are affected by changes in temperature, which, for instance, might arise as an important effect to account in winter sports applications. Moreover, accelerometers and gyroscopes usually operate within a specific range, and, in the case of highly dynamic movements, the acceleration or angular velocity may exceed this range and saturate the sensor. Although saturation is generally temporary, it is particularly problematic

when studying the peak value or when an integration of the signal is required. Today, most commercial devices offer an operating range adequate for most sports applications, with $\pm 16\text{ g}$ for the accelerometers and $\pm 2000\text{ deg/s}$ for the gyroscopes. The same conclusion holds for the sampling frequency, typically set around 200-500 Hz in sports applications. Nonetheless, in two recent studies, Mitschke et al. (Mitschke et al., 2017, 2018) observed that both the sampling frequency and the operating range could affect the estimation of the running kinematics and recommended using sampling frequencies above 200 Hz.

Acceleration and angular velocity are not easily interpretable. Generally, users prefer the speed, the position, or the orientation to evaluate kinematics which are much more comprehensible. These metrics can be obtained with accelerometers and gyroscopes but require a time-integration of the signals. As the sensors' measurements are not error-free, and since the integration function acts as a cumulative sum, the noise and bias generate a time-dependent drift of the integrated signal. Drift may be slowly changing or can have discontinuities. Moreover, the source of the drift can be multifactorial; while it depends on the bias and noise of the sensor, it may change with the type and intensity of movement, the sampling frequency, and the signal pre-processing (e.g., filtering, interpolation). Also, since accelerometers are instruments that measure the acceleration relative to freefall (i.e., the kinematic acceleration), an accelerometer at rest will approximately measure a 1 g acceleration. Therefore, to express the motion of the sensor relative to an Earth-fixed reference frame, the acceleration associated with Earth's gravity needs to be subtracted from the three-dimensional accelerometer data. If not correctly removed, Earth's gravity can become an essential source of integration errors. Hence, many drift-correction techniques have been proposed, but the most common approaches are based strap-down integration (Favre et al., 2006; Sabatini, 2005), and complementary filters (Madgwick et al., 2011; Sabatini, 2006).

For the sake of completeness, other motion sensor such as barometers and magnetometers may be added to IMU, thus referred to as Magneto-Inertial Measurement Units (MIMUs). A recent review (Camomilla et al., 2018) showed that the number of papers reporting IMU-based sport-performance evaluation methods had grown gradually over the past decade. In the same paper, the authors also listed the different fixation methods observed in these papers, from tapes and straps to harnesses and suits. The fixation mean plays a crucial role in the assessment quality. If an IMU is not firmly attached to the body, its intrinsic motion interferes with the actual motion of the segment. This wobbling effect can be challenging to remove in the post-processing stage and alter the accuracy of the measurements particularly during or just after an impact.

For biomechanical analysis, different frames are interchangeably used to describe the position and orientation of a body segment. A global frame (GF) is a fixed (global) laboratory frame. This frame does not change its orientation or position over time. The directions of the global axes are consistent, no matter which activities or subjects are being studied, or which investigator is conducting the experiment¹. In comparison, a local frame typically refers to a frame attached to a body, possibly in motion. Hence, a local frame can change its orientation and position over

time with respect to the global frame. Three generic local frames are commonly employed with body-worn inertial sensors. The technical frame (TF) is a generic local frame rigidly associated with a bony segment. It generally refers to the intrinsic sensor frame, the frame in which the raw data are collected. Hence, this frame may be completely arbitrary as it depends on the orientation and position of the sensors on the body, making the comparison between two different configurations impossible. To avoid this issue, scientists prefer to use the anatomical frame (AF) to describe the motion of a segment. The definition of the AF should always be the same; its origin at the center of mass of the segment and the planes of the AF approximating the frontal, transverse and sagittal anatomical planes. So, to align the TF of the sensors with the AF of the segment, researchers have used a procedure called functional calibration. This process estimates the orientation of the anatomical frame based on movements restricted to a single plane (Favre et al., 2009; Lebleu et al., 2020). Thus, the functional frame is not exactly the anatomical frame and can, therefore, result in different 3D kinematics when compared with an anatomically set reference frame (e.g. in optical motion capture system).

Inertial sensors measure physical quantities related to the motion of a body and have shown to be promising instruments to estimate temporal, kinematic, and dynamic parameters in running. These parameters can be used in biomechanics research or in practice with coach-oriented needs. Although these two aspects are related, from of sport-science point of view, it is important to present the metrics obtained through inertial sensors in an intuitive and interpretable manner. For instance, directly commenting on the acceleration and angular velocity time-curves might be relevant in biomechanical studies, but less pertinent for coaches and athletes. Therefore, the following sections focus on the spatiotemporal parameters corresponding more to coach needs, as introduced in Chapter 1.

2.3.1 Temporal analysis of the running gait

The detection of initial and terminal contact events is paramount to the estimation of gait phases durations, such as contact time, flight time, swing duration, or step duration. Temporal events are the building blocks of the running gait and are necessary to provide a cycle-by-cycle analysis. Some studies have used IMUs on the upper body (Abt et al., 2011; García-López et al., 2005), other focused on the shank/tibia segments (Crowell et al., 2010; McGrath et al., 2012; Ogueta-Alday et al., 2013) and some used foot-worn IMUs (Mercer, Devita, et al., 2003; M. Norris et al., 2013). However, few studies have validated the results against a gold standard measurement.

Mo & Chow (Mo & Chow, 2018) compared three methods during overground jogging and running, and evaluated the detection error of initial contact, terminal contact, and stride duration with a ground-integrated force plate. Each method was based on different sensor placement and used sensors on the foot, shank, and pelvis (Figure 2.3). The authors concluded that initial

¹The definition of reference frames follows a different convention than that used in earth sciences, astronomy or engineering disciplines as navigation and guidance. The employed global frame (GF) may not be parallel to the geographical coordinate system.

contact can be detected most accurately by using the peak foot-resultant acceleration and terminal contact as the minimum before positive peak shank vertical acceleration. Using this method, they reported a relative mean \pm STD error of $4.1 \pm 1.8\%$ for contact time and $26.6 \pm 4.3\%$ when only foot-worn IMUs were employed. The method based on the pelvic acceleration showed an $8.7 \pm 3.7\%$ error and confirm the previous observation from other studies (J. B. Lee et al., 2010; Wixted et al., 2010).

Similar methods based on shank-worn IMUs have also been used in other studies (Michelle Norris et al., 2016; Purcell et al., 2005). For instance, Mercer et al. (J A Mercer et al., 2003) used shank-worn accelerometers to estimate the stance phase duration. They defined initial contact as the minimum acceleration before the peak impact and terminal contact as the minimum acceleration after a second local maximum. Even though the authors did not evaluate the detection error, one study (Schmidt et al., 2016) used the same method for sprinting and reported a systematic error for contact time estimation of -2.5 ± 4.8 ms and a 95% limits of agreement range from -11.8ms to 6.8ms.

Weyand et al. (Weyand et al., 2001), used the acceleration peak from a foot-worn accelerometer to detect initial and terminal contact and compared their estimation of contact time with a treadmill-mounted force plate. They reported a bias (mean \pm STD) of $14.6 \pm 0.5\%$ when computed over 165 trials. In comparison, Chew et al. (Chew et al., 2017) used the first local minimum to define initial contact and the latter for terminal contact and compared the results with a force plate. They reported a precision 14 ms and 19 ms for initial and terminal contact, respectively. Noticeably, Strohrmann et al. (Strohrmann et al., 2012) also used the peak acceleration norm to define initial contact but proposed a 2 g threshold to detect terminal contact.

Gyroscopes based methods have also been proposed and adapted from walking gait analysis (Mariani et al., 2013). McGrath et al. (McGrath et al., 2012) used the shank angular velocity in the sagittal plane to detect initial and terminal contact events and compared the results to a marker-based data acquisition system. The two events were derived using an adaptive threshold approach and observed a mean error of 24 ms and -28 ms for initial and terminal contact, respectively.

Ammann, Taube & Wyss (Ammann et al., 2016), compared contact time estimations between shoe-worn IMUs and a high-speed video camera for 132 steps of 12 athletes at running speeds within 22.3 ± 5.8 km/h. Because data processing was done by proprietary software, the algorithms were not described in the methods.

Zhao et al. (Zhao et al., 2016) proposed a relatively different approach in the detection of the period of stance. They used foot-worn inertial sensors and a frequency-tracking algorithm from the field of audio analysis to obtain information about gait cycle duration and subsequently determined the stance phase point for the next gait cycle. Even though the authors did not validate the detection results, their approach differs from the more traditional methods based on heuristic feature detection. Besides, with the advances in machine learning techniques,

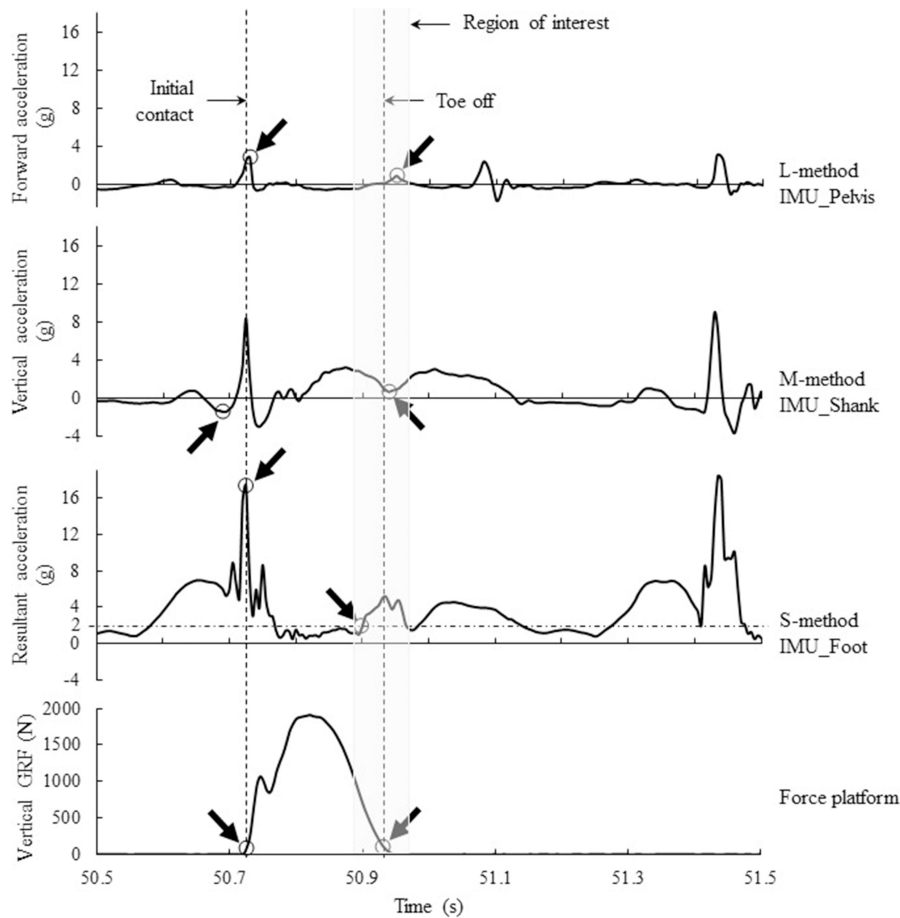


Figure 2.3 – Acceleration signals used in the detection of initial and terminal contact in the comparison study by Mo & Chow (Mo & Chow, 2018).

some researchers have investigated whether these techniques could improve temporal events detection in running. For instance, Robberechts et al. (Robberechts et al., 2019) evaluated gait event detection from 3D tibial acceleration signals using a heuristic-based method and two machine learning methods. Their results suggest that machine learning approaches better predict the timing of initial and terminal contact. However, machine learning methods are prone to overfitting and would require validation with large data sets to concluded on the actual performance of the system.

Furthermore, several commercialized devices are available on the market for running gait assessment, but only a few have been validated against gold-standard reference systems. A recent paper (García-Pinillos et al., 2019), however, evaluated the concurrent validity of two commercialized foot-pods systems (i.e., Stryd and RunScribe systems) during treadmill running. Detection times were compared with a 1000 fps high-speed camera. They observed that the Stryde system underestimated contact time (5.2%) and overestimated flight time (15.1%), whereas the RunScribe system underestimated contact time (2.3%) and overestimated flight time (3.2%).

Based on this review, the best detection performance seems to be obtained when initial contact is detected by a foot-worn IMU and terminal contact using a shank-worn IMU. However, no study compared the performance of a multitude of kinematic features in detecting initial and terminal contact. The majority of the existing literature focused on peak detection methods assuming that the landing impact would create large high-frequency oscillations in the acceleration signal. Even though the latter is relevant, there is usually more than a single peak, and these peaks can be separated by a few milliseconds; this enhances the chances to observe a relatively high random error in the detection performances. Moreover, the precision of these methods could be largely affected if the sensor is not firmly fixed on the body segment.

2.3.2 Foot strike patterns and rear-foot eversion

Two different approaches have been proposed for the assessment of the foot strike patterns: (1) estimation of the foot orientation in the sagittal plane at initial contact, and (2) model-based classification of the foot strike pattern. The first method typically involves the integration of the angular velocity measured on foot and is prone to orientation drift. Therefore, the first attempts were more oriented towards the latter type of approach, modeling.

Strohrmann et al. (Strohrmann et al., 2011) classified the foot strike type using the minimum and maximum peak of the unfiltered foot's pitch angular velocity in a 0.2 s window around initial contact. They compared their results with foot strike patterns derived from video observations but only reported the performance of the system with a figure (Figure 2.4, left).

Giandolini et al. (Giandolini et al., 2014) validated a method to identify the running pattern based on accelerometers located on the heel and metatarsals. They calculated the reference foot strike angle using retroreflective markers placed on the lateral side of the right shoe at the heel and the fifth metatarsal head. Their proposed method used delay between heel and metatarsal peak accelerations to estimate the foot strike angle and obtained an overall classification of 86.3% accuracy (Figure 2.4, right).

Recently, van Werkhoven et al. (van Werkhoven et al., 2019) showed that shoe-worn sensors were able to accurately (92.2% success) distinguish between rearfoot and non-rearfoot foot strikes using an angular velocity cut-off value of 0 deg/s. However, when estimating the foot strike angle by direct integration of the angular velocity, the authors only reported a correlation of 86%. The reference system was a traditional 2D video analysis.

The methods based on foot-worn inertial sensors that estimate the 3D orientation of the foot first emerged from the field of walking analysis. Although different methods have been proposed (Mariani et al., 2010; Sabatini et al., 2005) most share the same underlying structure: (1) integration of the angular velocity obtained from a foot-mounted gyroscope to calculate orientation in the fixed global frame and (2) combine the measurements from other sensors (e.g., accelerometer, magnetometer, GPS) to estimate and remove the orientation drift. Such method, for instance, was used in a validation study (Brégou Bourgeois et al., 2014) on walking

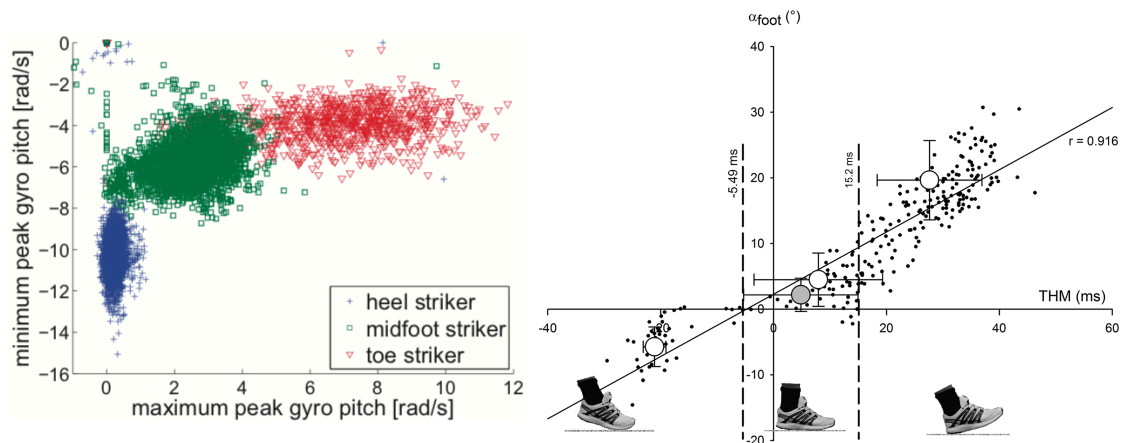


Figure 2.4 – (Left) Cluster method based on foot-worn inertial sensors proposed in (Strohrmann et al., 2011) to discriminate heel, midfoot, and toe strikers. (Right) The overall correlation between timing-based method (THM) and the reference system used in (Giandolini et al., 2014). Black dots represent the mean of each participant within each condition.

analysis and reported accuracy and precision of $0.5 \pm 2.9^{\circ}$ and $3.9 \pm 5.8^{\circ}$ in the estimation of the pitch angle at initial and terminal contact, respectively.

In order to compensate for the orientation drift during the integration of angular velocity, methods such as the zero-velocity-update (Skog et al., 2010; Zhang et al., 2017) usually require the presence of low accelerations or low magnetic disturbances during the period of stance. Although these periods are generally present during low-speed human locomotion, they are either rare or inexistent as the speed increases and thus are likely to underperform in running. Nevertheless, studies have proposed a hard reset of the drift based on the hypothetical presence of a foot-flat period during the stance phase of running. Bailey & Harle (Bailey & Harle, 2014) tested two methods (linear de-drifting and extended Kalman filter) to compute the orientation of the foot in 5 subjects based on shoe-mounted IMUs. They reported an error (mean + STD) in foot strike angle of $1.92 \pm 1.09^{\circ}$ at 8.28 km/h and $3.18 \pm 1.19^{\circ}$ at 12.24 km/h. Using a similar approach, Koska et al. (Koska et al., 2018) reported error biases ($^{\circ}$) \pm 95% limits of agreement ($^{\circ}$) of $-3.1 \pm (-7, 3.4)$ at 10 km/h, $-3.8 \pm (-7.6, 2.1)$ at 12 km/h and $-5.9 \pm (-11.1, 1.8)$ at 15 km/h.

Shiang et al. (Shiang et al., 2016) also assumed the presence of a foot-flat period during the period of stance and defined the difference between two local maximums as the strike index. Their results show a good correlation between the strike index and the pitch angle obtained with optical motion capture. Although this approach seems reasonable for rearfoot strikers, it is not appropriate for forefoot strikers as their rearfoot segment possibly never comes into contact with the ground. Also, typically-rearfoot strikers tend to switch from a rearfoot to a forefoot strike pattern when the running speed increases; speed might likewise be a confounding factor for any drift reduction method.

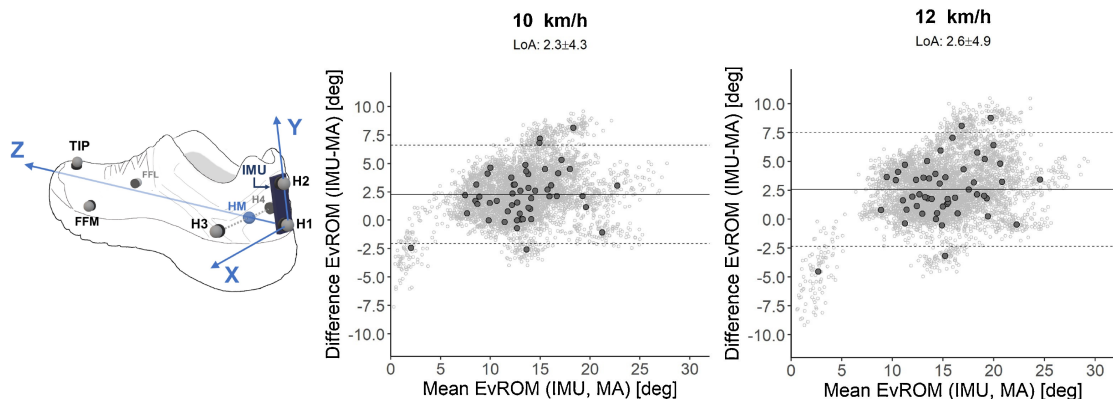


Figure 2.5 – (Left) Reflective markers (MA method) and IMU placement on the right shoe. (Right) Bland-Altman plot of the agreement between the eversion range (EvROM) and the optical motion capture system at 10 and 12 km/h. Source (Koska et al., 2018).

Assessing the rear-foot eversion in running is slightly more complicated than the foot strike angle since the range of the eversion movement is usually low. Moreover, the methods based on foot-worn inertial sensors usually require an initial value to start the drift correction, and this initial value should be subject-specific in order to be accurate. Assuming that the eversion angle is null at mid-stance is not a reliable correction, since each individual demonstrates a different degree of pronation while running. To avoid this correction problem, Koska et al. (Koska et al., 2018) compared two parameters related to the inversion/eversion rotation of the rearfoot: (1) the eversion range of motion (i.e., difference between maximum and minimum of the integrated gyroscope in frontal plane); (2) the maximum eversion velocity (i.e., maximum of the angular velocity in the frontal plane). They compared their estimation against an optical motion tracking system and showed the limitation of such an approach (Figure 2.5).

2.3.3 Stride length and speed

Stride or step length are two metrics closely related to the running speed. As discussed previously (section 2.3.1), temporal parameters can be measure quite accurately using body-worn inertial sensors. Thus, if the distance covered during one step (or stride) can be estimated, then the running speed can be calculated by dividing this value by the duration of the step (or stride). Hence, when discussing the matter of speed estimation, it is important to consider both step/stride length and their duration. Some studies proposed an accurate ambulatory method, based on body-worn IMUs, to estimate the overground speed of running but few did so for instantaneous speed estimation. There are two main categories of methods that are described below. The first category relies on the direct integration of the IMU acceleration and angular velocity data, and the second on machine learning models.

Regarding the first category, Yang et al. (Yang et al., 2011) developed an algorithm to estimate the running speed using a single shank-mounted IMU. Through integration, the orientation of the shank segment in the sagittal plane was determined, and an estimate of stride-by-

stride running speed was calculated by integrating the acceleration data. They validated their method with seven individuals running on an instrumented treadmill at speeds between 2.50 m/s and 3.50 m/s. For each subject, the speed estimation error of each trial was calculated as the difference between the average estimated speed over 30 stride cycles and the treadmill speed (i.e., bias). The authors reported the inter-trial mean \pm STD of the bias and showed errors of 0.11 ± 0.03 m/s for 2.5 m/s treadmill speed, and 0.09 ± 0.02 m/s at 3.5 m/s. Chew et al. (Chew et al., 2017) used the same method as in Yang et al. (Yang et al., 2011) but used shoe-worn inertial sensors and considered the shank and foot as a single rigid body that rotates about the ankle joint during the period of stance. The bias of this method was between 0.16 to 0.41 m/s depending on the running speed (2.2 m/s to 3 m/s) and the precision between 0.23 to 0.32 m/s. The authors also validated the stride length and obtained a bias between 0.14 to 0.45 m and precision between 0.46 to 0.62 m.

In the second category, several models have been discussed in the existing literature. Some of the models were generic, but the majority aimed to personalize their estimation either based on the input of other devices or on a subject-specific calibration procedure. The models are generally based on a set of features interrelated with the running speed. For instance, Provot et al. (Provot et al., 2019) investigated the effect of running speed on acceleration measured at three different positions: the foot, the tibia, and the L4-L5 lumbar. The authors concluded that the features associated with the signal energy (e.g., RMS value) were highly correlated ($r^2 > 0.9$) with the overground velocity. A recent study (Soltani et al., 2019) proposed a real-world speed estimation method based on wrist-worn inertial sensors. The authors obtained a median [IQR] (Inter-Quantile Range) bias of $-0.02 [-0.2 \ 0.18]$ m/s and precision of $0.31 [0.26 \ 0.39]$ m/s for a non-personalized method. These results improved to $0.00 [-0.01 \ 0.02]$ and $0.18 [0.14 \ 0.23]$ for the bias and precision, respectively, when they used a personalization method based on the sporadic speed of a GNSS device. Researchers in (De Ruiter et al., 2016) proposed a personalized speed estimation model based solely on the measurement of the contact time. They measured contact time using shoe-worn inertial sensors and personalized a model for each of the 14 participants. They personalized the model based on the average speed obtained over several bouts of 125 meters and compared their speed estimation with those obtained with a stopwatch over the same 120-meters bouts. This method reported a median RMSE of 2.9 and 2.1% (two runs). Similarly, but with different instrumentation, de Ruiter & van Dieën (de Ruiter & van Dieën, 2019) proposed a method based on feet sensors and timing-gates to estimate the step length during maximal sprint acceleration. They fitted a mono-exponential function to the time-gait measurements to estimate the instantaneous speed and divided this estimation by the duration of the steps detected with the IMUs. Their method showed a bias \pm limit of agreement of -0.00 ± 0.11 m. Another study (Hauswirth et al., 2009) compared in-lab a commercialized speed estimation device (i.e., Polar RS800sd foot pod) with the speed of a treadmill and reported an inter-trial mean \pm STD bias of -0.03 ± 0.14 m/s. The accuracy of the system is relatively low, considering that it required a subject-specific calibration before the measurement. Finally, in a study (Herren et al., 1999) conducted in outdoor conditions, the authors explored whether triaxial accelerometer can be combined with subject-specific

neural networks to assess the speed and incline of running accurately. The authors reported an RMSE of 0.12 m/s for the average speed within the trials.

Overall, a variety of methods have been proposed to estimate the step length and the running speed based on body-worn inertial sensors. However, most were evaluated for jogging and level running. As the performance of some of the studies mentioned above suggests, the actual running speed seems to affect the error, especially for the methods based on the direct integration of the acceleration. Hence, there is a need for more real-world validated speed estimation algorithms, where the validation is carried at multiple speeds and with a wide range of incline.

2.3.4 Impacts and ground reaction forces

Inertial sensors can not directly measure forces. However, according to Newton's second law, researchers have associated the impact forces with the maximum values (or peaks) observed on the accelerometer data. Based on this simple association, studies that investigated the effects of the repetitive loads during running were among the first to use body-worn accelerometers in the field of sports science. Some studies, for instance, acquired head acceleration data to examine the capacity of the body in absorbing the repetitive landing shocks (Abt et al., 2011; Crowell et al., 2010). Others have used accelerometers on the trunk to investigate shock attenuation in the human lumbar spine during running (Castillo & Lieberman, 2018). However, most of the studies used accelerometers on the lower limbs, and especially on the tibia.

A recent review (Sheerin et al., 2019) on the measurement of tibial acceleration in runners concluded that this metric is clearly affected by running technique, running velocity, lower extremity stiffness, as well as surface and footwear compliance. The review also highlighted the interrelationships between fatigue, effective mass, and tibial acceleration which still require further investigation, and their impact on risk of injury. Moreover, the authors also proposed some guidelines to avoid common handling and processing mistakes. They advised for a capture sampling frequency between 300–600 Hz and recommended a “heel drop” test to allow confirmation of the integrity of attachment before testing begins.

Even though tibial acceleration is a proxy measurement for the impact forces, it does not correspond to a direct estimate of the ground reaction forces (GRF). As discussed in section 1.5.2, the kinematic parameters of running have been widely examined from the standpoint of the effective load applied to the musculoskeletal structure of the human anatomy. Logically, with the advents in wearable sensors, scientists have investigated whether body-worn inertial sensors could be used to estimate the GRF through biomechanical models and machine learning methods. According to a recent literature survey (Ancillao et al., 2018), most of the validated methods focused on the vertical component of GRF and attained acceptable results, while a few focussed on the lateral components and found poor reliability in the estimation of such quantities.

Neugebauer et al. (Neugebauer et al., 2012) proposed a model based on a hip-worn accelerometer to estimate the peak of the vertical component of GRF during walking and running. Their model relied on a statistical model based on repeated measures and achieved an average absolute difference between the predicted and the reference force plate GRF of 9% while the maximum observed error was 17.5%. Wundersitz et al. used an accelerometer on the upper back to estimate the peak GRF and compared the output of their model with a force plate. The authors reported a step-by-step absolute error of 24%. The model was based on the hypothesis that the measured acceleration is proportional to force. Using a similar approach, Charry et al. (Charry et al., 2013) preferred using an accelerometer affixed on the tibia. The main advantage of this sensor placement is its capacity to detect the gait events accurately and that a logarithmic fitting can approximate the correlation between acceleration and peak GRF. This method reached an average error of 150 N when compared with a treadmill at different running speeds.

More recent attempts were more directed towards machine learning approaches. Raper et al. (Raper et al., 2018) designed a protocol to measure the continuous GRF during the stance phase employing a single IMU mounted on the tibia. The results showed that the IMU could underestimate the force up to 400 N. The authors attributed this error to a delay between the peak in acceleration and the peak measured by the force plate. Recently also, Wouda et al. (Wouda et al., 2018) estimated the vertical GRF during running using a combination of three inertial sensors placed on the lower legs and pelvis. Two neural networks were used subsequently in this method; first, to derive the lower joints kinematics and second, to estimate the vertical GRF. The model achieved low estimations error when trained on subject-specific data. Nevertheless, the authors concluded that the proposed method has the potential to be applied for individual subjects, and with additional research can be extended for running in various environments.

Despite the latest and promising results, the current state-of-the-art is not reliable and robust enough to monitor GRF in real-world settings. Other studies (Clark et al., 2014, 2017), however, have suggested that GRF might be estimated from temporal and kinematic features, such as flight time, vertical acceleration of the lower limb during landing, and ground contact time. However, these models require highly accurate spatiotemporal input and have never been tested with inertial sensors.

2.3.5 Overall conclusions

This chapter reviewed the reference measurement systems used in the assessment of the running gait and discussed their advantages and limitations. Despite their high accuracy, reliability, and repeatability, this chapter showed that force plates and optical motion capture system have several disadvantages. They are:

1. They are inherently bulky and require dedicated space to function optimally.

2. They are sensitive to changes in the environment (e.g., ambient light, vibrations).
3. They are expensive.
4. They require highly skilled operators.
5. Their limited volume of capture often restrains their use to in-lab treadmill running.

Due to the latter constraints, investigating the use of body-worn inertial sensors in real-world conditions is a continuing concern within the field of running biomechanics. These wearable sensors retrieve physical measures of motion that can be processed to estimate the temporal, kinematic, and dynamic parameters of running. However, accelerometers and gyroscopes are subject to measurement errors, and their utilization as a research-grade instrument is prone to misinterpretations. The fixation of the device, its configuration, the transformations between of the different reference frames, the subtraction of the gravitational acceleration (in a fixed frame), and the integration drift are some of the most prominent challenges encountered with inertial sensors. It is, therefore, necessary to consider their potential limitations before handling these devices and to evaluate their reliability against gold-standard systems. Sadly, few studies have carefully reported on the error of their algorithms.

Therefore, this chapter reviewed the methods which have been validated against gold standard systems and primarily focused on spatiotemporal and coach oriented running metrics. First, temporal event detection appears to perform best when the IMU is located on the shank or foot, with most of the existing methods considering the acceleration peak to detect the gait events. Yet, no study compared the performance of a variety of kinematic features to estimate the gait phases nor have assessed which features are affected by the running conditions (i.e., speed, slope, terrain). Second, lower-limb orientation drift correction methods are usually based on zero-velocity-updates during the stance phase. Although static periods are generally present during low-speed human locomotion, they are either rare or inexistent when the speed increases and thus are not suited for running. Moreover, the drift correction method directly affects the estimation of speed and position; an error in the calculation of the global frame orientation will resume an inaccurate correction of the gravitational acceleration and in the erroneous estimation of speed and position. Overall, a variety of methods have been proposed to estimate the step length and running speed. However, few of these methods were validated in real-world conditions, at multiple velocities, and with a wide range of incline. Also, the state-of-the-art in ground reaction force estimation with body-worn inertial sensors suggests that the current systems are not yet reliable in the real-world conditions and that models based on spatiotemporal features should be preferred. Meanwhile, tibial accelerations have shown to be a valid proxy and have been examined in many outdoor studies. This lack of methods explicitly designed for running and the divergence of the results in the literature have raised concerns about the actual capacity of inertial sensors to provide research-grade evaluations of real-world running. It is, therefore, essential to provide validated algorithms and to state the limitations of the results based on the validation protocol. Ideally, lab-validated algorithms should also be tested in applied settings, to evaluate their applicability in real-world conditions.

Algorithms Development and Validation

Part II

3 Accurate Estimation of Running Temporal Parameters

Abstract

This study aimed to assess the performance of different kinematic features measured by foot-worn inertial sensors for detecting running-gait temporal events (e.g., initial contact, terminal contact) in order to estimate inner-stride phases duration (e.g., contact time, flight time, swing time, step time). Forty-one healthy adults ran multiple trials on an instrumented treadmill while wearing one inertial measurement unit on the dorsum of each foot. Different algorithms for the detection of initial contact and terminal contact were proposed, evaluated, and compared with a reference-threshold on the vertical ground reaction force. The minimums of the pitch angular velocity within the first and second half of a mid-swing to mid-swing cycle were identified as the most precise features for initial and terminal contact detection with an inter-trial median \pm IQR precision of 2 ± 1 ms and 4 ± 2 ms respectively. Using these initial and terminal contact features, this study showed that the ground contact time, flight time, step, and swing time can be estimated with an inter-trial median \pm IQR bias less than 12 ± 10 ms and a precision less than 4 ± 3 ms. Finally, this study showed that the running speed can significantly affect the biases of the estimations, suggesting that a speed-dependent correction should be applied to improve the system's accuracy.

Keywords: running, inertial measurement unit (IMU), validation study, temporal parameters, contact time

Chapter adapted from Falbriard, M., Meyer, E., Mariani, B., Millet, G. P., & Aminian, K. (2018). Accurate estimation of running temporal parameters using foot-worn inertial sensors. *Frontiers in physiology*, 9, 610

Contributions: conceptualized the study design; conducted the data collection; designed the algorithms; contributed to the analysis and interpretation of the data; drafted the manuscript.

3.1 Introduction

In running, two temporal events (initial contact or touchdown and terminal contact or toe-off) need to be detected in order to extract the main temporal parameters of each step: cadence, contact time, flight phase duration, and swing phase duration. Initial contact (IC) is defined as the time instant when the foot initiates contact with the ground at landing. Terminal contact (TC) corresponds to the end of the pushing phase when the foot ends contact with the ground. The intrinsic relationships between the different inner-stride temporal parameters and running speed, shoe configuration, running economy, running performance, injury risks have been widely investigated. Therefore, accurate detection of IC and TC are paramount.

In the literature, the majority of studies that investigated temporal parameters in running have used force plates, contact mats or high-speed cameras as reference measurement systems (García-López et al., 2005; Handsaker et al., 2016; Leitch et al., 2011; Ogueta-Alday et al., 2013; Viitasalo et al., 1997). Although force plates are accepted as state-of-the-art systems for temporal events detection in running, they suffer from several limitations. The detection timing of the IC and TC on the vertical ground reaction force depends on the filtering method, and the detection threshold used (Cronin & Rumpf, 2014). Moreover, their lack of portability and their setup complexity restrict their use for in-laboratory experiments, which is a major drawback given the in-field nature of the running activity.

Thanks to the recent improvements in MEMS inertial sensors, their low production cost, their decrease in weight and size, and their ability to measure kinematics over large periods, inertial sensors are now widely accepted systems to analyze human locomotion. In fact, studies on gait analysis have shown that inertial measurement units (IMUs), when used with state-of-the-art algorithms, can reliably fill the gap between subjective observational analysis and bulky in-laboratory installations (Mariani et al., 2012, 2013). In running, inertial sensors have predominantly been used to detect inner-stride temporal events and derive temporal parameter estimations from them. Some studies have used IMUs on the upper body (Bergamini et al., 2012; M. Norris et al., 2013), other focused on the shank/tibia segments (Crowell et al., 2010; McGrath et al., 2012; John A. Mercer et al., 2003) and some used foot-worn IMUs (Brahms, 2017; Chapman et al., 2012; Y. S. Lee et al., 2015; Reenalda et al., 2016; Strohrmann et al., 2011). However, to the authors' knowledge, only a few studies have reported on the validity of their algorithms when compared with a state-of-the-art reference system. In Ammann et al. (2016), CT estimations were compared between shoelaces worn IMUs and a high-speed video camera for 132 steps of 12 athletes at running speeds within 22.3 ± 5.8 km/h. Because data processing was done by proprietary software, the algorithms used to estimate CT were not described in the methods. In Weyand et al. (2001), the authors used the acceleration peak from a foot-worn accelerometer to detect IC and TC and compared their estimation of CT with a treadmill-mounted force plate. The exact method used to detect IC and TC is not documented in this study, and only the bias (mean \pm STD) of the 165 trials is provided in the results. There is, therefore, no information about the precision of the proposed system. For all other methods, where no validation was reported, there is no evidence that the parameters

measured are within an acceptable error range and that this error range does not change with the running conditions.

Therefore, the present study aimed to investigate different algorithms to detect IC and TC from different features measured by foot-worn IMU kinematic signals and estimate the main inner-stride temporal parameters. The performance metrics (bias and precision) of each algorithm were assessed in comparison with a reference system (instrumented force plate treadmill), that allowed a validation of inner-stride temporal parameters over a high number of steps and a large range of running speeds.

3.2 Methods

3.2.1 Measurement protocol

In total, 41 healthy adults (13 females and 28 males, age 29 ± 6 years, weight 70 ± 10 kg, height 174 ± 8 cm, running weekly 2.1 ± 1 hour, 11 being affiliated to a running club) running at least once a week and without any symptomatic musculoskeletal injuries volunteered to participate to this study. The study was approved by the local ethics committee (CCER-VD 2015-00006), was conducted according to the declaration of Helsinki, and written informed consent was obtained from all the participants prior to the measurements. Each participant was asked to run multiple trials of 30 seconds each, wearing their usual shoes on an instrumented treadmill, starting at 8 km/h and increasing by 2 km/h up to their maximum speed. A 6 minutes familiarization period (Lavcanska et al., 2005) was carried out on the treadmill and served as a warm-up for the participants. The participants were free to decide on the rest duration in-between the trials.

3.2.2 Wearable device and temporal features estimation

IMU-based system - One inertial measurement unit (IMU) (Physilog 4¹, Gait Up, Switzerland, weight: 19 g, size: 50 x 37 x 9.2 mm) was worn on the dorsum of each foot and measured both 3D acceleration and 3D angular velocity at 500 Hz. Each IMU was affixed to the foot using an adhesive strap around the shoe. The range of the accelerometer was set to ± 16 g and ± 2000 °/s for the gyroscope.

Functional calibration - In order to use single axes of the inertial sensors in a meaningful and reproducible manner, we designed a functional calibration method to automatically align the technical frame of the foot-worn IMUs with the functional frame of the foot. The functional frame of the foot was defined as in Figure 3.1: the origin is at the base of the second metatarsal bone, Y_F is orthogonal to the horizontal plane defined by the ground surface, X_F lies on the horizontal plane projection of the line joining the center of the calcaneus bone and the head of the second metatarsal bone, pointing distally, and Z_F is orthogonal to the $X_F Y_F$ plane

¹Datasheet available in the Appendix.

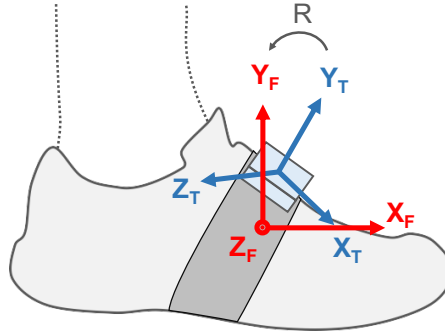


Figure 3.1 – Technical frame of the foot-worn IMU (X_T , Y_T , Z_T) and the functional frame of the foot (X_F , Y_F , Z_F). The 3 by 3 rotation matrix R aligns the IMU's technical frame with the functional frame of the foot.

pointing to the right-hand side of the subject. The functional calibration process requires static standing periods in order to align Y_T with Y_F using the gravitational acceleration measured by the IMU. Then, using the hypothesis that most of the foot's angular rotations occur along the Z_F axis while running, we used Principal Component Analysis to find the rotation angle around the Z_T axis which aligns Z_T with Z_F . Finally, X_T is the result of the cross-product $\langle Z_T, X_T \rangle$.

Gait cycle detection- Using the cyclic nature of the running movement, an algorithm was designed to segment a complete trial into mid-swing to mid-swing cycles. Following previous work on gait analysis (Aminian et al., 2002; Sabatini et al., 2005), we hypothesized that the pitch angular velocity (Ω_p) of the foot is maximum at mid-swing. To enhance and detect the mid-swing peak, a 2nd-order Butterworth low-pass filter was designed with an adaptive cut-off frequency. The cut-off frequency was set at 60% of the stride frequency estimated using an auto-correlation method over a 5 seconds sliding window. This adaptive filtering method was used to cope with the range of running speeds used in this study. The length of the sliding window (5 seconds) was selected empirically and based on our observations of the signals.

Temporal features detection - The estimation of inner-stride phases relies on two main temporal events: initial and terminal contact. The initial contact (IC) event corresponds to the time instant when the foot initiates contact with the ground at landing. The terminal contact (TC) event, also known as toe-off, corresponds to the end of the pushing phase when the toes terminate contact with the ground. For each cycle, we identified kinematic features that seemed to be valid candidates to detect IC and TC. Such features varied from global maximum (MAX), local maximum (MAX_{loc}), global minimum (MIN), local minimum (MIN_{loc}) and zero-crossing ($ZeroX$) time samples and were detected on the following signals: the pitch angular velocity (Ω_p : angular velocity around Z_F), the pitch angular acceleration (Ω'_p), the pitch angular jerk or first derivative of the pitch angular acceleration (Ω''_p), the roll angular velocity (Ω_r : angular velocity around X_F), the norm of the angular velocity ($\|\Omega\|$), the vertical axis acceleration (A_{vert} : acceleration along Y_F), the longitudinal axis of the acceleration

(A_{long} : acceleration along X_F), the coronal axis acceleration (A_{coro} : acceleration along Z_F), the norm of the acceleration ($\|A\|$) and the first derivative of the acceleration norm or jerk ($\|A\|'$). In some cases, an empirically chosen threshold was also used to improve the feature detection (e.g. $< -100^\circ/s$). All these detection rules are detailed in Table 3.1 and illustrated in Figure 3.2. Prior to the detection, the acceleration and angular velocity signals were filtered using a 2nd-order low-pass Butterworth filter ($F_c = 30$ Hz) to minimize the influence of the IMU fixation artifacts, and a temporary estimation of mid-stance was carried out for each gait cycle in order to separate the detection zones for IC and TC. The detection zone for IC was set as the period between the first zero-crossing of the pitch angular velocity (Ω_p) and mid-stance. For TC, the detection zone was set as the period between mid-stance and the last zero-crossing of the pitch angular velocity. Mid-stance was set as the time instant when the angular velocity norm ($\|\Omega\|$) is minimum within the 30% to 45% time-range of each mid-swing to mid-swing cycle. Finally, the IC and TC events of left and right foot were combined in order to estimate for each step i the ground contact time (CT), the flight time (FLT), the swing time (SWT) and the step time (SPT) using the following relations:

$$CT_i = TC_i - IC_i \quad (3.1)$$

$$FLT_i = IC_{i+1} - TC_i \quad (3.2)$$

$$SWT_i = IC_{i+2} - TC_i \quad (3.3)$$

$$SPT_i = IC_{i+1} - IC_i \quad (3.4)$$

3.2.3 Reference system and temporal features

Force plate - This study used an instrumented treadmill (T-170-FMT, Arsalis, Belgium) sampling at 1000 Hz as a reference system for the validation. The force plate system and the inertial sensors were electronically synchronized using a 5V pulse triggered manually and recorded on each system while IMUs were synchronized with each others using radio frequencies. To reduce the noise inherent to the treadmill's vibrations, we first applied, on the vertical ground reaction force (GRF) signal, a 2nd-order stop-band Butterworth filter with edge frequencies set to 25 and 65 Hz. The filter configuration was chosen empirically to obtain a satisfactory reduction of the oscillations observed during flight phases (i.e., subject not in contact with the treadmill) while minimizing its widening effect during ground contact time.

Temporal features detection - IC and TC events were detected using a threshold on the filtered vertical GRF signal, setting the first threshold-crossing occurrence as IC and the second as TC for each step. As previous studies (Cronin & Rumpf, 2014; Weyand et al., 2001) used different reference thresholds, we have decided to investigate the effect of eight reference thresholds on

Detection zone	Feature		Description
	Signal	Rule	Label
Initial contact (IC)	Ω_p	MIN	k1
		<i>ZeroX</i>	k2
		$MIN_{loc} < -100^\circ/s$	k3
	Ω'_p	<i>MAX</i>	k4
		<i>MIN</i> before k4	k5
	Ω''_p	<i>ZeroX</i>	k6
	$\ \Omega\ $	<i>MAX</i>	k7
	A_{vert}	<i>MAX</i>	k8
	$\ A\ $	<i>MAX</i>	k9
		<i>MIN</i> before k9	k10
		MIN_{loc}	k11
	$\ A\ '$	<i>ZeroX</i>	k12
		<i>MIN</i>	t1
	Ω_p	<i>ZeroX</i> after t1	t2
Terminal contact (TC)	Ω'_p	<i>ZeroX</i> after t1	t3
	Ω_r	<i>MAX</i>	t4
	$\ \Omega\ $	MAX_{loc} after t1	t5
	A_{vert}	<i>MIN</i>	t6
	A_{long}	MAX_{loc} after t1	t7
	A_{coro}	<i>MAX</i>	t8
	$\ A\ $	MAX_{loc} after t1	t9

Table 3.1 – Summary of the features used on the inertial sensors signals to detect initial contact and terminal contact. IC candidates are identified by kj with $j \in \{1 \dots 12\}$ and TC candidates are identified by tj with $j \in \{1 \dots 9\}$. The features presented in this table were used in the respective detection zone of IC and TC.

the validation results. Four thresholds were set to 20 N, 30 N, 40 N and 50 N, independently of the subjects' body weight (BW) and four others were set to 3 %BW, 5 %BW, 7 %BW, and 9 %BW. Finally, we combined IC and TC events to find the reference inner-stride phases durations (CT, FLT, SWT, and SPT) as in Eq. 3.1 - 3.4.

3.2.4 Statistical analysis and error estimation

In order to avoid developing algorithms that over-fits our data set and would, therefore, bias the results, the first 10 subjects were randomly selected and dedicated to the development set while the remaining subjects were only used as the validation set. The design of the algorithms described in section 3.2.2 was conducted using the data from the development set solely. No algorithms debugging was done over signals from the validation set.

To evaluate the error of the proposed system against the reference force plate, we computed for each temporal feature, the bias (intra-trial mean) and precision (intra-trial STD) for all steps within a trial. We then combined the results from each trial and computed the median and IQR of both the bias and precision over all trials. These two steps resulted in four inter-trial statistics per temporal feature for both sets (development and validation sets): b_μ is the inter-trials median bias, b_σ is the inter-trials IQR of the bias, σ_μ is the inter-trials median precision and σ_σ is the inter-trials IQR of the precision. Note that we have used the median and IQR functions for the inter-trial statistics as the intra-trial bias and precision were not normally distributed.

A similar method was used for the inner-stride phases. However, to avoid having a large number of candidates for each parameter (12 IC candidates * 9 TC candidates = 108 possible pairs of candidates for each phase estimation), we have decided to keep only the three most precise candidates for IC, the three most precise candidates for TC and to combine them into 9 pairs of estimates for CT, FLT, SWT, and SPT. Then, similarly, the inter-trials bias (b_μ , b_σ) and the inter-trial precision (σ_μ , σ_σ) were evaluated. Precision (i.e. intra-trial STD) was chosen as selection criteria for IC and TC candidates as it informs about the range of random errors made by the system among the steps of a trial. The bias, however, can potentially be decreased using an appropriate model of the errors.

To investigate if the speed affects the intra-trial bias of the IC and TC candidates, we used the Kruskal-Wallis test with a significance level of 0.05. We preferred this non-parametric test to the one-way ANOVA because the Lilliefors test rejected, in most cases, the hypothesis that the intra-trial biases were normally distributed among the running speeds. Consequently, in this study, the null hypothesis was accepted only if the rank of the biases were equal among the running speeds. The same hypothesis has also been tested on the precision. Note that this test was applied to the complete data set (development and validation set) as there were no speed-depend adaptations of our detection algorithms.

Finally, we used Bland-Altman plots and the best linear fit, in the least-squares sense, to show

the trend in the CT estimation errors on the development set. Finding the best linear fit on the development set allowed us to further use the linear coefficients to correct the inter-steps errors in the validation set. The inter-steps errors refer to the error of all steps within a group, independently of the trial they belong to. The inter-steps bias is defined as the mean error of all steps and the inter-steps precision as the STD of the error of all steps.

3.3 Results

3.3.1 Temporal events detection

Out of the 41 participants, 35 were kept for the evaluation of the proposed system. Within the 6 participants removed, 2 were removed because the data loss rate was above 20%, and 4 were removed because of calibration errors of the systems. The results for the development set and the validation set were computed from 10 subjects with 59 trials (4836 steps) and 25 subjects with 146 trials (12092 steps), respectively. Trials with running speed at 8 km/h were removed due to the presence of steps with double support for some subjects that makes the detection of IC and TO impossible with the GRF of the reference system.

The minimum number of steps per trial was 67, and the maximum number of steps per trial was 105, given that the running speed recorded ranged from 10 km/h to 20 km/h. Figure 3.2 illustrates the features used to detect IC and TC with the vertical grey dashed lines showing the limits of the detection zones for IC and TC candidates. The signals showed in Figure 3.2 belong to the same step and are represented during one mid-swing to mid-swing cycle.

Table 3.2 summarizes the IC and TC events detection error for development and validation sets, and for each kinematics feature candidate (kj and tj) extracted by applying the specific detection rule on the kinematics signal. The results are obtained by using the reference value estimated with a threshold at 7 %BW on the vertical GRF. The differences shown in the table were computed such that a positive difference indicates that the event was detected later in the signal than the reference. The three most precise IC candidates (median \pm IQR) with respect to the results from the validation set are k1 (2 ± 1 ms), k3 (2 ± 1 ms) and k8 (3 ± 2 ms). The three most precise TC candidates (median \pm IQR) with respect to the results from the validation set are t1 (4 ± 2 ms), t4 (4 ± 2 ms) and t5 (4 ± 2 ms). One TC candidate shows a noticeably lower inter-trial bias IQR: t5 with $b_{\sigma} = 7$ ms.

Figure 3.3 shows the influence of the running speed on the IC and TC inter-trials bias for the features (k1, k3, k8) and (t1, t4, t5). The graph was generated using the complete data set (development and validation set) as it is solely used for visualization purposes. When the trials are grouped according to the running speed, the Kruskal–Wallis test applied on the biases shows that the running speed significantly affects the biases in k8 ($p = .001$), t1 ($p < .001$), t4 ($p < .001$), t5 ($p < .001$) and precision in t1 ($p < .001$), t4 ($p = .014$) and t5 ($p < .001$).

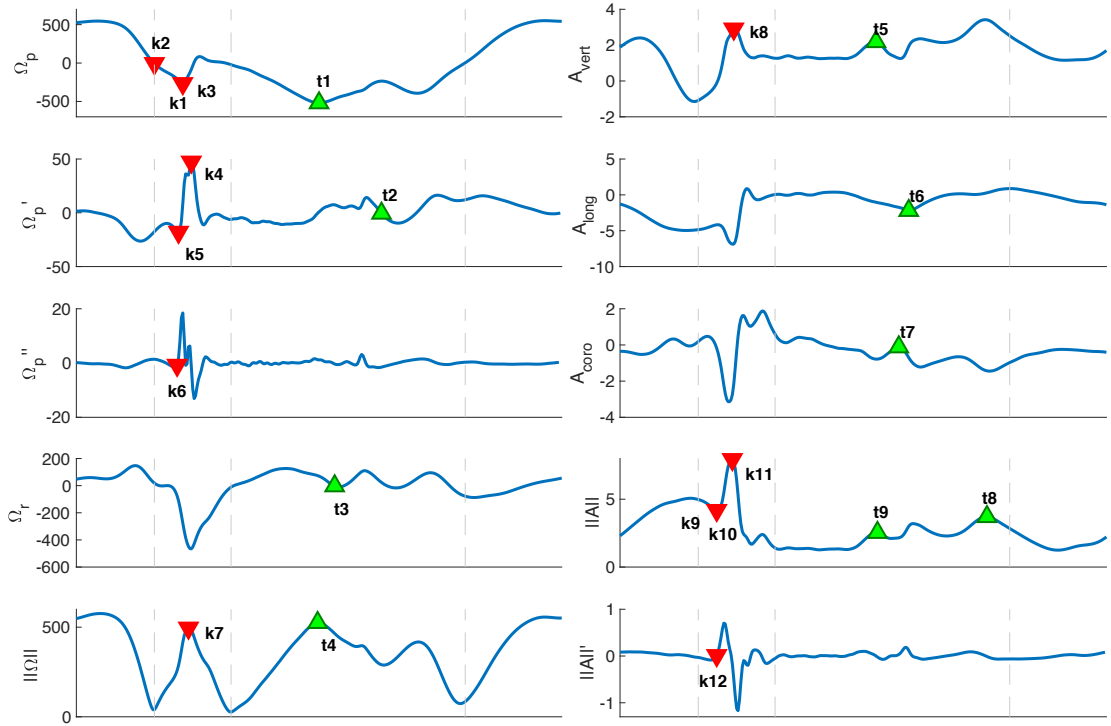


Figure 3.2 – Features used on the kinematic signals recorded by the foot-worn inertial sensors. IC candidates are identified by k_j with $j \in \{1 \dots 12\}$ and TC candidates are identified by t_j with $j \in \{1 \dots 9\}$. The vertical grey dashed lines show the limits of the detection zones for IC and TC candidates. The signals showed in this figure belong to the same step and are represented during one mid-swing to mid-swing cycle.

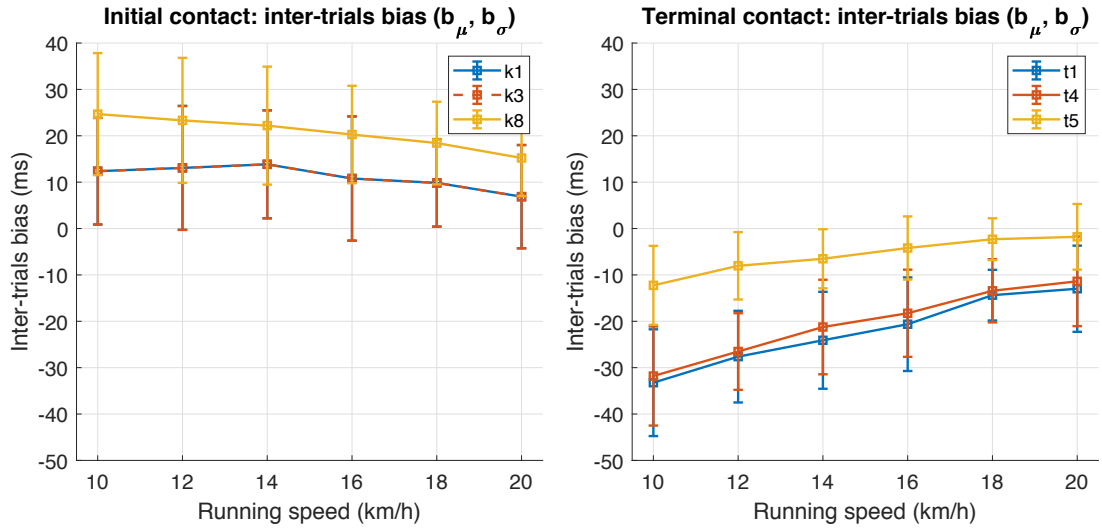


Figure 3.3 – Initial contact (left graph) and terminal contact (right graph) inter-trials bias for the features (k_1 , k_3 , k_8) and (t_1 , t_4 , t_5), respectively. The graph was computed using the complete data set (development set and validation set) and using the reference threshold on the vertical GRF at 7 %BW. Each group of speed contains $N=35$ trials except the 20km/h group, where $N=30$.

Feature			Development set (N=59) errors (ms)				Validation set (N = 146) errors (ms)				
Signal	Rule	Label	b_μ	b_σ	σ_μ	σ_σ	b_μ	b_σ	σ_μ	σ_σ	
Initial contact (IC)	Ω_p	MIN	k1	11	14	2	1	11	10	2	1
		ZeroX	k2	-30	11	6	3	-29	11	6	2
		MINloc <-100 °/s	k3	11	14	2	1	11	10	2	1
	Ω'_p	MAX	k4	22	20	3	2	23	15	4	2
		MIN before k4	k5	-5	7	3	4	-4	7	4	4
	Ω''_p	ZeroX	k6	-3	11	2	3	-2	8	3	3
	$\ \Omega\ $	MAX	k7	14	4	3	2	14	5	4	2
	A_{vert}	MAX	k8	19	13	3	2	20	13	3	2
	$\ A\ $	MAX	k9	19	18	3	3	17	17	3	3
		MIN before k9	k10	1	19	3	5	0	13	5	6
		MINloc	k11	6	19	7	5	4	13	7	5
		ZeroX	k12	2	17	2	4	2	13	3	4
Terminal contact (TC)	Ω_p	MIN	t1	-24	14	3	2	-21	13	4	2
	Ω'_p	ZeroX after t1	t2	31	18	10	13	29	17	9	10
	Ω_r	ZeroX after t1	t3	33	24	13	39	39	33	14	25
	$\ \Omega\ $	MAX	t4	-22	14	3	2	-18	13	4	2
	A_{vert}	MAXloc after t1	t5	-7	8	4	3	-4	7	4	2
	A_{long}	MIN	t6	20	18	5	9	18	15	6	7
	A_{coro}	MAXloc after t1	t7	-2	14	21	9	1	11	22	9
	$\ A\ $	MAX	t8	33	38	24	28	37	57	22	40
		MAXloc after t1	t9	-3	11	4	2	0	13	5	6

Table 3.2 – List of time differences for all the initial and terminal contact candidates computed over 4836 and 12092 steps for the development set and the validation set, respectively. The reference system used in this table is the vertical GRF with a threshold set at 7% BW. IC candidates are identified by k_j with $j \in \{1 \dots 12\}$ and TC candidates are identified by t_j with $j \in \{1 \dots 9\}$. “b” and “ σ ” are the abbreviations for accuracy (intra-trial mean error) and precision (intra-trial STD of the error), respectively, while suffix “ μ ” and “ σ ” represent the median and the IQR over all the trials.

3.3.2 Inner-stride phases estimation

Table 3.3 lists absolute and relative errors obtained for the estimations of CT, on the validation set, when compared with the force plate estimation found using the reference threshold at 7 %BW. The bias and precision obtained when comparing the other force plate thresholds with the 7 %BW reference threshold are also listed at the end of Table 3.3.

The most precise pair of IC and TC candidates for CT was (k1, t1) with an inter-trial median \pm IQR precision of 4 ± 2 ms or 1.8 ± 0.9 %. CT estimators (k1, t5) and (k3, t5) both have the lowest absolute inter-trial IQR of the biases ($b_\sigma = 12$ ms) while (k1, t5) has the lowest IQR in relative values ($b_\sigma = 5.0$ %). The reference values observed in this study ranged from 132 to 354 ms for CT, from 29 to 238 ms for FLT, from 367 to 613 ms for SWT and from 254 to 435 ms for SPT. Table 3.4 shows the relative and absolute errors for FLT, SWT, and SPT estimations for both (k1, t1), (k1, t5), and (k3, t5) pairs.

Finally, Figure 3.4 shows the Bland-Altman plot for the CT estimation of the (k1, t1) and (k1, t5) estimators. The orange dashed line represents the best linear fit according to the least-squares method. These graphs were computed using all the steps in the development set ($N = 4836$), independently of the trials.

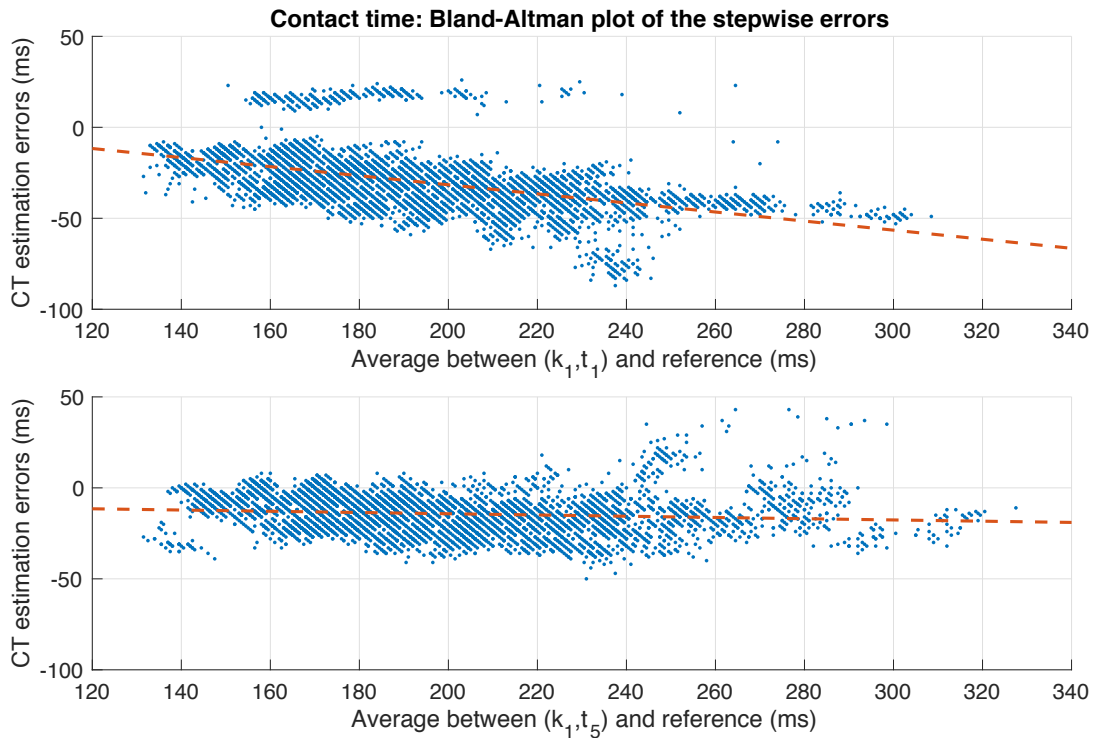


Figure 3.4 – Bland-Altman plot of the ground contact time (CT) estimation errors for the (k1, t1) (top graph) and (k1, t5) (bottom graph) candidates. The error is measured on all the steps of the development set ($N = 4836$). The orange dashed line represents the best linear fit according to the least square method.

Chapter 3. Accurate Estimation of Running Temporal Parameters

Features		Absolute CT errors (ms)				Relative CT errors (%)			
IC	TC	b_{μ}	b_{σ}	σ_{μ}	σ_{σ}	b_{μ}	b_{σ}	σ_{μ}	σ_{σ}
k1	t1	-30	17	4	2	-13.8	5.5	1.8	0.9
k1	t4	-27	17	4	2	-12.9	5.5	1.9	1.2
k1	t5	-15	12	5	3	-7.1	5.0	2.1	1.0
k3	t1	-30	18	4	2	-13.8	5.6	1.8	1.0
k3	t4	-27	17	4	3	-12.9	5.5	1.9	1.4
k3	t5	-15	12	5	3	-7.1	5.2	2.2	1.1
k8	t1	-38	21	5	3	-18.1	6.0	2.1	1.0
k8	t4	-35	21	5	3	-17.4	6.1	2.2	1.3
k8	t5	-23	15	5	3	-10.8	5.5	2.2	1.3
20 N			8	6	3	1	4.0	2.2	1.3
30 N			5	4	2	1	2.2	1.6	1.0
40 N			2	3	1	1	0.9	1.2	0.6
50 N			0	2	1	1	-0.1	1.1	0.4
3 %BW			9	5	3	2	3.9	1.7	1.3
5 %BW			4	2	2	1	1.7	0.6	0.8
9 %BW			-3	2	2	1	-1.4	0.5	0.7

Table 3.3 – List of the duration differences for contact time (CT) estimation (N = 146 trials, 12092 steps) when compared with reference at 7 %BW in the validation set. The first nine rows show the estimation errors of the three most precise candidates for IC and TO detection arranged as pairs while the last seven rows show the difference observed when using other reference thresholds on the vertical GRF signal. “b” and “ σ ” are the abbreviations for bias (intra-trial mean error) and precision (intra-trial STD of the error), respectively, while subscript characters μ and σ represent the median and the IQR over all the trials in the validation set.

Parameter	Estimator	Absolute errors (ms)				Relative errors (%)			
		b_{μ}	b_{σ}	σ_{μ}	σ_{σ}	b_{μ}	b_{σ}	σ_{μ}	σ_{σ}
FLT	(k1, t1)	30	17	4	3	22.8	17.2	4	2.8
	(k1, t5)	15	12	5	3	10.7	10.7	3.7	2.7
	(k3, t5)	15	12	5	3	10.7	10.7	3.9	2.6
SWT	(k1, t1)	30	17	4	2	6.3	3.7	0.9	0.4
	(k1, t5)	15	12	5	3	3.2	2.6	1	0.6
	(k3, t5)	15	12	5	3	3.2	2.6	1	0.6
SPT	(k1, t1)	0	0	3	2	0	0	0.8	0.5
	(k1, t5)	0	0	3	2	0	0	0.8	0.5
	(k3, t5)	0	0	3	2	0	0	0.8	0.5

Table 3.4 – Flight phase duration (FLT), swing phase duration (SWT) and step time duration (SPT) estimations errors for the (k1, t1), (k1, t5) and (k3, t5) candidates when compared with reference threshold at 7 %BW. The results were computed from the data in the validation set (N = 146 trials, 12092 steps). “b” and “ σ ” are the abbreviations for bias (intra-trial mean error) and precision (intra-trial STD of the error), respectively, while subscript characters μ and σ represent the median and the IQR over all the trials in the validation set.

3.4 Discussion

In this study, we proposed, evaluated, and compared how different algorithms based foot-worn IMU kinematic features performed in detecting IC and TC during running and in estimating the main inner-stride temporal parameters: CT, FLT, SWT, and SPT. The errors (Table 3.2) show that the bias and precision for IC and TC could reach very low values depending on the kinematic features used. Therefore, by considering the most efficient kinematic features, an accurate and precise estimation of inner-stride temporal parameters was proposed and validated against a force plate as a reference system.

Table 3.3 shows that the three most precise IC candidates (k1, k3, and k8) and TC candidates (t1, t4, and t5) can be combined to provide a precise estimation of ground contact time (CT). The most precise pair of features obtained from the two minimums of pitch angular velocity in IC and TC detection zones (k1, t1) had an inter-trials median \pm IQR precision of 4 ± 2 ms (1.8 ± 0.9 %). However, the accuracy of the t1 candidate is speed-dependent ($p < .001$). This explains the relatively high inter-trial IQR of the biases ($b_\sigma = 17$ ms) of CT for the (k1, t1) candidate. In Figure 3.3, the median of the biases for the t1 candidate (as well for t4 and t5) seem to linearly decrease as the speed increases. However, even though the Kruskal–Wallis test shows that speed also affects t5 ($p < .001$), the range of the median biases is approximately two times shorter for t5 (10 ms) than for t1 (21 ms).

To reduce the effect of the running speed on the bias, the minimums of pitch angular velocity in the IC zone and the maximum of vertical acceleration in TC zone, i.e. (k1, t5) candidate can be used. Although it is slightly less precise on the detection of CT, the results in Table 3.4 show better results in the estimation of FLT for both accuracy and precision. Given that the CT decreases as the speed increases, a measure of the CT itself already contains information about the running speed. Therefore, using the coefficients from the best linear fit (development set data) showed on the Bland-Altman plots in Figure 3.4, the validation set inter-trials median \pm IQR bias decreased to -2 ± 14 ms (-1 ± 6.2 %) and 1 ± 10 ms (0.3 ± 4.9 %) for the (k1, t1) and the (k1, t5) pairs, respectively. For both the (k1, t1) and the (k1, t5) candidates, the precision did not change after the aforementioned correction. Note that the outliers observed on the top graph of Figure 3.4 correspond to the detection errors of the t1 feature due to a second minimum happening later in the pitch angular velocity signal.

Moreover, Table 3.2 reveals that the most precise features for IC detection were found on the measurements from a single axis of the IMUs (k1, k3, and k8). This observation emphasizes the importance of the functional calibration, which aligns the technical frame of the inertial sensors with the biomechanically meaningful axes of the foot.

Table 3.2 also shows that, in general, the kinematic features used in this study tend to better detect IC than TC. Considering that the IC event comes with a landing impact, while no abrupt variation in the foot's motion occurs at TC, the odds of missing the exact instant of TC are higher. Moreover, the vertical force applied by the foot on the ground decreases drastically at the end of the CT although foot is still in contact with the ground leading to a potentially

early detection of TC. Similar observations were reported by Weyand et al. (2001). In fact, we observed that the 3%BW detection threshold showed a bias ($b_{\mu} \pm b_{\sigma}$) of -2 ± 2 ms and 7 ± 4 ms for IC and TC when compared to the 7%BW reference threshold. For both IC and TC, the bias was the highest when compared to a force threshold set at 20N. These results show that the detection accuracy of the force plate for TC, is more sensitive to the variations in the reference threshold than IC.

Lastly, the inter-step errors of the k1 feature seem to follow a bimodal distribution when including all step of the validation set, independently of the trials ($N = 12092$ steps). This implies that there might be an additional source of variance other than running speed that affects the detection of IC. Because the k1 feature is based on the angular velocity of the foot at landing, we assume that the type of foot-strike employed (fore-foot strike or rear-foot strike) could also introduce an error in the detection of IC. Further study would be required to evaluate how foot-strike angle influences detection accuracy and precision of temporal events during running. In addition, determining the applicability of the algorithms developed for level running in this study to uphill or downhill running would also need further study.

This study used a different method to express the CT errors than in Ammann et al. (2016). In the aforementioned study, the authors reported an inter-steps bias ($N = 132$ steps) of -1.9 ms (-1.3%) and a random error (95% confidence interval) of 17.4 ms (6.1%) for CT. The inter-steps bias and precision for the (k1, t1) pair showed comparable results. In fact, the validation set inter-steps bias ($N = 12092$ steps) was -2 ms (-0.5%) for CT, after applying the linear fit correction showed in the Bland-Altman plots in Figure 3.4. However, the inter-steps random error (95% confidence interval) was slightly higher (23 ms) for the (k1, t1) pair than in (Ammann et al., 2016). This can be explained by the fact that t1 precision is affected by speed ($p < .001$) and that the range of speed in this study ($10 - 20$ km/h) is larger than in (Ammann et al., 2016) (22.3 ± 5.8 km/h). In Weyand et al. (2001), the authors reported a bias (mean \pm STD) of $14.6 \pm 0.5\%$ when computed over 165 trials. These results are in accordance with the biases showed in Table 3.3.

To the authors' knowledge this study is the first to quantitatively demonstrate how, when using foot-worn IMUs in running, the choice of kinematic features affects the detection accuracy and precision of IC, TC and the inner-stride parameters derived from these two events. Consequently, it is important that researchers report on the methods applied to detect IC and TC events as it provides some information about the confidence interval of the measurements.

3.5 Conclusions

This study aimed to validate, against a gold standard reference system, the performance of several algorithms using foot-worn inertial sensors to detect running gait temporal events and estimate inner-stride phases duration. The results highlighted the importance of suitable kinematic signals and features to avoid large errors in detecting initial and terminal contact.

The two minimum values of the pitch angular velocity in the first half and second half of a mid-swing to mid-swing cycle provide the best estimation of IC and TC. Also, the maximum value of vertical acceleration during the second half mid-swing to mid-swing cycle provides a good estimation of TC which is less dependent on running speed. Using these initial and terminal contact features, we showed that the ground contact time, flight time, step and swing time can be estimated with an inter-trial median \pm IQR bias less than 15 ± 12 ms and the inter-trial median \pm IQR precision less than 4 ± 3 ms. Running speed could have a significant impact on the biases of the estimations, and therefore, the knowledge about the speed could improve the results. Further studies should investigate the effect of the foot-strike angle on the errors made by the features during initial contact.

Funding

This study was supported by the Swiss CTI grant no 17664.1 PFNM-NM

3.A Additional Results: Automatic Detection of Body-Worn Sensors Location in Running

Abstract

When wearable motion monitoring systems are used with multiple sensors, it is convenient to automatically identify sensor locations to avoid error and time-consuming attachment procedure. This study aimed to design a method that automatically recognizes six sensor locations (feet, shanks, thorax, and sacrum) of a body-worn inertial measurement unit (IMU) during running. The method was trained and tested on a data set of 41 healthy subjects running on a treadmill at speeds ranging between 12km/h to 22 km/h. We obtained the best classification performance using a decision tree with binary K-NN classifiers at its nodes. The proposed classification method achieved an accuracy of 99.4% in the distinction between the upper vs. lower body sensors, 95% accuracy between the trunk and sacrum sensors, 97.3% accuracy between the foot and shank sensors, 79.6% accuracy between the left and right foot-worn sensors, and 88.2% between the left and right shank-worn sensors.

Keywords: inertial sensors, IMU-to-segment, decision tree, K-NN classifier, running

3.A.1 Introduction

In recent years, new wearable sensors with a broad range of applications arose in running. However, these systems have yet to overcome several limitations, one of which being the correct placement of the wearable sensors. Robust automatic detection of body-worn sensors position has been proposed to improve their ease of use drastically (Amini et al., 2011; Graurock et al., 2016; Kunze et al., 2005; Mannini et al., 2015; Saeedi et al., 2014; Shi et al., 2011; Weenk et al., 2013; Zimmermann et al., 2018). In the case of multi-sensor configuration, no preparation would be required before using the system, therefore removing the need for a time-consuming set up prone to error and discomfort. Moreover, the versatility of the sensors would be enhanced as their location could be adapted according to clothing or activity.

Previous studies have shown that IMU-to-segment assignment is feasible and reliable, through various classification means, with 95% accuracy or above (Kunze et al., 2005; Saeedi et al., 2014; Weenk et al., 2013). However, to the authors' knowledge, the existing methods in the literature have been designed for walking and other daily activities (e.g., talking on the phone, cleaning) and thus may not be appropriate for running. Also, most previous studies (Graurock et al., 2016; Kunze et al., 2005; Saeedi et al., 2014; Shi et al., 2011; Weenk et al., 2013) collected data on a small number of participants, ranging from only 1 to 17 people with multiple trials of each participant. Therefore, the models might be biased towards the gait of a few individuals

Publication accepted as Falbriard, M., & Aminian K. (2021). Sixteenth International Symposium on the 3-D Analysis of Human Movement, Ames, Iowa, USA.

Contributions: conceptualized the study design; conducted the data collection; designed the algorithms; contributed to the analysis and interpretation of the data; drafted the manuscript.

and thus less able to generalize to unseen data. Some studies (Amini et al., 2011; Graurock et al., 2016; Mannini et al., 2015) relied solely on the measurements from accelerometers and did not consider other data such as angular velocity. While other focalized on the angular velocity measurements only (Shi et al., 2011). Finally, it is worth noting that only a few research (Saeedi et al., 2014; Weenk et al., 2013; Zimmermann et al., 2018) aimed to differentiate between sensors placed on the left and right sides of the body (e.g., right foot and left foot).

In this research, we proposed a new classification method to automatically assign an IMU to the left foot, right foot, left shank, right shank, upper trunk, or sacrum segments. The model relied on a binary decision tree and was tested for running speeds between 12km/h to 20 km/h. We investigated both K-NN and K-Mean as candidate classifiers at the nodes and used features from both the accelerometer and gyroscope sensors. Finally, our method aims to classify each IMU individually; hence, any sensor configuration is possible (e.g., one IMU, several IMUs on multiple segments, and multiple IMUs on the same segment).

3.A.2 Material and Methods

Protocol

In total, 41 healthy adults (13 females and 28 males, age 29 ± 6 years, weight 70 ± 10 kg, height 174 ± 8 cm) running at least once a week and without any musculoskeletal injuries volunteered to participate to this study. The local ethical committee approved the protocol (CCER-VD 2015-00006) and the measurement sessions we conducted according to the declaration of Helsinki. Each participant ran multiple trials of 30 seconds on an instrumented treadmill at speeds ranging between 12 to 22 km/h. The participants were free to decide on the rest duration in-between the trials and performed a 6 minutes warm-up on the treadmill before starting the measurements.

Instrumentation and pre-processing

The participants were equipped with one IMU (Physilog 4¹, Gait Up, Switzerland, weight: 19 g, size: 50 x 37 x 9.2 mm) on the following body-segments: left and right foot, left and right shank, sacrum, and thorax (near the T2 vertebrae). The IMUs were recording the acceleration and angular velocity with a 500 Hz sampling frequency and an operating range of $\pm 16g$ and ± 2000 deg/s, respectively. The shoe-worn and the shank-worn IMUs were fixed to their respective body-segments using Silicon/Velcro elastic straps, while the sacrum and thorax IMUs were fixed using adhesive tape.

To help with the distinction between the left and right leg sensors, we applied a previously validated functional calibration (FC) algorithm (Falbriard et al., 2018) on the foot-worn and shank-worn sensors. This step allowed the binary classifiers to dissociate the left and right foot, and the left and right shank using the features from the different axes of the sensors. We then applied a moving average filter (window length = 50 ms) on the data from each axis and

¹Datasheet available in the Appendix.

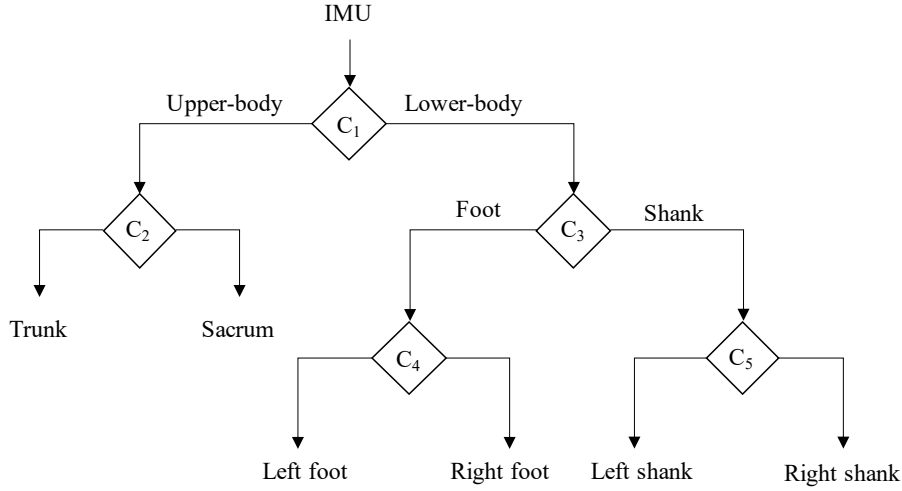


Figure 3.5 – The tree structure of the classification steps identified as C_i where $i = 1, \dots, 5$

the L2 norm.

Decision tree and classifiers

The classification was based on the tree structure shown in Figure 3.5. When designing the structure of the tree, we prioritized the nodes where we expected the greatest differences in the quantity of movement. Hence, each IMU was first classified as an upper or a lower body sensor (C_1). Upper-body sensors were then classified as a sacrum or thorax sensor (C_2). If an IMU was labeled as lower-body sensors at C_1 , it then went through a second classification where the distinction between the foot-worn and shank-worn IMUs was made (C_3). Finally, we used the third level of classifiers (C_4 and C_5) to determine whether the foot-worn or shank-worn IMU was placed on the right or the left leg. Moreover, for each of the C_i classifiers, we evaluated the performance of both the K-Means and the K-NN techniques.

Feature extraction and selection

The first step aimed to select the most relevant features to separate the classes. The features extracted for the accelerometer and angular velocity norm of all IMUs are listed in Table 3.5. Besides, the same features were extracted for the three axes of the foot-worn and shank-worn sensors, hence replacing the final letter N by either X, Y, or Z for the parameter's label. We did not consider the axes of the thorax and sacrum sensors due to the lack of plug-and-play FC algorithms for these locations. The majority of the features inform about the intensity of the signal, with only the skewness and the kurtosis describing the shape of the distribution. Also, since the classification must occur for all the IMUs independently, no inter-sensor features were used in the analysis.

Feature selection was performed on the running trials of 7 subjects and using 100-fold cross-validation, where, for each fold, we attributed 1/3 of the trials to the training set and 2/3 to

Label	Description
rmsAccN, rmsGyrN	Root mean square (RMS)
stdAccN, stdGyrN	The standard deviation
maxAccN, maxGyrN	Maximum value
minAccN, minGyrN	Minimum value
medAccN, medGyrN	Median
iqrAccN, iqrGyrN	Interquartile range (IQR)
peakAccN, peakGyrN	The ratio of maximum value to RMS
skewAccN, skewGyrN	Skewness
kurtAccN, kurtGyrN	Kurtosis
momAccN, momGyrN	Moment of order 5
modeAccN, modeGyrN	The most frequent value (mode)

Table 3.5 – List of the features extracted for the accelerometer norm (AccN) and angular velocity norm (GyrN).

the validation set. These 7 participants were later excluded from the data set used to assess the performance of the model. The features were selected using the wrapper method; the algorithm first selected the feature with the highest the F1-score (Eq. 3.5) and successively repeated this process, adding the next feature with the highest F1-score at each iteration, until no significant increase or decrease in performance occurred. Note that we computed the F1-score on the validation set only.

$$F1 = 2 * \frac{P * R}{P + R} \quad (3.5)$$

With P the precision and R the recall (or sensitivity). We applied this selection procedure for each of the classification stages (i.e., each of the C_i classifiers, $i = 1, \dots, 5$) with K-NN and K-Mean used separately.

Evaluation of the model

To assess the performance of the model, we divided the data from 34 participants (we excluded the 9 participants used for feature selection) into two sets: the training and test set using a leave-one-subject-out approach. We used the F1-score, accuracy, specificity, sensitivity, and precision for each of the C_i classifiers, where $i = 1, \dots, 5$, to assess the performance of the proposed method.

To determine the optimal value for K for each C_i classifiers, we plotted the F1-measure as a function of the number of nearest neighbors K and selected the K value with the best classification results. Moreover, since the performance of the models may vary for different running speeds, we have trained and tested the classifiers for each speed individually and investigated whether differences occurred in the classification performances.

3.A.3 Results

In total, 198 trials were used in this study: 28 for feature selection and 170 for the evaluation of the model. We extracted 17 features from the acceleration and angular velocity norm of each of the 6 body-worn IMUs. Also, these 17 features were extracted for each axis of the foot-worn and shank-worn IMU after we applied the transformation obtained from the functional calibration. Hence, a total of 121176 data points were available to train and evaluate the model.

Classifiers	Features	Method	K	FC	F1-score
C_1	rmsAccN, medAccN, medGyrN, skewAccN	K-NN	5	No	0.996
C_2	rmsAccN, medAccN, medGyrN, stdAccN	K-NN	3	No	0.951
C_3	stdAccN, stdGyrN, rmsAccN, rmsGyrN	K-NN	5	No	0.968
C_4	skewGyrX, skewGyrY, maxAccY, maxAccZ, kurtGyrX	K-NN	3	Yes	0.785
C_5	medAccX, medAccZ, medGyrX, medGyrY	K-NN	5	Yes	0.904

Table 3.6 – Results from the feature selection process.

In Table 3.6, the features and configuration that obtained the highest F1-score are shown for each classifier. Note that, at each node, the K-NN method outperformed the K-Mean approach. Consequently, the general performances of the decision tree have been further assessed only with the K-NN classifiers at its nodes. The accuracy, specificity, sensitivity, and precision statistics of the proposed decision tree are summaries in Table 3.7, with each column of the table corresponding to one of the C_i classifiers (Figure 3.5). Finally, the effect of running speed on the F1-score is displayed in Table 3.8.

Statistics	C_1	C_2	C_3	C_4	C_5
Accuracy (%)	99.4	95	97.3	79.6	88.2
Specificity (%)	99.7	96.5	96.4	76.3	85.8
Sensitivity (%)	99.2	93.8	98.1	83.4	90.9
Precision (%)	99.8	96.8	96.4	75.4	84.8

Table 3.7 – Accuracy, specificity, sensitivity, and precision obtained using the leave-one-subject-out process.

Speed (km/h)	C_1	C_2	C_3	C_4	C_5
12	1	0.98	1	0.91	0.92
14	1	0.99	1	0.89	0.92
16	1	0.99	1	0.90	0.95
18	1	0.98	1	0.89	0.97
20	0.99	0.93	0.99	0.90	0.95
All	0.99	0.95	0.97	0.81	0.91

Table 3.8 – F1-score of the different classifiers with the running speeds considered separately.

3.A.4 Discussion

In this study, we proposed a simple decision tree structure to assign body-worn sensors to the thorax, the sacrum, the left or right shank, the left foot, or the right foot. The results suggest that the K-NN method outperforms the K-Means approach for all the nodes of the decision tree (Table 3.6). Overall, the C_1 , C_2 , and C_3 classifiers achieved good accuracy, specificity, sensitivity, and precision using features extracted on the norm of the accelerometer and from the gyroscope measurements. Hence, no function calibration was required for such classification. Although the distinction between the left and right leg at C_4 achieved lower performances than the C_1 , C_2 , and C_3 classifiers, the results from Table 3.8 suggest that these results could be improved by using the running speed as an additional input to the model. The current results are nevertheless acceptable if the proposed method serves as a warning to the end-user in case the system expects an incorrect configuration. Hence, further research should be carried to assign a probability of error for each class. Also, we used a time window of 29 seconds for feature extraction, but a shorter window length could also be implemented for embedded scenarios. Indeed, whereas multiple cycles would ensure more robustness of the classifier by decreasing the importance of any unusual steps due to obstacles or unexpected movement, theoretically, a single cycle would be sufficient.

The IMU-to-segment assignment results obtained in this study are comparable to those previously reported for walking. The method, however, used a simple decision tree with K-NN classifiers at its nodes, while other researchers have proposed more sophisticated approaches such as support vector machines (Amini et al., 2011; Mannini et al., 2015; Saeedi et al., 2014; Shi et al., 2011) and deep-learning techniques (Zimmermann et al., 2018).

Acknowledgment

The authors would like to acknowledge Maury-Larivière Pauline for her contribution to the implementation of the methods.

Funding

This study was supported by the Swiss CTI grant no 17664.1 PFNM-NM.

4 Drift-Free Foot Orientation Estimation in Running Using Wearable IMU

Abstract

This study aimed to introduce and validate a new method to estimate and correct the orientation drift measured from foot-worn inertial sensors. A modified strap-down integration was proposed to decrease the orientation drift, which, in turn, was further compensated by estimation of the joint center acceleration of a two-segment model of the foot. This method was designed to fit the different foot strike patterns observed in running and was validated against an optical motion-tracking system during level treadmill running at 8, 12, and 16 km/h. The sagittal and frontal plane angles obtained from the inertial sensors and the motion tracking system were compared at different moments of the ground contact phase. The results obtained from 26 runners showed that the foot orientation at mean stance was estimated with an accuracy (inter-trial median \pm IQR) of $0.4 \pm 3.8^\circ$ and a precision (inter-trial precision median \pm IQR) of $3.0 \pm 1.8^\circ$. The orientation of the foot shortly before initial contact was estimated with an accuracy of $2.0 \pm 5.9^\circ$ and a precision of $1.6 \pm 1.1^\circ$; which is more accurate than commonly used zero-velocity update methods derived from gait analysis and not explicitly designed for running. Finally, the study presented the effect initial and terminal contact detection errors have on the orientation parameters reported.

Keywords: running, inertial measurement units (IMU), validation study, orientation, drift, angles, foot strike

Chapter adapted from Falbriard M, Meyer F, Mariani B, Millet GP and Aminian K (2020) Drift-Free Foot Orientation Estimation in Running Using Wearable IMU. *Front. Bioeng. Biotechnol.* 8:65. doi: 10.3389/fbioe.2020.00065

Contributions: conceptualized the study design; conducted the data collection; designed the algorithms; contributed to the analysis and interpretation of the data; drafted the manuscript.

4.1 Introduction

The orientation of the foot recorded slightly before, during, or after the ground contact phase is an essential parameter for running analysis. Many studies have investigated how different foot landing techniques give rise to kinematic and kinetic differences between subjects. For instance, the foot strike patterns (i.e., rearfoot, midfoot and forefoot) and their association with injury risks (Peter R. Cavanagh & LaFortune, 1980; Daoud et al., 2012; Goss & Gross, 2012), running economy (Gruber et al., 2013; Joseph Hamill & Gruber, 2017; Miller & Hamill, 2015; Perl et al., 2012), running performance (de Almeida et al., 2015; Kasmer et al., 2013; Larson et al., 2011), collision forces (Boyer et al., 2014; Gruber et al., 2014; Lieberman et al., 2010), muscle activity (Ahn et al., 2014; Yong et al., 2014) and footwear (Horvais & Samozino, 2013; Larson, 2014; Lorenz & Pontillo, 2012; C. Meyer et al., 2018) have been at the core of many research studies and changes of running paradigms within the last decades. The orientation of the foot in different planes or relative to the shank has also been extensively analyzed and now constitutes a primary marketing argument for the running industry (e.g., eversion/inversion, pronation/supination) (Monaghan et al., 2014; Muñoz-Jimenez et al., 2015; B. M. Nigg et al., 1993; Perry & LaFortune, 1995).

In research, the continuous measurement of the 3D orientation of the foot is generally obtained using optical motion capture systems (Altman & Davis, 2012; Arndt et al., 2007; Riley et al., 2008). While these systems measure the foot pose (i.e., orientation and position) accurately, they are often restricted to well-equipped laboratories and treadmill running. As an alternative to this lack of portability, a growing number of studies have shown that wearable inertial sensors, if combined with state-of-the-art algorithms, can be used to provide reliable spatiotemporal information (Camomilla et al., 2018).

Historically, the methods based on foot-worn inertial sensors that estimate the fixed-frame orientation of the foot first emerged from the field of gait analysis. Although different methods have been proposed (Mariani et al., 2010; Sabatini, 2005; Skog et al., 2010), most share the same underlying structure: (1) integration of the angular velocity obtained from a foot-mounted gyroscope to calculate the global frame orientation and (2) combine the measurements from other sensors (e.g., accelerometer, magnetometer, GPS) to estimate and remove the orientation drift. Methods such as the zero-velocity-update usually require the presence of low accelerations or low magnetic disturbances during the period of stance to estimate the orientation drift. Although these periods are generally present during low-speed human locomotion, they are either rare or inexistent as the speed increases (Foxlin, 2005; Park & Suh, 2010; Zhang et al., 2017), and thus are likely to underperform in running.

Nevertheless, studies have proposed a hard reset of the drift based on the hypothetical presence of a foot-flat period during the stance phase of running (Bailey & Harle, 2014; Chew et al., 2017; Yuan et al., 2019). Although this approach seems reasonable for rearfoot strikers, it is not appropriate for forefoot strikers as their rearfoot segment possibly never comes into contact with the ground. Also, typically-rearfoot strikers tend to switch from a rearfoot to a forefoot

strike pattern when the running speed increases (Breine et al., 2014); speed might likewise be a confounding factor for any drift reduction method. Note that if the continuous orientation is not required, different approaches have been proposed to classify the foot-strike patterns with foot-worn IMUs (Marlène Giandolini et al., 2014; Strohrmann et al., 2011).

The combination of strap-down integration with the difference between proximal and distal accelerations at any joint center has been used to estimate the joint orientation and to model the drift in dynamic movements (Dejnabadi et al., 2006; Fasel et al., 2018). To the authors' knowledge, this method has never been tested to estimate the orientation drift of the foot in running.

Hence, the objective of this research was to propose a novel drift-free orientation estimation method for running built on a two-segment model of the foot and explore the abovementioned combination of proximal and distal accelerations using a single inertial measurement unit (IMU) placed on the rear foot. We assumed that, regardless of the foot strike pattern, a forefoot-flat period is always present, and it can be used to estimate and compensate the foot orientation drift. The proposed method provides an estimate of the orientation drift for each stance period and can, therefore, be used for online analysis of the running gait. Moreover, the proposed method does not require the presence of a second IMU on the forefoot, for such complicated instrumentation would reduce its applicability for field studies.

4.2 Materials and Methods

4.2.1 Protocol

A total of 26 volunteers (9 females and 17 males, age 29 ± 6 years, weight 70 ± 10 kg, height 174 ± 8 cm, running weekly 2.1 ± 1.0 h, 11 affiliated to a running club) participated in this study. They were running at least once a week and had no symptomatic musculoskeletal injuries. Participants gave their written informed consent before the measurements and ran for 45 seconds at 8, 12, and 16 km/h on a level instrumented treadmill, wearing their regular shoes. A 6 min familiarisation period (Lavcanska et al., 2005) was performed on the treadmill and served as a warm-up for the participants. This protocol was approved by the local ethical committee (CCER-VD 2015-00006) and conducted according to the declaration of Helsinki.

4.2.2 Wearable systems

Inertial measurement units

One Inertial Measurement Unit (Physilog 4¹, GaitUp SA, CH, weight: 19 g, size: 50 x 37 x 9.2 mm) was fixed on the dorsum of each foot using a Silicon/Velcro elastic strap. The accelerometer operated at 500 Hz (± 16 g), the gyroscope at 500 Hz (± 2000 deg/s), and sensors' calibration was performed according to Ferraris et al. (1995). We modeled the foot with two rigid segments:

¹Datasheet available in the Appendix.

the rearfoot and forefoot segments (Figure 4.1). Note that there was no sensor located on the forefoot segment. We aligned the IMU's technical frame (TF) with the rearfoot Functional Frame (FF_{rear}), as described by Falbriard et al. (2018); we recorded a standing period and used the gravitational acceleration to set the FF_{rear} y-axis parallel to the vertical axis of the foot. Then, using principal component analysis (PCA) on the running measurements, we aligned the FF_{rear} z-axis with the principal vector, which we assumed parallel to the mediolateral axis of the foot. Finally, we defined the FF_{rear} x-axis as the cross-product between the FF_{rear} y-axis and the z-axis. Note that the calibration matrix was considered constant within the duration of the trial.

Temporal events detection

Temporal events detection was based on previously validated algorithms (Falbriard et al., 2018). We segmented the trials into running strides and extracted four events per stance phase. The Initial (IC) and Terminal (TC) contact events, when the foot initializes and terminates ground contact, were found using local minima on the pitch angular velocity. Also, the mean-stance (MS) was defined as the mean time between IC and TC, and MinRot as the time-point of stance when the norm of the foot angular velocity is minimum.

Orientation estimation

Strap-down integration of the angular velocity (Favre et al., 2008) is frequently used to obtain the orientation of a body segment in the Global Frame (GF). However, this operation generates a drift which accumulates with time. In this study, orientation estimation was performed in three phases: (i) modified strap-down integration, (ii) drift modeling, (iii) drift estimation and reduction. The modified strap-down integration method provides a first estimate of the orientation. It assumes that, at MinRot of each stance phase, the FF_{rear} and the GF are aligned. In other words, it supposes that a rearfoot strike is used and that, at MinRot, the rearfoot segment is flat on the ground. Since this hypothesis is not general enough (i.e., it does not consider all the possible foot strike patterns), the subsequent phases (ii) and (iii) aims to remove the drift further.

Modified strap-down integration (MSDI)

First, we set the quaternion ${}^{GF}_{FF} \hat{q}(t)$ to transform the IMU 3D kinematics from the FF_{rear} into the GF. The x-axis of the GF was parallel to the longitudinal axis of the treadmill's belt, the z-axis to the lateral axis, and the y-axis was perpendicular to the ground surface, pointing upward (Figure 4.1). Typically, strap-down integration is computed between time-points at which the orientation of the FF_{rear} in the GF can be estimated. In walking, short zero-velocity periods during foot-flat are often used to reset the integration drift (Sabatini, 2005). As these static periods were not observed during running, we implemented a new integration method that relies on a quasi-zero velocity update at MinRot and a bidirectional strap-down integration. This method merges the strap-down integration results calculated in a forward and backward

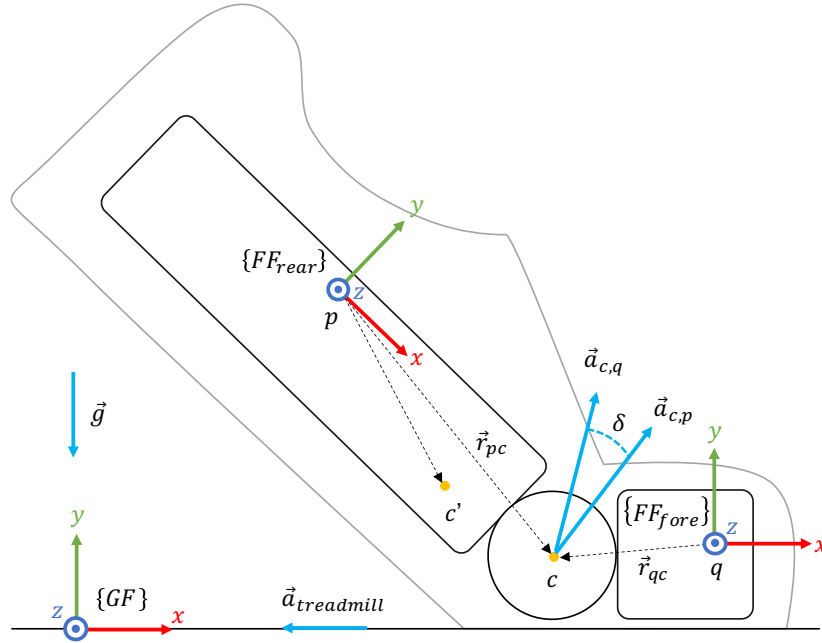


Figure 4.1 – The two-segments model of the foot during the stance phase. Using the RGB convention, $\{FF_{rear}\}$ represents the functional frame of the rearfoot segment, $\{FF_{fore}\}$ the functional frame of the forefoot segment and $\{GF\}$ the room's global frame. Points p and q are arbitrarily placed on rearfoot, and forefoot segments, c' and c are respectively hypothetical and optimum rearfoot-forefoot joint's center. $\vec{a}_{c,q}$ is the acceleration at c estimated from q , $\vec{a}_{c,p}$ the acceleration at c estimated from p , $\vec{a}_{treadmill}$ the acceleration of the treadmill and \vec{g} the Earth gravitational acceleration. Finally, δ is the orientation difference (i.e., quaternion) between $\vec{a}_{c,p}$ and $\vec{a}_{c,q}$ while \vec{r}_{pc} and \vec{r}_{qc} are the distance vectors from point p to c and from q to c , respectively.

direction, awarding higher weight to the estimation originating from the closest MinRot. So, for each stride $i \in [2, N-1]$, N is the total number of strides, we performed strap-down integration in two directions. The quaternion ${}^{GF}_{FF} \hat{q}_{backward,i}(t)$ with $t \in [\text{MinRot}(i), \text{MinRot}(i+1)[$ results from the forward strap-down integration and the quaternion ${}^{GF}_{FF} \hat{q}_{backward,i}(t)$, with $t \in]\text{MinRot}(i-1), \text{MinRot}(i)]$, from the backward integration. Note that, we assumed the FF_{rear} at MinRot (${}^{GF}_{FF} \hat{q}(\text{MinRot})$) to be aligned with the GF. The orientation difference was obtained as in Eq. 4.1:

$${}^{GF}_{FF} \hat{q}_{diff}(t) = {}^{GF}_{FF} \hat{q}_{backward,i+1}(t) * {}^{GF}_{FF} \hat{q}_{forward,i}(t)^{-1} \quad (4.1)$$

We then weighted the contribution of the “backward” and “forward” estimations in the actual orientation ${}^{GF}_{FF} \hat{q}_{diff}(t)$ through the correction of the helical angle ($\alpha(t)$) obtained by the transformation from the quaternion notation to the axis-angle notation (*quat2helic*):

$$(\vec{u}(t), \alpha(t)) = \text{quat2helic}({}^{GF}_{FF} \hat{q}_{diff}(t)) \quad (4.2)$$

$$\alpha_w(t) = \alpha(t) * \frac{t - \text{MinRot}(i)}{|t - \text{MinRot}(i+1)|} \quad (4.3)$$

The corrected helical angle $\alpha_w(t)$ and vector $\vec{u}(t)$ were then transformed back into quaternion notation (*helic2quat*) and used to estimate the weighted orientation difference:

$${}_{FF}^{GF}\hat{q}_{diff,w}(t) = \text{helic2quat}(\vec{u}(t), \alpha_w(t)) \quad (4.4)$$

Finally, we found the rearfoot orientation as:

$${}_{FF}^{GF}\hat{q}(t) = {}_{FF}^{GF}\hat{q}_{diff,w}(t) * {}_{FF}^{GF}\hat{q}_{forward,i}(t) \quad (4.5)$$

Since the forward and backward orientation estimations are linearly weighted (Eq. 4.3), this technique does not have jumps in the final orientation estimate ${}_{FF}^{GF}\hat{q}(t)$.

Drift modeling based on joint center acceleration (JCA)

During the stance phase of running, the kinematics of the rearfoot and forefoot segments vary upon the landing technique. The forefoot segment always has a short flat period, independently of the foot strike pattern (i.e., rearfoot strike, midfoot strike, or forefoot strike), while the rearfoot segment is usually flat only for rearfoot strikes. However, all runners have the forefoot segment that remains flat on the ground shortly after toe-strike and toward most of the pushing phase (Peter R. Cavanagh & Lafortune, 1980; De Cock et al., 2005). The previously calculated rearfoot orientation ${}_{FF}^{GF}\hat{q}(t)$ could, therefore, be incorrect due to this potential absence of the rearfoot-flat period. By modeling the foot with two segments, one can estimate the acceleration at their joint center (i.e., point *c* in Figure 4.1) based on the rearfoot $\vec{a}_{c,p}(t)$ and forefoot $\vec{a}_{c,q}(t)$ accelerations. The above can be done using the function $\varphi(\vec{a}, \vec{\omega}, \vec{r})$ which shifts the acceleration $\vec{a}(t)$ of any point of a segment to another point of the same segment based on the segment's angular velocity $\vec{\omega}(t)$ and the translation between the two points \vec{r} :

$$\varphi(\vec{a}(t), \vec{\omega}(t), \vec{r}) = \vec{a}(t) + \vec{\omega}(t) \times \vec{r} + \vec{\omega}(t) \times (\vec{\omega}(t) \times \vec{r}) \quad (4.6)$$

The drift model in this study assumes that, during the forefoot-flat period, $\vec{a}_{c,p}(t) - \vec{a}_{c,q}(t) = \vec{0}$. Consequently, the orientation difference of the joint center accelerations ($\delta(t)$) should also be zero or minimal. During forefoot-flat, $\vec{a}_{c,q}(t)$ can be estimated from Eq. 4.6 by assuming no angular rotation:

$$\vec{a}_{c,q}(t) = \vec{a}_q(t) = \vec{g} + \vec{a}_{treadmill}(t) \quad (4.7)$$

where \vec{g} is the earth gravitational acceleration and $\vec{a}_{treadmill}(t)$ the acceleration of the treadmill. Note that, even if the treadmill velocity was set constant, the shearing forces acting on the belt, shortly after landing, change the speed of the treadmill, hence generating a non-zero acceleration $\vec{a}_{treadmill}(t)$. The model also assumes that each point on the rearfoot segment has a trajectory which lies on the surface of a sphere during forefoot-flat; hence, Eq. 4.8 describes the accelerations acting at point p :

$$\vec{a}_p(t) = \vec{a}_{p,tang}(t) + \vec{a}_{p,cent}(t) + \vec{g} + \vec{a}_{treadmill}(t) \quad (4.8)$$

where $\vec{a}_{p,tang}(t)$ is the tangential and $\vec{a}_{p,cent}(t)$ the centripetal acceleration at point p .

Drift estimation and reduction

To estimate the orientation drift $\delta(t)$, the accelerations $\vec{a}_{c,p}(t)$ and $\vec{a}_{c,q}(t)$ were calculated based on the acceleration and angular velocity at point p and q , respectively. As the exact position (p) of the IMU is unknown (i.e., somewhere on the dorsum of the foot), we designed a two-step optimization process to find the \vec{r}_{pc} vector, necessary to find $\vec{a}_{c,p}(t)$. In the first step, the point c' is selected as the candidate position, which minimizes the norm of the tangential and centripetal accelerations. This point c' is chosen among all the rearfoot points j for which $\vec{r}_{pj,x} < 30\text{cm}$, $\vec{r}_{pj,y} < 10\text{cm}$ and $\vec{r}_{pj,z} < 5\text{cm}$ in FF_{rear}. We used Eq. 4.6 to find an estimate of \vec{r}_{pc} , namely $\vec{r}_{pc'}$, which minimizes Eq. 4.9 after removing the contribution of \vec{g} (inclination) from the acceleration at point j :

$$\vec{r}_{pc'} = \underset{\vec{r}_{pj}}{\operatorname{argmin}} \left(\left\| \varphi \left(\vec{a}_p(t) - \overset{GF}{FF} \hat{q}(t)^{-1} * \overset{GF}{g}, \vec{\omega}_p(t), \vec{r}_{pj} \right) \right\| \right), t \in S \quad (4.9)$$

The function argmin returns the \vec{r}_{pj} vector at which the input function is minimized. S is the set of samples within the pushing phase of each stride i , defined as $t \in [\text{MinRot}(i), \text{TC}(i)]$. During the pushing phase, the tangential and centripetal accelerations are maximum. This high signal-to-noise ratio optimizes the outcome of the minimization function in Eq. 4.9. As a result, Eq. 4.6 and $\vec{r}_{pc'}$ can be used to estimate the acceleration at the point c' :

$$\vec{a}_{c',p}(t) = \varphi \left(\vec{a}_p(t), \vec{\omega}_p(t), \vec{r}_{pc'} \right) \quad (4.10)$$

If the point c' is reasonably close to the joint center c , the tangential and centripetal accelerations should approximately be null and, based on Eq. 4.7, $\vec{a}_{c',p}(t) - \vec{g}$ can be used as an estimate of $\vec{a}_{treadmill}(t)$.

$$\vec{a}_{c',p}(t) \cong \vec{a}_{c,q}(t) = \vec{g} + \vec{a}_{treadmill}(t) \quad (4.11)$$

$$\vec{a}_{c',p}(t) - \vec{g} \cong \vec{a}_{treadmill}(t) \quad (4.12)$$

In the second step of optimization, $\vec{a}_{c',p}(t)$ was used as in Eq. 4.9 to refine the estimate of \vec{r}_{pc} :

$$\vec{r}_{pc} = \underset{\vec{r}_{px}}{\operatorname{argmin}} \left(\left\| \varphi \left(\vec{a}_p(t) - \vec{a}_{c',p}(t), \vec{\omega}_p(t), \vec{r}_{px} \right) \right\| \right) \quad (4.13)$$

$$\vec{a}_{c,p}(t) = \varphi \left(\vec{a}_p(t), \vec{\omega}_p(t), \vec{r}_{pc} \right) \quad (4.14)$$

Using Eq. 4.7 and Eq. 4.14 in GF, the orientation drift ($\delta(t)$) was estimated, for each step, as the orientation difference between $\vec{a}_{c,p}(t)$ and $\vec{a}_{c,q}(t)$:

$$\delta(t) = \left[\cos \left(\frac{\beta(t)}{2} \right), \sin \left(\frac{\beta(t)}{2} \right) * v(t) \right] \quad (4.15)$$

where $v(t)$ is a unit vector perpendicular to $\vec{a}_{c,p}(t)$ and $\vec{a}_{c,q}(t)$ and $\beta(t)$ is the rotation around $v(t)$:

$$\beta(t) = \arccos \left(\frac{|\vec{a}_{c,q}(t) * \vec{a}_{c,p}(t)|}{|\vec{a}_{c,q}(t)| * |\vec{a}_{c,p}(t)|} \right) \quad (4.16)$$

$$v(t) = \frac{\vec{a}_{c,q}(t) \times \vec{a}_{c,p}(t)}{\|\vec{a}_{c,q}(t) \times \vec{a}_{c,p}(t)\|} \quad (4.17)$$

The orientation drift of the i th stance phase, namely δ_i , was defined as the average quaternion (Cheng et al., 2007) of $\delta(t)$ where $t \in [t_m - \varepsilon, t_m + \varepsilon]$. The parameter t_m was found as in Eq. 4.18 and $\varepsilon = 5\text{ms}$.

$$t_m = \min_t (\|\vec{a}_{c,p}(t)\| - 1) \quad (4.18)$$

$$\delta_i = \operatorname{mean}(\delta(t)), t \in [t_m - \varepsilon, t_m + \varepsilon] \quad (4.19)$$

We then estimated the rearfoot orientation based on Eq. 4.5 and obtained the drift correction with Eq. 4.20:

$${}_{FF}^{GF}q(t_m) = {}_{FF}^{GF}\hat{q}(t_m) * k * \delta_i \quad (4.20)$$

$$k = 1 / \left(1 + e^{100 * (\|\vec{a}_{c,p}(t_m)\| - 1.1)} \right) \quad (4.21)$$

Note that the sigmoid function in Eq. 4.21 aims to reduce the weight of the update the further the norm of $\tilde{a}_{c,p}(t_m)$ is from the unit norm. The parameters of the sigmoid function were selected such that a 10% error corresponds to a coefficient k equal to 0.5. Finally, we used the same MSDI process to correct the estimate of ${}^{GF}_{FF}\hat{q}(t)$: for each stance phase a new ${}^{GF}_{FF}\hat{q}_{forward,i}(t)$ and ${}^{GF}_{FF}\hat{q}_{backward,i}(t)$ was computed, with the center time $t_{m,i}$ and with an initial orientation defined as in Eq. 4.19.

4.2.3 Reference system

Temporal events detection

We used an instrumented treadmill (T-170-FMT, Arsalis, Belgium) as a reference system for temporal events detection. The force plate recorded the 3D ground reaction forces (GRF) at 1000Hz, and a 5V analog trigger synchronized the system with the IMUs. To reduce the noise on the vertical GRF signal due to the treadmill's vibration, we first applied a 2nd-order stopband Butterworth filter with edge frequencies set to 25 and 65 Hz. Finally, the initial and terminal contact events were found using a threshold on the vertical GRF set at 7% of the participant's body weight (Falbriard et al., 2018).

The 3D orientation of the foot with stereophotogrammetry

Motion tracking of the lower limbs was achieved using eight motion cameras (BTS Smart 400, BTS Bioengineering, USA) and 21 reflective markers placed on body landmarks. The system operated at 100Hz and was synchronized with the IMUs and the force plate using an analog trigger (i.e., 5V pulse trigger recorded on all the systems). We defined the GF of the system using three reflective markers on the horizontal plane of the treadmill; the GF x-axis set parallel to the belt (i.e., in the running direction) and the z-axis laterally to the belt, and the y-axis perpendicular to the x and z axes (Figure 4.2).

Calibration in standing posture

The malleolus markers (Figure 4.2, m5-6) were frequently torn off while running, so we recorded a 5-seconds standing posture at the beginning of each session. The calibration phase aimed to obtain the matrix ${}^{FF}_{TF}R_{calib}$ which transforms the vector space from the Technical Frame (TF) to the Functional Frame (FF). The position of the markers of the shoe remained unchanged throughout a session, so the matrix ${}^{FF}_{TF}R_{calib}$ was considered constant and was used to process the running trials. The TF was defined using the mean position of 4 reflective markers firmly fixed around the IMU (Figure 4.2, m1-4) and the matrix ${}^{GF}_{TF}R_{calib}$ was set to transform the vector space from the TF to the GF (Eq. 4.22 - 4.23). In Eq. 4.22, the N symbol represents the normalization function, and the circumflex indicates that the average position of the marker was considered.

$$\tilde{x}_{TF} = N(\tilde{m}_2 - \tilde{m}_4), \tilde{z}_{TF} = N(\tilde{m}_3 - \tilde{m}_4), \tilde{y}_{TF} = N(\tilde{z}_{TF} \times \tilde{x}_{TF}), \tilde{x}_{TF} = \tilde{y}_{TF} \times \tilde{z}_{TF} \quad (4.22)$$

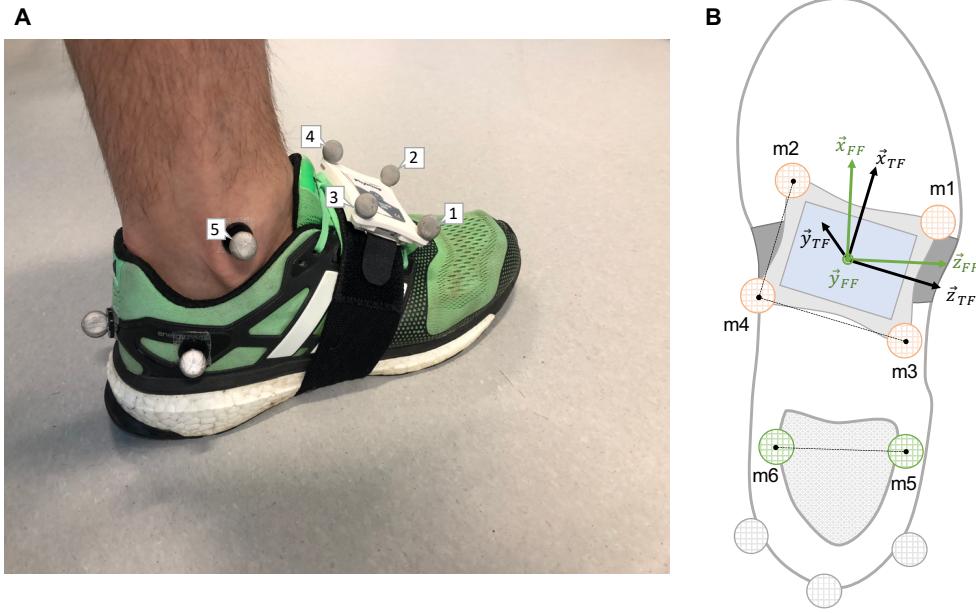


Figure 4.2 – (A) Rear/lateral view of the markers' configuration used in this study. (B) Top scheme of the markers' configuration required in the definition of the foot's technical (TF) and functional (FF) frames. Markers illustrated in orange are the one needed to set the TF, in green the FF, and in grey the duplicates which were not used in this study. Also, note that markers 5 and 6 were kept only during the calibration trials.

$${}_{TF}^{GF}R_{calib} = [\vec{x}_{TF}, \vec{y}_{TF}, \vec{z}_{TF}] \quad (4.23)$$

We defined the orientation of the FF (${}_{FF}^{GF}R_{calib}$) using the two malleolus markers (m5-6) and the GF vertical axis, as shown in Eq. 4.24 - 4.25.

$$\vec{z}_{FF} = N(\vec{m}_5 - \vec{m}_6), \vec{y}_{FF} = [0, 1, 0], \vec{x}_{FF} = N(\vec{y}_{FF} \times \vec{z}_{FF}), \vec{z}_{FF} = \vec{x}_{FF} \times \vec{y}_{FF} \quad (4.24)$$

$${}_{FF}^{GF}R_{calib} = [\vec{x}_{FF}, \vec{y}_{FF}, \vec{z}_{FF}] \quad (4.25)$$

Finally, we obtained the matrix ${}_{TF}^{FF}R_{calib}$ using the two calibration matrices from Eq. 4.23 and Eq. 4.25.

$${}_{TF}^{FF}R_{calib} = {}_{FF}^{GF}R'_{calib} * {}_{TF}^{GF}R_{calib} \quad (4.26)$$

Reference orientation during running

During the running trials, only the markers m1 to m4 were kept. We calculated the TF of the foot as in Eq. 4.22 except that the markers' position at each time t was considered and not their average position as for the calibration trials.

$${}_{TF}^{GF}R(t) = [\tilde{x}_{TF}(t), \tilde{y}_{TF}(t), \tilde{z}_{TF}(t)] \quad (4.27)$$

Finally, we transformed the TF into the FF using the matrix from the calibration trial.

$${}_{FF}^{GF}R(t) = ({}_{TF}^{FF}R_{calib} * {}_{TF}^{GF}R(t))' = {}_{TF}^{GF}R(t) * {}_{TF}^{FF}R'_{calib} \quad (4.28)$$

By definition, the columns of ${}_{FF}^{GF}R(t)$ correspond to the coordinates of the TF basis vectors in the GF. The TF was computed based on the markers affixed on the IMU and was, therefore, subject to fixation artifact. Three additional markers were placed on the subtalar region as duplicates in case of unsatisfactory data quality. These markers were fixed on the shoe but suffered from recurrent marker loss as the marker on the medial side was frequently hit by the opposite foot during running. When present, however, these markers were used to visually assess the sensor-to-foot motion (i.e., wobbling of the sensor) with an average RMS difference of 3.68° obtained after the low-pass filtering of the pitch angle.

4.2.4 Validated angles

We calculate two reference angles using the 3D orientation of the foot measured by stereophotogrammetry (${}_{FF}^{GF}R(t)$): the pitch angle (θ_{ref}), defined as the projection of the FF x-axis onto the sagittal plane in the GF and the roll angle (ρ_{ref}), defined as the projection of FF z-axis onto the frontal plane in the GF. These angles were also computed for the IMU system using the MSDI (${}_{FF}^{GF}\hat{q}(t)$) method (θ_{MSDI} , ρ_{MSDI}) and the JCA (${}_{FF}^{GF}q(t)$) method (θ_{JCA} , ρ_{JCA}). By definition, the pitch angle is zero when the rear foot remains flat on the ground and is positive when the forefoot segment is higher than the rearfoot segment. The Root Mean Square error of $\theta_{ref}(\text{stance}) - \theta_{MSDI}(\text{stance})$ and $\theta_{ref}(\text{stance}) - \theta_{JCA}(\text{stance})$ was estimated for each stance phase. In addition, the value of the pitch angle at initial contact, i.e., the foot strike angle ($\theta_{ref}(\text{IC})$, $\theta_{MSDI}(\text{IC})$, $\theta_{JCA}(\text{IC})$), at terminal contact, i.e., the pushing angle ($\theta_{ref}(\text{TC})$, $\theta_{MSDI}(\text{TC})$, $\theta_{JCA}(\text{TC})$) and at mean-stance ($\theta_{ref}(\text{MS})$, $\theta_{MSDI}(\text{MS})$, $\theta_{JCA}(\text{MS})$) were extracted from the different methods. These parameters rest on the detection accuracy of the IC and TC, so they were computed based on the results of both the force plate (i.e., reference system) and the IMU (Falbriard et al., 2018). Note that, because of the potential detection error of the IMU-based method, we used the mean angle within an 8-millisecond window (i.e., ± 2 samples at 500Hz) instead of the exact angle at IC, MS, and TC. Moreover, the time (AC) and value of the pitch angle last local maximum before IC was extracted and defined as the pre-activation pitch angle ($\theta_{ref}(\text{AC})$, $\theta_{MSDI}(\text{AC})$, $\theta_{JCA}(\text{AC})$). This feature describes the orientation of the foot

shortly before landing when muscle pre-activation occurs (Kyröläinen et al., 2005). Also, as the range of the roll angle was small, therefore potentially suffering from low signal-to-noise ratio, only the activation roll angle ($\rho_{ref}(AC)$, $\rho_{MSDI}(AC)$, $\rho_{JCA}(AC)$) was defined as the last local minimum before IC. A negative roll angle corresponds to an inversion of the foot and a positive angle to an eversion.

4.2.5 Statistical analysis and error computation

This study focused on the trials at 8, 12, and 16 km/h, which corresponds to slow, moderate, and fast running. Trials were either removed because of instrumentation errors, protocol errors, or marker loss. We also removed the outliers steps from the data set according to the following criteria: $\theta_{ref}(MS) > 10^\circ$ and $\theta_{ref}(AC) < -80$. After the outliers were removed, trials with less than five strides were dropped from the study.

To evaluate the error of the IMU estimations against the reference motion tracking system, we computed four statistics on the entire data set for each parameter. The bias (intra-trial mean) and precision (intra-trial STD) were computed on the strides from the same foot and the same trial. We considered the feet independently as runners may use different patterns for the left and right foot. The bias and precision were later combined among all the trials: b_μ the inter-trials median of the bias, b_σ the inter-trials IQR of the bias, σ_μ the inter-trials median of the precision and σ_σ the inter-trials IQR of the precision. We used the median and IQR statistics because the biases and precisions were not normally distributed.

The influence of the running speed on the intra-trial biases and precision values was tested using the non-parametric Kruskal-Wallis test with a significance level set at $p < 0.1$. This test was preferred to an ANOVA analysis because of the low number of trials and the lack of prior knowledge about the seemingly not normal distributions. Also, boxplots were used to visualize the biases and precision differences among the running speeds. Finally, we graphically assessed the agreement between the IMU-based system and the reference motion capture system using Bland-Altman plots (Bland & Altman, 1986).

4.3 Results

In total, 4252 steps were analyzed in this study. The mean \pm STD (min, max) number of recorded strides per trial was 36 ± 6 (10, 45) for a total of 59 trials (23 at 8 km/h, 23 at 12 km/h, and 13 at 16 km/h). The pitch angles during the stance phase and obtained from the different estimation methods are shown for a rearfoot (left) and a forefoot (right) striker in Figure 4.3. We emphasized on the IC and TC detection differences between the force plate and the IMU-based method using vertical dashed lines.

Table 4.1 shows the results of the inter-trials error statistics for the MSDI and JCA orientation estimation methods. The range (95% interval) observed on the reference system for the pitch

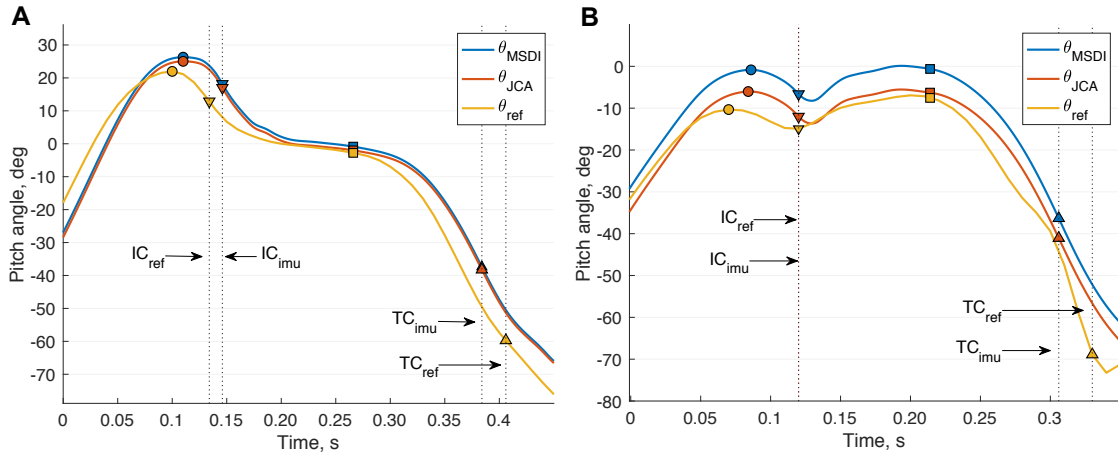


Figure 4.3 – Comparison of the pitch angle measured from different measurement systems for a rearfoot (A) and forefoot (B) striker. The blue curve is the estimation from the IMU-based MSDI method (θ_{MSDI}), the orange curve from the IMU-based JCA method (θ_{JCA}), and the yellow curve from the reference motion tracking system (θ_{ref}). The IC events are shown using down-pointing triangles, TC events with up-pointing triangles, MS events with squares, and the AC peaks using circles. The black vertical dashed lines accentuate the detection differences, for the IC and TC events, between the IMU and the force plate system.

and roll angles are: $\theta_{ref}(IC)$ (-12.5, 18.2), $\theta_{ref}(MS)$ (-11.8, -1.2), $\theta_{ref}(TC)$ (-68.9, -41.6), $\theta_{ref}(AC)$ (-7.8, 28.9) and $\rho_{ref}(AC)$ (-29.5, -7.6). The error statistics are expressed in degrees and are shown for two different temporal events detection systems: the IMUs and the force plate. When the steps are gathered regardless of their trial and using the IMU-based event detection, the mean \pm STD error ($^{\circ}$) of the JCA method are: $\theta_{JCA}(IC)$ (0.8 ± 5.9), $\theta_{JCA}(MS)$ (0.2 ± 4.7), $\theta_{JCA}(TC)$ (17.0 ± 9.0), $\theta_{JCA}(AC)$ (2.1 ± 5.5) and $\rho_{JCA}(AC)$ (3.1 ± 4.9). Similarly, for the MSDI method: $\theta_{MSDI}(IC)$ (3.9 ± 5.7), $\theta_{MSDI}(MS)$ (3.6 ± 3.9), $\theta_{MSDI}(TC)$ (20.2 ± 8.8), $\theta_{MSDI}(AC)$ (5.3 ± 5.2) and $\rho_{MSDI}(AC)$ (4.6 ± 4.9).

Figure 4.4 illustrates the intra-trial biases (b) and precision (σ) statistics obtained for the $\theta_{JCA}(AC)$ parameter at 8, 12, and 16 km/h. Two trials at 8 km/h had large biases (23.2 $^{\circ}$ and -14.8 $^{\circ}$) and were cut-off from the graph for the sake of illustration. The results from the Kruskal-Wallis test suggest that the biases (b) and precision (σ) values for $\theta_{JCA}(AC)$ and $\theta_{JCA}(MS)$ are not affected by the running speed. However, for the parameters $\theta_{JCA}(IC)$, $\theta_{JCA}(TC)$ and $\rho_{JCA}(AC)$ the precision (σ) of the system was significantly affected ($p < 0.05$) but the intra-trial biases (b) were not ($p = 0.11$, $p = 0.21$, $p = 0.42$).

Finally, a Bland & Altman plot (Figure 4.5) shows the agreement between the IMU-based system and the reference motion capture system, with the mean ($2.1^{\circ} \pm \text{STD } 5.2^{\circ}$) of the error displayed with yellow horizontal lines.

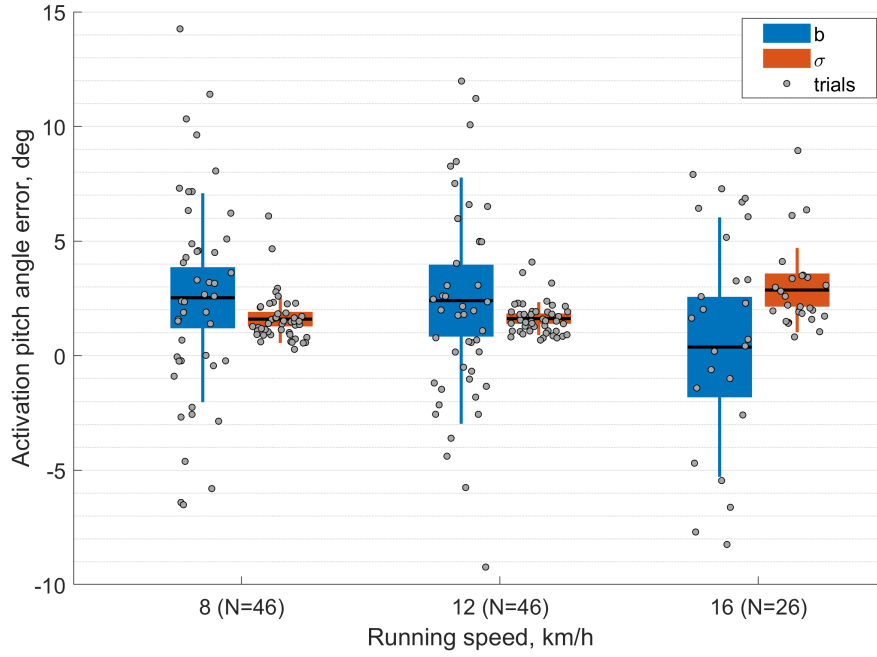


Figure 4.4 – Boxplot of the intra-trial biases and precision results for the foot pitch activation angle ($\theta_{JCA}(AC)$) measured with the proposed method (JCA). In the figure, the intra-trial biases are shown in blue and the precision values in orange. The grey dots represent the statistic of each trial. Note that there are two dots per trial because the feet were considered independently.

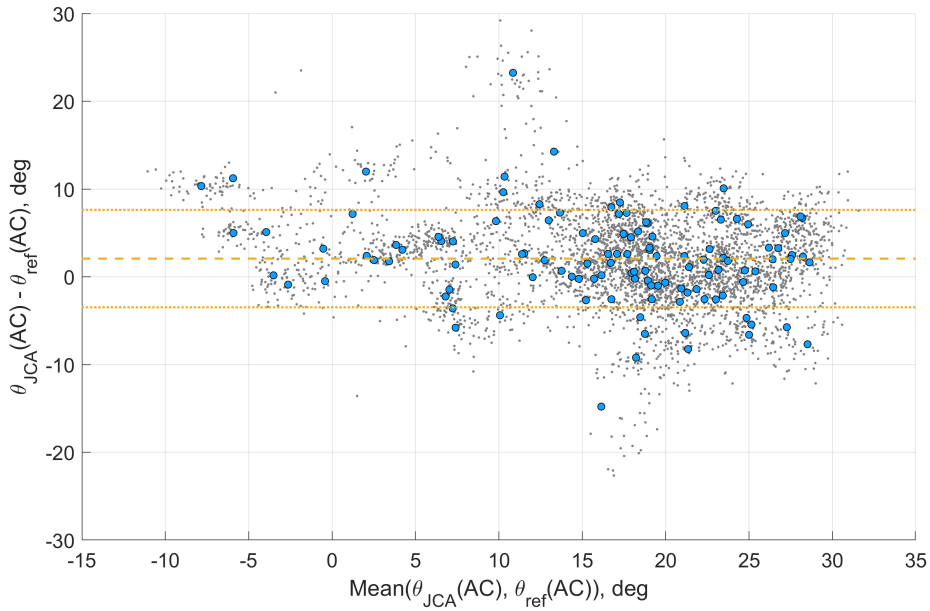


Figure 4.5 – Bland-Altman plot of the activation pitch angle ($\theta_{JCA}(AC)$) for the JCA method. The grey dots show the agreement of each step, the blue circles the agreement of the intra-trial mean, and the yellow lines the mean \pm STD of the error.

Parameter	IMU-based event detection				FP-based event detection			
	Bias (°)		Precision (°)		Bias (°)		Precision (°)	
	b_μ	b_σ	σ_μ	σ_σ	b_μ	b_σ	σ_μ	σ_σ
$\theta_{JCA}(\text{IC})$	0.9	6.7	2.4	1.5	6.2	6.9	2.2	1.1
$\theta_{MSDI}(\text{IC})$	3.7	6.0	2.1	1.1	9.9	7.2	1.8	0.8
$\theta_{JCA}(\text{IC}) - \theta_{MSDI}(\text{IC})$	-2.9	0.7	0.3	0.4	-3.7	-0.3	0.3	0.3
$\theta_{JCA}(\text{MS})$	0.4	3.8	3.0	1.8	1.1	3.5	1.3	1.1
$\theta_{MSDI}(\text{MS})$	3.8	3.8	2.0	1.7	4.3	3.1	0.8	0.4
$\theta_{JCA}(\text{MS}) - \theta_{MSDI}(\text{MS})$	-3.5	0.0	0.9	0.1	-3.2	0.4	0.5	0.8
$\theta_{JCA}(\text{TC})$	17.4	8.7	3.2	1.7	2.6	8.0	2.8	1.5
$\theta_{MSDI}(\text{TC})$	20.8	7.6	2.8	1.3	4.8	7.1	2.4	1.4
$\theta_{JCA}(\text{TC}) - \theta_{MSDI}(\text{TC})$	-3.4	1.1	0.3	0.4	-2.2	0.9	0.4	0.1
$\theta_{JCA}(\text{AC})$	2.0	5.9	1.6	1.1				
$\theta_{MSDI}(\text{AC})$	5.0	5.7	1.2	0.9				
$\theta_{JCA}(\text{AC}) - \theta_{MSDI}(\text{AC})$	-3.0	0.2	0.3	0.2				
$\theta_{JCA}(\text{stance})$	4.5	2.8	0.8	0.6				
$\theta_{MSDI}(\text{stance})$	6.2	4.1	0.6	0.3				
$\theta_{JCA}(\text{stance}) - \theta_{MSDI}(\text{stance})$	-1.7	-1.3	0.2	0.3				
$\rho_{JCA}(\text{AC})$	3.0	5.7	1.5	1.3				
$\rho_{MSDI}(\text{AC})$	4.4	5.5	1.5	1.2				
$\rho_{JCA}(\text{AC}) - \rho_{MSDI}(\text{AC})$	-1.4	0.2	0.0	0.1				

Table 4.1 – Inter-trial analysis of the IMU-based pitch (θ) and roll (ρ) angles estimation errors with motion tracking cameras used as a reference. The MSDI and JCA methods are evaluated in two scenarios: (1) using temporal event detection from the IMU and (2) using temporal event detection from the force plate (FP). The selected events are initial contact (IC), mean-stance (MS), terminal contact (TC), and activation peak (AC). The results of the inter-trials median (b_μ) and IQR (b_σ) of the bias, the inter-trials median (σ_μ) and IQR (σ_σ) of the precision and the root mean square error (RMSE) of the continuous pitch angle ($\theta_{JCA}(\text{stance})$, $\theta_{MSDI}(\text{stance})$) between IC and TC are presented in this table.

4.4 Discussions

In this study, we proposed a new method to estimate the foot orientation during running, based on a single IMU on the rear foot. While IMU-based estimation generates drift due to strap-down integration operation, we proposed a modified strap-down integration (MSDI) supplemented with a drift compensation method (JCA). The technique relies on the assumption of a flat period in the forefoot, which is accurate for all landing strike pattern. Assuming dynamic rearfoot kinematics during the pushing phase and a static period on the forefoot segment, a two-segment biomechanical model of the foot is, therefore, well suited for running. Also, the system requires no prior knowledge about the sensor's location. The IMU must be fixed on rearfoot, and the functional calibration is automatically performed. Validated against gold standard stereophotogrammetry system, the proposed drift correction method allowed to estimate the foot orientation at mean stance phase with a bias of $0.4 \pm 3.8^\circ$ and precision of $3.0 \pm 1.8^\circ$. Note that the validation was restricted to the stance phase due to the occlusion of the markers' position during the swing phase.

In this study, the drift correction of the MSDI method is hypothetical and enforced. An implication of this is the possibility that the biases (b_μ and b_σ) observed for this method cannot be extrapolated to other populations or other running conditions (e.g., various speed and style); we would certainly expect more significant biases in the case of forefoot strikers (Figure 4.3, right). Instead, the JCA method uses a real measure of the orientation drift and correctly estimated the pitch angle around MS, while the MSDI method remained around 0° (Figure 4.3). The RMSE analysis (Table 4.1) also reveals better results for the JCA method with better accuracy (b_μ and b_σ statistics). In contrary, the σ_μ and σ_σ statistics suggest that the JCA method is slightly less precise. Note that these precision differences are always below 1° (Table 4.1) and seem reasonable given that the $\theta_{MSDI}(MS)$ precision exposes the inter-steps variability of the participants (i.e., of the reference system). Besides, the precision of the JCA system could be improved by tuning the parameters of the sigmoid function of Eq. 4.21 in order to reduce the effect of outlier estimations. Also, the algorithm provides near-real-time processing of the orientation (i.e., in the order of a step), and could potentially be improved by considering the orientation of the few preceding steps in the estimation of the drift (e.g., using a weighted average).

Table 4.1 and Figure 4.3 highlight the importance of temporal events detection accuracy in the estimation of the pitch angle at IC, MS, and TC. Large errors in the measured angles result from the fact that IC and TC events are detected during phases of rapid change in pitch angle. Table 4.1 reveals that, when the force plate system detected TC, the median bias (b_μ) of the JCA and the MSDI methods improved by 14.8° and 16° , respectively. Similarly, the biases were worsened by 5.3° and 6.2° for IC. These findings can be explained by the fast-changing slope of the pitch angle (θ) around the IC, while it is continuously negative around TC. In consequence, the detection biases of IC and TC have dissimilar effects on $\theta_{JCA}(IC)$, $\theta_{MSDI}(IC)$, $\theta_{JCA}(TC)$ and $\theta_{MSDI}(TC)$. Furthermore, these estimations are sensitive to synchronization delays between the reference systems and the IMUs.

Because the AC event is not affected by the temporal events detection technique, a more detailed analysis was performed on the $\theta_{JCA}(AC)$ parameter. The parameter $\rho_{JCA}(AC)$ is also unaffected by the detection accuracy of the temporal events; however, the pitch angle was preferred because of the lack of generality in the roll angle drift correction hypothesis. The assumption of a null roll angle for the forefoot segment may be incorrect for subjects with pathological pronation/supination. In Figure 4.5, the optical motion-tracking system and the IMU-based system demonstrate a good agreement across the range of angles.

Bailey & Harle (2014) used two methods (linear de-drifting and extended Kalman filter) to compute the orientation of the foot in 5 subjects based on shoe-mounted IMUs. They reported an error (mean + STD) for $\theta(IC)$ of $1.92 \pm 1.09^\circ$ at 8.28 km/h and $3.18 \pm 1.19^\circ$ at 12.24 km/h. The present JCA results ($0.8 \pm 5.9^\circ$) show a better bias but a lower precision. The lower performance in precision might be associated with the higher diversity of subjects and speeds analyzed in this study. Also, the authors assumed that the pitch and roll angles were similar for every stance phase, hence reducing the inter-steps variability of the system. Koska et al. (2018) used trapezoidal integration of gyroscopic measurements to estimate the orientation of the foot during the stance phase. The authors reported error biases ($^\circ$) \pm 95% limits of agreement ($^\circ$) of $-3.1 \pm (-7, 3.4)$ at 10 km/h, $-3.8 \pm (-7.6, 2.1)$ at 12km/h and $-5.9 \pm (-11.1, 1.8)$ at 15 km/h in the estimation of the sagittal plane (i.e., pitch angle) range of motion during stance phase. Although heel-off events were defined using a fixed time window, their observations corroborate with the results of the MSDI method. Shiang et al. (2016) also assumed the presence of a foot-flat period (i.e., pitch angle = 0°) during stance, as for the MSDI method used in the present study, and defined the difference between two local maximums as the strike index. The range of angles ($-5^\circ, 27^\circ$) reported for the strike index reflect those obtained for $\theta_{JCA}(AC)$ and $\theta_{MSDI}(AC)$ parameters in this study. Also, in Altman & Davis (2012), the authors concluded that the foot strike angle, obtained from an optical motion capture system, is an acceptable measure of foot strike pattern, and proposed the following classification limits: rearfoot strike $> 8^\circ$, midfoot strike between -1.6° and 8° , and forefoot strike $< 1.6^\circ$. These results, with a midfoot strike classification range of 9.6° , suggest that the JCA method provides an acceptable measure of the pitch angle, with an accuracy of $2.0 \pm 5.9^\circ$ and $0.9 \pm 6.7^\circ$ for the $\theta_{JCA}(AC)$ and $\theta_{JCA}(IC)$ parameters, respectively. However, such a conclusion does not hold for the MSDI method (Table 4.1). A validation study on walking analysis (Brégou Bourgeois et al., 2014) reported accuracy and precision of $0.5 \pm 2.9^\circ$ and $3.9 \pm 5.8^\circ$ in the estimation of the pitch angle (θ) at initial and terminal contact, respectively. In comparison, we observed (when the steps were gathered regardless of their trial) a $0.8 \pm 5.9^\circ$ and $17.0 \pm 9.0^\circ$ accuracy and precision for $\theta_{JCA}(IC)$ and $\theta_{JCA}(TC)$ parameters. The lower performance may partly be explained by the lower detection accuracy of the initial and terminal contact in running and by the highly dynamic motion of the foot in running generating a greater level of noise during the period of stance.

The results from the Kruskal-Wallis test suggest that neither the bias nor the precision of the $\theta_{JCA}(AC)$ and $\theta_{JCA}(MS)$ parameters were significantly affected by the running speed. However, we observed significant differences in the precision of $\theta_{JCA}(IC)$ and $\theta_{JCA}(TC)$. This

possibly results from the effect speed has on the detection precision and accuracy of IC and TC (Falbriard et al., 2018). Note that there is a performance trade-off made by the system and associated with the running speed. At low running speeds, the norm of the tangential and centripetal accelerations during the pushing phase is small and therefore decreases the performance of the automatic estimation of \vec{r}_{pc} in Eq. 4.9 - 4.13. Conversely, ground contact times are longer at low running speeds (Nummela et al., 2007), increasing the probability of sufficiently long static periods to directly estimate the 3D orientation of the rearfoot segment.

It is essential to bear in mind that the present study was performed on a 0° inclined treadmill. Consequently, the results reported in this document cannot be generalized to uphill and downhill running. Also, we obtained the reference orientation based on markers on the sensors rather than on the shoe; therefore, the protocol constraints such as the lightweight IMU and the IMU fixation are aspects that could affect the detection results. Finally, the present study raises the possibility for the JCA method to be tested on active gait methods other than running (e.g., Nordic walking).

4.5 Conclusions

In this study, we proposed and validated a new method to estimate and correct the orientation drift estimation based on a foot-worn IMU using a two-segment model of the foot for drift removal. The validation compared sagittal and frontal plane angles obtained from an optical motion-tracking system with the estimation based on wearable inertial sensors. We showed that the pitch angle at mid-stance can be estimated with an inter-trial median \pm IQR of $0.4 \pm 3.8^\circ$ and an inter-trial precision median \pm IQR of $3.0 \pm 1.8^\circ$. Although running speed can affect the detection performance, the system showed a good agreement with the gold standard optical motion-tracking system. Apart from the short standing period used for the functional calibration, the proposed system is fully plug-and-play. It requires no prior knowledge about the position of the sensors and needs no magnetometer.

Funding

This study was supported by the Swiss CTI grant no. 17664.1 PFNM-NM.

4.A Additional Results: How Accurate is Visual Determination of Foot Strike Pattern and Pronation Assessment

Abstract

Nowadays, choosing adequate running shoes is very difficult, due to the high number of different designs. Nevertheless, shoes have two main characteristics to fit the runners' technique and morphology: drop and arch support. Retailers' advices are usually based on the visual assessment of the customer's running technique. Such a method is subjective and requires an experimented examiner, while objective methods require expensive material, such as a 3D motion system and pressure insoles. Therefore, this study aimed to determine the accuracy of foot strike pattern and pronation assessment using video cameras, compared to a gold standard motion tracking system and pressure insoles. Thirty-four subjects had to run at 8, 12, and 16 km/h shod and 12 km/h barefoot during 30 s trials on a treadmill. The agreement between foot strike pattern assessment methods was between 88% and 92%. For pronation, agreement on assessment methods was between 42% and 56%. The results obtained indicate a good accuracy on foot strike pattern assessment, and high difficulty to determine pronation with enough accuracy. There is, therefore, a need to develop new tools for the assessment of the runner's pronation.

Keywords: running, foot strike, visual assessment

4.A.1 Introduction

Running has become a very popular sport in the last decades, thanks to its accessibility, ease of practice, and health benefits (Taunton et al., 2002). Nevertheless, injury risks are usually underestimated by non-professional runners. In a prospective study, Macera et al. (Macera et al., 1989) reported that each year, approximately one out of two runners gets injured. Assessing foot strike and pronation is paramount as directly linked to injury risk (Stacoff et al., 2016). Moreover, shoes adapted to the runner's technique and foot morphology may reduce the risk of injury (McKenzie et al., 1985). As a consequence, retailers usually propose shoes with two main characteristics: soles with different drops to fit foot strike pattern (rearfoot, midfoot and forefoot strikers), and neutral shoes vs. shoes with arch support for pronators. The Foot Strike Index (FSI) indicates the location of the center of pressure when the foot hits the ground (Peter R. Cavanagh & Lafortune, 1980). The foot is separated into three areas: rearfoot, midfoot, and forefoot. Altman & Davis (Altman & Davis, 2012) showed the agreement between FSI and Foot Strike Angle (FSA), the angle of the foot in the sagittal plane, measured using 3D motion system (82% for shod condition and 60% barefoot) and between a direct visual classification and FSI (75%). The pronation of the foot has also been measured using different methods.

Chapter adapted from Meyer, E, Falbriard, M., Aminian, K., & Millet, G. P. (2018). How accurate is visual determination of foot strike pattern and pronation assessment. *Gait & posture*, 60, 200-202

Contributions: conceptualized the study design; conducted the data collection; contributed to the designed the algorithms; contributed to the interpretation of the data.

Brody proposed a method called “navicular drop” (ND) (Brody, 1982), where the navicular height difference was measured seated (without body weight) and in a standing position (with bodyweight). Foot characteristic was defined as follows: Under pronation: $ND < 4$ mm, Normal pronation: 4-10 mm, Overpronation: >10 mm. Clarke et al. (Clarke et al., 1984) and then McClay & Manal (McClay & Manal, 1998) defined the rearfoot eversion (EVA) as the angle between tibia and heel, measured on the frontal plane. The following classification was defined: Under pronation: $EVA < 8^\circ$, Normal pronation: $8-15^\circ$, Overpronation: $>15^\circ$. Except for ND and a direct visual classification, all methods require extensive material and data processing. In this context, using video cameras could allow for accurate and straight forward foot strike patterns and pronation classification. The aim of this study was, therefore, to compare the accuracy of the previously cited methods with a visual determination from experts who analyzed slow-motion videos from cameras placed laterally and behind the runner: The lateral and the back visual classification methods (LVC and BVC respectively).

4.A.2 Methods

Thirty-four healthy adults (12 females and 22 males) aged 21-46 years, height 158-193 cm, weight 51-92 kg, running at least once a week and without any symptomatic musculoskeletal injuries volunteered to participate to this study. The study was approved by the local ethics committee. All participants signed an informed consent form before beginning the test. Participants were first asked to run six minutes on a force plate treadmill (FMT170, Arsalis, The Netherlands) at a self-selected speed, as a familiarization and warm-up (Schieb, 1986). Shoes were removed, ND measured, and markers placed on each barefoot using the Heidelberg Foot Measurement Method (Simon et al., 2006) for the back of the foot. The front foot markers were substituted by a 4 markers-cluster. A 30 s trial was then recorded by the motion tracking system at 100 Hz (Smart400, BTS Bioengineering, Italy), with the participants running at 12 km/h. Participants then wore their usual running shoes with pressure insoles (Pedar-X, Novel, Germany). Markers were fixed on each shoe using the same configuration (only the navicular marker was not repositioned). The participants had then to run 30 s at 8, 12, and 16 km/h. All trials were also recorded using a lateral (left) and a back camera at 240 Hz (GoPro 3, GoPro, USA). Direct comparison of running kinematics with vs. without shoes was possible at 12 km/h.

The time of initial contact was determined using the ground reaction forces recorded at 1000 Hz, for a 7% bodyweight threshold. Synchronized pressure insoles data were computed to determine FSI as a foot strike pattern reference system. Three-dimensional orientations of each were also computed (Smart Tracking, BTS Bioengineering, Italy) to calculate FSA and EVA. Finally, three experts (biomechanists) used LVC to determine foot strike pattern, and BVC was used by three other experts (clinicians) to determine over, normal, or under pronation of the foot.

Confusion matrix was built to determine accuracy, precision, sensitivity, and specificity and

compare consistency between foot strike pattern assessment methods and between pronation assessment methods using the average values over each trial. Accuracy between expert classification was also calculated. Finally, the Intraclass Correlation Coefficient (ICC) was calculated to assess observer variability (Bartko, 1966). ICC values were interpreted according to often quoted guidelines: Poor < 0.4 < Fair < 0.6 < Good < 0.75 < Excellent < 1 (Cicchetti, 1994).

4.A.3 Results

The results between foot strike pattern determination methods are presented in Table 4.2, while the results between pronation determination methods are presented in Table 4.3. The average standard deviation intra-trial was 1.88° for EVA and 2.00° for FSA.

Experts proposed accuracy between 86% and 94% for LVC classification, with an excellent inter-assessors ICC of 0.89. For the barefoot condition, the accuracy between FSA and LVC was 75%, while shod condition gave 97%. Figure 4.6 illustrates the relationship between FSI, FSA, and LVC. Concerning BVC, experts proposed accuracy between 73% and 76%, for a poor inter-assessors ICC of 0.05.

	FSI - FSA (n = 93)			FSI - LVC (n = 101)			FSA - LVC (n = 128)		
	Rear. (n = 65)	Mid. (n = 11)	Fore. (n = 17)	Rear. (n = 70)	Mid. (n = 11)	Fore. (n = 20)	Rear. (n = 73)	Mid. (n = 18)	Fore. (n = 37)
accuracy	88			92			91		
precision	92	55	94	96	55	100	97	67	89
sensitivity	92	55	76	96	55	80	97	67	97
specificity	100	50	94	100	67	100	92	71	89

Table 4.2 – Overall accuracy, precision, sensitivity, and specificity given in percent for the comparison between the foot strike pattern assessment methods. Values are given in % for Foot Strike Index (FSI), Foot Strike Angle (FSA), Lateral Visual Classification (LVC) and for each type of foot strike (rear., mid. and fore.).

	EV - BVC (n = 55)			EV - ND (n = 51)			ND - BVC (n = 102)		
	Under (n = 33)	Normal (n = 15)	Over (n = 7)	Under (n = 39)	Normal (n = 14)	Over (n = 7)	Under (n = 50)	Normal (n = 40)	Over (n = 12)
accuracy	56			49			42		
precision	7	88	14	64	50	14	0	82	17
sensitivity	7	88	20	64	50	14	0	82	20
specificity	100	59	14	41	68	14	0	45	17

Table 4.3 – Overall accuracy, precision, sensitivity, and specificity given in percent for the comparison between pronation assessment methods. Values are given in % for Eversion Angle (EVA), Navicular Drop (ND), and Back Visual Classification (BVC) comparison.

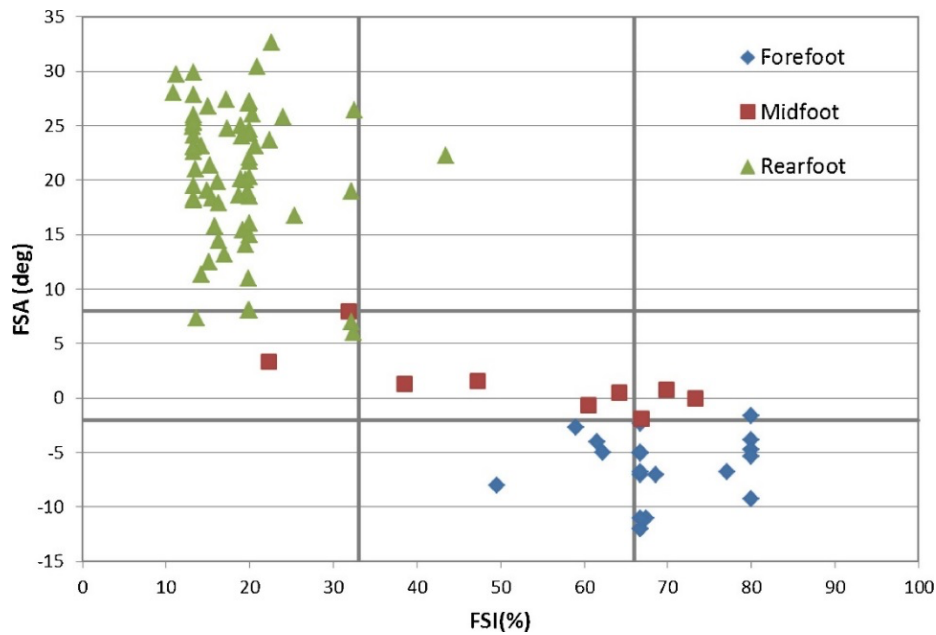


Figure 4.6 – Agreement between Foot Strike Index (FSI), Foot Strike Angle (FSA), and Lateral Visual Classification (LVC) (color boxes)

4.A.4 Discussion

Classifying foot strike patterns using a single camera placed laterally seems appropriate to determine rearfoot, midfoot, and forefoot strikers. There is a good agreement between the three methods used in this project. Experts also gave accurate results for LVC, as expected by Altman & Davis (2012). In their study, an overall 71% of correct classification between FSA and direct visual classification was observed. The barefoot condition also scored with a lower agreement between FSA and LVC. The difference between shod and barefoot condition is probably due to the higher difficulty to determine two parameters: the initial contact, and the orientation of the foot. Indeed, the shoes offer more contrast than the barefoot on images. Concerning the shod condition, the few classification errors were probably caused by the difficulty to estimate both the initial contact and the angle of the foot at that time. The midfoot condition is more problematic to assess, and Figure 4.6 provides a visual incentive that only a few runners land midfoot.

Classifying the pronation of the foot using the back camera leads to different conclusions: the agreement between the ND, EVA, and BVC methods is very low. This can probably be explained by the fact that the three different methods measure slightly different parameters: EVA determines only the rearfoot eversion at ground contact, ND classifies the foot in a non-dynamic way, while experts tried to estimate a malfunction (i.e., under or over-pronation) of the foot that increases the risk of injury. The small number of under pronators also requires interpreting the confusion matrix with caution. The fact that experts proposed different estimations illustrates two points: the difficulty to accurately define the pronation, even

among experts, and the difficulty of observing the movement of pronation from back videos. Indeed, as described by Stacoff et al. (2016), forefoot movement may also influence pronation at initial contact, implying a correlation between strike angle and pronation. The difference between shod and barefoot running was measured only at 12 km/h. At different velocities, one may assume that the bias would be higher with footwear since there are many additional confounding factors (insole height, shoe drop, lateral support) that would likely make the assessment more difficult and more variable.

One limitation of the present study was that FSA and the EVA were calculated by using the markers of the Heidelberg foot model but with only a limited set of available markers. This study showed the benefit of using video cameras to determine the foot strike pattern and the limitation when determining pronation during stance in running. Defining more accurately the foot pronation seems paramount since this factor is clinically important. Experts will also be able to determine pronation with greater accuracy according to the definition, and the inter-assessor ICC will probably increase.

Funding

This study was supported by the Swiss CTI grant no 17664.1 PFNM-NM.

5 Running Speed Estimation Using Shoe-Worn Inertial Sensors

Abstract

The locomotion speed is the main outcome in running analysis. Today, most wearable systems for running speed estimation are based on GNSS devices. However, these devices have a high power consumption and can suffer from sparse communication with the satellites. In this study, we proposed three different approaches to estimate the overground speed in running based on the measurements of foot-worn inertial sensors and compare them to GNSS considered as reference. First, a method is proposed by direct strapdown integration of the foot acceleration. Second, a feature-based linear model and finally a personalized online-model based on the recursive least squares method were devised. We also evaluated the performance differences between two sets of features; one automatically selected set (i.e., optimized) and a set of features based on the existing literature. The data set of this study was recorded in a real-world setting, with 33 healthy individuals running at low, preferred, and high speed. The direct estimation of the running speed achieved an inter-subject mean \pm STD accuracy of 0.08 ± 0.1 m/s and a precision of 0.16 ± 0.04 m/s. In comparison, the best feature-based linear model achieved 0.00 ± 0.11 m/s accuracy and 0.11 ± 0.05 m/s precision, while the personalized model obtained a 0.00 ± 0.01 m/s accuracy and 0.09 ± 0.06 m/s precision. The results of this study suggest that (1) the direct estimation of the velocity of the foot are biased, and the error is affected by the overground velocity and the slope; (2) the main limitation of a general linear model is the relatively high inter-subject variance of the bias, which reflects the intrinsic differences in gait patterns among individuals.; (3) this inter-subject variance can be nullified using a personalized model.

Keywords: IMUs, speed, running, linear prediction, personalization

Chapter to be submitted as Falbriard, M., Soltani, A., & Aminian, K. (2020). Running speed estimation using shoe-worn inertial sensors: direct integration, linear and personalized model.

Contributions: designed the algorithms (except the personalization model); contributed to the analysis and interpretation of the data; drafted the manuscript.

5.1 Introduction

The overground speed is the most useful metric in training and performance analysis of running. Researchers have tried for decades to understand the physiological and biomechanical adjustments occurring at different ranges of running speeds (Moore, 2016; Nummela et al., 2007; Thompson, 2017; K. R. Williams & Cavanagh, 1987). However, most of the existing studies were performed in a controlled environment (i.e., treadmill running inside a laboratory) where the runner has to adapt his gait to run at a constant speed. In overground running, change of environment, surface, slope, obstacles, and turns alter the gait and the running speed. Many studies have discussed the biomechanical adaptations associated with running on a treadmill versus running overground (Van Hooren et al., 2019). While standard motion capture (i.e., stereophotogrammetry and force plate) offers accurate measurements in laboratories, the recent emergence of wearable systems is paving the shift towards studies carried overground and in real-world conditions (Benson et al., 2018).

The real-world estimation of the overground speed is generally obtained using a body-worn Global Navigation Satellite System (GNSS). Although these systems provide accurate and reliable measurement of the locomotion speed (Terrier et al., 2000; Witte & Wilson, 2004), they suffer from several limitations: (1) their high power consumption restricts their duration of use in portable devices, (2) the communication between the receiver and the satellite is not always guaranteed (e.g., indoor, near high buildings), and (3) the measurement accuracy decrease during rapid changes of speed and position (Rawstorn et al., 2014; Varley et al., 2012). As a solution to the latter limitation, systems based on the data fusion of body-worn inertial and GNSS sensors have been proposed to monitor sports activities (Brodie et al., 2008; Waegli & Skalous, 2009; Zihajehzadeh et al., 2015). However, to address the issue of power consumption and communication losses, IMU-based systems must be able to estimate the speed without or with very limited input from a GNSS device.

Several methods have been proposed to estimate the walking speed using IMUs attached to different body-segments (Aminian et al., 2002; Hu et al., 2013; Miyazaki, 1997; Sabatini et al., 2005; Salarian et al., 2013; Zijlstra & Hof, 2003). One solution would be to extend and adapt these methods to running. However, these methods often relied on walking models or on the estimation of step length, which can not be directly applied to running because of the aerial phases, where accelerometers are erroneous. Other studies have used machine learning techniques to estimate the walking speed but did not validate the results for running (Fasel et al., 2017; Zihajehzadeh & Park, 2016).

To the authors' knowledge, few studies proposed an accurate ambulatory method, based on body-worn IMUs, to estimate the overground speed of running, and even less did so for instantaneous speed estimation. Two studies used a similar method (integration of the acceleration signal) to calculate the velocity of the shank (Yang et al., 2011) and foot (Chew et al., 2017) segments. However, the error of the system was computed over multiple strides, in a small range of speeds, and for level treadmill running. As mentioned previously, the

velocity estimated from the integration of segment acceleration has limitations, particularly when the flight phase varies in a wide range or when various slopes are experienced as it is the case in overground running. Another study (Hauswirth et al., 2009) compared in-lab a commercialized speed estimation device with the speed of a treadmill and reported a relatively low accuracy considering that the system required a subject-specific calibration. Subject-specific neural networks were also devised to assess the running speed in free-living conditions using only triaxial accelerometric measurements, but the model needed a calibration/learning phase for each runner and was validated for the mean speed using few trials (Herren et al., 1999). One study, however, exploited the personalized calibration and proposed a model based solely on the contact time (De Ruiter et al., 2016). Although the authors obtained a low root-mean-square error ($<3\%$), these results were not instantaneous estimations but rather the average speed over bouts of 125 meters. Besides, a more recent study (Soltani et al., 2019) based on wrist-worn inertial sensors suggested that better results could be achieved by including more features to the model.

The objective of the current study was three-fold: first, we aimed to extend an existing walking algorithm based on strapdown integration of foot acceleration and show its limitation for running speed estimation. Then we proposed a new linear model to predict the running speed at each step and in real-world condition, based on relevant features extracted from feet acceleration and angular velocity. Finally, we investigated how personalization improved the performances of the system using additional data, such as occasional GNSS inputs. We compared each method to the GNSS speed, considered as the ground truth, obtained during outdoor measurements of overground running, at different speeds and slopes.

5.2 Methods

5.2.1 Protocol and instrumentation

33 healthy and active participants (18 males (age: 38 ± 9 y.o.; size: 180 ± 7 cm; weight: 76 ± 9 kg), 15 females (age: 36 ± 10 y.o.; size: 165 ± 7 cm; weight: 59 ± 7 kg)) without any symptomatic musculoskeletal injuries participated to this study. The measurements were performed in real-world conditions with sections of uphill, downhill, and level running. We asked the participants to run the same circuit three times, once at self-adjusted normal, fast, and slow speeds (Figure 5.1, left). The periods of rest and the walking bouts, in between the running segments, were manually removed from the analysis. The local ethics committee approved the present protocol, and we conducted the measurements in agreement with the declaration of Helsinki.

Each participant was equipped with two time-synchronized sensors (Physilog 4¹, Gait Up, Switzerland) strapped on the dorsum of the shoe. Each sensor included a triaxial accelerometer, a triaxial gyroscope, and a barometer. The barometer was sampled at 50 Hz. Acceleration (\pm

¹Datasheet available in the Appendix.

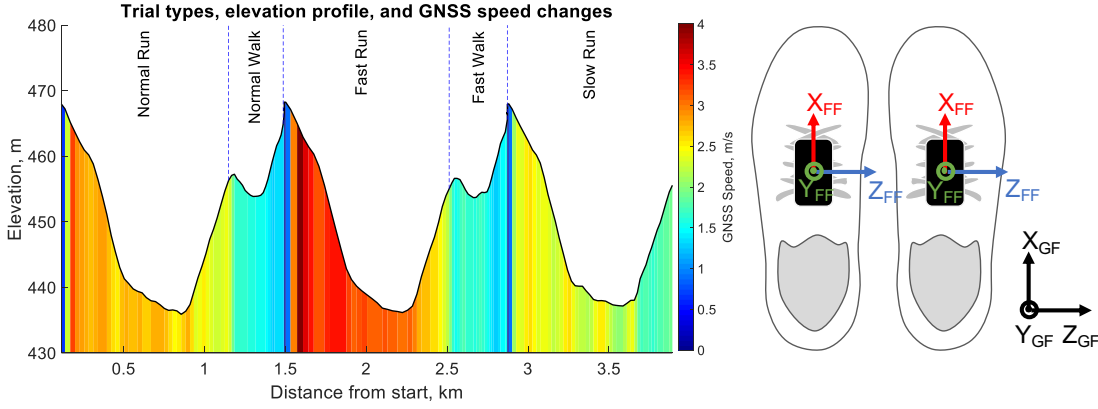


Figure 5.1 – (Left) The elevation and speed of the running circuit. This figure was adapted from (Soltani et al., 2019). (Right) the definition of the foot functional frame (FF) and global frame (GF) used in this study.

16g) and angular velocity (± 2000 deg/s) were recorded at 500 Hz and were calibrated according to (Ferraris, F., Grimaldi, U., & Parvis, 1955) before each measurement session. Furthermore, a GNSS receiver (Camm8Q, u-blox, CH) with an external active antenna (ANN-MS, u-blox, CH) was mounted on the head using Velcro attached to a cap. GNSS was used as a reference system for the estimation of the running speed. The GNSS receiver was set to pedestrian mode with a sampling frequency of 10 Hz. With such a configuration, the datasheet of the manufacturer reported a median error of 0.05 m/s for instantaneous speed estimation. MATLAB software (R2018b, MathWorks, Natick, MA USA) was used for all the data processing steps without the need for publicly available libraries.

5.2.2 Estimation of reference GNSS speed

The reference speed obtained from the GNSS receiver was processed according to (Soltani et al., 2019) and in two steps (Figure 5.2). First, we enhanced the signal by removing the outliers that did not correspond to running; hence, we removed all recorded speed samples outside of the 5-20 km/h range. Moreover, the GNSS receiver provided an estimation of the accuracy of each observation; hence we discarded any data-point with an error higher than 0.15 m/s. This process retrieved an unevenly sampled reference speed signal. We applied a moving average of 0.5-second width (in 10 Hz), followed by linear interpolation to obtain an equally-spaced time series at 10 Hz. In the second step, the signal was down-sampled to provide the reference speed (v_{ref}), after a fourth-order low-pass Butterworth filter with the cut-off frequency at 0.25 Hz to reduce the noise.

5.2.3 Speed estimation based on direct integration of foot acceleration

In this section, we describe the sequence of transformations that we applied on the IMU and barometer data to extract the gait features. The whole process can be summarized in four tasks:

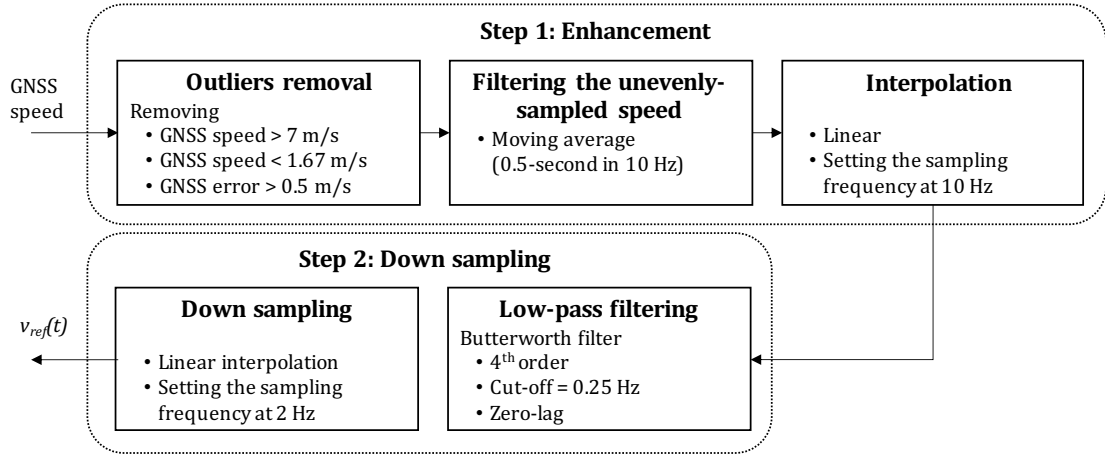


Figure 5.2 – Pre-processing steps applied to the GNSS measurements of speed to obtain the reference speed estimation. This figure was adapted from (Soltani et al., 2019).

pre-processing, temporal analysis, spatial analysis, and foot speed estimation (Figure 5.3).

Pre-processing

First, a 4th-order low-pass Butterworth filter ($F_c = 50$ Hz) was applied on the raw acceleration (a_t) and angular velocity (ω_t) signals to reduce the noise. Then the IMU signals were aligned with the foot segment by computing the rotation matrix that transforms the data recorded in the technical frame of the sensors into the functional frame (FF) of the foot (Figure 5.1, right). For this purpose, we used the measurements of level normal walking (Figure 5.1, left) and a previously reported calibration method (Falbriard et al., 2018). This process aligned the y-axis of the IMU with the vertical axis of the foot, pointing upward, the z-axis to the mediolateral axis, pointing to the right side of the subject, and the x-axis to the longitudinal axis, pointing towards the forefoot. Throughout this paper, if not mentioned otherwise, the data are reported in the functional frame of the foot.

The last phase in pre-processing was estimating the overground slope. As the mechanics of running differ between level, uphill, and downhill running (Vernillo, Giandolini, et al., 2017), we assumed that the elevation difference between successive steps would be a relevant input for the model. Therefore, the barometric pressure was converted by the hypsometric equation to the altitude signal (Bolanakis, 2017) smoothed by applying a 4-seconds moving average filter and down-sampled to 1 Hz time-series. The slope (st) was defined as the altitude difference between two samples spaced by 5 seconds, by assuming that changes of altitude shorter than 5 seconds would not have a significant effect on the running speed.

Temporal analysis

Temporal events detection was performed as described in Falbriard et al. (2018) by segmenting the race into midswing-to-midswing cycles and detecting of several temporal events within

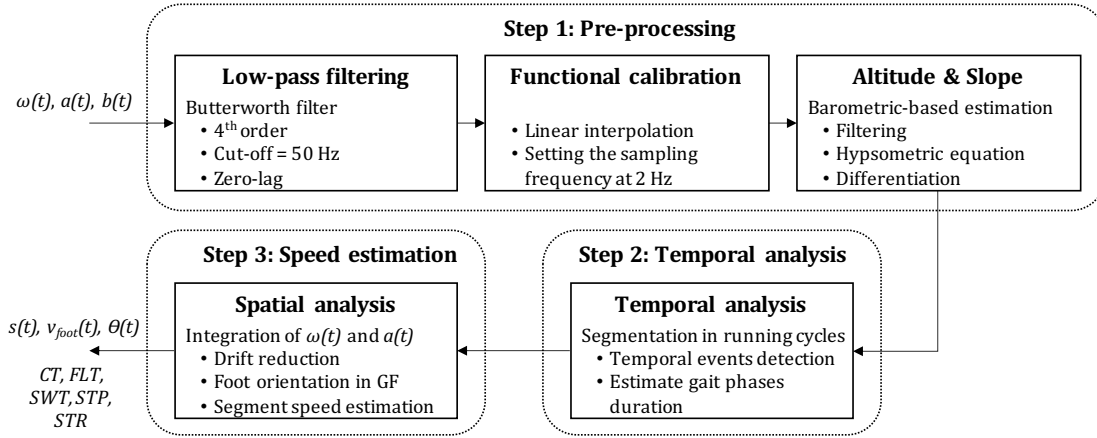


Figure 5.3 – Steps performed on the IMU acceleration $a(t)$, angular velocity $\omega(t)$, and barometric pressure $b(t)$ measurements. The outputs were later used for feature extraction; the slope $s(t)$, the speed of the foot $v_{foot}(t)$, the pitch angle $\theta(t)$, contact time CT, flight time FLT, swing phase duration SWT, step duration STP and stride duration STR

each cycle. Midswing was detected as the positive peaks observed on the pitch axis (FF z-axis) of the angular velocity measurements. Moreover, we improved the robustness of the peak detection algorithm by applying the YIN auto-correlation method (De Cheveigné & Kawahara, 2002) over a 10-seconds sliding window (5-seconds overlap) to obtain an approximation of the cadence and set an adequate minimum time difference between two peaks. The initial contact event (IC), defined as the moment when the foot initiates contact with the ground at landing, and terminal contact (TC), defined as the instant when the toes leave the ground during the pushing phase, were then detected within each cycle using the two minimums of the pitch angular velocity. Moreover, we defined the event MinRot as the time-point where the norm of the angular velocity ($\|\omega_t\|$) is minimum within the stance phase (i.e., between IC and TC).

Spatial analysis and foot speed estimation

This process aimed to measure the orientation of the foot in the global frame (GF), remove the Earth's gravitational acceleration from the recorded acceleration, and integrate the corrected acceleration to obtain the speed of the foot. In GF, the x-axis was in the running direction, the z-axis corresponds to the axis perpendicular to the ground surface, and the y-axis was defined by the cross-product of the z and x-axes (Figure 5.1). Using a previously validated technique (Falbriard et al., 2020), foot orientation was obtained in GF and foot acceleration in FF was expressed in GF and the gravitational acceleration ($g = [0 \ 0 \ 9.81] \text{ m/s}^2$) removed. The resulting acceleration (in GF) was integrated using a trapezoidal rule to get a first estimate of the speed of the foot. We considered the speed of the foot to be zero during the stance phase and, therefore, estimated and removed the integration drift by linearly resetting the speed between MinRot and TC of each stance phase. Note that we preferred MinRot to the IC for drift resting since MinRot corresponds to the time sample when the foot is the closest to a static

state, reportedly used as the integration limits in walking gait analysis (Mariani et al., 2010). We finally applied the inverse of the quaternions mentioned above to get the drift-corrected speed of the foot segments ($v_{foot}(t)$) in the FF.

5.2.4 Development of a linear model for speed prediction

Feature extraction, linearization, and outliers removal

First, we extracted several parameters (p_j) for each step, which were later used as inputs for the speed estimation model. As several studies reported on the association between the changes in the duration of the gait phases and the running speed (Högberg, 1952; Nummela et al., 2007; Saito et al., 1974), we computed the ground contact time (CT), the flight time (FLT), the swing time (SWT), the step duration (STP), and the stride duration (STR) for each step i , where $i = 1 \dots N$, and N is the total number of steps (Eq. 5.1-5.5).

$$CT_i = TC_i - IC_i \quad (5.1)$$

$$FLT_i = IC_{i+1} - TC_i \quad (5.2)$$

$$SWT_i = IC_{i+2} - TC_i \quad (5.3)$$

$$STP_i = IC_{i+1} - IC_i \quad (5.4)$$

$$STR_i = IC_{i+2} - IC_i \quad (5.5)$$

As a few strides suffered from misdetections, outliers were removed according to (1) a valid stride must last between 0.37 and 2.5 seconds, and (2) the flight phase (FLT) must be greater than zero. Pitch angle (θ) at the IC was extracted as the angle between the longitudinal axis of the foot (FF x-axis) and the ground surface (x and y-axis in GF). A positive pitch angle corresponds to a rear-foot landing (i.e., talus region lower than the toes) and a negative pitch angle to a forefoot strike.

We also extracted several statistics from the acceleration $a(t)$, the angular velocity $\omega(t)$, the foot speed $v_{foot}(t)$, and the slope $s(t)$ time-series. Moreover, since $a(t)$, $\omega(t)$, and $v_{foot}(t)$ were 3-dimensional signals, these statistics were computed for each axis (i.e., x, y, and z) and the norm of the signal. Note that the features were captured on the signals of a single stride (i.e., between IC_i and IC_{i+2} , where $i = 1 \dots N$) before applying the statistical functions. We opted for a stride-based segmentation instead of the step-based segmentation because a stride corresponds to one period of gait and, therefore, is more likely to capture the complete pattern of a cycle. Besides, the list of selected features (Table 5.1) aimed to collect information in the

Type	Feature	Description
Intensity	mean_<T>_<C>	Mean value
	std_<T>_<C>	Standard deviation
	med_<T>_<C>	Median
	iqr_<T>_<C>	Interquartile range
	max_<T>_<C>	Maximum
	rms_<T>_<C>	Root-mean-square
Shape	kurt_<T>_<C>	Kurtosis
	skew_<T>_<C>	Skewness
Compression	arm1_<T>_<C>	First coefficient of the auto-regressive model of order 3
	arm2_<T>_<C>	Second coefficient of the auto-regressive model of order 3
	arm3_<T>_<C>	Third coefficient of the auto-regressive model of order 3

Table 5.1 – List of the features extracted for each stride on the continuous acceleration $a(t)$, the angular velocity $\omega(t)$, the foot speed $v_{foot}(t)$, and the slope $s(t)$. In the name of the feature, variables <T> and <C> correspond to the label of the signal and to the channel, respectively. Hence <T> must be replaced by a , ω , v_{foot} , or s while <C> must be replaced by x, y, z, or norm.

intensity of the signal (e.g., mean, STD, RMS), the shape of its distribution (e.g., skewness, kurtosis) and its shape in a compressed format (e.g., coefficient of the auto-regressive model). Moreover, as the temporal parameters (Eq. 5.1-5.5) already hold relevant periodic information, we did not consider features in the frequency domain.

Before proceeding to the selection of the best features, we visualized the relation between the reference speed $v_{ref}(t)$ and the features individually. Based on our observations, we identified three functions that improved the linear relationship between the reference speed and some of the input features; $f_1(p) = p^2$, $f_2(p) = p^3$, and $f_3(p) = 1/p$. The functions f_1 , f_2 , and f_3 were applied to all the features, and the results added to the list of features. Finally, we also included several anthropometric parameters to the collection of features, such as the size, weight, gender, and age of the participants.

Data set configuration

We divided the data into three subsets: validation, training, and testing sets. The participants were randomly distributed into the three subsets. It is important to note that all the steps of a single individual were attributed to only one of the subsets; this removed the performance bias associated with the models trained and tested on measurements originating from the same subjects (Halilaj et al., 2018). Figure 5.4 shows the data from each set with different colors and illustrates their functions.

We used the 10 subjects (30%) from the validation set for feature selection (in orange in Figure 5.4), and the 23 remaining participants (70%) were used interchangeably for training (in blue in Figure 5.4) and testing (in green in Figure 5.4) of the model according to the leave-one-subject-out cross-validation method. We emphasize on the fact that the validation set

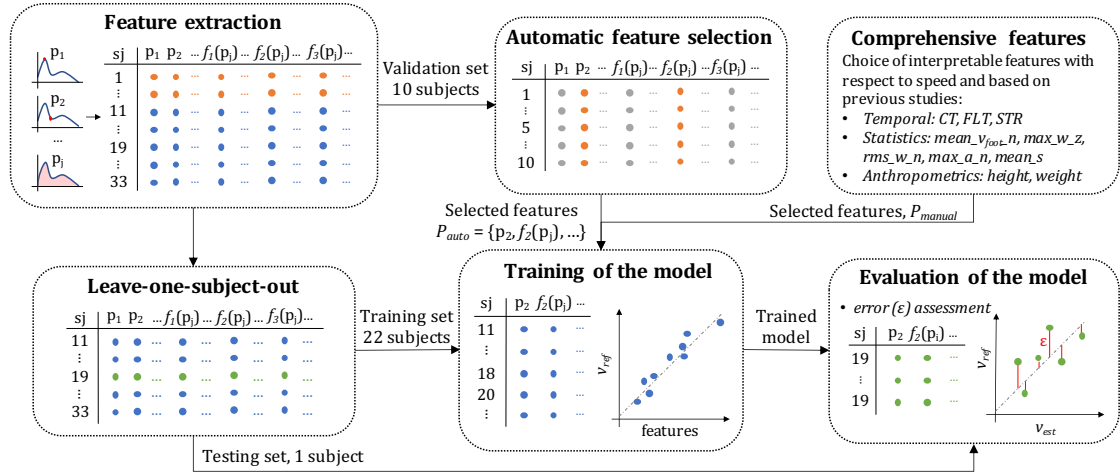


Figure 5.4 – Schematic representation of the data organization into the validation (blue), training (orange), and testing (green) set. The validation set was used for feature selection, the training set to train the coefficients of the linear model, and the testing set to evaluate the performance of the predictions. The features are represented as p_j and the linearization function as $f_1(p_j)$, $f_2(p_j)$, and $f_3(p_j)$.

was not included in the evaluation of the model and served exclusively for feature selection. We distinguished the development set from the other sets to lessen the risks of overfitting and preferred a leave-one-subject-out approach for the assessment of the model's performance due to the relatively low number of individuals present in this study. Moreover, such a method allowed us to identify potential outliers in the participants and later find collections of subjects with similar biases.

The leave-one-subject-out cross-validation method functioned as followed: we trained the model using the data from 22 subjects (training set) and tested on the data from one individual (testing set). We then repeated this process, such that each participant appeared once in the testing set.

Automatic feature selection

Here, we selected the features (P_{auto}) to minimize the mean-square error (MSE) of the speed estimation model using the ordinary least squares method. The leave-one-subject-out method was applied with 11 subjects for training and one subject to evaluate the error of the predictions (Figure 5.4). The automatic feature selection process started with an empty set of inputs and sequentially added the parameters p_j or their transform (f_1 , f_2 , f_3), which minimized the average MSE among all the subjects. This method is known as the forward stepwise selection process and has proven to be reliable on large feature space (John et al., 1994; Kohavi & John, 1997). The algorithm stopped including new parameters if the gain in the average MSE was lower than 1% of the previous MSE recorded. We deliberately set a low 1% criterion to obtain a possibly unnecessary large number of inputs knowing that the model is trained using the

LASSO method (Tibshirani, 1996) with shrinkage of the redundant features. To ensure that the features contributed equally to the MSE estimation, we rescaled the inputs using a robust z-score normalization method (Jain et al., 2005); after normalization, the feature's mean was equal to zero, and median absolute deviation equal to one (less sensitive to outliers than the variance of one).

Comprehensive selected features

Although a supervised and automatic feature selection method may retrieve the subset with the best prediction performance on a given set of parameters, the results are sometimes difficult to interpret. Hence it is generally recommended also to evaluate the performance of a comprehensive set of features selected based on their biomechanical relevance (Halilaj et al., 2018). Based on the findings of previous research in running, we defined a list of features (P_{manual}) known to be affected by variations in the running speed. Similarly to the automatic selection of features, we willingly selected a large number of input features, potentially inter-correlated, knowing that optional inputs will be discarded later in the training stage. In summary, comprehensive features included the following:

- Anthropometric features: the height because taller individuals are likely to have longer step length, thus higher speed, than shorter individuals with similar flight times.
- Temporal features: the CT, FLT, and STR contain relevant information about the stride frequency and were shown to decrease with an increase in the running speed (Chapman et al., 2012; Nummela et al., 2007; Saito et al., 1974).
- Speed and spatial features: the average speed of the foot ($mean_v_{foot_norm}$) obtained with a direct integration; the maximum angular velocity of the foot in the sagittal plane (max_w_z) assuming faster swing involves higher speed; the RMS value of the angular velocity norm (rms_w_norm) since higher speed should result in higher dynamic movements; the maximum of the acceleration norm (max_a_norm) as it was demonstrated in previous studies that tibial peak accelerations increased with faster-running velocities (Sheerin et al., 2019); and the average slope ($mean_s$) since uphill and downhill may affect the running speed.

Training and testing of the model

The linear model was trained and tested with the leave-one-subject-out cross-validation method. For each individual, the performance of the speed prediction was evaluated with the model's coefficients trained on 22 other subjects. This approach was preferred to a traditional split of the data into two data sets (e.g., 70% training and 30% testing) due to the restricted number of subjects available after the feature selection phase. Besides, the leave-one-subject-out procedure allowed us to detect potential outliers in the participants and, therefore, possibly identify the sources of poor estimation results.

The least-squares regression coefficients were trained using the LASSO method (Tibshirani, 1996), with scaled inputs to have zero mean and a variance of one, and equally distributed the observations' weights at the initialization stage. To limit the risks of overfitting, we selected the model with the smallest number of inputs, if any new input would improve the MSE by less than 2%.

Since we observed some disparity in the data set (the steps between 2.5 m/s to 4 m/s were over-represented), we used a random under-sampling (RUS) method to deal with the issue of class imbalance (Pes, 2020). This process started by dividing the range of reference speeds into five equally spaced groups, from 1.4 to 2.2 m/s, 2.2 to 3 m/s, 3 to 3.8 m/s, 3.8 to 4.6 m/s, and 4.6 to 5.4 m/s. We then randomly selected the same number of steps from each group based on the group with the least amount of steps (i.e., down-sampling of the majority). We repeated this process ten times, generating ten versions of the under-sampled data set and used these subsets independently. In other words, we trained and tested the model ten times for each individual.

Finally, we investigated the changes in the speed prediction when input features were averaged over consecutive steps. Instead of using a single step granularity for running speed, averaging over several steps might conceivably improve the precision (i.e., random error) of the model. We tested this approach on an even number of steps (i.e., 2, 4, 6, 8, and 10), for it equally includes the sensor's information from both feet. In order to avoid grouping non-consecutive steps, we applied this averaging process before under-sampling the inputs.

5.2.5 Personalized model

Running speed estimation algorithm

Recently, online personalization methods have emerged in the field of human movement analysis. For instance, such an approach demonstrated significant improvement in speed estimation performances (Soltani et al., 2019). The objective is to personalize a generic speed estimation model based on the sporadic reference data obtained from a GNSS device. We describe the online-learning procedure used in this study in the following; we define n as the observation (or sample) index used for the personalization where each sample corresponds to one stride. Therefore, if we have M samples (i.e., strides) for the personalization, then $n \in \{1, 2, 3, \dots, M\}$.

Let's Q be the number features in each stride. We defined \vec{p}_n as the feature vector and sl_n as the reference stride length for the n -th stride according to Eq. 5.6-5.7. Here, $p_j[n]$ is a symbolic name for the j -th feature of the n -th stride. Moreover, $v_{ref}[n]$ is the GNSS speed of the n -th stride.

$$\vec{p}_n = [1 \quad p_1[n] \quad p_2[n] \quad \cdots \quad p_Q[n]] \quad (5.6)$$

$$sl_n = v_{ref}[n] \times \frac{1}{STR_n} \quad (5.7)$$

For \vec{p}_n we used the selected features in P_{manual} or P_{auto} based on results obtained in the linear model. We first modeled the stride length through Recursive Least Square (RLS) and then multiplied that by the stride frequency to obtain the running speed. The RLS is a real-time and computationally effective online learning method, which does not need to have or store all the training data from the beginning of training.

Let P_n and SL_n be the feature matrix and the vector of actual stride length defined in Eq. 5.8-5.9, respectively.

$$P_n = \begin{bmatrix} \vec{p}_1 \\ \vdots \\ \vec{p}_n \end{bmatrix} \quad (5.8)$$

$$SL_n = \begin{bmatrix} sl_1 \\ \vdots \\ sl_n \end{bmatrix} \quad (5.9)$$

Using the RLS approach, SL_n can be modeled as in Eq. 5.10, where β_n is the coefficient of the model trained using n observations. If P_{n-1} and β_{n-1} are the feature matrix and model coefficients estimated using $n-1$ samples, then once we obtain a new sample (\vec{p}_n and sl_n) for the personalization, β_n can be recursively estimated through Eq. 5.10.

$$\beta_n = \beta_{n-1} + D_n \vec{p}_n (sl_n - \vec{p}_n^T \beta_{n-1}) \quad (5.10)$$

Where D_n , known as the dispersion matrix, itself, is recursively estimated by having only D_{n-1} (i.e., the dispersion matrix estimated using $n-1$ samples) and the new personalization data (i.e. \vec{p}_n and sl_n) according to Eq. 5.11. Here, K_n is defined as Eq. 5.12.

$$D_n = D_{n-1} (I - \vec{p}_n (I + K_n)^{-1} \vec{p}_n^T D_{n-1}) \quad (5.11)$$

$$K_n = \vec{p}_n^T D_{n-1} \vec{p}_n \quad (5.12)$$

For each individual, ten strides from the training set were used to initialize the recursion process of the RLS.

Cross-validation

The data set was organized differently for the personalization process to consider the gait style of each individual and minimize the training data from GNSS. Data from each individual was divided into bouts of 10 strides, and half of these bouts were assigned randomly to the training set and the other half to the testing set of that same individual. Consequently, we trained and evaluated the models for each individual separately, using the uniquely the data from that same individual.

5.2.6 Statistical analysis

We evaluated the performance of the model by computing the error on the training and testing sets. We did so going from a single step to a ten-steps resolution according to the configuration of the inputs. For each of the RUS iteration, the intra-subject accuracy (or bias) and precision were estimated using the mean and standard deviation, respectively. The normality of the speed error was tested using the Lilliefors test, and in the case of non-normal distribution, the mean was replaced by the median and standard deviation by the Inter-Quartile Range (IQR). To better understand the performance of the system, the intra-subject RMS error was calculated, and the Pearson correlation coefficient was used to assess the linear dependence of the predictions. Since we used the leave-one-subject-out method for training and testing, the results were reported by computing the mean, the standard deviation, the minimum and the maximum on the intra-subject biases, precision, RMS error, and correlation coefficients. Agreement between the reference GNSS speed and the estimated speed was illustrated with Bland & Altman plots (Bland & Altman, 1986). Furthermore, to evaluate the distribution of the errors and possible overfitting, we used the cumulative distribution function (CDF) of step absolute error for both training and testing sets.

5.3 Results

5.3.1 Direct speed estimation

Two subjects were excluded from the data set; because of the poor quality of the GNSS measurements or because of an improper fixation of the IMU on the shoe and high Signal to Noise Ratio (SNR) of the kinematic data. Since it required no learning, the direct speed estimation method was performed on the 63'435 steps available in this study. We observed an inter-subject mean \pm STD (min, max) of 0.08 ± 0.10 (-0.12, 0.27) m/s for the bias, 0.16 ± 0.04 (0.08, 0.25) m/s for the precision, 0.20 ± 0.06 (0.08, 0.34) for the RMSE. The relation between the speed estimation error and the overground velocity is presented in Figure 5.5, and the effect of the slope in Figure 5.6.

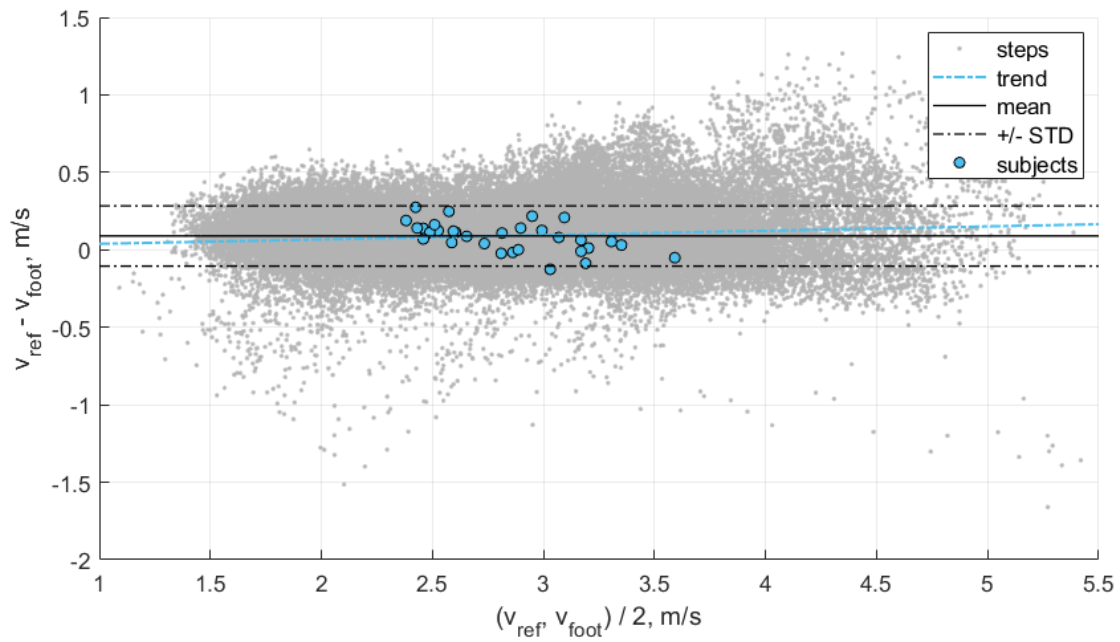


Figure 5.5 – Bland-Altman plot of the agreement between the direct speed estimation method (v_{foot}) and the GNSS reference (v_{ref}). The error was estimated with a granularity of one step. The dashed blue line represents the best linear fit according to the least square method.

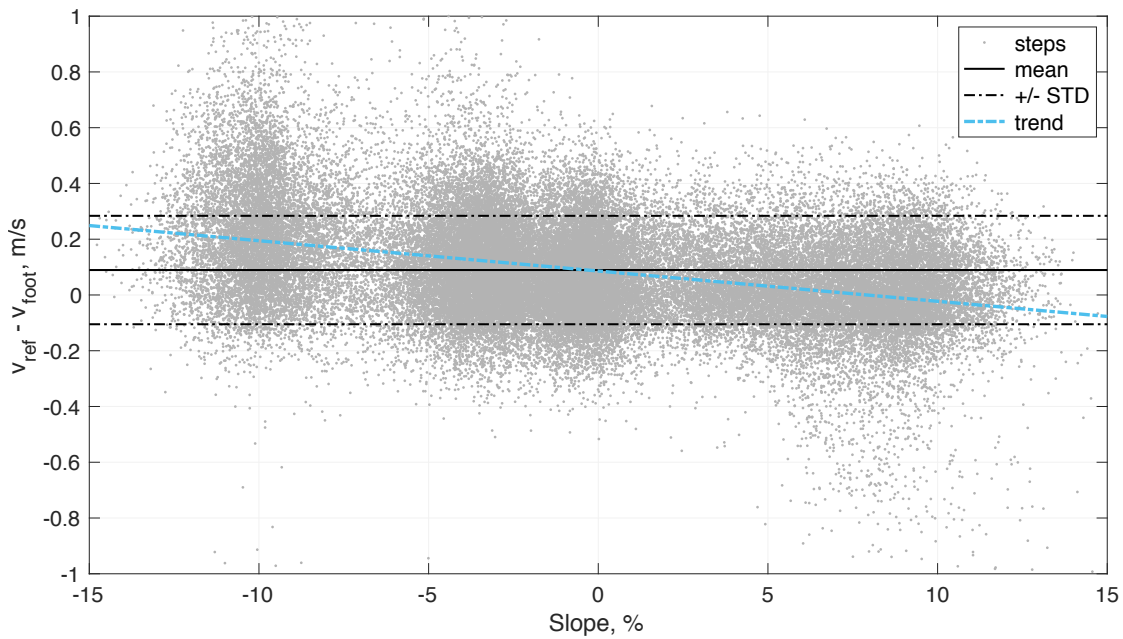


Figure 5.6 – The step by step error of the direct speed estimation method (v_{foot}) in relation to the slope of the ground surface. The dashed blue line represents the best linear fit according to the least square method.

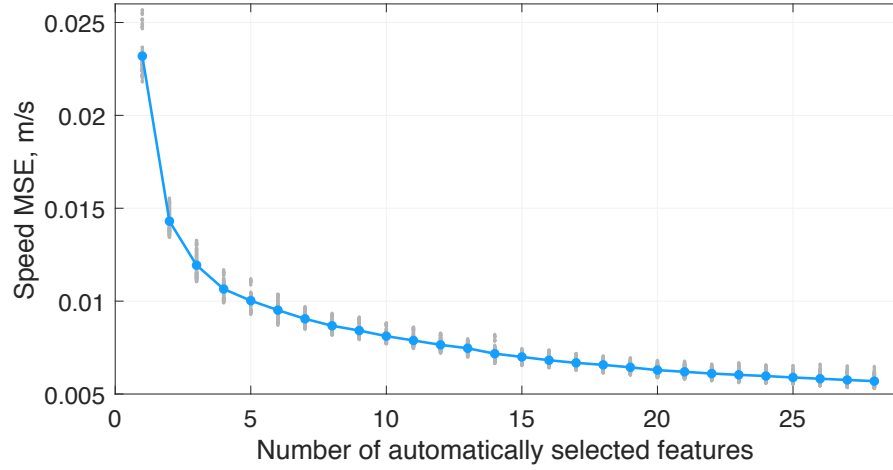


Figure 5.7 – Mean Square Error (MSE) of the speed estimation during the forward step-wise selection process. In grey, the MSE of each subject and blue the inter-subject average.

Automatic feature selection

In total, we used the 20'084 strides of the validation set to select 28 features out of the 668 features available. The feature selection process stopped at average Mean Square Error (MSE) of 0.0057 m/s (Figure 5.7), which corresponded to a 1.12% improvement compared to the previous step with 27 features. The selection process was repeated 100 times (i.e., 10 times for each of the 10 subjects) and led to the set of features presented in Table 5.2.

Out of the 28 features selected, 16 (57%) resulted from one of the three linearization functions (f_1 , f_2 , f_3), one feature from the temporal analysis (STR), one from the orientation estimation (θ). The other features are statistics extracted from the different time series (i.e., acceleration $a(t)$, angular velocity $\omega(t)$, the velocity of the foot segment $v_{foot}(t)$, and the slope $s(t)$).

5.3.2 Linear model

In total, 43'351 steps were used to train and test the linear model. Due to the subdivision of the data associated with the leave-one-subject-out method, we used, for each individual, an average \pm STD (min, max) of 41'287 \pm 188 (41'032, 41'642) steps for training and 2'064 \pm 188 (1'709, 2'319) steps for testing. When the P_{auto} feature set was used for training, the LASSO method always favored the same 7 inputs $P_{auto,best}$ among the 28 features previously selected (Table 5.2):

$$P_{auto,best} = \begin{bmatrix} mean_a_norm & f_1(mean_s) & f_3(STR) & f_2(median_w_z) & \dots \\ max_v_{foot_norm} & f_1(mean_v_{foot_norm}) & f_3(median_w_norm) \end{bmatrix} \quad (5.13)$$

#	Label	f(p)	#	Label	f(p)
1	<i>mean_a_norm</i>	-	15	<i>mean_v_foot_y</i>	p^2
2	<i>mean_v_foot_norm</i>	-	16	<i>median_ω_norm</i>	p^{-1}
3	<i>iqr_a_norm</i>	-	17	<i>median_ω_x</i>	-
4	θ	-	18	<i>skew_v_foot_norm</i>	-
5	<i>mean_s</i>	p^2	19	<i>iqr_v_foot_norm</i>	p^{-1}
6	STR	p^{-1}	20	<i>max_v_foot_y</i>	p^{-1}
7	<i>median_a_x</i>	p^3	21	<i>mean_ω_y</i>	-
8	<i>median_ω_z</i>	p^3	22	<i>rms_a_x</i>	p^3
9	<i>max_v_foot_norm</i>	-	23	<i>median_v_foot_x</i>	-
10	<i>median_a_y</i>	p^3	24	<i>std_a_norm</i>	p^{-1}
11	<i>mean_v_foot_x</i>	p^2	25	<i>skew_ω_norm</i>	-
12	<i>skew_v_foot_y</i>	p^{-1}	26	<i>skew_ω_z</i>	p^2
13	<i>median_v_foot_y</i>	-	27	<i>std_a_x</i>	p^{-1}
14	<i>std_ω_z</i>	-	28	<i>arm3_v_foot_y</i>	p^{-1}

Table 5.2 – The ordered list of the features automatically selected by the forward stepwise selection algorithm.

In comparison, with P_{manual} the LASSO method selected 4 inputs ($P_{manual,best}$):

$$P_{manual,best} = [rms_ω_norm \quad mean_v_foot_norm \quad mean_s \quad CT] \quad (5.14)$$

The performances of the linear predictor over the testing set are shown in Table 5.3; the inter-subject mean, STD, minimum, and maximum are presented for the bias, the precision, the RMSE, and the correlation coefficients. The results of the running speed estimation are presented for single-step resolution and also where the inputs were averaged over 2, 4, 6, 8, and 10 steps before being used by the linear model.

In comparison, when we used a moving average (4 steps) on the output of the speed estimation model (i.e., not the inputs as in Table 5.3), then we obtained an inter-subject mean \pm STD (min, max) bias of 0.00 ± 0.10 (-0.17, 0.17) m/s, precision of 0.13 ± 0.05 (0.06, 0.23) m/s, RMSE of 0.14 ± 0.05 (0.08, 0.28) m/s, and correlation coefficients of 0.985 ± 0.010 (0.956, 0.997). The agreement between the speed estimation using $P_{auto,best}$ (v_{est}) and the reference GNSS system is presented for each stride (grey dots) and each individual (blue circles) in Figure 5.8.

Figure 5.9 (left) shows the CDF of the speed estimation error for each subject (grey lines) and the subjects aggregated (blue line). In total, 56% of the recorded steps have an error below 0.1 m/s and 86% below 0.2 m/s. Finally, as illustration of overground measurement of speed over a various range of self-adjusted speed, the speed obtained with the reference GNSS system was compared for a typical subject with the speed estimation at step level ($v_{est,1}$), and the estimation when averaged over four steps ($v_{est,4}$) in Figure 5.9 (right).

Features	Steps	Bias (m/s)			Precision (m/s)			RMSE (m/s)			R		
		mean	STD	min	max	mean	STD	min	max	mean	STD	min	max
$P_{auto,best}$	1	0.00	0.10	-0.17	0.17	0.14	0.05	0.08	0.24	0.16	0.05	0.10	0.28
	2	0.00	0.11	-0.17	0.18	0.13	0.05	0.06	0.23	0.14	0.05	0.08	0.27
	4	0.00	0.11	-0.17	0.19	0.12	0.06	0.05	0.24	0.12	0.05	0.07	0.24
	6	0.00	0.11	-0.17	0.18	0.11	0.05	0.05	0.23	0.12	0.04	0.06	0.21
	8	0.00	0.11	-0.18	0.19	0.11	0.05	0.05	0.23	0.12	0.05	0.06	0.23
	10	0.00	0.11	-0.17	0.19	0.11	0.05	0.05	0.23	0.11	0.04	0.06	0.23
$P_{manual,best}$	1	0.00	0.11	-0.22	0.17	0.15	0.06	0.09	0.29	0.18	0.07	0.11	0.37
	2	0.00	0.11	-0.23	0.18	0.13	0.06	0.07	0.26	0.15	0.06	0.09	0.29
	4	0.00	0.11	-0.23	0.20	0.12	0.06	0.06	0.26	0.14	0.06	0.08	0.24
	6	0.00	0.12	-0.23	0.19	0.12	0.06	0.06	0.24	0.13	0.06	0.06	0.24
	8	0.00	0.12	-0.23	0.20	0.11	0.06	0.05	0.24	0.13	0.06	0.06	0.24
	10	0.00	0.12	-0.24	0.20	0.11	0.06	0.05	0.24	0.12	0.06	0.06	0.24

Table 5.3 – Inter-subject mean, STD, minimum, and maximum of the system's bias, precision, Root-Mean-Square error (RMSE), and the linear correlation coefficient (R). The results are presented for each configuration of inputs ($P_{auto,best}$ and $P_{manual,best}$).

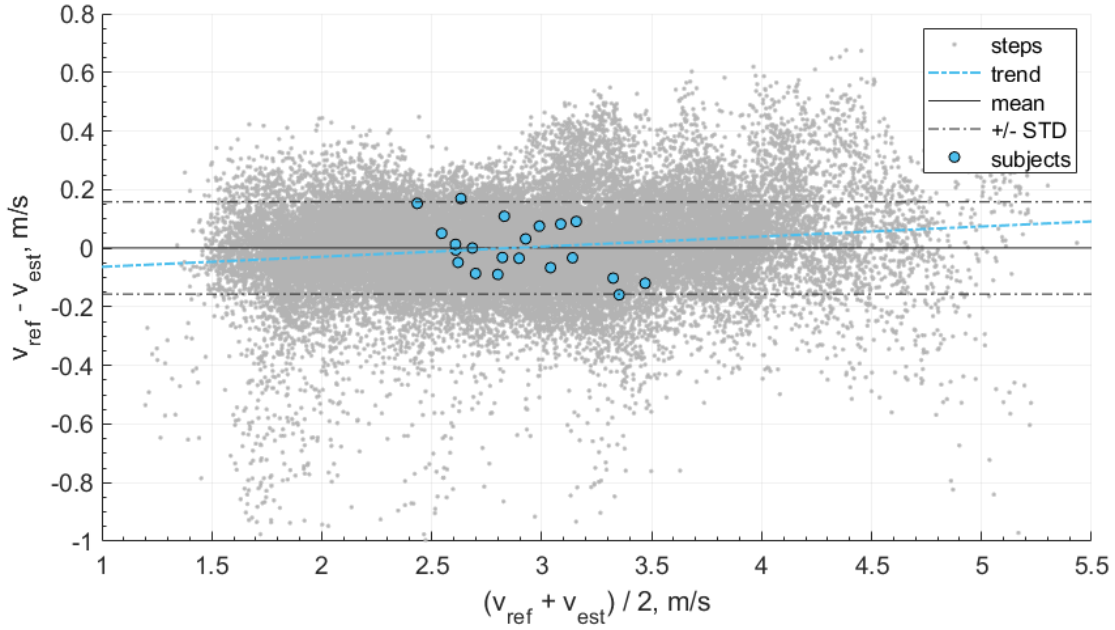


Figure 5.8 – Bland-Altman plot of the speed estimation (v_{est}) obtained with the features automatically selected ($P_{auto,best}$) and compared with the reference GNSS speed (v_{ref}). The grey dots represent the steps, the blue circle the average results of each subject, the solid black line the mean of the steps, the dashed black lines the STD of the steps, and the dashed blue line the linear trend of the steps.

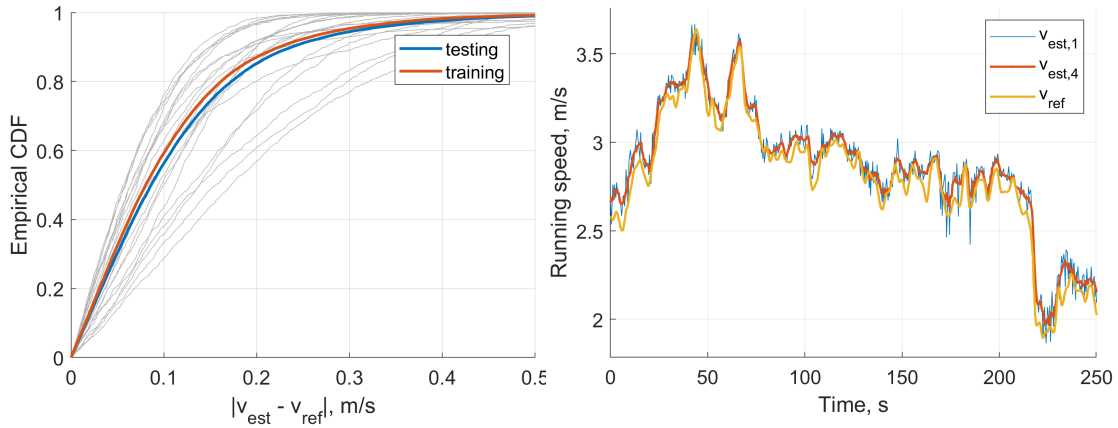


Figure 5.9 – (Left) The Cumulative Density Function (CDF) of the speed estimation error of each step ($|v_{ref} - v_{est}|$). The speed was estimated using the automatically selected inputs ($P_{auto,best}$). The grey curves represent the CDF of each individual in the testing set, the blue line the inter-subject CDF of the testing set, and the orange line the inter-subject CDF of the training set. (Right) Comparison between the speed estimation of each step ($v_{est,1}$), the speed estimation averaged over four steps ($v_{est,4}$), and the reference GNSS speed (v_{ref}).

Bias (m/s)		Precision (m/s)		RMSE (m/s)	
median	IQR	median	IQR	median	IQR
0.00	0.01	0.09	0.03	0.09	0.06

Table 5.4 – Inter-subject median and Inter-Quartile Range (IQR) of bias, precision, and RMSE of the personalized model.

5.3.3 Personalization

We used the features in P_{manual} to train and test the personalized model since the results of the generic model show little differences between $P_{auto,best}$ and $P_{manual,best}$, and because, with P_{manual} , we could include the 10 subjects from the validation set in the training and testing process without any risk of overfitting. For each subject, the training samples (i.e., half of the data of the subject, randomly selected) were fed one-by-one to the RLS, and the speed was estimated with the complete test set of the subject. Figure 5.10 shows this process for the first 150 strides used for personalization of the model; the solid line and the shaded area represents the inter-subject mean and standard deviation of the RMSE, respectively. Also, the evaluation error for the first 10 strides is not displayed in Figure 5.10; these strides were used to initialize the RLS algorithm.

In total, we used 1139 ± 149 strides for training and 1132 ± 149 strides for testing for each individual. Table 5.4 reports the bias, precision, and RMSE of the personalized model. Figure 5.11 also shows the Bland-Altman plot of the personalized model where the mean and standard deviation of the error is displayed by the dark and dotted lines, respectively. Moreover, the Spearman's test showed a high correlation of 0.97 between the estimated and the reference values of running speed.

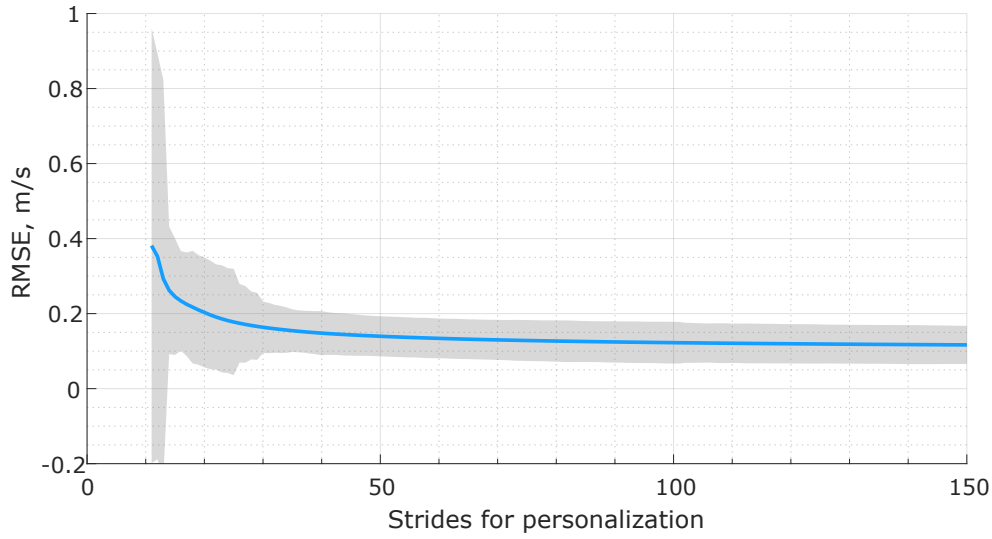


Figure 5.10 – Evolution of the RMSE error during the personalization of the speed model. Here, the solid line and the shaded area represent, respectively, the inter-subject mean and standard deviation of the RMSE. The x-axis corresponds to the number of strides used for the personalization. Note that, for a better visualization of the error evolution, the figure is zoomed only on the first 150 samples used for personalization.

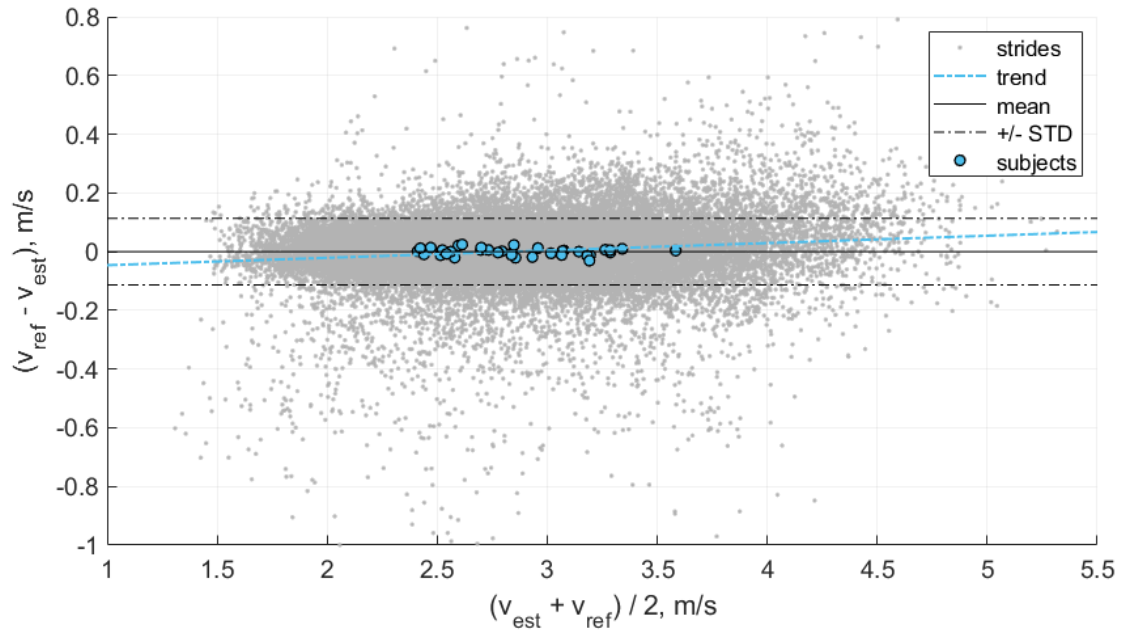


Figure 5.11 – Bland-Altman plot of the proposed personalized model. Here, the points represent samples in the testing of all subjects. The dark and dotted and lines show a mean and standard deviation of the error, respectively.

5.4 Discussion

In this study, we proposed three methods to estimate overground running speed using feet worn sensors. First, we estimated the overground speed using solely the velocity of the foot obtained through the direct integration of the acceleration. We evaluated this direct method to test our hypothesis that the accelerometer fails to provide the correct value during the flight phase due to the combination of rotational and translational accelerations. Nevertheless, the velocity of the foot, with other relevant features, was selected as the input of the second method based on a linear model to predict the running speed. Thanks to an exhaustive features selection procedure and cross-validation approach, the model predicted the running speed with better accuracy. Finally, we assumed that the running technique varies among individuals, but that it should be well correlated with individual gait features. Therefore, we showed that the performance of running speed could be improved using an online-personalization method with sporadic access to some GNSS data. It is important to note that the same method could be extended to less complicated instrumentation (e.g., a stopwatch over a fixed distance).

The speed estimation result for the method based on v_{foot} only confirmed our hypothesis that the direct integration of the acceleration, as proposed for walking, cannot be generalized to running due to the presence of aerial phases. The inter-individual mean bias (0.08 m/s) we observed indicates that the direct integration method underestimates the speed during the phase of flight. This underestimation confirms the inexact measure of the translational movement by the accelerometer during the flight phase. Moreover, the trend displayed in the Bland & Altman plot (Figure 5.5) indicates that the system underestimates the velocity more at faster speeds. This observation is coherent with our hypothesis; the higher the speed, the greater the distance covered during the phase of flight (i.e., longer step length) (Nummela et al., 2007). Slope also seems to be a confounding factor of the error (Figure 5.6), with higher errors obtained during downhill running. In conclusion, v_{foot} itself does not characterize the speed of the subject as it cannot measure the distance covered during the period of the flight, but v_{foot} was a good proxy for speed and was one of the main features for speed prediction based on the linear model.

The selection of relevant features in the linear model was a crucial phase. Feature selection was carried over 20'084 steps and aimed to retrieve the most relevant features among the 668 variables available. Although we used a high-dimensional feature space, the curse of dimensionality issue did not apply as we used approximately 30 times more observations for feature selection. The results of the feature selection process show that the cost function (i.e., MSE) decreased quickly with the first few inputs and then stabilized as additional features were included (Figure 5.7). We set the stopping criteria intentionally low (i.e., 1% improvement in the MSE), knowing that the LASSO method used for training the model would ignore the inputs with redundant information. Interestingly, several of the features manually selected (P_{manual}) were among the first to be selected by the automatic process (P_{auto}); however, using different linearization functions (Table 5.2).

The linear model required inputs parameters from the temporal and spatial domain, as well as overground slopes. Hence a precise estimation of related parameters is paramount to optimize the precision of the speed estimation. The methods used to obtain these parameters should always be carefully reported and, ideally, previously validated. Interestingly, the model did not select the FLY parameter and instead favored the inverse of the stride duration (i.e., the stride frequency); hence none of the features selected required a bipedal configuration of the sensors allowing us to use the model with a single foot-worn IMU in the future. Also, none of the anthropometric parameters was necessary for the estimation of the running speed. This result is somewhat surprising, as we expected the height to be an essential input.

Apart from its computation time greediness, one reported issue of the forward selection algorithm is that decisions made early in the process cannot be changed, therefore potentially affecting its performance when the inputs are correlated (Derksen & Keselman, 1992). Although we observed some correlation in the inputs, we presumed that the two-fold selection process (i.e., stepwise selection and LASSO) would not be significantly affected by that matter. Moreover, the linearization of the feature-space was an essential component of this study. We selected f_1 , f_2 , and f_3 functions based on visual inspection of the data, and out of the 28 pre-selected features, 16 (57%) resulted from these linearization functions.

Although the performance of the automatically selected set of features ($P_{auto,best}$) performed slightly better than the comprehensive set of features ($P_{manual,best}$), the differences remain in the order of a few centimeters per second (Table 5.3). Indeed, the estimations based on $P_{auto,best}$, with a granularity of 1, over-performed the ones using $P_{manual,best}$ by 0.01 m/s in the inter-subjects STD of the bias, 0.01 m/s in average precision, and display a slightly lower RMSE. These differences are relatively little since several elements in $P_{manual,best}$ were among the most relevant features selected by the LASSO regression method in $P_{auto,best}$, or at least were highly correlated. The results also show that averaging the inputs over several steps had a moderate effect on the performance of the system; it reduced the random error of the system with mean precision values consistently decreasing from 0.14 m/s for the step level estimation to 0.11 m/s when the granularity decreased to 10 steps. Also, when the output of step level estimated speed was averaged over four steps, the precision slightly improved (0.13 ± 0.05 m/s). Hence, whether the inputs or the outputs are averaged does not seem to affect the performances of the model.

Overall, the linear method showed good prediction results across a wide range of speed and slope, observed in real-world conditions (Figure 5.9, right). It principally removed the mean bias of the method based on v_{foot} only and slightly improved the precision. The Bland-Altman plot in Figure 5.8 shows a good agreement between the linear model and the reference GNSS system. The linear trend of the error (dashed blue line) is almost horizontal ($y = 0.0034x + 0.098$), which suggests that the running speed has little effect on the error. These results support the usage of the RUS technique on the training data; the model ensured that all the ranges of speeds observed were equally represented. Although procedures more sophisticated than the RUS method have been proposed, they do not always provide a clear

advantage in the results (Japkowicz, 2000). Moreover, the CDF curves of the training and testing sets do not indicate clear overfitting of the training data (Figure 5.9, left) as the training set attains better performance than the testing set, but these are within an acceptable range.

It seems challenging to reduce further the STD of the bias using such a linear model since it depends on the inter-subject differences as it has previously been reported that individuals use different spatiotemporal adaptations at similar speeds. For instance, previous studies have shown that the relationship between stride frequency and stride length was specific to each subject (Nummela et al., 2007; Saito et al., 1974). These limitations were also encountered by previous studies that aimed to estimate the running speed based on body-worn inertial sensors. In (Yang et al., 2011), the authors used a shank-worn IMU to measure the velocity of the shank and compared it with the speed of a motored treadmill. The study was conducted at five predefined speeds (2.5, 2.75, 3, 3.25, 3.54 m/s), with seven participants, and the error was calculated as the difference between the average estimated speed over 30 strides and the constant speed of the treadmill (i.e., the bias). The results show inter-trial mean and STD of the bias of 0.11 ± 0.03 m/s at 2.5 m/s, 0.10 ± 0.03 m/s at 2.75 m/s, 0.08 ± 0.02 m/s at 3 and 3.25 m/s, and 0.09 ± 0.02 at 3.5 m/s. The biases reported in (Yang et al., 2011) are in range with those obtained in our study. However, the measurements were performed on a leveled treadmill at a discrete and limited number of running speeds, and the results were averaged over 30 strides (i.e., 60 steps). By considering the foot and shank as a single rigid body, the authors in (Chew et al., 2017) used foot-worn inertial sensors with ten participants and a similar approach as in (Yang et al., 2011). Based on the errors reported at each speed (8, 9, 10, 11 km/h), our method outperformed the one proposed in (Chew et al., 2017). Aiming to evaluate the accuracy and the repeatability of a commercialized foot-worn running assessment system (RS800sd, Polar, Kempele, Finland), the authors in (Hauswirth et al., 2009) performed 30-seconds measurements at multiple speeds (from 12 to 18km/h) and compared the speed estimations with the speed of the treadmill. Even though the commercialized system required a subject-specific calibration, the reported mean \pm STD bias of -0.03 ± 0.14 m/s indicates a slightly less accurate estimation of the running speed than the method proposed in this study. In a study (Herren et al., 1999) conducted in outdoor conditions, the authors explored whether triaxial accelerometric measurements can be combined with subject-specific neural networks to assess speed and incline of running accurately. The authors reported an RMSE of 0.12 m/s for average speed the whole running trial which is similar to our linear model estimations when the inputs are averaged at least four steps.

In a recent effort to reduce the inter-subject differences in the bias, researchers in De Ruiter et al. (2016) proposed a personalized speed estimation model based solely on the measurement of the contact time (CT). They obtained the CT using shoe-worn inertial sensors and conducted the measurements on an outdoor 2 km long tarmac. First, they personalized a model ($\text{speed} = \alpha CT_d$) for each of the 14 participants based on the average speed over several bouts of 125 meters. Then, they compared the personalized estimation results with those obtained with a stopwatch over a fixed 120-meters distance ($N = 35$ bouts) and reported a median RMSE of 2.9 and 2.1% (two runs). In comparison, our linear model method obtained a mean RMSE

of 5.1% at step level estimation, and the personalized method a median RMSE of 3.1%. This slightly higher RMSE in our study is partly reflecting the variety of slopes in our measurements in comparison to the level running in (De Ruiter et al., 2016).

A recent study (Soltani et al., 2019) proposed a real-world speed estimation method based on wrist-worn inertial sensors. The authors obtained a median [IQR] (Inter-Quantile Range) bias of -0.02 [-0.2 0.18] m/s and precision of 0.31 [0.26 0.39] m/s for the non-personalized method. These results improved using a personalization technique similar to this study, with 0.00 [-0.01 0.02] and 0.18 [0.14 0.23] for the bias and precision, respectively. Hence, for both the personalized and non-personalized methods, this study out-performed the wrist-based estimation of the running speed.

The linear model is accurate for “average people” (i.e., individuals with typical running patterns), and individuals with an atypical running technique will give rise to higher speed estimation errors (Figure 5.8). In comparison, the personalized model adapts to the movements of each individual; thus, it ensures a bounded error for “average” and “atypical” individuals (Figure 5.11).

The proposed personalization demonstrates significant improvements in the performance of the real-world running speed estimation. As reported in Table 5.4, the personalization process improved the IQR of the bias by at least a factor of 10 and the median precision by roughly 30% by employing approximately 35 times less training data than the non-personalized linear model. The personalized model bypasses the bias caused by the intrinsic variation of individuals during real-world running. This observation is best characterized by Figure 5.10, which demonstrates the relatively fast convergence of the proposed RLS-based personalization; after roughly 50 strides, the model stabilized. As a consequence, the personalized model does not require continuous GNSS value to be updated. Once a good performance is reached, GNSS switch to off to save batteries. Moreover, the proposed personalized method is based on an online learning technique that does not require a database; hence it saves time and energy. It allows real-time speed estimation, computationally optimized, and does not need to store training data.

5.5 Conclusion

In this study, we proposed and evaluated three different methods for real-world speed estimation in running: direct speed estimation, training based linear model, and a personalized model. The direct estimation of the foot velocity confirmed the hypothesis that accelerometers inaccurately measure the translational motion of an individual during the flight phase; therefore, techniques developed for walking analysis can not be generalized to running. We evaluated the linear model for two sets of features: automatically selected (i.e., optimized) or manually selected (i.e., comprehensive features). The model performed best when we averaged its output over a few steps and showed that 4 steps (i.e., two left strides and two right strides) provided an acceptable trade-off between performance (bias: 0.00 ± 0.11 m/s;

precision: 0.12 ± 0.06 m/s) and time-resolution. The personalized method tested in this study, used an online-learning technique based on recursive least-squares to personalize the speed estimations for each individual. Our results indicate that such an approach primarily helps to reduce the inter-subject bias (0.01 m/s) but also improves the average random error by more than 30%.

Based on the results of this study, we recommend using the linear model for speed estimation when the recordings of other accurate devices are temporarily unavailable and personalized the model when these recordings are available. For instance, the system can be used as a complement to a GNSS device experiencing sparse communication, either due to a reduced transmission bandwidth (e.g., indoor running, city centers) or because of electrical power limitations (e.g., low power systems).

Acknowledgment

The authors thank M. Ziqi Zhao for his participation in the data analysis of the personalized model.

Real-World Applications **Part III**

6 Gait Changes, Foot Strike Pattern and Stiffness During Marathon Running

Abstract

Achieving a marathon race has become one of the ultimate objectives of a high number of runners. It has also become the favorite playground on running research, as it involves multiple and complex mechanisms (e.g., biomechanics, physiology, fatigue, injury prevention). New opportunities appeared with the emergence of new lightweight wearable sensors allowing the continuous recording of relevant parameters. This study aimed to assess the evolution of spatiotemporal parameters, stiffness, and foot strike angle during a marathon and determine possible breaks in running patterns. Twelve recreational runners were equipped with a GNSS watch, and two inertial measurement units clamped on each foot to run the 2017 Geneva marathon. Data were processed and split into 8 sections of 5 km. Using a linear mixed model, we observed significant changes around the 25th kilometer. Contact time, fly time, swing time, speed, duty factor, stride length, maximal ground reaction force, vertical stiffness, leg stiffness, and foot strike angle were affected, and two breaks between consecutive sections were observed: one around Km 25 and another around Km 35. No changes were observed on stride duration, vertical oscillations of the center of mass, and leg length. Surprisingly, the average foot strike angle decreased during the race. However, each participant kept a rearfoot strike. This could be explained by the effect of fatigue on the running gait. Moreover, the two breaks we observed are possibly due to the alteration of the stretch-shortening cycle and by reaching physiological limits. This study highlights new measurable phenomena that can be analyzed through continuous monitoring of athletes and recreational runners.

Keywords: IMU, marathon running, temporal parameters, foot strike, stiffness

Chapter to be submitted as Meyer, E, Falbriard, M., Mariani, B., Millet, G. P., & Aminian, K. IMU-based measurement of changes in gait, foot strike pattern and stiffness during a marathon.

Contributions: conceptualized the study design; conducted the data collection; designed the algorithms; contributed to the interpretation of the data.

6.1 Introduction

The number of recreational runners participating in marathon races has drastically increased in the past decade, with approximately one million participants in 2018. There is also a large body of scientific literature on marathon running (i.e., Pubmed: over 2000 publications with “marathon” in the title), including many studies describing how running-induced fatigue can alter the runners’ gait which in turn can lead to running-related injuries. Marathon running is considered as the pinnacle of distance running and therefore constitutes a logical playground for the analysis of gait alterations with the increase of fatigue (Larson et al., 2011; Joseph Mizrahi et al., 2000; Paquette & Melcher, 2017).

Different setups have been proposed to investigate fatigue in marathon running. The most common one is based on the comparison of Post- versus Pre- responses as in Nagel et al. (Nagel et al., 2008). In this study, the authors reported an increase of peak plantar pressure beneath the metatarsal head in 200 runners. Similarly, Post-to-Pre comparison showed differences in 3D knee kinematics both in walking and running on 20 participants (Tian et al., 2020).

An alternative method consists of carrying several biomechanical measurements during a marathon race, as used by Bertram et al. (Bertram et al., 2013). They compared the gait characteristics obtained with a force plate in 84 runners at Pre-, km 18, and km 36. They observed a progressive decrease of speed but little changes in maximal ground reaction forces. Similarly, Larson et al. (Larson et al., 2011) recorded foot contact videos of only one left and one right step at km 10 and 32 for 936 runners during a marathon race. The results show an increase of rearfoot strikers between these points. A similar method was used on elite runners at four laps of a marathon (Hanley et al., 2019), where a minimum of 54% of male runners were rearfoot strikers and 67% for women. These values stayed consistent throughout the four laps of the race. Recently, a decrease in tibial acceleration peaks measured by an inertial measurement unit (IMU) was reported in 222 runners between km 10 and km 40, with rearfoot strikers seemingly more affected (Ruder et al., 2019). However, the relationship between foot strike pattern and injury risks has been debated for long (Stacoff et al., 2016).

Nicol et al. (Nicol, Komi, & Marconnet, 1991b) investigated the changes in running mechanics by performing one maximal sprint test every 10 km during a simulated overground marathon. They observed a significant decrease in the maximal sprinting speed after 20 km, with an increase in the significance level at 30 and 42 km. The contact time during these sprints increased from the beginning to the end of the race, and the average vertical force significantly decreased. The authors noted that the repetitive impacts altered the stretch-shortening cycle and consequently reduced the efficiency of the locomotion.

Another method of investigation consists of a laboratory simulation. For instance, in (Kyrö-lainen et al., 2000) participants were asked to run a marathon on a treadmill at a constant speed, and only a minor increase in stride frequency and decrease in stride length was observed while the kinematic parameters (hip, knee, and ankle angular displacements and velocities), contact time, external mechanical work and power were maintained.

Overall, there is a scarcity of reports on the changes in running mechanics (kinetics or kinematics) observed continuously. Wearable sensors could be a valuable alternative for providing continuous data throughout the marathon races. In a preliminary study with only three athletes, Reenalda et al. (Reenalda et al., 2016) used eight IMUs. Each participant was followed by a cyclist to allow recording of the IMUs data on a datalogger connected by Bluetooth. Recently, Clermont et al. (Clermont et al., 2019) equipped 27 runners with a commercial IMU placed on the sacrum, allowing the report of subject-specific changes in the spatiotemporal parameters of gait during a marathon race. To our knowledge, these later studies are the firsts to provide a continuous biomechanical analysis of marathon competitions and confirm that body-worn sensors are valuable tools to analyze the biomechanics of locomotion (running or walking) in real-world settings.

However, one limitation of the previously cited study is its use of commercial body-worn inertial sensors without publicly available and validated estimation methods for spatiotemporal and kinematic estimations. Nowadays, emerging literature provides validated methods to determine the running spatiotemporal and kinetic parameters (Falbriard et al., 2018, 2020). Hence, the present study aimed to assess the continuous changes in spatiotemporal parameters, stiffness, and foot strike angles (FSA) in a marathon race by using foot-worn inertial sensors in recreational runners based on validated algorithms. This study is one of the first to investigate the continuous changes in foot strike patterns and stiffness during “real” marathon competition.

6.2 Material and Methods

6.2.1 Protocol

A total of 12 recreational runners (age: 36 ± 10 year; size: 178 ± 7 cm; weight: 72 ± 6 kg; race time: 231 ± 27 min [179 – 246 min]) participated in this study. Each participant was equipped with a shoe-worn IMU (Physilog 5¹, Gait Up SA, CH) located on the dorsum of each foot. The accelerometer and gyroscope were recording at 512 Hz with an operating range of $\pm 16g$ and ± 2000 deg/s, respectively. We set the barometer to record the atmospheric pressure at 64 Hz with an operating range of 260 to 1260 hPa. The participants also wore their personal Global Navigation Satellite System (GNSS) tracking system (i.e., commercialized watch or belt). The measurements were performed during the 2017 Geneva (CH) marathon (average temperature: 13°C), which has the particularity of having the same section run twice during the race (5-10 km and 25-30 km). This protocol was approved by the local ethical committee (CER-VD 2015-00006) and conducted according to the declaration of Helsinki.

¹Datasheet available in the Appendix.

6.2.2 Data processing

GNSS system - Since the configuration of the GNSS systems was different for each participant because participants used their own GNSS device, we started by pre-processing the position data to harmonize the subsequent processing tasks. We first low pass filtered the position using a 2nd-order low-pass Butterworth filter ($F_c = 0.25$ Hz) and then linearly resampled the time series at 1Hz. To compute the distance covered, we used a cumulative sum on the position difference samples. Finally, we obtained the running speed through the derivation of the position and then pre-processed the signal similarly to Soltani et al. (Soltani et al., 2019). First, we enhanced the signal by removing the outliers that did not correspond to running; hence, we removed all recorded speed samples outside of the 5-20 km/h range. This process retrieved an unevenly sampled reference speed signal; hence we applied a 3-second moving average, followed by linear interpolation to obtain an equally-spaced time series at 1Hz. Finally, we applied a fourth-order low-pass Butterworth filter with the cut-off frequency at 0.25 Hz to reduce the noise.

Foot-worn IMUs - We pre-processed the raw acceleration and angular velocity using a 4th-order low-pass Butterworth filter ($F_c = 50$ Hz) and applied the functional calibration method described in (Falbriard et al., 2018) to align the technical frame of the IMUs with the functional frame of the foot. As some of the GNSS systems did not provide the elevation signal, we obtained the running slope using the hypsometric equation on the barometric pressure data and restrained the analysis to the bout of level running (Bolanakis, 2017). Temporal events detection was performed as described in Falbriard et. al (Falbriard et al., 2018); we first segmented the race into midswing-to-midswing cycles and carried the detection of initial contact, terminal contact, and mid-stance events within the cycles. Using the event detection results, we then derived the ground contact time (CT), the flight time (FLT), the swing time (SWT), and the stride duration (STR). We also computed the duty factor (DF) (McGhee & Jain, 1972) and the stride length (STRL) by multiplying STR and the GNSS speed. In addition, we estimated the orientation of the foot in the global frame to investigate the continuous changes in FSA throughout the race. This method used a two-segment model of the foot (i.e., rear-foot and fore-foot segments) in conjunction with a bidirectional strap-down integration to estimate and reduce the orientation drift accumulating with time (Falbriard et al., 2020). Finally, we used the method proposed by Morin et al. (J. B. Morin et al., 2005) to estimate vertical (K_{vert}) and leg (K_{leg}) stiffness during the race (Eq. 6.1 - 6.2). This model allowed us to estimate the downward oscillation of the center of mass (Δz), the compression of the leg (ΔL), the maximal ground reaction force (F_{max}) from body mass, running velocity, leg length, FLT, and CT by assuming sine-wave profile for vertical ground reaction force.

$$K_{vert} = \frac{F_{max}}{\Delta z} \quad (6.1)$$

$$K_{leg} = \frac{F_{max}}{\Delta L} \quad (6.2)$$

K_{vert} and K_{leg} are often used in running to characterize the storage and return of elastic energy by a spring-mass modeling of running.

6.2.3 Statistical analysis

Before computing the statistics over the different part of the race, we targeted only level running by excluded walking and inclined period based on the following criteria: (1) the GNSS speed must be higher than 6 km/h and the time of flight greater than 0 seconds (i.e., the subject is running), and (2) the slope must be lower than 1% (i.e., level running). We then computed the mean and standard deviation for each temporal, spatial, and stiffness parameters over bouts of 5 kilometers long and investigated how these features changed throughout the race. We then applied a linear mixed model on the eight 5km-long sections, one fixed effect on the race section and a random intercept effect. All the statistical comparisons were obtained using Jamovi Software (Jamovi project 2020, Version 1.2). The overall significance level was set at $p < 0.05$, and trends discussed at $p < 0.10$. The Bonferroni pairwise comparison tests were then applied to identify differences between sections.

Since small differences in ground conditions (e.g., surface, slight incline) may influence the biomechanical responses, a comparison of the two strictly identical sections (5-10 km vs. 25-30 km) is also displayed.

6.3 Results

Running a marathon significantly alters several spatiotemporal parameters early in the race. A first significant change is visible since the Km15-20 section with a $p < 0.05$ for both the FLT (Figure 6.1) and the DF (Figure 6.2B). The SWT and CT were then significantly affected, starting at the Km 25-30 section. Figure 6.1 shows the evolution of the temporal parameters as the distance increased. Speed and STRL (Figure 6.2A and 6.2C) also show a significant decrease ($p < 0.05$ and $p < 0.001$ respectively) between the first and the last section of the race. Except for STRT, which indicates no significant difference throughout the race, all the other spatiotemporal parameters suffered from two significant breaks; first between Km 20-25 and Km 25-30 sections, and then from Km 30-35 to the last section of the race (Figure 6.1 and 6.2).

The vertical oscillations (Δz ; Figure 6.3A) and leg compression (ΔL ; Figure 6.3B) values remained constant across the marathon race, while F_{max} was already lower than at start after km15 (Figure 6.3C). A significant break in F_{max} was observed between the 20-25 and 25-30 sections and later between the 3-35 and 35-42 sections. K_{vert} and K_{leg} showed a significant decrease after km 25 (Figure 6.3D and 6.3E), and the broken trend was visible for K_{vert} between Km 20-25 and Km 25-30 sections.

Figure 6.4 shows the evolution of FSA across the different sections of the race. FSA ranged [8° - 14°], indicating that all participants were rearfoot strikers from the start and across all

Chapter 6. Gait Changes, Foot Strike Pattern and Stiffness During Marathon Running

sections (Altman & Davis, 2012; F. Meyer et al., 2018). Surprisingly, The FSA significantly decreased during the race, and after km 25, the FSA values became significantly lower than at the start.

Table 6.1 provides a detailed comparison of the race section traveled twice by the participants, first at Km 5-10 and then at Km 25-30. Relative differences between 5% and 14% were obtained for the parameters with significant differences.

Parameters	km 5-10	km 25-30	Difference (%)
FSA [deg]	10.75 ± 1.5	9.24 ± 0.58*	-14.0
K_{vert} [KN/m]	31.7 ± 7.36	29.66 ± 5.57	-6.4
K_{leg} [KN/m]	15.2 ± 3.29	13.97 ± 2.34	-8.1
F_{max} [N]	1901 ± 254	1798 ± 210*	-5.4
CT [s]	0.214 ± 0.03	0.228 ± 0.037*	6.5
FLT [s]	0.138 ± 0.02	0.126 ± 0.024*	-8.7
SWT [s]	0.490 ± 0.023	0.479 ± 0.025	-2.2
DF	0.30 ± 0.03	0.32 ± 0.04*	6.7
Speed [m/s]	3.29 ± 0.35	3.16 ± 0.42	-4.0
STRL [m]	2.31 ± 0.18	2.23 ± 0.20	-3.5

Table 6.1 – Biomechanical parameters for the two identical sections (5-10 vs. 25-30 km). Values are presented as mean ± SD. * $p < 0.05$ (Bonferroni Post hoc) between the two sections.

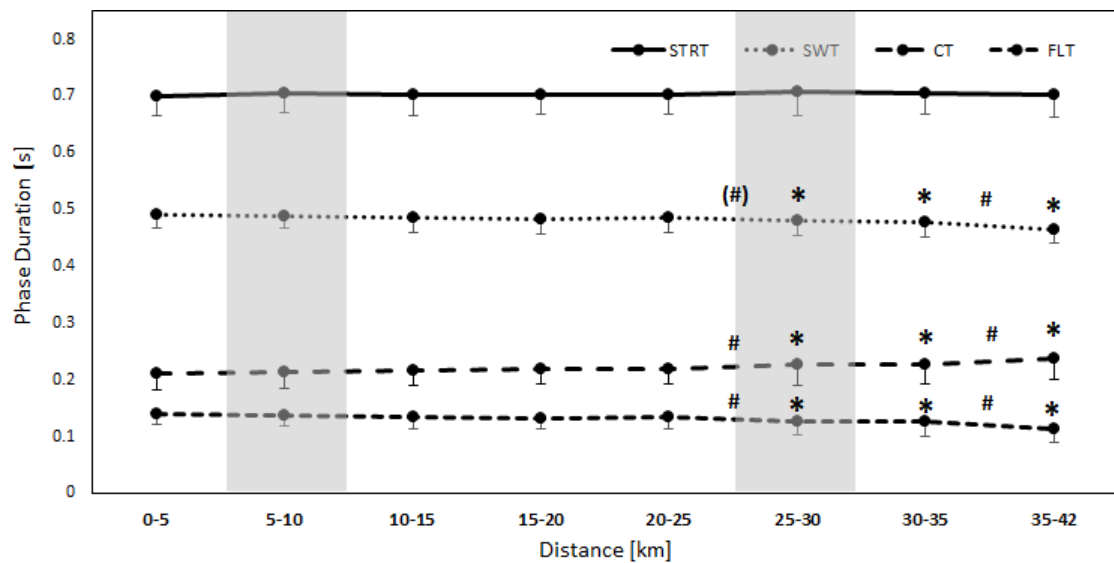


Figure 6.1 – Evolution of the temporal parameters, with changes in contact time (CT), flight time (FLT), Swing time (SW), and Stride time (STRT). A grey area indicates the two identical sections of the race. * Significant difference compared to the first section ($p < 0.05$). # Significant difference and (#) trend between two consecutive sections ($p < 0.05$).

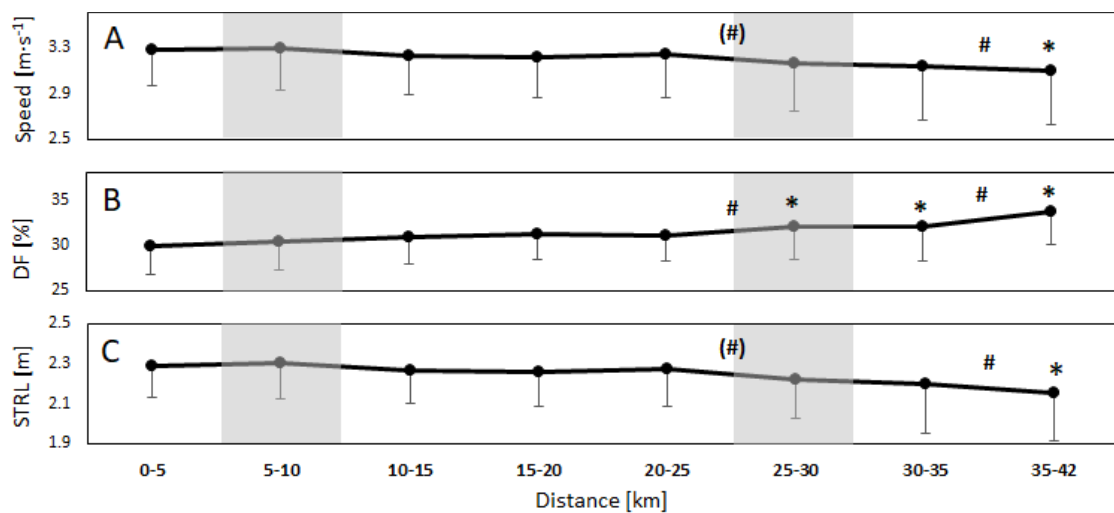


Figure 6.2 – (A) Evolution of running speed during the marathon. (B) Changes in duty factor (DF). (C) Changes in Stride length (STRL). A grey area indicates the two identical sections of the race. * Significant difference compared to the first section ($p < 0.05$). # Significant difference and (#) trend between two consecutive sections ($p < 0.05$).

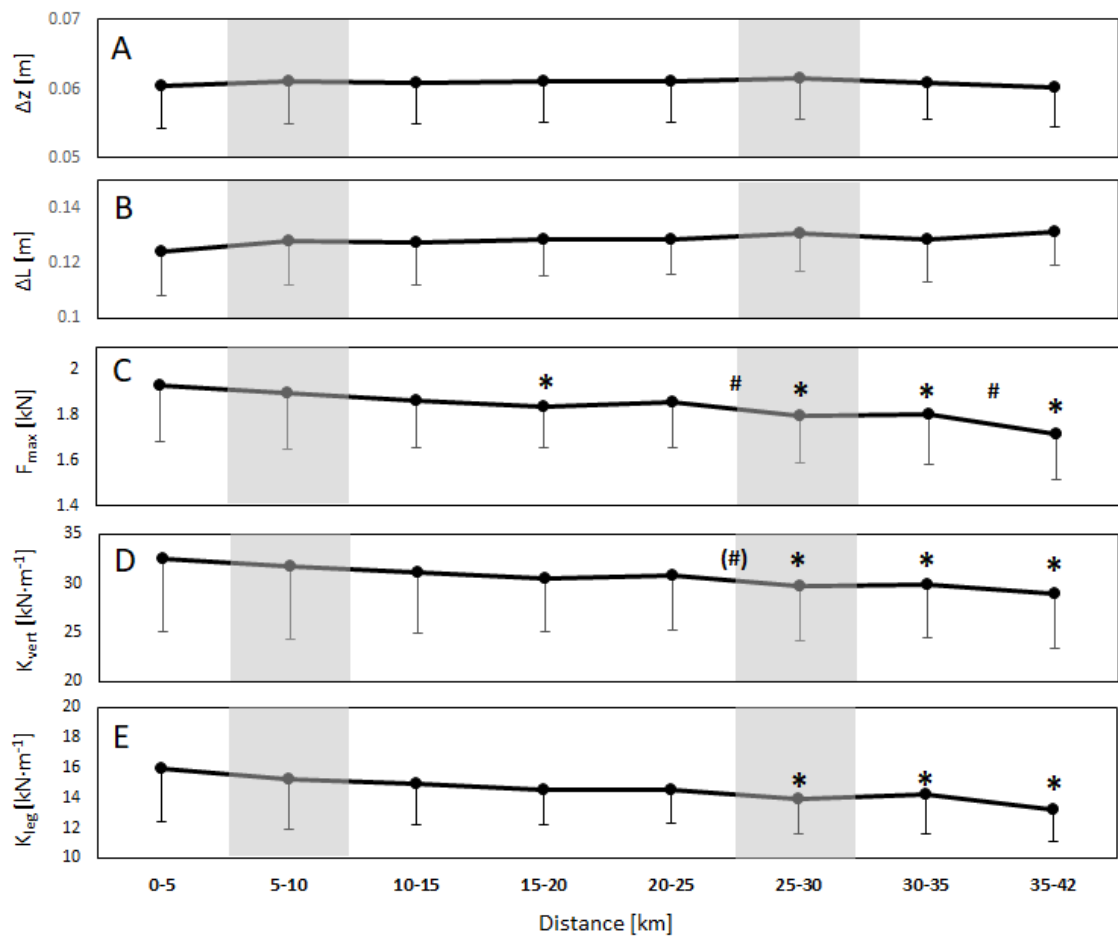


Figure 6.3 – (A) Evolution of vertical stiffness (K_{vert}). (B) Evolution of leg stiffness (K_{leg}). (C) Changes in maximal ground reaction force (F_{max}). (D) Changes in the downward displacement of the center of mass (Δz). (E) Changes in leg length (ΔL). A grey area indicates the two identical sections of the race. * Significant difference with the first (0-5 km) section ($p < 0.05$). # Significant difference and (#) trend between two consecutive sections ($p < 0.05$).

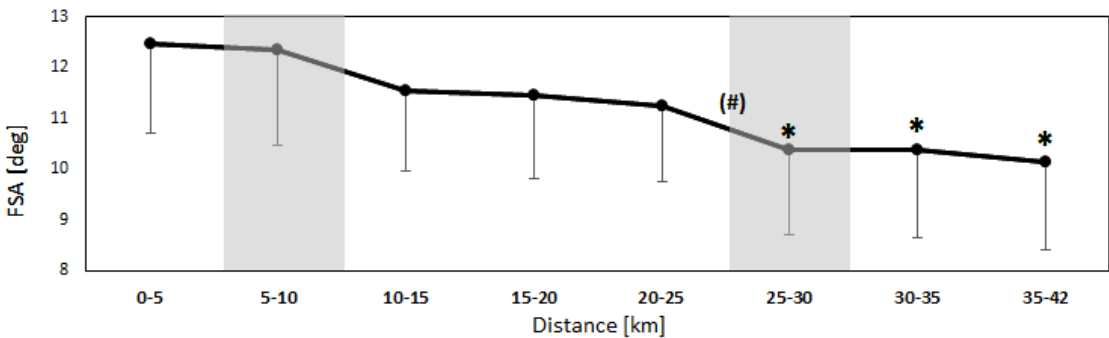


Figure 6.4 – Evolution of foot strike angle (FSA) during the marathon. Grey area indicates the two identical sections of the race. * Significant difference compared to the first (0-5 km) section ($p < 0.05$). (#) Trend for difference between two consecutive sections ($p < 0.01$).

6.4 Discussion

The current study presents novel findings regarding the alteration mechanism occurring for several biomechanical parameters of the running during marathon race measured through foot-worn inertial sensors. Also, to the authors' knowledge, it is the first attempt to report the dynamics of the main spatiotemporal parameters and more interestingly, of FSA and stiffness during a "real" marathon race.

The main finding of this work is the highlight of two breaks on the evolution of running pattern during the race: A first occurring around Km 25, and the second occurring around Km 35. It is the first time that such behavior is highlighted, and it was made possible by the continuous analysis of the marathon race. Moreover, a global look at the different curves (Figure 6.1 - 6.4) indicates a progressive alteration of several parameters during the race, reaching a significant difference around Km 25-30. This general observation is in line with the results obtained by Nicol et al. (Nicol, Komi, & Marconnet, 1991b), who assessed in a simulated marathon the changes in running mechanics by doing a maximal sprint test every 10 Km. They showed a significant decrease in the maximal sprinting speed that was significant after 20 Km, and that decreased even more at 30 and 42 Km. Using a biomechanical index, Clermont et al. (Clermont et al., 2019) observed significant changes from Km 20-22 of the race, compared to a Km 4-14 baseline. Using such an index helps to emphasize the global changes in biomechanical patterns, but also remove the possibility to analyze the behavior of each parameter individually. However, the authors did not investigate changes between consecutive sections, that could highlight sudden modifications of the biomechanical parameters.

The temporal parameters measured in the current study showed a simultaneous increase of CT and DF and a decrease of FLT during the race, resulting in a constant STR (and, therefore, a constant stride frequency) (Figure 6.1). Tests carried on a treadmill showed different results, with higher step frequency and constant CT (Nicol, Komi, & Marconnet, 1991a). Having the constraint to follow a given speed on a treadmill implies that the runners cannot change their speed and have to find another strategy to compensate for neuromuscular fatigue. Chan-roper et al. (Chan-Roper et al., 2012) observed similar differences in running speed, CT, and STRL between km 8 and km 40 of a marathon race and explained the changes by fatigue.

K_{vert} and K_{leg} obtained in this study follow the same trend, as they both decrease progressively during the marathon and reach a significant difference with the first section from Km 25-30 section (Figure 6.3). Previous studies showed that running different distances should not have the same effect on the force-production ability of the runners and their leg and vertical stiffness (Degache et al., 2013; Farley & González, 1996; J. B. Morin et al., 2011). Compared to our results, Girard et al. (O. Girard et al., 2013) obtained a similar decrease in K_{vert} during a 5 Km self-paced run, also caused by a decrease in F_{max} and a constant Δz . Nevertheless, they did not observe changes in K_{leg} . Running shorter distances, such as repeated sprinting, followed the same principle (Olivier Girard et al., 2011; Hobara et al., 2010; Jean Benoît Morin et al., 2006). On the other end, results from long-distance events such as ultra-marathon of

Chapter 6. Gait Changes, Foot Strike Pattern and Stiffness During Marathon Running

170 Km or more showed a modification of the running patterns with an increase of stride frequency, a decrease of FLT, F_{max} , and Δz resulting in a decrease of K_{leg} , but no effect on K_{vert} (Degache et al., 2016; Guillaume Y. Millet et al., 2009). According to our results, we deduce that running a marathon is short enough to affect K_{vert} and long enough to affect K_{leg} .

Stiffness and the stretch-shortening cycle have always been implicitly linked to neuromuscular fatigue. However, there is no consensus on the subjacent mechanisms. Rabita et al. (Rabita et al., 2013) found a correlation between the decrease in K_{leg} and the increase in energy consumption during a running test to exhaustion. In a second study, the same author explained the decrease of K_{leg} by changes in muscle activation using electromyography.

The FSA between 8 and 16 degrees obtained in this study corresponds to a rearfoot strike, as proposed by Altman and Davis (Altman & Davis, 2012). Therefore, each participant in this study was categorized as a rearfoot striker, like approximately 85% of recreational long-distance runners (Degache et al., 2016; Hanley et al., 2019; Larson et al., 2011). Larson et al. (Larson et al., 2011) observed changes in the foot-strike pattern between Km 10 and Km 32, with significant shifts from forefoot and midfoot to rearfoot strike. Almost no participant switch from rearfoot to another category. This corresponds to the results obtained in this study, even if a significant decrease in FSA was observed (Figure 6.4). Our method allows a deeper investigation than the evolution of the foot-strike pattern, for it provides the strike angle continuously throughout the race. The decrease of FSA observed in this study can be explained by the effect of neuromuscular fatigue. Mizrahi et al. (Joseph Mizrahi et al., 2000) reported a decrease in knee flexion after a 30 min high intensity run, suggesting that a lower amplitude in the running pattern would also reduce the FSA. Moreover, Willson and Kernozek (Willson & Kernozek, 1999) observed a decrease of heel loading after a fatigue running test and explained it by an adoption of a more midfoot landing. Their results are aligned with our findings and clearly indicate an adaptation of the runner during the race.

The Geneva marathon has the particularity to have a section ran twice by the participants, first at Km 5-10 and then at Km 25-30. This section provides twice identical conditions during the race and removes the undesired effects of slope and surface change. The results obtained (Table 6.1) reinforce the validity of the results obtained on the other sections of the race, by removing confounding factors.

Based on our observations, it was possible to find the onset of two significant breaking point during the marathon. Analyzing the groups of runners with a more homogeneous level would probably retrieve more details on the evolution of specific running parameters and linked them more accurately with the onset of fatigue. We decided to divide the race into eight sections to offer easy to read and interpret results, but the proposed system can provide a granularity up to a single step, allowing the analysis of cycle variability.

6.5 Conclusions

It is the first time that such a large amount of data was extracted from only two small and autonomous devices attached to the runners' feet. This study aimed to answer the gap between laboratory experiments and practitioners' concerns and needs in the field. Using a linear mixed model, we observed significant changes in the running gait around the 25th kilometer. Contact time, fly time, swing time, speed, duty factor, stride length, maximal ground reaction force, vertical stiffness, leg stiffness, and foot strike angle were affected. We also observed two breaks between consecutive sections: one around Km 25 and another around Km 35. No changes were observed on stride duration, vertical oscillations of the center of mass, and leg length. Future utilization of such systems will allow a more individualized analysis of the evolution of running parameters, but also provide accurate and continuous data to understand when and how runners respond to fatigue.

Acknowledgments

Special thanks to Guillaume Callias and Manuel Reynaert for their assistance during the data collection.

7 Gait Parameters and Vertical Speed During a Mountain Ultra-Marathon

Abstract

The aim of the present study was to investigate the effects of altitude and distance on uphill vertical speed and the main spatiotemporal gait parameters during an extreme mountain ultra-marathon. The vertical speed (VS), stride height (SH), and stride frequency (SF) of 27 runners were measured with an inertial sensor at the shank for two different altitude ranges (low 1300-2000 m vs. high 2400-3200 m) of 10 mountains passes distributed over a 220 km course. There was a significant interaction ($F(4,52) = 4.04$, $p < 0.01$) for the effect of altitude and distance on VS. During the first passes, the mean VS was faster at lower altitudes, but this difference disappeared at a quarter of the race length, suggesting that neuromuscular fatigue influenced the uphill velocity to a larger extent than the oxygen delivery. The average VS, SH, and SF were 547 ± 135 m/h, 0.23 ± 0.05 m, and 0.66 ± 0.09 Hz. The individual VS change for each uphill portion was more strongly correlated with the changes in SH ($r = 0.80$, $P < 0.001$, $n = 321$) than SF ($r = 0.43$, $P < 0.001$, $n = 321$). This suggests a large effect of the knee extensors strength loss on the diminution of VS.

Keywords: ultra-endurance, fatigue, altitude, uphill walking

Chapter adapted from David Jeker, Mathieu Falbriard, Gianluca Vernillo, Frederic Meyer, Aldo Savoldelli, Francis Degache, Federico Schena, Kamiar Aminian & Grégoire P Millet (2020) Changes in spatio-temporal gait parameters and vertical speed during an extreme mountain ultra-marathon, European Journal of Sport Science, DOI: 10.1080/17461391.2020.1712480.

Contributions: conceptualized the study design; conducted the data collection; designed the algorithms; contributed to the interpretation of the data.

7.1 Introduction

Mountain ultra-marathons (MUMs) have gained popularity in recent years (Hoffman et al., 2010). These events are of interest to better understand how healthy subjects cope – from both physiological and biomechanical points of view – with extreme loads and fatigue (G. P. Millet & Millet, 2012).

Similarly to running events of shorter duration, maximal oxygen uptake ($\text{VO}_{2\text{max}}$) and the fraction of its utilization are important determinants of ultra-marathon performance (G. Y. Millet et al., 2011). However, the measurement of the energy demand over the complete course of a MUM is difficult if not impossible, and the results of laboratory studies can hardly be extrapolated to a mountainous environment (Savoldelli et al., 2017). Altitude, exercise duration, elevation changes, and temperatures are making the determination of the energy cost of locomotion particularly difficult in the case of a MUM (Vernillo, Millet, et al., 2017). At the moderate altitudes (2000–3000 m a.s.l.) often encountered during a MUM, $\text{VO}_{2\text{max}}$ is reduced by 7–8% per 1000 meters above sea level (Wehrlin & Hallén, 2006). Additionally, exposure to moderate hypoxia exacerbates the development of peripheral fatigue (Amann et al., 2006; Fan & Kayser, 2016). Therefore, the negative effect of altitude on uphill performance should be greater the further an athlete gets on the racecourse during a MUM.

MUMs provide opportunities to assess the effects of prolonged uphill and downhill walking/running periods over extremely long distances on biomechanical parameters (Degache et al., 2016; J. B. Morin et al., 2011). Previous studies have measured running mechanics either at set points during a race (Degache et al., 2016; J.-B. Morin et al., 2011), or after the completion of the event (Giandolini, Gimenez, et al., 2016; Lazzer et al., 2015; J. B. Morin et al., 2011; Vernillo et al., 2014). Besides a case study (Savoldelli et al., 2017), there is a paucity of data collected during real racing conditions, thereby limiting our understanding of the changes in running mechanics during MUMs. Recording the gait parameters with an inertial sensor in the context of going up a mountain pass would broaden our knowledge in this area.

An increased stride frequency (SF) - or reduced stride length (SL) - at a constant speed is known to diminish the impact shock and the energy absorbed at the ankle, knee, and hip (Schubert et al., 2014). Despite some debate regarding the importance of the cost of running in MUM performance (Vernillo, Millet, et al., 2017), preferred SF and optimal SF remained the same following a 6-hour trail run suggesting that, despite fatigue, athletes optimize their running gait to preserve energetic efficiency (Vernillo et al., 2019). Furthermore, the muscle preservation strategies used during a MUM of extreme duration did not lead to a modification of SL or SF from pre- to post-race when tested at the same speed (Vernillo et al., 2014). However, the speed loss expected during the climbs of a MUM (Saugy et al., 2013) must be related to a reduction of the SF and/or SL. As the speed of locomotion is expressed vertically in this study, the amplitude of the strides will be referred to as stride height (SH) rather than SL. Considering that knee extensors (KE) force loss during a MUM was shown to be correlated with performance time (Balducci et al., 2017) and that SF was not affected by an improvement

in maximal strength (Sardroodian et al., 2015), loss of strength over the course of MUM should primarily affect SH. Consequently, one may hypothesize that the expected decrease in vertical speed (VS) throughout the race is mostly correlated with a decrease in the SH rather than a reduction of the SF.

To our knowledge, the combined effects of altitude and distance on uphill running/walking performance and biomechanics have never been studied to date. Therefore, the evolution of VS and other spatiotemporal gait variables during the climbs of a MUM remains unclear and would provide novel insights into the respective influence of (1) physiological factors, i.e., the convective oxygen transport altered by altitude, compared to (2) neuromuscular factors, i.e., KE muscle fatigue induced by prolonged exercise, on the performance and pacing during MUMs. The primary aim was to use an inertial sensor to investigate the effect of altitude and fatigue on VS during a MUM of extreme duration. The secondary aim was to assess the relationship between VS and SH and SF. We hypothesized that VS would be lower at higher altitude and that the decrease in VS would be greater for the highest portion of each mountain pass.

7.2 Methods

7.2.1 Participants

Twenty-seven athletes (3 women and 24 men) volunteered to participate in this study. Their characteristics are presented in Table 7.1. All subjects were experienced MUM athletes, 15 of them had finished a previous edition of the race studied. The participants were informed of the procedure and the risks involved. They gave their consent and could refuse to take part in any of the tests. The study was approved by the Institutional Ethics Committee of the University of Verona, Italy (Department of Neurosciences, Biomedicine and Movement Sciences) and carried according to the Declaration of Helsinki.

N = 27	Age (y)	Height (cm)	Weight (kg)	BMI (kg m ⁻²)	Performance index
Mean	45.3	176.7	72.8	23.3	549
SD	9.5	8.0	9.0	2.4	76.6
Range	22-64	158-193	59.8-93	19.7-28.7	412-743

Table 7.1 – Age, height, weight, body mass index and the International Trail Running Association performance index of the participants.

7.2.2 Design

The international race supporting the study was the 2015 Tor des Géants (TdG). Considered as one of the world's most challenging mountain ultra-marathon (Vernillo et al., 2016), it covers a total of 330 km and includes 24,000 m of elevation gain and loss. The maximum and minimum

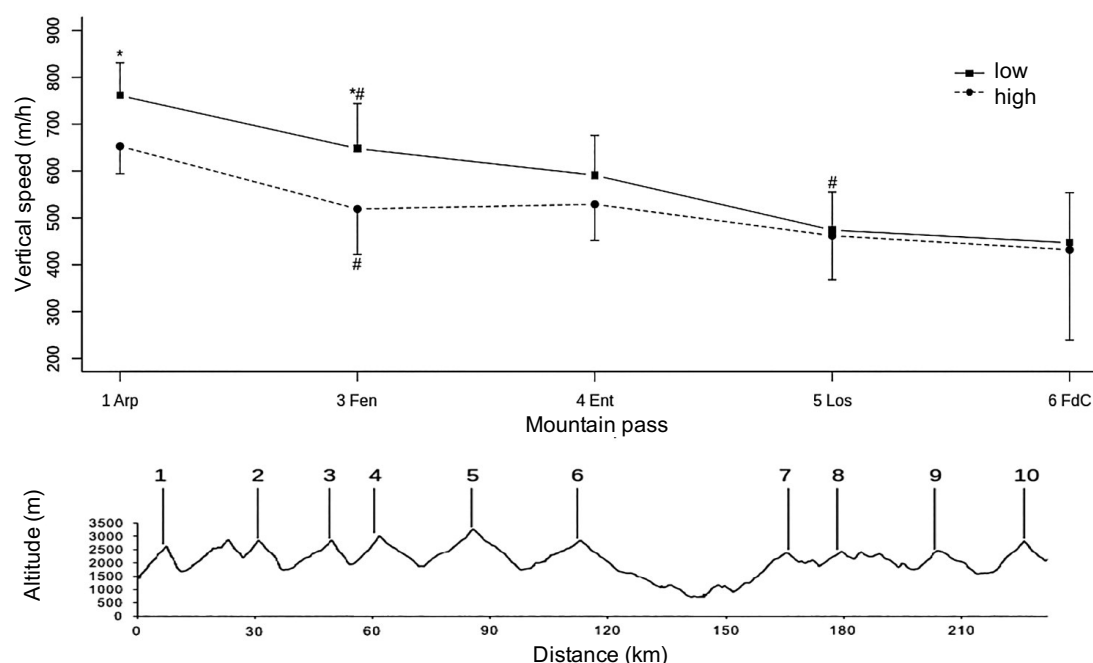


Figure 7.1 – Average vertical speed for the low (1298 to 2086 m) and high (2392 to 3204 m) portions of the first five mountain passes with both a low and high-altitude portions (A). * $p < 0.05$ for differences with high altitude. # $p < 0.05$ for differences with previous pass. Values are mean \pm SD. Mountain passes used for the measurement of vertical speed, stride height, and stride frequency (B).

altitudes are 3300 and 322 m, respectively, with 25 passes over 2000 m. The distance is divided by six major aid stations where sleeping is allowed. Ten mountain passes were divided into sections of 147-368 m of elevation gain and categorized as in high altitude (2392-3204 m a.s.l.) and low altitude (640 to 2086 m a.s.l.) portions (Table 7.2). Each section was selected to avoid flat portions or aid stations and did not start immediately after an aid station. The race was stopped a few hours after the 80-hour mark due to bad weather conditions - athletes normally have 150 h to cover the distance. Therefore, only the measurements up to the ascent of Col Pinter, which correspond to pass number 10 (Figure 7.1), were used, and only the first 5 passes with both a low and a high altitude section were used for the comparison of the VS between low and high altitudes.

7.2.3 Methodology

The movement was recorded using Physilog 4¹ Silver device (Gait Up SA, Lausanne, Switzerland). The 19 g device was attached to each participant's shank close to the ankle, encapsulated in a waterproof elastic band, and securely placed over the lateral malleoli. The device was recording tri-axial acceleration at 100 Hz, tri-axial angular velocity at 100 Hz, and the baro-

¹Datasheet available in the Appendix.

	Low				High			
	Altitude (m)			Slope (%)	Altitude (m)			Slope (%)
	Start	End	Gain		Start	End	Gain	
1. Arp	1298	1639	341	23.7	2392	2539	147	20.1
2. Crosatie	-	-	-	-	2506	2828	322	29.8
3. Fenêtre	1681	2032	351	21.7	2576	2815	239	19.1
4. Entrelor	1756	2086	330	23.2	2529	2822	293	32.2
5. Loson	1757	2010	253	13.8	2948	3204	256	23.3
6. F. di Champorcher	1614	1818	204	22.4	2508	2813	305	15.4
7. Coda	640	818	178	16.3	-	-	-	-
8. Marmontana	1683	1936	253	16.4	-	-	-	-
9. Lasoney	1707	2031	324	24.9	-	-	-	-
10. Pinter	1422	1790	368	33.5	2573	2765	192	29.1

Table 7.2 – Characteristics of the portions of the mountain passes used for the analysis of vertical speed, stride height, and stride frequency.

metric pressure at 50 Hz. First, altitude was estimated using the barometric pressure signals as in the ICAO Standard Atmosphere model and then linearly corrected using the 10 passes as altitude landmarks. A calibration process was designed to align the technical frame of the sensors with the functional frame of the shank (Falbriard et al., 2018). Knowing the time ($Time_k$) spent in each section k of the pass and the elevation difference between the lowest ($Altitude_{low}^k$) and highest limits ($Altitude_{high}^k$) of the section, average vertical velocity of each portion was estimated by Eq. 7.1:

$$\frac{Altitude_{high}^k - Altitude_{low}^k}{Time_k} \quad (7.1)$$

For each section, stride frequency (SF_k) was estimated using a 4 seconds sliding-window and was set as the fundamental frequency component of the mediolateral angular velocity of the shank obtained by Fast Fourier Transform (FFT) (Fasel et al., 2017). We then used this fundamental frequency f_0 to set the cut-off frequency ($F_c = 1.5 f_0$) of the low-pass Butterworth filter applied on the sagittal plane angular velocity signal. We used this highly filtered signal (almost a sinusoid) to find the local peaks, which we assumed to correspond to the mid-swing moment. Finally, we detected initial contact within each midswing-to-midswing period and use the detection results to compute the stride frequency (Aminian et al., 2002). There was no need to apply a high-pass filter. The determination of stride frequency using step by step detection is more accurate than using FFT that gives only a rough estimation. Stride height SH_k within each pass section was defined as Eq. 7.2, where $N_{strides}^k$ is the number of strides

detected in the k th section.

$$SH_k = \frac{Altitude_{high}^k - Altitude_{low}^k}{N_{strides}^k} \quad (7.2)$$

7.2.4 Statistical Analysis

The statistical analysis was performed using the R software (R Foundation for Statistical Computing, Vienna, Austria) using a significance level of 0.05. Two-way repeated measures analysis of variances (ANOVA) was used to determine the effect of altitude (low vs. high section of mountain passes) and distance covered (number of mountain pass during the race) on VS. Sphericity was tested using Mauchly's test, and Greenhouse-Geisser correction was applied when sphericity was violated. Normality was confirmed with the Shapiro-Wilks test. Post hoc comparisons were made using Tukey honestly significant difference. Pearson's correlations were calculated to evaluate the association between VS, SH, and SF.

7.3 Results

Of the 27 athletes participating in this study, 4 withdrew from the race before it was stopped. None of the 23 remaining athletes completed the whole 330 km. Only 6 athletes who were not involved in the study reached the finish line before the race was stopped. For the five first passes with both a low-altitude (1300-2000 m) and a high-altitude (2400-3200 m) portions, there was a significant interaction [$F(4,52) = 4.04$, $p < 0.01$]. Figure 7.2 and 7.3 shows the Tukey HSD post hoc comparison for the low and high-altitude sections of each mountain pass analyzed. The average VS, SH, and SF were 547 ± 135 m/h, 0.23 ± 0.05 m, and 0.66 ± 0.09 Hz. As shown in Figure 7.2 and 7.3, VS was more strongly correlated with SH than SF.

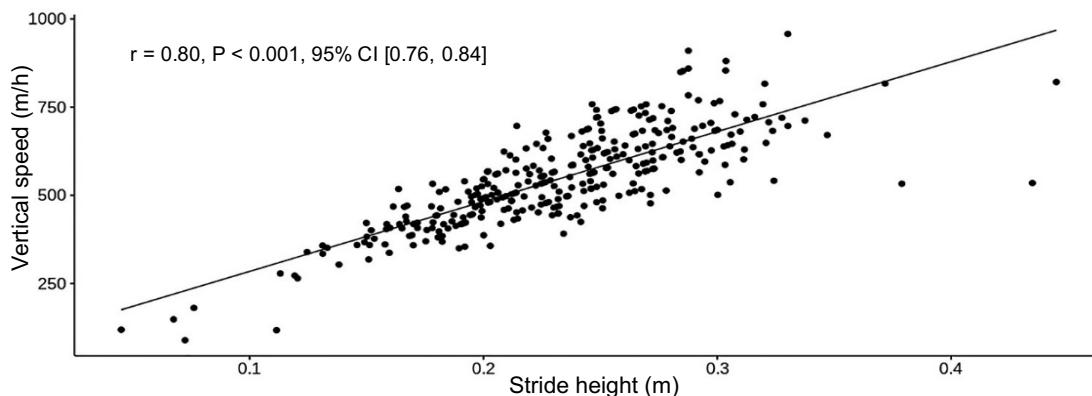


Figure 7.2 – Correlation between vertical speed and stride height for the selected uphill portions of the mountain passes.

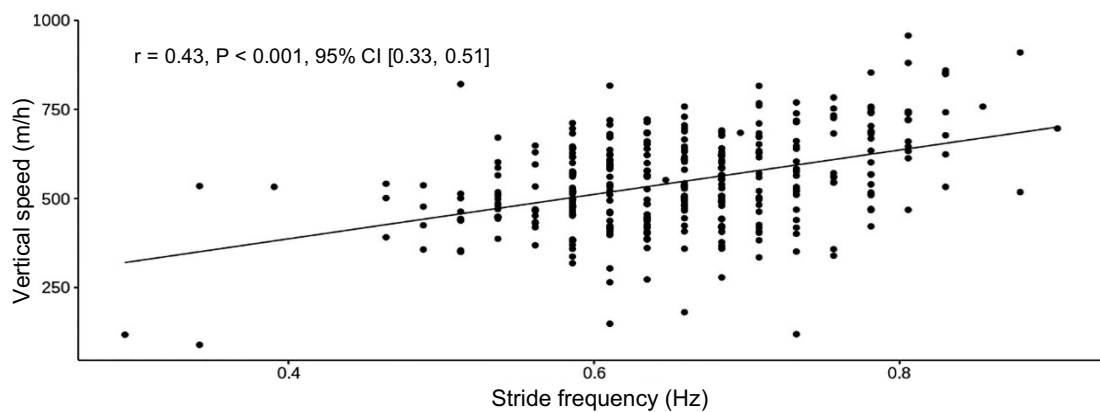


Figure 7.3 – Correlation between vertical speed and stride frequency for the selected uphill portions of the mountain passes.

7.4 Discussion

The purpose of this study was to investigate the effects of altitude and distance on VS during an extreme mountain ultra-marathon (Tor des Geants). The main findings were: (1) VS was progressively diminished with race progression, and this decrease in speed was greater at low than at high altitude; (2) the reduction in VS throughout the race is mainly related to a reduction in stride height (SH).

The VS was lower at higher altitude for the first and third pass, but the deceleration was greater at low altitude, which is contrary to the initial hypothesis. After the third mountain pass, there was no more difference in VS between the two altitude portions studied. A case study about an experienced athlete showed no metabolic fatigue during the major climbs of the TdG (Savoldelli et al., 2017). The large decrease of speed in the second half of TdG has previously been associated with sleep deprivation and fatigue (Saugy et al., 2013). Maximal aerobic speed was shown to be more strongly related to performance in a MUM than KE force or KE force loss (Balducci et al., 2017). These results were obtained during a shorter race (75 km with 3930 m of elevation gain). They do not contradict our findings, as the reduced VS at higher altitudes in the first quarter of TdG indicates that the effect of aerobic capacity on performance is only reduced beyond 75 km. Also, it is worth pointing out that there were no effects of the slope on VS ($p = 0.279$). One may argue that central or neuromuscular fatigue may be different between the low-altitude (at the beginning of the pass) and the high-altitude (at the upper part of the pass) sections. In such an ecological set-up, it was impossible to measure fatigue at the bottom and at the summit of each pass. This can be seen as a confounding factor since the differences between low and high altitudes may be due to other factors than the altitude-induced changes in aerobic capacity.

As expected, the reduction in VS was more strongly correlated with the reduction of SH than the reduction of SF. Changes in running biomechanics during the TdG have been associated with nociceptive feedback and the use of a smoother running pattern, which involved an increase in

SF (Degache et al., 2016). In that case, the measurements were made on a treadmill at 12 km/h before and after the race. With the speed being constant, the increase in SF was accompanied by a reduction in stride length. However, the etiology of neuromuscular fatigue differs between level and graded running where the decrease in maximal voluntary force observed for uphill running is associated with metabolic fatigue whereas it is associated with mechanical damages for downhill running (Giandolini, Vernillo, et al., 2016). A reduction in the strength of the KE and the plantar flexors (PF) have previously been reported for the TdG and could explain the reduction in SH observed in the present study (J.-B. Morin et al., 2011). We have previously shown large fatigue in plantar flexors during hilly running (Fourchet et al., 2012). Strength loss is similar in PF and KE during MUM (Saugy et al., 2013), while during level ultra-running, greater stress occurs on PF compared with KE (24-h running exercise on a treadmill) (V. Martin et al., 2010). Despite that there are no data available on hip flexors/extensors during or after MUM, it is likely that a strength loss of the hip flexors or extensors could also be involved. Moreover, the present results are in line with the previously reported decrease in uphill energy cost following the TdG that was associated with a modification of the uphill running mechanics presumably caused by a decrease in KE strength (Vernillo et al., 2014). Considering that the preferred SF seems to be adjusted to be metabolically optimal despite the fatigue encountered during a prolonged trail running exercise (Vernillo et al., 2019), the reduction in SF observed may not be detrimental to the energy cost of movement. Overall, our results indicate that the speed loss observed is likely related to a loss of KE strength; however, a voluntary reduction of intensity could also explain the reduction in VS observed.

A positive pacing strategy, where the speed progressively decreases, is the most common during ultra-endurance events (Abbiss & Laursen, 2008) and is the one adopted, consciously or not, by every athlete of this study. Participants with a higher performance level generally show greater speed loss during ultra-marathon events (Angus & Waterhouse, 2011; Kerhervé et al., 2015; Lambert et al., 2004). The observed reduction in speed could have been partly related to the athletes' perceived exertion (Marcora, 2009), which – based on the psychobiological model of endurance performance – plays a crucial role in the self-regulation of pacing (Pageaux, 2014). Future studies regarding MUM should consider the role of motivation and rate of perceived effort in the regulation of pace and their effects on performance. Because of the cancellation of the event before its completion, it was not possible to determine if the athletes would increase their speed in the last part of the race and whether or not this increase in speed would be influenced by the altitude.

7.5 Conclusion

During the TdG, the pacing was different between low and high altitudes only in the first quarter of the race suggesting that exertion influenced the uphill velocity to a larger extent than the oxygen delivery. The reduction in VS was more strongly correlated to the decrease in SH than SF and implies an effect of the KE strength loss.

8 Hurdle Clearance Detection and Spatiotemporal Analysis in Hurdling

Abstract

This research aimed to determine whether: (1) shoe-worn magnetic and inertial sensors can be used to detect hurdle clearance and identify the leading leg in 400-m hurdles, and (2) to provide an analysis of the hurdlers' spatiotemporal parameters in the intervals defined by the hurdles' position. The data set is composed of MIMU recordings of 15 athletes in a competitive environment. The results show that the method based on the duration of the flight phase was able to detect hurdle clearance and identify the leading leg with 100% accuracy. Moreover, by combining the swing phase duration with the orientation of the foot, we achieved, in unipedal configuration, 100% accuracy in hurdle clearance detection, and 99.7% accuracy in the identification of the leading leg. Finally, this study provides statistical evidence that contact time significantly increases, while speed and step frequency significantly decrease with time during 400 m hurdle races.

Keywords: inertial sensors, 400m hurdles, magnetometer, hurdle clearance, flight time, speed

Chapter adapted from Falbriard, M., Mohr, M., & Aminian, K. (2020). Hurdle Clearance Detection and Spatiotemporal Analysis in 400 Meters Hurdles Races Using Shoe-Mounted Magnetic and Inertial Sensors. *Sensors*, 20(2), 354.

Contributions: conceptualized the study design; conducted the data collection; designed the algorithms; contributed to the analysis and interpretation of the data; drafted the manuscript.

8.1 Introduction

The last decade has seen a growing trend towards magnetic inertial measurement units (MIMU)- based studies in track and field races, with the majority focusing on sprint distances. These studies differ in terms of sensor configuration, sensor location, and type of parameter measured (Macadam et al., 2019). Several groups have used inertial sensors in sprint running to characterize temporal parameters (Ammann et al., 2016; Bergamini et al., 2012; Purcell et al., 2005), body-segment orientation (Bergamini et al., 2013; Channells et al., 2006), ground reaction forces (Gurchiek et al., 2017; Setuain et al., 2018), and speed (Gurchiek et al., 2018, 2019; Mertens et al., 2018). Surprisingly, only a few studies used MIMU to quantify spatiotemporal parameters in hurdle races. Recently Ho, Chang and Lin (Ho et al., 2019) used high-speed video cameras and inertial sensors strapped on the dorsal surface of each foot to analyze flight time, hurdle cycle time (i.e., the time between hurdles) and hurdle cycle velocity (i.e., hurdle cycle time divided by the distance between hurdles) in 110-m hurdles. Unfortunately, the authors offered no explanation about the method employed to detect the time point of hurdle clearance (HC) or how they measured the parameters above. The authors in (Iskra et al., 2017) used inertial measurement units (IMU) to evaluate the kinematics of the hurdlers' upper limbs and reported the linear velocities and the trajectory of the segments during hurdle clearance. Overall, little research has been performed specifically on 400-m hurdles (Iskra & Coh, 2011), and no wearable system has been proposed to detect HC and identify the leading leg (LL), i.e., the leg attacking the hurdle.

The variations in the average speed, contact time, flight time, and step frequency in between the hurdles and the side of the leading leg are all relevant indicators of the athletes' racing strategy, and thus can have a significant impact on performance. Currently, such analysis requires a set-up with multiple video cameras around the track and time-consuming manual post-processing of the data. A wearable system capable of providing instant feedback would significantly improve our capacity to monitor the training status and performance of athletes.

In alpine skiing, gate crossings have been detected through the use of magnets placed into the snow and a magnetometer worn by the athlete (Fasel et al., 2019). Although potentially transferable and useful, this technique has not yet been tested to measure the timing of hurdle crossings. Therefore, the primary aim of this study was to propose and test different methods based on foot-worn MIMU to detect HC and identify the LL. Furthermore, magnets fixed on the hurdles were tested as a complementary method to detect HC. As a secondary aim of this study, the changes throughout the race of contact time, flight time, running speed, and step frequency were analyzed to explore the relationship between the athlete's caliber and racing strategy.

8.2 Materials and Methods

8.2.1 Protocol

In this study, 16 athletes ($n = 10$ males (age: 22 ± 4 years, height: 183 ± 2 cm, weight: 69 ± 6 kg, time: 57 ± 3 s), $n = 6$ females (age: 23 ± 3 years, height: 165 ± 4 cm, weight: 55 ± 2 kg, time: 64 ± 3 s)) volunteered to perform one 400 m hurdles race equipped with IMUs. The measurement took place during an outdoor competition with participants aiming for a qualification, thus running at their maximum speed. The athletes were equipped before the warm-up session to not disturb their preparation routine, and the sensors were collected at the end of the race. Moreover, each of the 10 hurdles in the second lane was equipped with two magnet bars (Figure 8.1). In 400 m hurdling, the distance (D_H) in between two hurdles is 35 m. The distance (D_H) between the starting line and the first hurdle is 45 m, and the distance between the last hurdle and the finish line is 40 m, hence $D_H = \{45, 35, \dots, 35, 40\}$ with $\dim(D_H) = 11$ intervals. The study was conducted in accordance with the Declaration of Helsinki, and the protocol was approved by the local Ethics Committee. All subjects gave their written informed consent for inclusion in the study.

8.2.2 Instrumentation

Each participant was equipped with one shoe-mounted inertial measurement unit (IMU) (Physilog 4¹, Gait Up SA, Lausanne, Switzerland, weight: 19 g, size: $50 \times 37 \times 9.2$ mm) affixed on the dorsum of the foot with a D_H esive tape (Figure 8.1). The left and right foot IMUs were synchronized using radio frequencies. The configuration included an accelerometer at 500 Hz ($\pm 16g$ operating range), a gyroscope at 500 Hz (± 2000 °/s operating range) and a magnetometer at 71Hz (± 1000 μ T operating range). The magnets were constructed by vertically stacking 8 small neodymium magnets (S-20-10-N, Supermagnete, Uster, Switzerland) spaced by 5 mm into a 12 cm long stick. The magnets were fixed on each side of the hurdle at the top of the vertical poles (Figure 8.1). We aimed for the magnets to be as close of possible to the foot-worn magnetometers when passing over the hurdle. Finally, the video of each race was recorded at 25 frames/s and used for verification purposes in this study (leading leg identification and the number of steps per interval manually labeled). All the subsequent data processing tasks described in this manuscript, the implementation of the HC and LL detection algorithms, and the analysis of the results were performed using the MATLAB software (R2018b, MathWorks, Natick, MA USA) and required no external libraries.

8.2.3 Data processing

Preprocessing, Calibration, and Segmentation

The accelerometer and gyroscope sensors were calibrated, as described in (Ferraris et al., 1995). The magnetometer offset, sensitivity, and axis-misalignment were corrected using

¹Datasheet available in the Appendix.

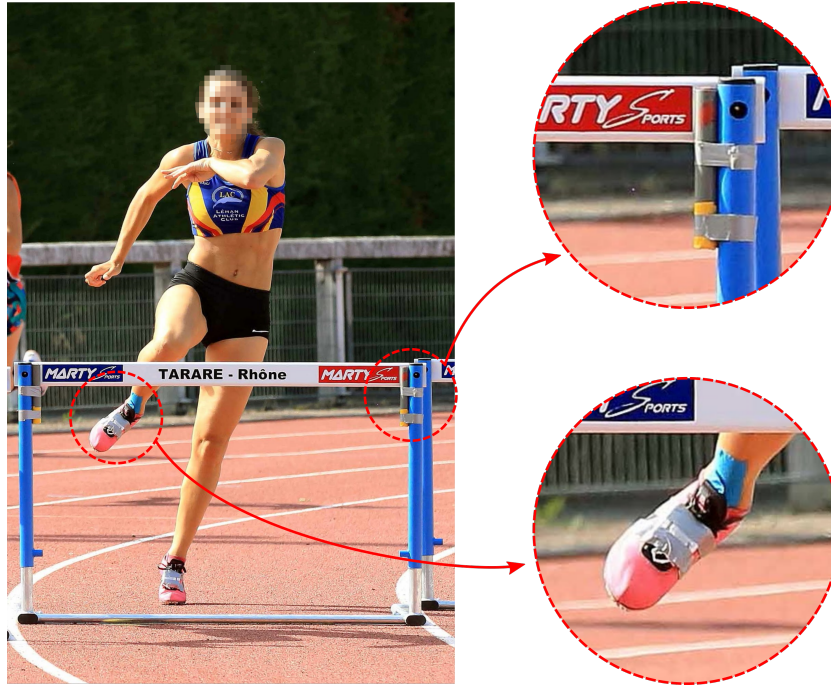


Figure 8.1 – One participant clearing a hurdle with two shoe-mounted IMUs and one magnet bar on each of the vertical poles of the hurdle.

the method proposed in (Bonnet et al., 2009) with calibration data recorded on-site the day of the event. The angular velocity and acceleration signals were low-pass filtered using a 2nd-order Butterworth filter with a cut-off frequency at 70 Hz. Functional calibration of the IMUs was performed as described in (Falbriard et al., 2018): we used a standing period to define the functional frame (FF) vertical axis, the first component resulting from the principal component analysis (PCA) of the angular velocity during running to define the mediolateral axis of the foot, and we set the anterior-posterior axis orthogonally to the first two (Figure 8.2). The accelerometer, gyroscope, and magnetometer data were then expressed in the FF.

We defined the start of the race as the time t_{start} , which occurred 200 ms before the first manually detected acceleration peak measured when the athlete was still in the starting blocks. The 200 ms offset corresponds to the estimated response-time of the participants (Brosnan et al., 2017), and the acceleration peak to the instant when the athlete starts pushing on the starting blocks. The races were then segmented using t_{start} and the official race time (T_{race}) of the participants.

Temporal Analysis and Orientation Estimation

The stepwise temporal analysis was carried out as in (Falbriard et al., 2018) with minor adaptations to improve the robustness of event detection (i.e., mid-swings, initial contact, and terminal contact). The performance of the detection algorithm was indeed affected by the noise generated by the hurdle clearance movements, the adaptation steps occurring before

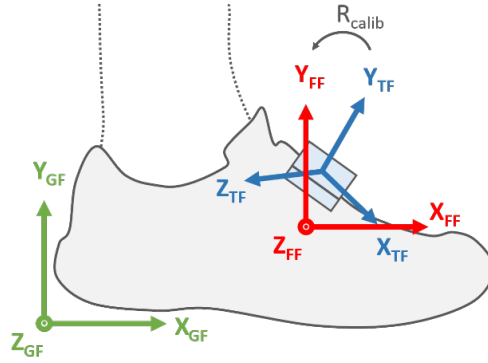


Figure 8.2 – The orientation of the IMU technical frame (blue), the foot functional frame (red) and global frame (green) when standing. R_{calib} is the rotation matrix obtained by the functional calibration.

and after the hurdle, and by the high running speeds. Since initial (IC) and terminal contact (TC) generate high-frequency oscillations in the acceleration signal, we restrained the search window for IC and TC events using the envelope of the signal. We computed the envelope using two successive wavelet transforms. First, we applied a high-pass filter ($F_c = 100$ Hz) on the acceleration norm, which preserved only the high-frequency oscillations at IC and TC. We then rectified the signal and applied a low-pass filter ($F_c = 5$ Hz). Although the successive filters resulted in a low amplitude signal, the shape of the envelope preserved two peaks where the high-frequency oscillations of IC and TC occurred. Features detection within these IC and TC limits was carried out as in (Falbriard et al., 2018), and the detection results of each trial were visually inspected to ensure that the algorithm correctly detected IC, TC, and mid-stance (MS) at each step. Note that MS corresponds to the event where the angular velocity in the sagittal plane of the foot is minimum.

We obtained the 3D orientation of the foot using strap-down integration (Favre et al., 2006) and a drift correction method based on the assumption that the global frame (GF) and the FF were aligned at MS (Figure 8.2). Hence, the orientation of the foot between two successive strides i and $i+1$ was computed in the GF set at MS(i). Furthermore, the inclination of the foot in the starting-blocs was found using the orientation of the gravitational acceleration in the FF. Two Euler angles were extracted from the quaternion notation in the ZYX order: (1) the pitch angle (θ) defined as the rotation in the sagittal plane, and (2) the yaw angle (ψ) defined as the rotation in the horizontal plane.

8.2.4 Hurdle Clearance Detection

Three methods have been implemented to detect HC and identify LL; (1) MAG: using the magnetometer signal, (2) TEMP: using the temporal events, and (3) ORIENT: using the foot orientation (i.e., pitch and yaw angles). For each of these methods, both a unipedal (i.e., one foot-worn IMU) and a bipedal (i.e., one IMU on each foot) configuration were tested.

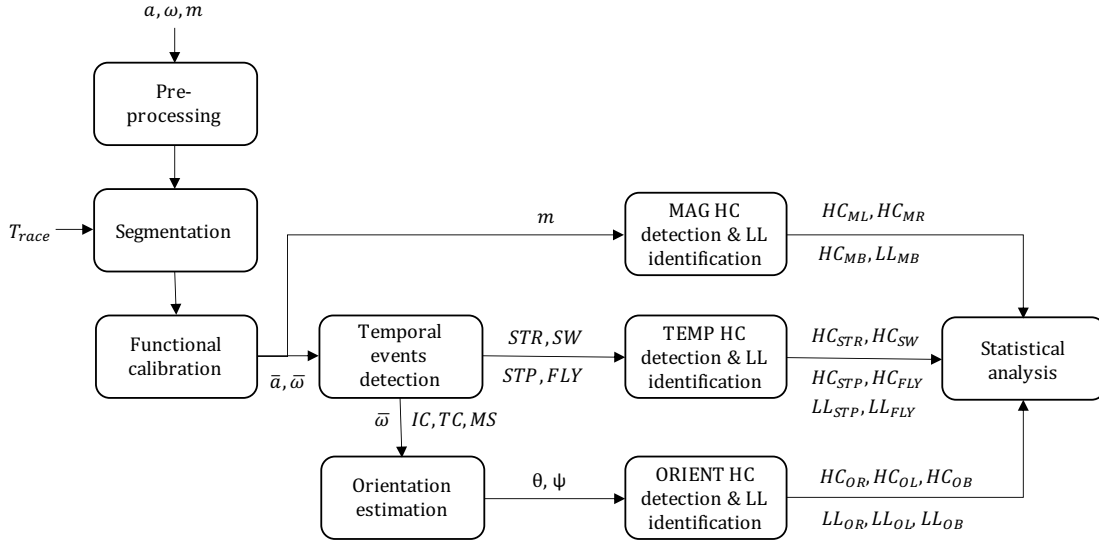


Figure 8.3 – Flow chart of the proposed hurdle clearance detection method. We defined the inputs as follows: a the accelerometer data, ω the gyroscope data, m the magnetometer data, T_{race} the official race duration, θ the pitch angle, and ψ the yaw angle of the foot. Initial contact (IC), terminal contact (TC), mid-stance (MS), stride time (STR), swing phase duration (SW), step duration (STP), and flight phase duration (FLY) result from the temporal analysis. Hurdle clearance (HC) detection results are shown as HC_{XX} and leading leg detection results as LL_{XX} , where XX describes the detection method.

Each method was developed independently of the two others and used different parameters. Because the total number of hurdles ($N_{hurdles}$) and the distance between the hurdles (D_H) were fixed, these parameters were considered as inputs of the system. The general flow chart of the methods is described in Figure 8.3.

MAG: Magnets and Magnetometer Based Detection

This method assumes that the two magnets affixed on each side of the hurdle (Figure 8.1) locally increased the magnitude of the magnetic field. The HC detection, therefore, consisted of finding peaks on the filtered magnetometer norm (Figure 8.4).

We computed the upper envelope of the magnetometer norm using spline interpolation over local maxima separated by at least 0.5 s (maximum step frequency reported in (Hanon & Gajer, 2009)). The envelop signal was then normalized by its mean to facilitate the comparison of the peak absolute values between the two feet. Unipedal HC detection involved finding the $N_{hurdles}$ highest peaks separated by at least τ second (Eq. 8.1) on \hat{m}_{right} and \hat{m}_{left} for the right and left leg, respectively:

$$\tau = \min(D_H) / V_{max} \quad (8.1)$$

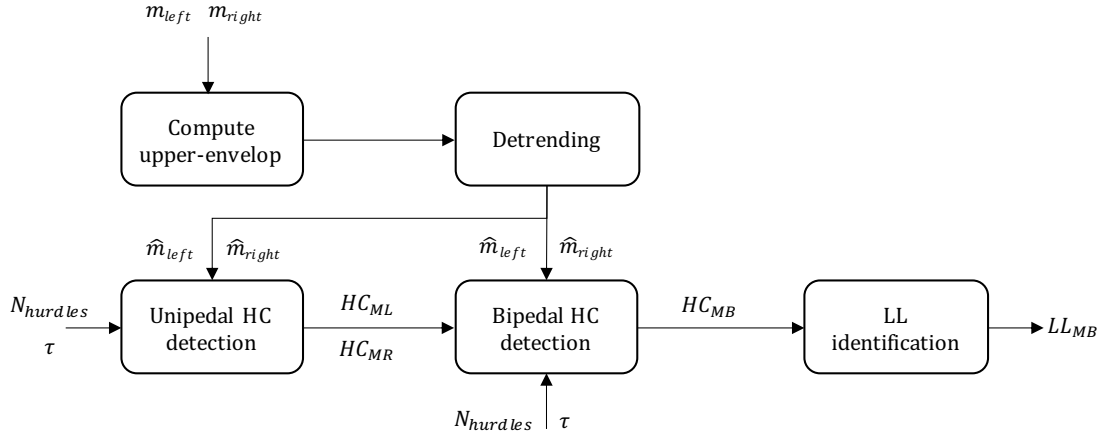


Figure 8.4 – Block diagram of the MAG method. In this figure, m_{left} and m_{right} represent the magnetometer norm of the left and right foot, $N_{hurdles}$ the number of hurdles to detect and τ the minimum time difference between two consecutive HC.

where D_H is the set of interval length and V_{max} , the maximum running speed considered. As $\min(D_H) = 35$ m and V_{max} was set at 11.67 m/s (42 km/h), which is slightly faster than the average speed of the current 100m sprint World Record, τ was set at 3s. The times of the $N_{hurdles}$ highest peaks were then labeled as HC_{ML} and HC_{MR} for the left and right leg, respectively, with $\dim(HC_{ML}) = \dim(HC_{MR}) = N_{hurdles}$. We obtained the bipedal detection results, namely HC_{MB} , by combining HC_{ML} and HC_{MR} using the following rules:

1. If $|HC_{ML}(i) - HC_{MR}(j)| < 0.4$ s, i and $j \in \{1, \dots, N_{hurdles}\}$, then $0.5 * (HC_{ML}(i) + HC_{MR}(j))$ was added to HC_{MB} . Here, we assumed that if two HC events occurred within a short period (i.e., 0.4s = average flight time in (Salo et al., 1997)) and were detected on the left and right foot distinctively, then these events were likely to correspond to a true HC. As we could not predict which of the left or right event was more accurate, we defined the time of the true HC event as the average of the left and right foot events.
2. The i and j indices not considered in step 1 were recursively added to HC_{MB} until $\dim(HC_{MB}) = N_{hurdles}$. The greatest peaks were added first if they were minimum $\tau = 3$ s away from all the HC already in HC_{MB} . Finally, the results were sorted in their order of appearance within the race.

Leading leg identification was only possible for the bipedal detection (LL_{MB}), where we assumed that the leg with the earliest magnetic peak was the LL.

TEMP: Temporal Event-Based Detection

This method supposes that the HC strides have longer phase duration in comparison to regular running strides. The phases considered were stride time (STR), swing phase duration

(SW), step duration (STP), and flight phase duration (FLY) with the time series estimated as in Eq. 8.2 - 8.5:

$$STR(i) = IC(i + 2) - IC(i) \quad (8.2)$$

$$SW(i) = IC(i + 2) - TC(i) \quad (8.3)$$

$$STP(i) = IC(i + 1) - IC(i) \quad (8.4)$$

$$FLY(i) = IC(i + 1) - TC(i) \quad (8.5)$$

Note that the estimation of these four temporal parameters required the detection of different events and necessitated different sensor configurations (Table 8.1). Since IC is more precisely detected than TC in running (Falbriard et al., 2018), we decided to keep STR and STP in the analysis, although SW and FLY offer narrower windows for HC detection (i.e., SW and FLY occur within STR and SPT, respectively). Moreover, STP and FLY parameters both require a bipedal configuration while STR and SW can be estimated from a single IMU.

Parameters	Detection required		
	IC	TC	Configuration
STR	yes	no	Unipedal
SW	yes	yes	Unipedal
STP	yes	no	Bipedal
FLY	yes	yes	Bipedal

Table 8.1 – Features and configurations required in order to estimate, for each step/stride, the parameters used to detect hurdle clearance.

To remove the trend induced by fatigue (Hanon & Gajer, 2009), we subtracted the moving average from the STR, SW, STP, and FLY time series using a window of length K (K equal to 60 steps for STP and FLY and 30 strides for STR and SW). For each parameter, the indices of the $N_{hurdles}$ highest peaks (i.e., the longest phase durations), separated by at least $\tau = 3$ s, were defined as i_k where $k = 1 \dots N_{hurdles}$. Eq. 8.6 - 8.9 show how the exact times of the HC were obtained based on the selected i_k periods of each parameter:

$$HC_{STR}(k) = 0.5 \times (IC(i_k) + IC(i_k + 2)) \quad (8.6)$$

$$HC_{SW}(k) = 0.5 \times (TC(i_k) + IC(i_k + 2)) \quad (8.7)$$

$$HC_{STP}(k) = IC(i_k + 1) + 0.74 \times (IC(i_k + 2) - IC(i_k + 1)) \quad (8.8)$$

$$HC_{FLY}(k) = TC(i_k + 1) + 0.65 \times (IC(i_k + 2) - TC(i_k + 1)) \quad (8.9)$$

In the unipedal cases (Eq. 8.6 - 8.7), we used a 0.5 factor because the exact time point of the HC event depends on the location of the IMU (i.e., on the leading leg or the trailing leg) (Figure 8.5). In Eq. 8.8 - 8.9, the 0.74 and 0.65 coefficients were based on the results of previous research (Čoh et al., 2008; Lafortune, 1988; Mclean, 1994). In these studies, the last ground contact time before HC lasted for approximately 25% of the total step duration. Furthermore, hurdle clearance occurred after 65% of the total HC distance, so if the speed is considered constant, 65% of flight time. The 0.74 factor of Eq. 8.8 was found using the two coefficients mentioned above (Eq. 8.10):

$$0.74 = \text{round}(0.25 + 0.65 \times (1 - 0.25)) \quad (8.10)$$

Here the *round()* function rounds to the nearest two digits to the right of the decimal point. Finally, for LL identification using the STP and FLY parameters (LL_{STP} and LL_{FLY}), we defined as the trailing leg the side where HC was detected.

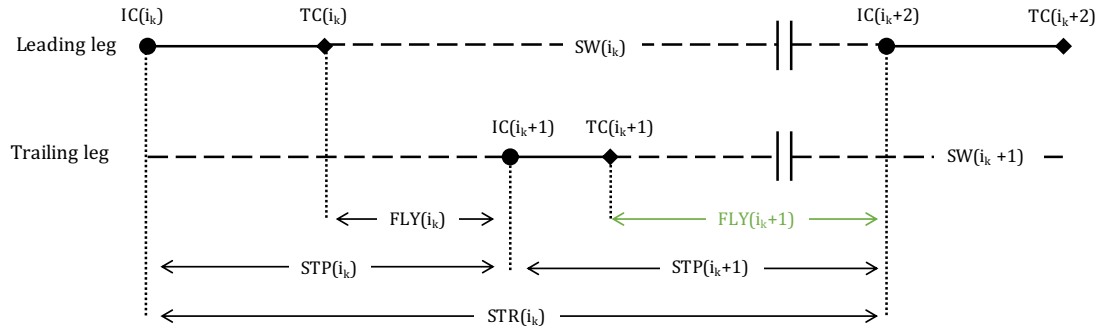


Figure 8.5 – A sequence of temporal events for the leading and trailing leg. IC events are shown with circles, TC events with diamonds. HC events are shown with two parallel vertical bars, ground contact with a solid horizontal line, and SW with a horizontal dashed line. In green, the flight phase within which HC detected from MAG, TEMP, and ORIENT method would be classified as correctly detected.

ORIENT: Orientation based Detection

In the hurdle clearing stride, the kinematics of the leading leg differ from those of the trailing leg (Tidow, 1991). Indeed, a large positive pitch angle (θ_{left} , θ_{right}) was expected for the leading leg during HC and large yaw angle (ψ_{left} , ψ_{right}) for the trailing leg. So, regardless of the IMU location (leading or trailing leg), it should always be possible to detect the HC events and determine the LL using only the pitch and yaw angles.

angle. The elements in $\hat{\theta}(HC_{\theta L}) \cup \hat{\psi}(HC_{\psi L})$ are then sorted in descending order and added to HC_{OL} recursively provided that each element in HC_{OL} is separated by at least by τ ($=3$ s). As a result, we defined HC_{OL} as the set of the HC events obtained for the left foot (i.e., the best HC candidates among $HC_{\theta L}$ and $HC_{\psi L}$). The same method was applied for the right foot to obtain HC_{OR} (Figure 8.6). Finally, HC_{OL} and HC_{OR} were combined to get the bipedal detection results, with a selection process similar to the magnetometer:

1. If $|HC_{OL}(i) - HC_{OR}(j)| < 0.4$ s, i and $j \in \{1, \dots, N_{hurdles}\}$, then $0.5 * (HC_{OL}(i) + HC_{OR}(j))$ was added to HC_{OB} . Here, we assumed that if two HC events occurred within a short period (i.e., 0.4 s = average flight time in (Salo et al., 1997)) and were detected on the left and right foot distinctively, then these events were likely to correspond to a true HC. As we could not predict which of the left or right event was more accurate, we defined the time of the true HC event as the average of the left and right foot events.
2. The i and j indices not considered in step 1 were recursively added to HC_{OB} until $dim(HC_{OB}) = N_{hurdles}$. The greatest peaks were added first if they were minimum $\tau = 3$ s away from all the HC already in HC_{OB} . Finally, the results were sorted in their order of appearance within the race.

Lastly, we used the following rule to detect the LL: the leg for which an HC event corresponded to a peak in the pitch angle was labeled as the leading leg. The results were kept in three LL identification sets: LL_{OL} and LL_{OR} for unipedal detection of the left and right leg and LL_{OB} for bipedal configuration.

8.2.5 Data Analysis

Ideally, the time when the athlete's center of mass cleared the hurdle should be used as a reference for HC time. However, due to the lack of synchronization between the camera and the IMUs, this reference was not available. Instead, we considered the time of HC_{FLY} (65% of flight phase) as the reference HC time (HC_{ref}) if it occurred inside of the flight phase of an HC observed on video. Note that the LL at each HC was manually labeled using the video.

The HC detected using the TEMP, ORIENT, and MAG methods were considered correctly detected if it occurred inside the flight phase of a reference HC_{ref} . Note that for HC_{STR} and HC_{SW} (TEMP methods in unipedal configuration), an HC was considered correctly detected if HC_{ref} occurred inside of a stride of HC_{STR} or inside of a swing of HC_{SW} (Figure 8.5). These two exceptions were necessary as the system could not identify the LL solely based on the STR and the SW parameters. We evaluated the performance of the proposed systems by computing the mean, SD, the minimum, and the maximum number of correctly detected HC per trial. Moreover, the mean \pm SD of the differences in HC detection time (Δt_{HC}) between HC_{ref} and HC detected from TEMP, ORIENT, and MAG methods were measured. Finally, all the correctly detected HC were collected, and the percentage of correctly identified LL was calculated regardless of the athlete.

As one of the goals of this study was to provide feedback to the participants and trainers, we extracted key performance features from the races (Amara et al., 2019; Otsuka & Isaka, 2019), such as contact time (CT), flight time (FLY), step frequency (STF) and speed (SPE). Moreover, we obtained the speed using the distance between the hurdles (D_H) and the time difference between two consecutive HC. The potential detection errors of IC and TC (Falbriard et al., 2018) combined with a $\pm 10\%$ error on the 65% reference threshold (Eq. 8.9) provided a confidence interval on the estimated speed. To assess how CT, STF, FLY, and SPE changed during the race, we extracted the mean of these parameters for the 11 intervals of the 15 races. We then grouped the results per interval and computed the inter-subjects mean and SD for each interval. Note that the first and last two steps of each interval were removed as these may be affected by the landing and takeoff phases. Also, we used a one-way ANOVA on the intra-interval means, with a significance level at 0.05 (*) and 0.01 (**), to assess any significant statistical differences between the second interval and the subsequent ones. The second interval was preferred to the first one as the latter was affected by the acceleration phase at the start of the race. Moreover, the intra-interval means of CT, STF, SPE, and FLY were expressed relative to the mean of the second interval (Eq. 8.13 - 8.16), and the evolution of these parameters during the race presented using boxplots:

$$AvCT(k) = \frac{mean(CT(t_k))}{mean(CT(t_2))} \quad (8.13)$$

$$AvSTF(k) = \frac{mean(STF(t_k))}{mean(STF(t_2))} \quad (8.14)$$

$$AvSPE(k) = \frac{mean(SPE(t_k))}{mean(SPE(t_2))} \quad (8.15)$$

$$AvFLY(k) = \frac{mean(FLY(t_k))}{mean(FLY(t_2))} \quad (8.16)$$

where k is the interval index (here $k = 3 \dots 11$), and t_k corresponds to the steps between interval k and $k+1$.

8.3 Results

In total, we analyzed the races of 15 athletes. One athlete had to be removed from the data set due to an instrumentation error. Such collection led to 300 HC for the evaluation in unipedal configuration (i.e., foot considered independently) and 150 HC for the assessment of bipedal configuration. According to the video-based validation of the HC detected in HC_{FLY} , all the 150 HC were correctly detected, with the correct number of steps in each interval and the correct leading leg identified. The results of the MAG, TEMP, and ORIENT detection methods are compared in Figure 8.7, where the processed signals and detected peaks are illustrated for both unipedal and bipedal configurations.

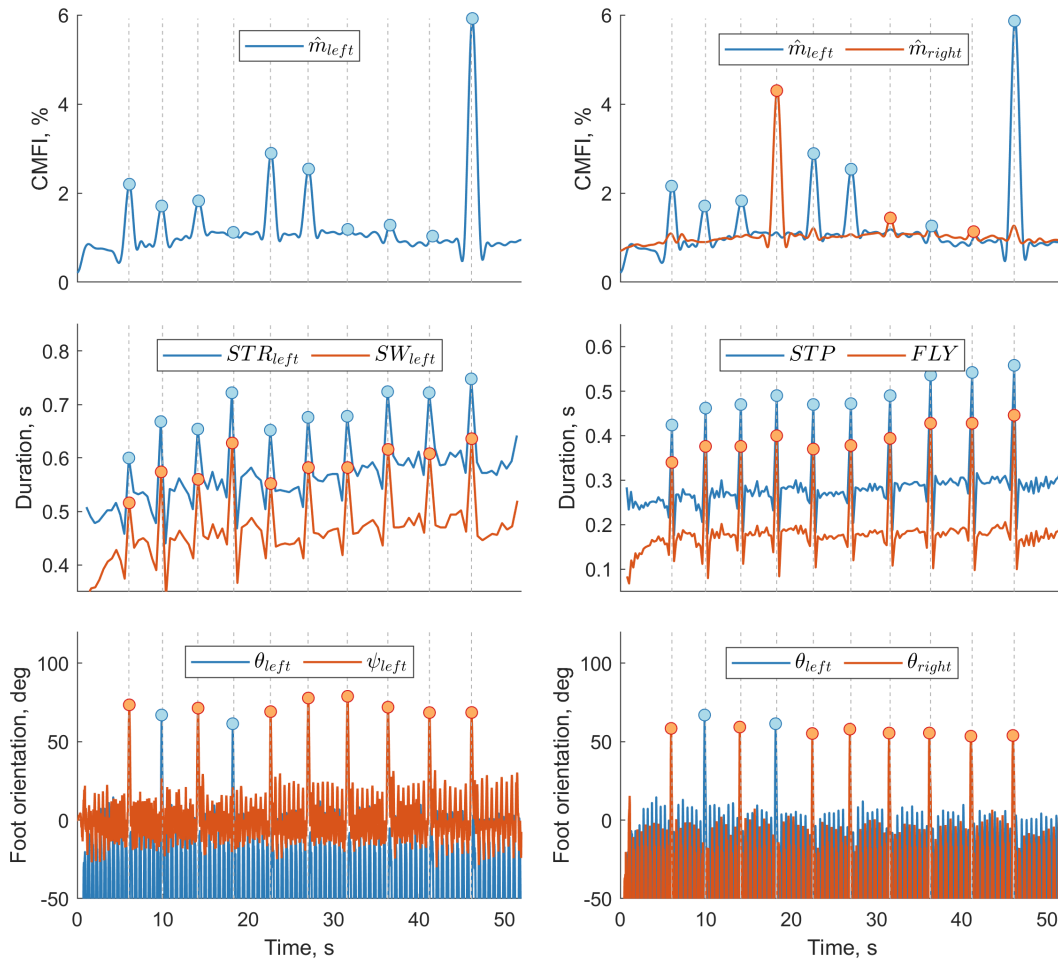


Figure 8.7 – Detection results obtained by MAG (top), TEMP (middle), and ORIENT (bottom) methods for one trial. The magnetometer graphs show the calibrated magnetic field intensity (CMFI) in percent of the Earth’s magnetic field. The column on the left shows the detection results in unipedal configuration and on the right for bipedal detection. The vertical grey dashed lines represent the reference HC events.

Table 8.2 compares the HC detection results in terms of correctly detected HC per trial and the mean \pm SD of Δt_{HC} . In unipedal configuration, LL detection accuracy is shown exclusively for the ORIENT method as the other methods cannot perform such analysis. Also, LL identification and Δt_{HC} statistics were computed on the correctly detected HC, hence the different N values for each method in Table 8.2.

Figure 8.8 presents the relative changes for the average speed ($AvSPE$), contact time ($AvCT$), step frequency ($AvSTF$), and flight time ($AvFLY$) throughout the race. These are expressed relative to the speed, contact time, step frequency, and flight time (Eq. 8.13 - 8.16) estimated in the second interval (i.e., 45-80 m). As the vertical color bar on the right side of the figures indicates, the values of the slowest athletes are shown in blue, and the fastest in orange - the boundary performances (i.e., the fastest and the slowest athlete) are shown with dashed lines.

Methods	HC detection per trial				Correct HC / Total HC	Δt_{HC} (ms)		LL accuracy % (Total)
	mean	SD	min	max		mean	SD	
Unipedal								
MAG	4.63	2.76	0	9	139 / 300	-12	100	-
TEMP _{STR}	9.97	0.18	9	10	299 / 300	-138	106	-
TEMP _{SW}	10	0	10	10	300 / 300	-78	104	-
ORIENT	9.53	0.82	7	10	286 / 300	-47	96	99.7 (285)
Bipedal								
MAG	7.33	1.76	2	9	110 / 150	15	94	39.1 (43)
TEMP _{STP}	10	0	10	10	150 / 150	2	4	100 (150)
TEMP _{FLY}	10	0	10	10	150 / 150	0	0	100 (150)
ORIENT	9.6	0.91	7	10	144 / 150	-42	33	99.3 (143)

Table 8.2 – Hurdle clearance and leading leg detection results for both unipedal and bipedal configurations. In total, 15 trials with each $N_{hurdles} = 10$ hurdle clearances were available.

Table 8.3 presents inter-subject mean and SD of the average CT, FT, STF, and SPE in each interval. The results from the one-way ANOVA test are shown for the intra-interval mean contact time, flight time, step frequency, and speed. On average, 18 steps (min = 11, max = 20) were available per interval. Finally, Figure 8.9 presents an overview of the average speed (blue) and the number of steps (orange) within each HC interval of a single athlete. The blue vertical lines represent the confidence interval of the average speed values, and the blue horizontal dashed line shows the average speed during the race. Also, we used R (right) and L (left) letters to indicate the side of the leading leg at each HC (vertical grey dashed lines). Such a graph provides an example of the type of feedback that can be instantly extracted using the proposed HC detection method.

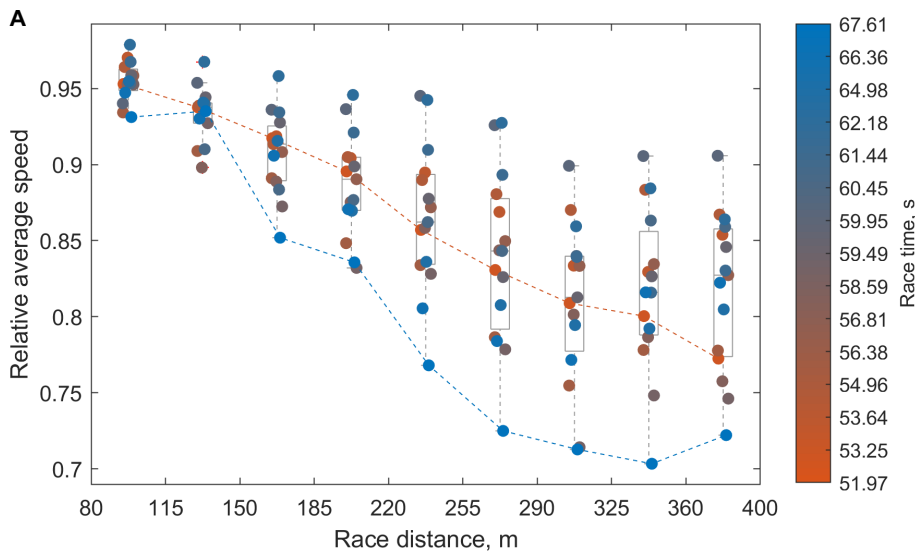


Figure 8.8 - Cont.

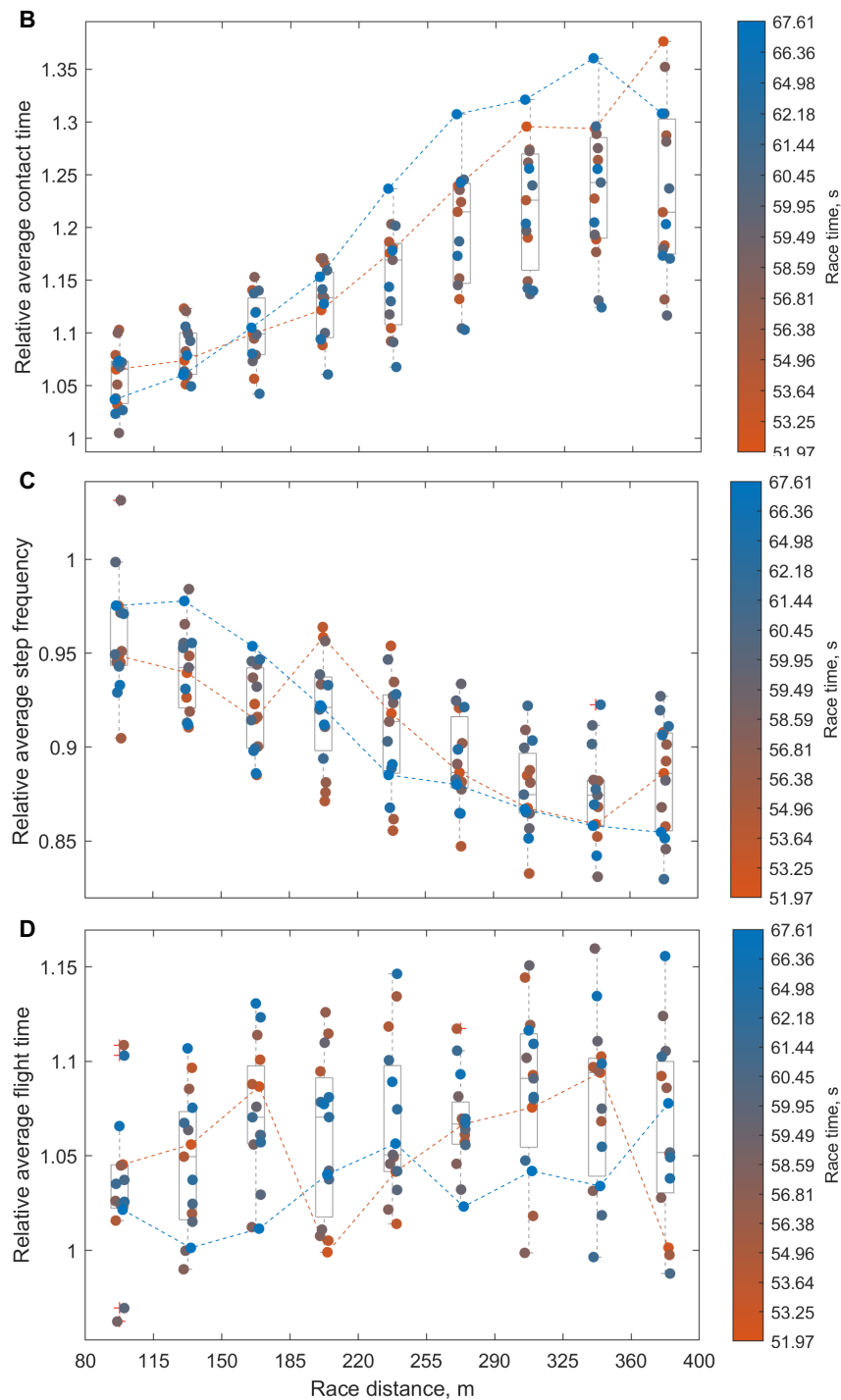


Figure 8.8 – Evolution of $AvSPE$ (a), $AvCT$ (b), $AvSTF$ (c), and $AvFLY$ (d) between the third and the last interval. The y-axis values are expressed relative to the average values obtained within the second interval (45 to 80 m). The orange to blue gradient is used to differentiate the athletes according to their performance time, with the boundary performances (slowest and fastest athlete) being illustrated with dashed lines. For better visibility of individual data points, a small scatter was introduced in the x-direction.

Chapter 8. Hurdle Clearance Detection and Spatiotemporal Analysis in Hurdling

Interval	Distance, m	CT, ms		FLY, ms		STF, Hz		SPE, ms ⁻¹	
		mean	SD	mean	SD	mean	SD	mean	SD
1	0-45	110	7	154	11	3.8	0.15	6.73	0.44
2	45-80	104	8	160	10	3.81	0.11	7.77	0.64
3	80-115	110	9	165	10	3.65*	0.13	7.41	0.61
4	115-150	113	9	167	10	3.59**	0.11	7.24	0.55
5	150-185	115	10	171	10	3.51**	0.1	7.05*	0.57
6	185-220	118**	10	169	7	3.5**	0.11	6.88**	0.56
7	220-255	120**	10	170	8	3.46**	0.11	6.72**	0.63
8	255-290	125**	11	170	9	3.4**	0.09	6.5**	0.64
9	290-325	127**	10	173*	11	3.35**	0.13	6.28**	0.61
10	325-360	129**	12	172*	13	3.33**	0.11	6.34**	0.59
11	360-400	128**	10	170	10	3.36**	0.11	6.34**	0.54

Table 8.3 – Inter-subject mean and SD of the average contact time (CT), flight time (FLY), step frequency (STF), and speed (SPE) within each interval. The results from the one-way ANOVA test, which compared the mean statistics between the second interval and the subsequent ones, are shown with significance level at 0.05 (*) and 0.01 (**).

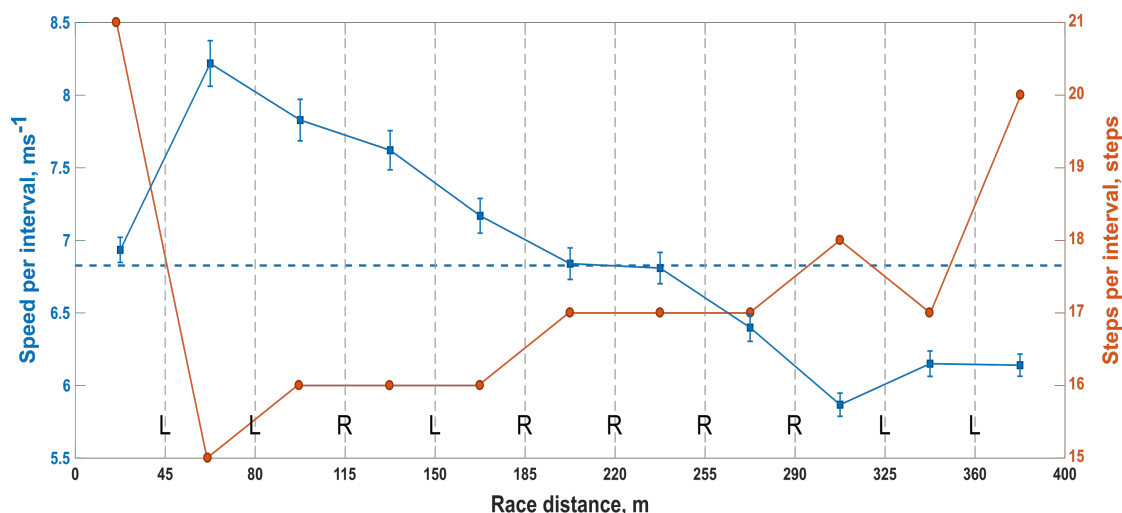


Figure 8.9 – Average speed, number of steps, and leading leg analysis for each interval between hurdles within a single race. The average speed between all HC is shown with blue squares and the confidence interval with vertical solid lines. The blue horizontal dashed line corresponds to the average race speed. Also, the number of steps is depicted with orange circles and the leading leg at each HC (vertical grey dotted line) with R (right), or L (left).

8.4 Discussion

The primary aim of this study was to evaluate the performance of three different MIMU-based methods in detecting HC events and identifying the leading leg in 400 m hurdles. In the unipedal configuration, the best HC detection results were obtained using the TEMP method and the swing phase duration (Table 8.2). This method was able to detect all the 300 HC available in the data set.

In contrast to the SW parameter, the ORIENT method delivered a slightly lower HC detection accuracy (95.3%), with one trial detecting only seven hurdles. The ORIENT method relies on the HC technique used by the athletes. It assumes a large pitch angle for the leading leg and a large yaw angle for trailing leg at HC (Figure 8.7). Its detection accuracy thus may decline the lower the performances, e.g., for beginners. However, ORIENT was the only method capable of identifying the leading leg in unipedal configuration and showed a high 99.7% accuracy with only one misclassification among all the 286 correctly detected HC.

The MAG method did not provide a reliable detection in unipedal configuration, with only 46.3% accuracy (Table 8.2). Closer inspection of the signals showed that most of the non-detected HC were caused by the absence of a peak in the raw data. A possible explanation for these results resides in the fact that the detectable distance between the foot-worn magnetometer and a hurdle depends on the setup of the magnet bars. As the weight of the hurdles is regulated, the number of vertically stacked magnets was limited, and so was the detectable distance. Also, fixing the magnets on the top bar of the hurdles would have reduced the foot-to-magnet distance but was not feasible in this study for practical reasons. Finally, the HC technique of the athlete may affect the detection results as an efficient technique minimizes the distance between the athlete center of mass and a hurdle. Although the results improved in the bipedal configuration (73.3%), this method remains the least accurate compared to the two others.

In the bipedal configuration, the flight time and step duration (TEMP method) provide a 100% accurate detection of HC and the ORIENT method 96% accuracy. These observations can be generalized to the identification of the leading leg in the bipedal configuration. Based on these findings, flight time seems to be the best indicator for both HC and LL identification and should be preferred to the step duration as it provides a narrower window around HC events (Figure 8.5). Yet, if only one foot-worn IMU is available, the swing phase duration in combination with the foot pitch and yaw angles also provides accurate detection for HC and LL.

A note of caution is due here since previous researches have shown that the vertical speed varies during the flight phase (Przednowek et al., 2014) and that the 65%–35% ratio used in this study may change among athletes (Čoh et al., 2008; Lafortune, 1988; Mclean, 1994). The estimated time of HC and the average speed between two hurdles must, therefore, be presented with an appropriate confidence interval (Figure 8.9). In future investigations, it would be interesting to investigate if: (1) the pitch angle of the leading leg and the yaw angle

of the trailing leg can be used conjointly to estimate the exact moment the athlete's center of mass clears the hurdle and (2) if instrumented magnetic hurdles with the magnet placed on the horizontal bar could be used to estimate the distance between the hurdle and the foot.

The secondary aim of this study was to investigate the evolution of contact time, running speed, flight time, and step frequency throughout the race. As shown in Figure 8.8 and Table 8.3, contact time increased, and speed decreased with the distance covered. A significant rise ($p < 0.01$) was found for contact time starting from the sixth interval in comparison to the second interval. However, the rate of these changes did not appear to be associated with the performances of the athlete as the slowest and fastest participants presented similar rates of change.

The running speed was significantly reduced as the distance covered increased, starting with the fifth interval ($p < 0.05$) and increasing ($p < 0.01$) from the sixth interval. As for the contact time, no association between the change in running speed during the race and athlete caliber was evident. These results support the evidence from previous studies (Hanon & Gajer, 2009; Nummela et al., 1992), who also observed a significant increase in contact time and a decrease in running speeds for 400-m sprints. Note that the average and SD of step frequency measured in this study (3.52 ± 0.19) are comparable with those of national-level hurdlers presented in (Otsuka & Isaka, 2019). We also observed that the step frequency significantly decreased starting from the third interval.

Interestingly, flight time did not follow the same trend, and no clear pattern emerged from data analysis. Although the average flight time increased as the race progressed, only intervals 9 and 10 provided significant differences. This observation suggests that the flight time is less affected by fatigue than the contact time. However, a measure of stride length would be useful in future studies to further investigate the evolution of spatiotemporal variables as a function of fatigue during 400 m hurdle races.

Finally, Figure 8.9 presents the example of a report which was provided to the athletes and trainers. Such a graph showcases the potential of the proposed system and the type of feedback that can be provided during field training. Overall, this research offers new insight into the performance of different wearable methods for detecting HC and will contribute to a deeper understanding of the discipline by providing a tool for researchers, athletes, and trainers.

8.5 Conclusions

This study showed that foot-worn inertial and magnetic sensors, combined with magnets bars, can be used to detect hurdle clearing events in 400-m hurdle. The results showed that both unipedal and bipedal configuration can provide reliable detection. When the sensor is placed on one foot (unipedal configuration), the swing phase duration was capable of detecting 100% of the hurdle clearances. When combined with the pitch and yaw angles of the foot, the unipedal configuration can correctly identify the leading leg with an accuracy of 99.7%.

These results were even improved to a 100% accuracy in both HC detection and leading leg identification when using flight phase duration in bipedal configuration (a sensor at each foot). Moreover, this study also showed that the use of additional magnets/magnetometer does not improve the detection results of the system. Finally, this study showcased the potential benefit of using foot-worn IMUs and validated algorithms in 400-m hurdle races as they can provide helpful feedback about the race and continuously assess the changes in spatiotemporal parameters.

Acknowledgments

The authors would like to thank all the athletes who participated in this study. We would also like to thank M. Manuel Reynaert for his support with the measurements and M. Lionel Cottin for sharing his knowledge about 400 m hurdles discipline. Finally, we would like to thank the organizers of the Meeting Quatrache Tarare for their most appreciated welcome and professionalism.

Funding

This research was funded by the Swiss CTI, grant number 17664.1 PFNM-NM.

Abbreviations

Acronyms	Definition
$AvCT(k)$	Average CT within the kth interval expressed relatively to $AvCT(2)$
$AvFLY(k)$	Average FLY within the kth interval expressed relatively to $AvFLY(2)$
$AvSPE(k)$	Average SPE within the kth interval expressed relatively to $AvSPE(2)$
$AvSTF(k)$	Average STF within the kth interval expressed relatively to $AvSTF(2)$
CMFI	Calibrated magnetic field intensity
CT	Contact time
DH	Distance between the hurdles
FF	Functional frame
FLY	Flight phase duration
GF	Global frame
HC	Hurdle clearance
HC_{FLY}	HC detection results of the FLY parameter in the TEMP method
HC_{MB}	Bipedal HC detection results of the MAG method
HC_{ML}	Left foot HC detection results of the MAG method
HC_{MR}	Right foot HC detection results of the MAG method
$HC_{\psi L}$	Left foot HC detection results based on ψ_{left} in the ORIENT method
$HC_{\psi R}$	Right foot HC detection results based on ψ_{right} in the ORIENT method
HC_{OB}	Bipedal HC detection results of the ORIENT method (HC_{OL} and HC_{OR})
HC_{OL}	Left foot HC detection results of the ORIENT method ($HC_{\theta L}$ and $HC_{\psi L}$)
HC_{OR}	Right foot HC detection results of the ORIENT method ($HC_{\theta R}$ and $HC_{\psi R}$)

HC_{ref}	Reference HC time
HC_{STP}	HC detection results of the STP parameter in the TEMP method
HC_{STR}	HC detection results of the STR parameter in the TEMP method
HC_{SW}	HC detection results of the SW parameter in the TEMP method
$HC_{\theta L}$	Left foot HC detection results based on θ_{left} in the ORIENT method
$HC_{\theta R}$	Right foot HC detection results based on θ_{right} in the ORIENT method
IC	Initial contact
IMU	Inertial measurement unit
LL	Leading leg
LL_{FLY}	Bipedal LL detection results of the TEMP method using the FLY parameter
LL_{MB}	Bipedal LL detection results of the MAG method
LL_{STP}	Bipedal LL detection results of the TEMP method using the STP parameter
m_{left}	Magnetometer signal recorded on the left foot
\hat{m}_{left}	Preprocessed magnetometer signal from the left foot
m_{right}	Magnetometer signal recorded on the right foot
\hat{m}_{right}	Preprocessed magnetometer signal from the right foot
MAG	Magnetometer based method for HC and LL detection
MIMU	Magnetic inertial measurement unit
MS	Mid-stance
$N_{hurdles}$	Total number of hurdles
ORIENT	Orientation based method for HC and LL detection
ψ	Yaw angle
$\hat{\psi}$	Normalized yaw angle
ψ_{left}	Yaw angle measured on the left foot
ψ_{right}	Yaw angle measured on the right foot
SPE	Speed
STF	Step frequency
STP	Step duration
STR	Stride time
SW	Swing phase duration
τ	Minimum time difference between two consecutive HC
T_{race}	Official race time of a participant
T_{start}	Time of the start of the race
ΔT_{HC}	Differences in HC detection time
TC	Terminal contact
TEMP	Temporal parameter-based method for HC and LL detection
θ	Pitch angle
$\hat{\theta}$	Normalized pitch angle
θ_{left}	Pitch angle measured on the left foot
θ_{right}	Pitch angle measured on the right foot
V_{max}	Maximum running speed considered (42 km/h)

Conclusions Part IV

9 General Discussion

9.1 Main contributions

The objective of this thesis was to expand the scope of running analysis through the design of a new wearable assessment device. The proposed system, based on foot-worn inertial sensors, uses lab-validated algorithms to quantify the temporal parameter of gait, estimate the fixed-frame orientation of the foot, and measure the overground running speed. It was validated against gold-standard reference systems, and its applicability tested in real-world and unconstrained conditions (marathon, trail running, and 400-m hurdling).

As introduced in the first part of this thesis (Part I, Introduction and Background), the exact relationship between the spatiotemporal parameters of gait and performances, or injuries, remains an open discussion among researchers. Hence, the proposed system does not have the pretentiousness to provide such a diagnostic. Instead, it provides scientists with new opportunities to monitor running in real conditions and over long periods. The system is non-invasive, lightweight, comfortable, and, as Part III revealed, can be introduced in different competition settings without disturbing the users.

The technical validation studies presented in Part II reveal the performance and limitations of the proposed methods. Characteristics such as bias and precision are essential to select the appropriate instrumentation for a given study; the precision (i.e., random error) of the system should be lower than any significant change in the measured parameters. Otherwise, these changes considered significant would disappear within the noise of the device.

However, as discussed in Part I, some of the methods reported in the literature are either not validated against gold-standard reference systems or derived from walking analysis without considering running-specific adaptations. Furthermore, the systems are often tested in controlled environments, such as on a level treadmill, and rarely accounted for the variety of settings that wearable sensors can undergo in real-world situations. In comparison, the current thesis (Part III) also tested the limitations of the proposed methods outdoor, in unconstrained environments, and for different types of running events: marathon, trail running,

and 400 meters hurdling.

The current thesis was organized into four parts, and each part was subdivided into different chapters. Part I introduced running and discussed the relevant temporal, kinematic, and kinetic parameters investigated in the literature (Chapter 1). It also briefly discussed the history of running assessments and provided evidence of growth in the number of participants. Chapter 2 then examined the current state-of-the-art in running assessment methods, starting with the gold-standard systems and followed with body-worn inertial sensors. On the latter subject, the performances and challenges associated with inertial sensing units in running were introduced.

Part II, focused on the technical description and validation of three novel methods for (1) temporal events detection and gait phases estimation, (2) measure the orientation of the foot by estimating and reducing the orientation drift, and (3) estimate the running speed using three different approaches. We showed that, in order for foot-worn inertial sensors to provide an accurate and precise evaluation of the running, the system must consider the underlying mechanics of the foot and adapt to the different landing techniques.

Part III tested the designed algorithms in three real-world applications (marathon race, ultra-marathon mountain race, and 400 meters hurdling event) and proposed amelioration when necessary. The system was able to observe trends in the average step height and vertical velocity in trail running, revealed statistically significant changes starting around the 25km of a marathon race and was able to detect the timing of hurdles crossings and to identify the leading leg. Moreover, the system was able to provide fast and relevant feedback to the track-and-field coaches of the hurdling study.

9.1.1 Part II – Algorithms development and validation

In Chapter 3, we validated against a force platform the performance of several algorithms to detect running temporal events and estimate inner-stride phases duration. The results showed that the two minimum values of the pitch angular velocity before and after a mid-swing event provided the best estimation of initial and terminal contact of the foot. The maximum vertical acceleration before a mid-swing event also provided a good estimation of terminal contact, and its accuracy seemed less associated with the running speed. Moreover, we showed that the ground contact time, flight time, step and swing time can be estimated with an inter-trial median \pm IQR bias less than 15 ± 12 ms and the inter-trial median \pm IQR precision less than 4 ± 3 ms. Besides, this chapter also described an automatic functional calibration method based on the motion of the foot during running. Such calibration method improves the user experience by reducing the tedious calibration movements to a short (3 seconds) standing period. As additional results , we proposed a decision tree structure to automatically assign body-worn sensors to the thorax, the sacrum, the left shank, the right shank, the left foot, or the right foot. The proposed classification method achieved an accuracy of 99.4% in the distinction between the upper vs. lower body sensors, 95% accuracy between the trunk and

sacrum sensors, 97.3% accuracy between the foot and shank sensors, 79.6% accuracy between the left and right foot-worn sensors, and 88.2% between the left and right shank-worn sensors. Hence, the current method provides a quasi-plug-and-play calibration method.

In Chapter 4, we introduced and validated a new method to estimate and correct the orientation drift estimation based on a foot-worn IMU using a two-segment model of the foot for drift removal. The validation compared sagittal and frontal plane angles obtained from an optical motion-tracking system with our inertial sensors-based estimation. The pitch angle at mid-stance was estimated with low errors (inter-trial median \pm IQR of $0.4 \pm 3.8^\circ$ and an inter-trial precision median \pm IQR of $3.0 \pm 1.8^\circ$). According to the results of a previous study (Altman & Davis, 2012), we argued that the performance of the proposed system should provide an acceptable classification of the foot strike pattern. Finally, as additional results, we discussed the accuracy of the foot strike pattern and pronation assessment using video cameras.

In Chapter 3 and Chapter 4, we showed that the accuracy of the proposed methods was affected by the running speed and suggested that, if known, the speed could be used to improve the system. Hence, in Chapter 5, we proposed and evaluated three different methods for real-world running speed estimation: direct speed estimation, training-based linear model, and a personalized model. The direct estimation of the foot velocity was sensitive to the changes in ground incline and confirmed the hypothesis that the techniques derived from walking can not be generalized to running due to the inaccurate measures of the accelerometer during the flight phase. We also showed that the linear model performed best when we averaged its output over a few steps and proposed 4 steps as an acceptable trade-off between performance (bias: 0.00 ± 0.11 m/s; precision: 0.12 ± 0.06 m/s) and time-resolution. Lastly, we presented the results from the personalized model and concluded that the inter-subject bias and precision could be improved, given intermittent access to some reference speed data.

Overall, the methods described in Part II led to the development of a collection of task-specific algorithms. The algorithms are interconnected in the sense that each plays an essential role in the subsequent ones. For instance, the automatic functional calibration developed in this thesis first needs to ensure that the IMU is actually located on foot, hence the importance of the automatic IMU-to-segment assignment. Similarly, initial and terminal contact events are detected the sagittal plane angular velocity signals and therefore depend on the quality of the functional calibration. Such comments also hold for the importance of temporal analysis in drift correction and drift correction in the estimation of the running speed.

9.1.2 Part III – Real-world applications

In Chapter 6, we tested the proposed methods during a marathon race and showed that the spatiotemporal parameters can be measured continuously throughout the race and provide relevant information about the mechanical alteration occurring as the distance increases. The main challenge we faced with the marathon was the presence of walking bouts within the

race. These bouts need to be removed from the analysis, and a simple speed-based threshold showed inconsistencies, especially in 6 to 8 km/h range. We, therefore, added criteria based on the duty factor. The analysis suggested the presence of two breaks on the running patterns during the race: a first occurring after approximately 25 km, and the second occurring after 35 km. Apart from the changes in contact time and flight phase duration, the continuous assessment of the foot strike angle provided new insight into its slowly decreasing pattern, which was not possible from the video-based analyses (Hasegawa et al., 2007).

In Chapter 7, we showed that the temporal analysis algorithms presented in Chapter 3 can be extended to IMUs located at the ankle joint and that these algorithms were able to investigate the effects of altitude and distance on the main spatiotemporal gait parameters during an extreme mountain ultra-marathon. In trail running, the racing conditions are frequently changing: the slope from uphill to down running, the surface from concrete to grass and rocky mountain trail, and the weather from warm and sunny to cold and humid. These challenging environments can potentially affect the foot kinematics and, consequently, also the robustness of temporal events detection. For instance, when trail participants are dealing with uneven surfaces, they adapt their gait according to the obstacles on the ground, possibly changing their step frequency very rapidly and causing misdetections in the analysis. Hence, to increase the time-resolution of cycle detection, we updated the sliding estimation method of the step frequency and added some timing-based criteria to check for missing steps. Moreover, over 20 hours of running, the attachment of the IMU sensors tends to loosen. We observed this issue in the kinematic data and improved the algorithms by adding an episodic recalibration of the sensors. This realignment of the IMUs' technical frame was only possible when the participants stopped running. Moreover, we showed that barometers could be used in conjunction with inertial sensors to estimate the average vertical speed.

Chapter 8 showed that the proposed algorithms can assess the spatiotemporal changes of gait and detect hurdle clearing events in a 400-m hurdling event. Compared to the previous applications, 400-m hurdling exhibit running patterns closer to sprinting, with higher running speed and a tendency to forefoot strike. The speed did not affect the detection thresholds set for treadmill running (i.e., set during the validation), but the jumping movements required to clear the hurdles did. Hence, we used the envelope of the high-frequency oscillations to narrow the search window around initial and terminal contact, and thus improved the robustness of step detection. The results showed that the method based on the duration of the flight phase was able to detect hurdle clearance and identify the leading leg with 100% accuracy. Moreover, by combining the swing phase duration with the orientation of the foot, we achieved, in unipedal configuration, 100% accuracy in hurdle clearance detection, and 99.7% accuracy in the identification of the leading leg. In addition, we also provided examples of performance feedback and provided a general analysis of the changes in spatiotemporal parameters among participants. Overall, this research might contribute to a deeper understanding of hurdling by providing a tool for researchers, athletes, and trainers. Today, the majority of the track and field coaches use a stopwatch to monitor the time at the hurdles and visually count the number of steps between the hurdles; such a method can be inaccurate and it only allows to

monitor one athlete at the time.

The variety of applications in which the system was evaluated revealed a need for a few adaptations. Although the primary purpose of the algorithms remained unchanged, these improvements constitute a critical step in making the system reliable in the wild. The need was rather directed toward more robust detection and lower sensitivity to abrupt artifacts in the data. While these issues can be avoided in-lab, they could become a reason of failure in-field. To summarize, we provide the list of improvements we implemented for the real-world studies

- Detection and suppression of the walking bouts in conjunction with a threshold on the running speed.
- Sliding window based estimation of the step frequency to improve the resolution of the step detection algorithm.
- Automatic and episodic recalibration of the technical frame with the functional frame of the foot.
- Improved step detection algorithm based on the high-frequency accelerations around initial and terminal contact, to cope with irregular jumping movements.
- Detection of hurdle crossing events in 400 meters hurdling events.
- Identification of the leading leg in 400 meters hurdling events.

In addition to the applications mentioned above, the algorithms proposed in Part II were also employed in two other research studies. Here, we briefly present the content and outcome of these studies and explain the contributions of our methods.

- The automatic functional calibration method described in Chapter 3 was used in a study published in the journal *Footwear Science* (C. Meyer et al., 2018). The objective of the study was to investigate the influence of perceived footwear comfort on the variability of running kinematics as a potential surrogate measure of comfort. Functional calibration was performed in post-processing using the running data from thirty-six recreational athletes in five different running shoes on an indoor track. For each trial, the algorithm was able to compute all the transformation matrices that aligned the shoe-worn IMU technical frame with the functional frame of the foot.
- The spatiotemporal evaluation methods presented in Chapters 3 and 4 were used in a study published in the journal *Current sports medicine reports* (Muniz-Pardos et al., 2018). Although preliminary in nature, this study illustrated the unique capacity of wearable devices to assess real-time running economy and foot mechanics in the field. The algorithms were used to analyze the real-world measurements of 8 Kenyan athletes and 4 adolescents.

9.2 The proposed system in the industry

To make the outcome of this thesis available for any user, most methods presented in this thesis were transferred into a commercialized product designed by Gait Up S.A. in the framework of an academic-industry agreement (CTI and Innosuisse grants). The product development was split into three sub-projects: (1) the design and implementation of a user interface, (2) the creation of a private web architecture to store and process the data, and (3) the adaptation of the validated algorithms into performance-efficient programming language (C++). I was involved in the latter two stages.

A first version of the system was designed as an Android application capable of quickly recording and analyzing running data wirelessly sent from two IMU units. The server architecture was designed such that the generated reports and raw data could be kept and reused in later times, for these reports to be recomputed after an update of the running analysis algorithms. The meta-information associated with a report (e.g., client size, shoe type, date) was also stored for further analysis. The cloud architecture was comprised of four elements: a public web API, a private web API, a document-oriented database, and storage units for the raw binary files. These elements were built using the latest technologies so that the cloud architecture and performances can be scaled in the future if needed. This version of the running analysis system won the first prize at the 2015/2016 Wearable Technologies Innovation World Cup in Sports & Fitness (Figure 9.1).

Today, the product evolved into a fast and precise system for stride-by-stride analysis of the running technique. Hence the algorithms of this thesis are now commercially available to coaches, shoe retailers, and athletes.

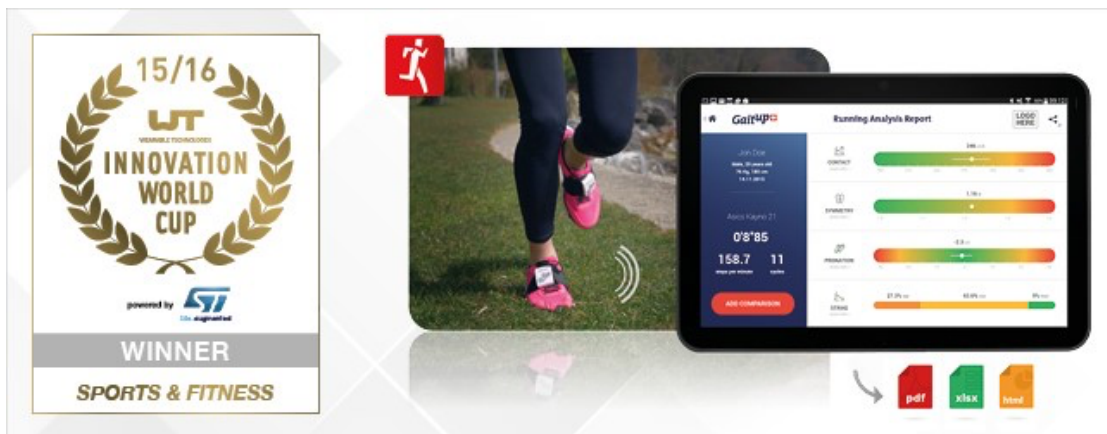


Figure 9.1 – WT Innovation World Cup award attributed to Gait Up S.A. for the running analyzer system. Source www.gaitup.com.

9.3 Limitations

The lab validation is a crucial step towards accurate and precise wearable systems. It allows comparing the system's performance with state-of-the-art devices for a variety of gait parameters. However, this controlled environment introduces some limitations in the methods, which only real-world testing can reveal. Outdoor applications provide useful insight into the robustness of the system, particularly about its capacity to perform in the presence of motion artifacts, such as sensors' attachment loosening, uneven surfaces, or intermittent non-running-related movements. Here, we discuss the limits observed both in-lab and in real-world conditions for the methods presented in this thesis.

Temporal event detection introduced in Chapter 3 was validated for level running, so the performance of the proposed algorithms can not be extended to uphill or downhill running. Even though we would expect the kinematics features used for initial and terminal contact to work on an inclined ground surface, the exact error of these features can not be extrapolated; for level running, we used the pitch angular velocity to detect the midswing events and find the timing of initial and terminal contact events. Since the range of motion in the sagittal plane of the lower-limbs is affected by the running slope (Vernillo, Giandolini, et al., 2017), the detection algorithms might require some adaptations to achieve comparable performance than for level running. Moreover, the accuracy of the initial and terminal contact was affected by the running speed. Since this study recorded running speeds between 10 to 20 km/h, the results reported in Chapter 3 are relevant within this range of velocities. For speed below 10 km/h, the less dynamic movement of the foot would probably lead to a higher overestimation of the timing of terminal contact. In contrast, initial contact error would remain roughly identical (Figure 3.3). At a certain extend, the subject would switch to walking, and the performance of these features (i.e., the local minimum of the pitch angular velocity) can be found in (Mariani et al., 2013). However, at speeds higher than 20 km/h, the results suggest that the bias of gait phases decreases as the running speed increases (Figure 3.4). Hence, by extrapolation of the linear trend, it is reasonable to assume that the bias would be relatively low. Correction of the bias based on the running speed would require a measure of the instantaneous speed to apply the right correction at each step. Hence the need for a reliable estimation of the overground speed in the system (Chapter 5). Finally, the footstrike pattern might lead to inter-subject differences in the detection performance of initial contact since the pitch angular velocity is used to detect the event.

The ground incline might also affect the orientation drift correction method proposed in Chapter 4. To model the drift, we hypothesized that the forefoot segment remained flat on the ground surface during a fraction of the stance phase, so we set its acceleration parallel to the gravity vector (i.e., perpendicular to the ground surface). However, this assumption is incorrect for uphill and downhill running; the orientation of the gravity vector depends on the ground incline. As shown in Chapters 6 and 7, the barometer can be used to estimate the ground incline, but whether the estimation is reliable enough for drift correction remains an open question. Consequently, the results reported in Chapter 4 can not be extended to inclined

running. Additionally, the automatic estimation of the sensor placement on the rear-foot was performed using two phases. The goal of the first phase was to remove the horizontal plane acceleration of the treadmill from the rearfoot acceleration. Theoretically, this first iteration should not be needed for overground running. Still, it is currently not possible to assess whether reducing to a single iteration would affect the error of the model. Also, the current model does not include a correction of the heading, but its structure could be adapted to include magnetometer-based heading estimation for field studies. Based on the above, further research in applied settings should be carried to assess the performance of the drift correction method proposed in Chapter 4.

As we observed with the marathon and ultra-trail measurements, the tracking of the time by the sensors can vary after an extended period of utilization. This issue is called jitter and, in short, occurs when the internal clock of an IMU records the time at a different rate than another device. Hence, even if two IMUs are synchronized at the start, they may experience a time difference of several milliseconds after a few minutes of recording. In research, jitter is usually compensated by recording the same movement simultaneously on the different sensors (e.g., shanking the IMUs while holding them in your hand) and interpolating the timestamps of each sensor to match the timing of movement. Although this procedure is adequate for research, it might not be applicable for long term measurements or when the participants are handling the start and stop of the sensors (e.g., typical in cohort studies). The issue with long-term measurements is the following: if the one of the foot-worn IMU stops before the end of the race (e.g., because of a discharged battery), then the post-race synchronization can not be recorded on both devices and jitter can not be removed. It is important to note that step duration and flight time are both affected by jitter. Flight time and step duration require the time of initial and terminal contact measured from both foot-worn IMUs. Therefore, when jitter occurs, the duration of these temporal parameters will be underestimated for one leg and overestimated for the other, which, in turn, leads to an inter-step variability increasing with the measurement duration. To avoid this issue, researchers should always prefer IMU devices with radio frequencies synchronization, which is not the case for all the commercially available devices.

As we mentioned previously, rapid changes in the step frequency and the presence of walking bouts can affect the performance of the temporal analysis method of Chapter 3. This method was validated using 30 seconds trials at constant-speed, where the stride frequency was roughly constant. Hence, the 5-second window we implemented for midswing detection performed adequately, whereas this time resolution was too low for the ultra-trail and hurdling applications. Even though we improved this functionality, these adaptations were explicitly set for each study and might not generalize to other applications.

Sensor attachment also revealed to be an essential component for the proposed method to work correctly. We obtained the validation results reported in this thesis using IMUs firmly fixed on the dorsum of the shoe, therefore, reducing the effect of sensor wobbling to a minimum. Moreover, once the sensor was attached it did not change its orientation relative

to the orientation of the foot. Thus, functional calibration was applied once for each trial, and this high fidelity in the sensor orientation allowed the proposed method to distinguish between the kinematics for each functional axis consistently. For instance, we showed that the two minimum values of the pitch angular velocity were the most stable features to detect initial and terminal contact. In real-world applications, however, sensor fixation is more challenging. For instance, firmly taping the sensors on the shoe is not possible in trail-running as the different surfaces and environments (e.g., rocks, snow) are likely to deteriorate the tape. Clips can be a good alternative, but the level of motion artifacts depends on the tightness of the shoelaces, which, throughout long-distance races, can start to loosen. In hurdling, athletes were particularly concerned about the fixation of the sensors and preferred using the tape. Such limitations were also reported in a recent review (Camomilla et al., 2018) about the in-field utilization of body-worn inertial sensors. Overall, the best solution seems to re-evaluate the quality of the sensors' calibration sporadically. The method proposed in this thesis can perform this re-evaluation but requires a short standing period. Although this was possible in trail running, it could not be applied in the marathon study (i.e., participants did not stop running).

There is evidence that real-time feedback can help reduce the types of lower extremity loading associated with stress fractures when real-time visual feedback is provided to the runners (Crowell et al., 2010). The methods presented in Part II could be used in quasi-real-time but would require a device capable of storing at least 3 seconds of accelerometer and angular velocity measurements. This limit depends on the smallest time resolution that the stride detection algorithm can achieve, but can not be shorter than one stride. Moreover, if the algorithms are embedded in a single measurement unit, flight time, and step duration can not be measured with the current methods.

Finally, the methods presented in this thesis were explicitly designed for foot-worn sensors. Even though we could apply the functional calibration and temporal analysis to inertial sensors located on the shank during trail running, the actual accuracy of initial contact and terminal contact detection can not be extrapolated from Chapter 3 for shank-worn sensors. Moreover, the drift correction method of Chapters 4 and 5 was based on a two-segments model of the foot. Using foot-worn sensors can be a limiting factor in some applications. For instance, it might not be possible to use such sensors configuration to assess the running biomechanics in soccer, as it could interfere with the ball contact. Nevertheless, the miniaturization advents in MEMS could solve this problem and allow shoe manufacturers to include the sensors directly in the sole. In such a configuration, the proposed method could be used in a wide range of applications.

9.4 Future developments

In addition to the improvements required by the current limitations of the methods presented in this thesis (e.g., occasional recalibration of the sensors, high-resolution stride detection,

uphill, and downhill running testing), several other features could significantly improve the system. Here, we introduce some ideas for future developments and research through the following topics: (1) integration of other sensors, (2) modeling of the running power, and (3) extension to other applications.

9.4.1 Integration of other sensor data

In this thesis, we have used the measurement from a barometer to estimate the elevation speed (Chapters 5 and 6) and, through multiplication with the running speed, obtained the ground inclination. We did not evaluate the error of the slope estimation but suggest that it might become necessary for further investigation of outdoor running. Hence, we propose the following improvements to the method discussed in Chapter 5. Instead of using the continuous barometer measurements, which are affected by the changes in air pressure during the period of swing, we propose to use the detection results from the temporal method and consider the mean barometric pressure during the stance phase. This process would result in a time series with one barometric measure per period of stance, and it is this time series, which should then be resampled and lowpass filtered to obtain the vertical velocity. With a reliable measure of the ground incline, we could further improve the orientation drift model and set the theoretical acceleration of the forefoot according to the slope.

Also, the current orientation drift correction method (Chapter 4) is not accounting for the changes in the azimuth. Hence, testing the effectiveness of several sensor fusion methods could significantly improve the overall usability of the system in-field. It is common to use magnetometers as an external source of information to account for the change in heading direction (Bergamini et al., 2014; Madgwick et al., 2011; Sabatini, 2006). Similar to gravity, the Earth's magnetic field provides a sufficiently constant vector field to derive the azimuth from the magnetometer's measurements. However, magnetometers are sensitive to ferromagnetic objects, making their utilization more challenging indoor, especially for sensors close to the ground, such as for foot-worn MIMU.

9.4.2 Modeling the running power

In running, the notion of mechanical work dates back to the early work of Fenn (W. O. Fenn, 1930; Wallace O. Fenn, 1930), where the author attempted to explain the metabolic cost of running by quantifying the mechanical work. Cavagna et al. (Cavagna et al., 1964) later extended the calculation of Fenn (Wallace O. Fenn, 1930) to a broader range of running speeds. In level running, different methods have been proposed to measure the total amount of work produced by the body and thus derive the mechanical power. Two distinct types of work have been identified: the external work, which sustains the motion of an individual's center of mass relative to the surrounding, and the internal work, which sustains the motion of the limbs relative to the center of mass. Currently, the instrumentation used to estimate power in running is primarily based on force plates and camera-based motion tracking systems.

Power-meters have been used for decades in cycling and are recognized as relevant tools for amateurs and professionals to optimize their training effort. In cycling, the power is directly measured from sensors integrated to the bike. In comparison, estimating the real-world power in running based on body-worn inertial sensors relies on indirect measurements. A model of running biomechanics is necessary to combine the relevant features obtained by the sensors. Based on the methods proposed in this thesis, temporal parameters, foot orientation, and overground speed are already available for the prediction of power. However, a method to estimate the ground reaction forces, a crucial component of the mechanical work, has yet to be implemented.

Although some studies (Sheerin et al., 2019) have proposed the tibial peak acceleration at landing as a proxy measurement for the impact forces, their methods were not able to reliably estimate the continuous profile of the ground reaction force and might not generalize to foot-worn accelerometers. Recently, however, Clark et al. (Clark et al., 2017) suggested that the vertical ground reaction force could be estimated from temporal and kinematic features, such as flight time, vertical acceleration of the lower limb during landing, and ground contact time. Since the model requires highly accurate spatiotemporal input, it has never been tested with inertial sensors. Given the results of the current thesis, it would be interesting to evaluate the model of Clark et al. (Clark et al., 2017) using IMU-based inputs against a reference force plate in level, uphill, and downhill running. For inclined running, it might be necessary to modify the model according to the observations by (Dewolf et al., 2016), which stated that adding a damper should be included in the model for downhill running, and a motor for uphill running.

By applying a validation method similar then described in Chapter 5 (i.e., feature selection and linear modeling), we designed and tested a model, 34 participants, to estimate the positive peak power in the anteroposterior direction of running. The algorithms were based on foot-worn inertial sensors and reached 14% precision and 2% accuracy for the whole population. Further, considering the specific running gait style of each individual, the general algorithm was personalized by adding a few data (5%) of each subject in the training phase. The performance of the personalized algorithm reached 5% precision and 0% accuracy for peak power estimation. The results of the personalized algorithm are encouraging and demonstrate the potential for improvements in the general algorithm. Several solutions have already been identified, such as adding new features, using non-linear models, or grouping the participants based on their technique and adapt the model accordingly. Moreover, we obtained the current results using foot-worn inertial sensors only, hence adding other sensors could contribute to improving the performances.

9.4.3 Relevance in other applications

The algorithms proposed in this thesis can have a variety of applications. In addition to running performance analysis, such as presented in Chapters 6-8, the system could be used for long term monitoring of the training load, for rehabilitation, or shoe fitting. For example,

an athlete recovering from a lower-limb injury might only be allowed back to the competition if the spatiotemporal parameters of the injured leg match those of the sound leg. However, to determine which parameter of gait best indicates such asymmetry will require further study. Also, shoe retailers could instrument their customers with the proposed system and use it to select the right footwear. As we introduced in Chapter 1, the notions of “preferred movement path,” and “habitual motion path” (B. M. Nigg et al., 2017; Trudeau et al., 2019) have recently emerged as a new alternative for the selection of the appropriate footwear, and the methods developed in this thesis could instrument such analysis.

Moreover, running occurs in a variety of team sports, such as soccer, rugby, football, or baseball. Thus the system designed in this thesis could be extended to these events. They could monitor the gait of athletes throughout a game or training, and report to the staff sudden changes in a player’s gait patterns as it might indicate the emergence of an injury or an advanced state of fatigue. For instance, rugby suffers from a high incidence of traumatic brain injuries, and these injuries can have different degrees of severity. In some cases, traumatic brain injuries are not directly visible from the sideline, and concussed players might remain in the game, risking the dangerous consequences of undergoing additional impacts to the head. However, concussions have shown (Ling et al., 2015) to affect the balance and coordination of individuals. Hence, inertial sensors placed into the sole of the rugby shoes, combined with the methods proposed in the current thesis, might be sensitive enough to detect an unusual asymmetry in the running gait of a concussed player and report this observation to the clinical staff.

Bibliography

- Abbiss, C. R., & Laursen, P. B. (2008). Describing and understanding pacing strategies during athletic competition. In *Sports Medicine*, 38(3), 239-252.
- Abt, J. P., Sell, T. C., Chu, Y., Lovalekar, M., Burdett, R. G., & Lephart, S. M. (2011). Running kinematics and shock absorption do not change after brief exhaustive running. *The Journal of Strength & Conditioning Research*, 25(6), 1479-1485. <https://doi.org/10.1519/JSC.0b013e3181ddfcf8>
- Aggarwal, P., Syed, Z., Niu, X., & El-Sheimy, N. (2008). A standard testing and calibration procedure for low cost MEMS inertial sensors and units. *Journal of Navigation*, 61(2), 323-336. <https://doi.org/10.1017/S0373463307004560>
- Ahn, A. N., Brayton, C., Bhatia, T., & Martin, P. (2014). Muscle activity and kinematics of forefoot and rearfoot strike runners. *Journal of Sport and Health Science*, 3(2), 102-112. <https://doi.org/10.1016/j.jshs.2014.03.007>
- Alexander McN., R. (1989). Optimization and gaits in the locomotion of vertebrates. *Physiological Reviews*, 69(4), 1199-1227. <https://doi.org/10.1152/physrev.1989.69.4.1199>
- Alexander, R. M. (1991). Energy-saving mechanisms in walking and running. *The Journal of Experimental Biology*, 160, 55-69.
- Altman, A. R., & Davis, I. S. (2012). A kinematic method for footstrike pattern detection in barefoot and shod runners. *Gait and Posture*, 35(2), 298-300. <https://doi.org/10.1016/j.gaitpost.2011.09.104>
- Amann, M., Romer, L. M., Pegelow, D. F., Jacques, A. J., Hess, C. J., & Dempsey, J. A. (2006). Effects of arterial oxygen content on peripheral locomotor muscle fatigue. *Journal of Applied Physiology*. <https://doi.org/10.1152/jappphysiol.01596.2005>
- Amara, S., Mkaouer, B., Chaabene, H., Negra, Y., & Ben-Salah, F. Z. (2019). Key kinetic and kinematic factors of 110-m hurdles performance. *Journal of Physical Education and Sport*, 19(1), 658-668. <https://doi.org/10.7752/jpes.2019.01095>
- Amini, N., Sarrafzadeh, M., Vahdatpour, A., & Xu, W. (2011). Accelerometer-based on-body sensor localization for health and medical monitoring applications. *Pervasive and Mobile Computing*, 7(6), 746-760. <https://doi.org/10.1016/j.pmcj.2011.09.002>

- Aminian, K., Najafi, B., Büla, C., Leyvraz, P. F., & Robert, P. (2002). Spatio-temporal parameters of gait measured by an ambulatory system using miniature gyroscopes. *Journal of Biomechanics*, 35(5), 689-699. [https://doi.org/10.1016/S0021-9290\(02\)00008-8](https://doi.org/10.1016/S0021-9290(02)00008-8)
- Ammann, R., Taube, W., & Wyss, T. (2016). Accuracy of PARTwear inertial sensor and optojump optical measurement system for measuring ground contact time during running. *Journal of Strength and Conditioning Research*, 30(7), 2057-2063. <https://doi.org/10.1519/JSC.0000000000001299>
- Ancillao, A., Tedesco, S., Barton, J., & O'flynn, B. (2018). Indirect measurement of ground reaction forces and moments by means of wearable inertial sensors: A systematic review. In *Sensors (Switzerland)* (Vol. 18, Issue 8). MDPI AG. <https://doi.org/10.3390/s18082564>
- Andersen, J. J. (2019). *The State of Running 2019*. RunRepeat. <https://runrepeat.com/state-of-running>
- Angus, S. D., & Waterhouse, B. J. (2011). Pacing strategy from high-frequency field data: More evidence for neural regulation? *Medicine and Science in Sports and Exercise*. <https://doi.org/10.1249/MSS.0b013e3182245367>
- Areblad, M., Nigg, B. M., Ekstrand, J., Olsson, K. O., & Ekström, H. (1990). Three-dimensional measurement of rearfoot motion during running. *Journal of Biomechanics*, 23(9), 933-940. [https://doi.org/10.1016/0021-9290\(90\)90358-A](https://doi.org/10.1016/0021-9290(90)90358-A)
- Arellano, C. J., & Kram, R. (2014). The metabolic cost of human running: Is swinging the arms worth it? *Journal of Experimental Biology*, 217(14), 2456-2461. <https://doi.org/10.1242/jeb.100420>
- Arndt, A., Wolf, P., Liu, A., Nester, C., Stacoff, A., Jones, R., Lundgren, P., & Lundberg, A. (2007). Intrinsic foot kinematics measured in vivo during the stance phase of slow running. *Journal of Biomechanics*, 40(12), 2672-2678. <https://doi.org/10.1016/j.jbiomech.2006.12.009>
- Bailey, G. P., & Harle, R. (2014). Assessment of foot kinematics during steady state running using a foot-mounted IMU. *Procedia Engineering*, 72, 32-37. <https://doi.org/10.1016/j.proeng.2014.06.009>
- Balducci, P., Cléménçon, M., Trama, R., Blache, Y., & Hautier, C. (2017). Performance Factors in a Mountain Ultramarathon. *International Journal of Sports Medicine*. <https://doi.org/10.1055/s-0043-112342>
- Bartko, J. J. (1966). The intraclass correlation coefficient as a measure of reliability. *Psychological Reports*, 19(1), 3-11. <https://doi.org/10.2466/pr0.1966.19.1.3>
- Bates, B. T., & Haven, B. H. (1974). Effects of fatigue on the mechanical characteristics of highly skilled female runners. *Biomechanics IV*, 121-125.

- Behling, A. V., Manz, S., von Tscharnier, V., & Nigg, B. M. (2019). Pronation or foot movement — What is important. *Journal of Science and Medicine in Sport*. <https://doi.org/10.1016/j.jsams.2019.11.002>
- Bélaise, C., Blache, Y., Thouzé, A., Monnet, T., & Begon, M. (2016). Effect of wobbling mass modeling on joint dynamics during human movements with impacts. *Multibody System Dynamics*, 38(4), 345-366. <https://doi.org/10.1007/s11044-016-9519-6>
- Belli, A., Bui, P., Berger, A., Geysant, A., & Lacour, J. R. (2001). A treadmill ergometer for three-dimensional ground reaction forces measurement during walking. *Journal of Biomechanics*, 34(1), 105-112. [https://doi.org/10.1016/S0021-9290\(00\)00125-1](https://doi.org/10.1016/S0021-9290(00)00125-1)
- Bénabou, M. (2009). Le mouvement. In *Médium* (Vols. 20-21, Issue 3). G. Masson. <https://doi.org/10.3917/mediu.020.0212>
- Benca, E., Listabarth, S., Flock, F. K. J., Pablik, E., Fischer, C., Walzer, S. M., Dorotka, R., Windhager, R., & Ziai, P. (2020). Analysis of Running-Related Injuries: The Vienna Study. *Journal of Clinical Medicine*, 9(2), 438. <https://doi.org/10.3390/jcm9020438>
- Benson, L. C., Clermont, C. A., Bošnjak, E., & Ferber, R. (2018). The use of wearable devices for walking and running gait analysis outside of the lab: A systematic review. In *Gait and Posture* (Vol. 63, pp. 124-138). Elsevier B.V. <https://doi.org/10.1016/j.gaitpost.2018.04.047>
- Bergamini, E., Guillon, P., Camomilla, V., Pillet, H., Skalli, W., & Cappozzo, A. (2013). Trunk inclination estimate during the sprint start using an inertial measurement unit: A validation study. *Journal of Applied Biomechanics*. <https://doi.org/10.1123/jab.29.5.622>
- Bergamini, E., Ligorio, G., Summa, A., Vannozzi, G., Cappozzo, A., & Sabatini, A. M. (2014). Estimating orientation using magnetic and inertial sensors and different sensor fusion approaches: Accuracy assessment in manual and locomotion tasks. *Sensors (Switzerland)*, 14(10), 18625-18649. <https://doi.org/10.3390/s141018625>
- Bergamini, E., Picerno, P., Pillet, H., Natta, F., Thoreux, P., & Camomilla, V. (2012). Estimation of temporal parameters during sprint running using a trunk-mounted inertial measurement unit. *Journal of Biomechanics*, 45(6), 1123-1126. <https://doi.org/10.1016/j.jbiomech.2011.12.020>
- Bertram, J. E. A., Prebeau-Menezes, L., & Szarko, M. J. (2013). Gait characteristics over the course of a race in recreational marathon competitors. *Research Quarterly for Exercise and Sport*. <https://doi.org/10.1080/02701367.2013.762259>
- Bland, J. M., & Altman, D. G. (1986). Statistical Methods for Assessing Agreement Between Two Methods of Clinical Measurement. *The Lancet*, 327(8476), 307-310. [https://doi.org/10.1016/S0140-6736\(86\)90837-8](https://doi.org/10.1016/S0140-6736(86)90837-8)
- Blickhan, R. (1989). The spring-mass model for running and hopping. *Journal of Biomechanics*, 22(11-12), 1217-1227. [https://doi.org/10.1016/0021-9290\(89\)90224-8](https://doi.org/10.1016/0021-9290(89)90224-8)

- Bolanakis, D. E. (2017). MEMS Barometers Toward Vertical Position Detection: Background Theory, System Prototyping, and Measurement Analysis. In *Synthesis Lectures on Mechanical Engineering* (Vol. 1, Issue 1). Morgan & Claypool Publishers. <https://doi.org/10.2200/s00769ed1v01y201704mec003>
- Bonnet, S., Bassompierre, C., Godin, C., Lesecq, S., & Barraud, A. (2009). Calibration methods for inertial and magnetic sensors. *Sensors and Actuators, A: Physical*, 156(2), 302-311. <https://doi.org/10.1016/j.sna.2009.10.008>
- Bovalino, S. P., Cunningham, N. J., Zordan, R. D., Harkin, S. M., Thies, H. H. G., Graham, C. J., & Kingsley, M. I. C. (2020). Change in foot strike patterns and performance in recreational runners during a road race: A cross-sectional study. *Journal of Science and Medicine in Sport*. <https://doi.org/10.1016/j.jsams.2019.12.018>
- Boyer, E. R., Rooney, B. D., & Derrick, T. R. (2014). Rearfoot and midfoot or forefoot impacts in habitually shod runners. *Medicine and Science in Sports and Exercise*, 46(7), 1384-1391. <https://doi.org/10.1249/MSS.0000000000000234>
- Brahms, C. M. (2017). *The assessment of fatigue-related changes in stride mechanics, variability and long-range correlations in recreational and elite distance runners using foot-mounted inertial sensors* (Issue March). University of Regina.
- Bredeweg, S. W., Kluitenberg, B., Bessem, B., & Buist, I. (2013). Differences in kinetic variables between injured and noninjured novice runners: A prospective cohort study. *Journal of Science and Medicine in Sport*, 16(3), 205-210. <https://doi.org/10.1016/j.jsams.2012.08.002>
- Brégu Bourgeois, A., Mariani, B., Aminian, K., Zambelli, P. Y., & Newman, C. J. (2014). Spatio-temporal gait analysis in children with cerebral palsy using, foot-worn inertial sensors. *Gait and Posture*, 39(1), 436-442. <https://doi.org/10.1016/j.gaitpost.2013.08.029>
- Breine, B., Malcolm, P., Frederick, E. C., & De Clercq, D. (2014). Relationship between running speed and initial foot contact patterns. *Medicine and Science in Sports and Exercise*, 46(8), 1595-1603. <https://doi.org/10.1249/MSS.0000000000000267>
- Brodie, M., Walmsley, A., & Page, W. (2008). Fusion motion capture: a prototype system using inertial measurement units and GPS for the biomechanical analysis of ski racing. *Sports Technology*, 1(1), 17-28. <https://doi.org/10.1002/jst.6>
- Brosnan, K. C., Hayes, K., & Harrison, A. J. (2017). Effects of false-start disqualification rules on response-times of elite-standard sprinters. *Journal of Sports Sciences*, 35(10), 929-935. <https://doi.org/10.1080/02640414.2016.1201213>
- Brown, J. P., & Josse, R. G. (2002). 2002 Clinical practice guidelines for the diagnosis and management of osteoporosis in Canada. *Cmaj*, 167(10).
- Bullimore, S. R., & Burn, J. F. (2007). Ability of the planar spring-mass model to predict mechanical parameters in running humans. *Journal of Theoretical Biology*, 248(4), 686-695. <https://doi.org/10.1016/j.jtbi.2007.06.004>

- Butler, R. J., Davis, I. S., & Hamill, J. (2006). Interaction of arch type and footwear on running mechanics. *American Journal of Sports Medicine*. <https://doi.org/10.1177/0363546506290401>
- Camomilla, V., Bergamini, E., Fantozzi, S., & Vannozzi, G. (2018). Trends supporting the in-field use of wearable inertial sensors for sport performance evaluation: A systematic review. *Sensors (Switzerland)*, 18(3). <https://doi.org/10.3390/s18030873>
- Castillo, E. R., & Lieberman, D. E. (2018). Shock attenuation in the human lumbar spine during walking and running. *Journal of Experimental Biology*, 221(9). <https://doi.org/10.1242/jeb.177949>
- Cavagna, G. A., Saibene, F. P., & Margaria, R. (1964). Mechanical Work in Running. *Journal of Applied Physiology*, 19, 249-256. <https://doi.org/10.1152/jappl.1964.19.2.249>
- Cavanagh, P. R. (1990). Biomechanics of distance running. *Choice Reviews Online*, 28(04), 28-2199-28-2199. <https://doi.org/10.5860/choice.28-2199>
- Cavanagh, Peter R., & Lafortune, M. A. (1980). Ground reaction forces in distance running. *Journal of Biomechanics*, 13(5), 397-406. [https://doi.org/10.1016/0021-9290\(80\)90033-0](https://doi.org/10.1016/0021-9290(80)90033-0)
- Cavanagh, Peter R., Pollock, M. L., & Landa, J. (1977). a Biomechanical Comparison of Elite and Good Distance Runners. *Annals of the New York Academy of Sciences*, 301(1), 328-345. <https://doi.org/10.1111/j.1749-6632.1977.tb38211.x>
- Chakravarty, E. F., Hubert, H. B., Lingala, V. B., & Fries, J. F. (2008). Reduced disability and mortality among aging runners: A 21-year longitudinal study. *Archives of Internal Medicine*, 168(15), 1638-1646. <https://doi.org/10.1001/archinte.168.15.1638>
- Challis, J. H. (2001). The variability in running gait caused by force plate targeting. *Journal of Applied Biomechanics*. <https://doi.org/10.1123/jab.17.1.77>
- Chan-Roper, M., Hunter, I., Myrer, J. W., Eggett, D. L., & Seeley, M. K. (2012). Kinematic changes during a marathon for fast and slow runners. *Journal of Sports Science and Medicine*.
- Channells, J., Purcell, B., Barrett, R., & James, D. (2006). Determination of rotational kinematics of the lower leg during sprint running using accelerometers - art. no. 603616. *BioMEMS and NanoTechnology II*, 6036, 3616. <https://doi.org/10.1117/12.638392>
- Chapman, R. F., Laymon, A. S., Wilhite, D. P., McKenzie, J. M., Tanner, D. a., & Stager, J. M. (2012). Ground contact time as an indicator of metabolic cost in elite distance runners. *Medicine and Science in Sports and Exercise*, 44(5), 917-925. <https://doi.org/10.1249/MSS.0b013e3182400520>
- Charry, E., Hu, W., Umer, M., Ronchi, A., & Taylor, S. (2013). Study on estimation of peak Ground Reaction Forces using tibial accelerations in running. *Proceedings of the 2013 IEEE 8th International Conference on Intelligent Sensors, Sensor Networks and Information Processing: Sensing the Future, ISSNIP 2013*, 1, 288-293. <https://doi.org/10.1109/ISSNIP.2013.6529804>

Chapter 9. General Discussion

- Cheng, Y., Markley, F. L., Crassidis, J. L., & Oshman, Y. (2007). Averaging quaternions. *Advances in the Astronautical Sciences*, 127 PART 2(4), 1675-1682.
- Chew, D.-K., Ngoh, K. J.-H., Gouwanda, D., & Gopalai, A. A. (2017). Estimating running spatial and temporal parameters using an inertial sensor. *Sports Engineering*, 21(2), 115-122. <https://doi.org/10.1007/s12283-017-0255-9>
- Cicchetti, D. V. (1994). Guidelines, Criteria, and Rules of Thumb for Evaluating Normed and Standardized Assessment Instruments in Psychology. *Psychological Assessment*, 6(4), 284-290. <https://doi.org/10.1037/1040-3590.6.4.284>
- Clark, K. P., Ryan, L. J., & Weyand, P. G. (2014). Foot speed, foot-strike and footwear: Linking gait mechanics and running ground reaction forces. *Journal of Experimental Biology*, 217(12), 2037-2040. <https://doi.org/10.1242/jeb.099523>
- Clark, K. P., Ryan, L. J., & Weyand, P. G. (2017). A general relationship links gait mechanics and running ground reaction forces. *Journal of Experimental Biology*, 220(2), 247-258. <https://doi.org/10.1242/jeb.138057>
- Clarke, T., Frederick, E., & Hamill, C. (1984). The Study of Rearfoot Movement in Running. *Sports Shoes and Playing Surfaces: Biomechanical Properties*, 166-189.
- Clermont, C. A., Benson, L. C., Edwards, W. B., Hettinga, B. A., & Ferber, R. (2019). New considerations for wearable technology data: Changes in running biomechanics during a marathon. *Journal of Applied Biomechanics*, 35(6), 401-409. <https://doi.org/10.1123/jab.2018-0453>
- Čoh, M., Dolenec, A., Tomažin, K., & Zvan, M. (2008). Dynamic and kinematic analysis of the hurdle clearance technique. *Biomechanical Diagnostic Methods in Athletic Training*, 109-116.
- Cronin, J. B., & Rumpf, M. C. (2014). Effect of four different step detection thresholds on nonmotorized treadmill sprint measurement. *Journal of Strength and Conditioning Research*, 28(10), 2996-3000. <https://doi.org/10.1519/JSC.0000000000000497>
- Crowell, H. P., Milner, C. E., Hamill, J., & Davis, I. S. (2010). Reducing impact loading during running with the use of real-time visual feedback. *The Journal of Orthopaedic and Sports Physical Therapy*, 40(4), 206-213. <https://doi.org/10.2519/jospt.2010.3166>
- Dalleau, G., Belli, a, Bourdin, M., & Lacour, J. R. (1998). The spring-mass model and the energy cost of treadmill running. *European Journal of Applied Physiology and Occupational Physiology*, 77(3), 257-263. <https://doi.org/10.1007/s004210050330>
- Daoud, A. I., Geissler, G. J., Wang, F., Saretsky, J., Daoud, Y. A., & Lieberman, D. E. (2012). Foot strike and injury rates in endurance runners: A retrospective study. *Medicine and Science in Sports and Exercise*, 44(7), 1325-1334. <https://doi.org/10.1249/MSS.0b013e3182465115>

- Davis, R. B., Öunpuu, S., Tyburski, D., & Gage, J. R. (1991). A gait analysis data collection and reduction technique. *Human Movement Science*, 10(5), 575-587. [https://doi.org/10.1016/0167-9457\(91\)90046-Z](https://doi.org/10.1016/0167-9457(91)90046-Z)
- de Almeida, M. O., Saragiotto, B. T., Yamato, T. P., & Lopes, A. D. (2015). Is the rearfoot pattern the most frequently foot strike pattern among recreational shod distance runners? *Physical Therapy in Sport*, 16(1), 29-33. <https://doi.org/10.1016/j.ptsp.2014.02.005>
- De Cheveigné, A., & Kawahara, H. (2002). YIN, a fundamental frequency estimator for speech and music. *The Journal of the Acoustical Society of America*, 111(4), 1917–1930. <https://doi.org/10.1121/1.1458024>
- De Cock, A., De Clercq, D., Willems, T., & Witvrouw, E. (2005). Temporal characteristics of foot roll-over during barefoot jogging: Reference data for young adults. *Gait and Posture*, 21(4), 432-439. <https://doi.org/10.1016/j.gaitpost.2004.05.004>
- De Cock, A., Vanrenterghem, J., Willems, T., Witvrouw, E., & De Clercq, D. (2008). The trajectory of the centre of pressure during barefoot running as a potential measure for foot function. *Gait and Posture*, 27(4), 669-675. <https://doi.org/10.1016/j.gaitpost.2007.08.013>
- De Cock, A., Willems, T., Witvrouw, E., Vanrenterghem, J., & De Clercq, D. (2006). A functional foot type classification with cluster analysis based on plantar pressure distribution during jogging. *Gait and Posture*, 23(3), 339-347. <https://doi.org/10.1016/j.gaitpost.2005.04.011>
- de Ruiter, C. J., & van Dieën, J. H. (2019). Stride and Step Length Obtained with Inertial Measurement Units during Maximal Sprint Acceleration. *Sports*, 7(9), 202. <https://doi.org/10.3390/sports7090202>
- De Ruiter, C. J., Van Oeveren, B., Francke, A., Zijlstra, P., & Van Dieen, J. H. (2016). Running speed can be predicted from foot contact time during outdoor over ground running. *PLoS ONE*, 11(9). <https://doi.org/10.1371/journal.pone.0163023>
- de Ruiter, C. J., Verdijk, P. W. L., Werker, W., Zuidema, M. J., & de Haan, A. (2014). Stride frequency in relation to oxygen consumption in experienced and novice runners. *European Journal of Sport Science*. <https://doi.org/10.1080/17461391.2013.783627>
- Degache, F., Guex, K., Fourchet, F., Morin, J. B., Millet, G. P., Tomazin, K., & Millet, G. Y. (2013). Changes in running mechanics and spring-mass behaviour induced by a 5-hour hilly running bout. *Journal of Sports Sciences*, 31(3), 299-304. <https://doi.org/10.1080/02640414.2012.729136>
- Degache, F., Morin, J. B., Oehen, L., Guex, K., Giardini, G., Schena, F., Millet, G. Y., & Millet, G. P. (2016). Running mechanics during the world's most challenging mountain ultramarathon. *International Journal of Sports Physiology and Performance*, 11(5), 608-614. <https://doi.org/10.1123/ijsp.2015-0238>

- Dejnabadi, H., Jolles, B. M., Casanova, E., Fua, P., & Aminian, K. (2006). Estimation and visualization of sagittal kinematics of lower limbs orientation using body-fixed sensors. *IEEE Transactions on Biomedical Engineering*, 53(7), 1385-1393. <https://doi.org/10.1109/TBME.2006.873678>
- Derksen, S., & Keselman, H. J. (1992). Backward, forward and stepwise automated subset selection algorithms: Frequency of obtaining authentic and noise variables. *British Journal of Mathematical and Statistical Psychology*, 45(2), 265-282. <https://doi.org/10.1111/j.2044-8317.1992.tb00992.x>
- Dewolf, A. H., Peñailillo, L. E., & Willems, P. A. (2016). The rebound of the body during uphill and downhill running at different speeds. *Journal of Experimental Biology*, 219(15), 2276-2288. <https://doi.org/10.1242/jeb.142976>
- Di Michele, R., & Merni, F. (2014). The concurrent effects of strike pattern and ground-contact time on running economy. *Journal of Science and Medicine in Sport*, 17(4), 414-418. <https://doi.org/10.1016/j.jsams.2013.05.012>
- Dierick, F., Penta, M., Renaut, D., & Detrembleur, C. (2004). A force measuring treadmill in clinical gait analysis. *Gait and Posture*, 20(3), 299-303. <https://doi.org/10.1016/j.gaitpost.2003.11.001>
- Dugan, S. a., & Bhat, K. P. (2005). Biomechanics and analysis of running gait. *Physical Medicine and Rehabilitation Clinics of North America*, 16(3), 603-621. <https://doi.org/10.1016/j.pmr.2005.02.007>
- Dumas, R., Camomilla, V., Bonci, T., Cheze, L., & Cappozzo, A. (2014). A qualitative analysis of soft tissue artefact during running. *Computer Methods in Biomechanics and Biomedical Engineering*, 17(SUPP1), 124-125. <https://doi.org/10.1080/10255842.2014.931518>
- Eichelberger, P., Ferraro, M., Minder, U., Denton, T., Blasimann, A., Krause, F., & Baur, H. (2016). Analysis of accuracy in optical motion capture - A protocol for laboratory setup evaluation. *Journal of Biomechanics*. <https://doi.org/10.1016/j.jbiomech.2016.05.007>
- Elliot, B., & Ackland, T. (1981). Biomechanical effects of fatigue on 10, 000 meter running technique. *Research Quarterly for Exercise and Sport*, 52(2), 160-166. <https://doi.org/10.1080/02701367.1981.10607853>
- Elliott, B. C., & Blanksby, B. A. (1979). Optimal stride length considerations for male and female recreational runners. *British Journal of Sports Medicine*, 13(1), 15-18. <https://doi.org/10.1136/bjism.13.1.15>
- Elliott, B. C., & Roberts, A. D. (1980). A biomechanical evaluation of the role of fatigue in middle-distance running. *Canadian Journal of Applied Sport Sciences*, 5(4), 203-207.
- Eslami, M., Begon, M., Farahpour, N., & Allard, P. (2007). Forefoot-rearfoot coupling patterns and tibial internal rotation during stance phase of barefoot versus shod running. *Clinical Biomechanics*, 22(1), 74-80. <https://doi.org/10.1016/j.clinbiomech.2006.08.002>

- Falbriard, M., Meyer, F., Mariani, B., Millet, G. P., & Aminian, K. (2018). Accurate estimation of running temporal parameters using foot-worn inertial sensors. *Frontiers in Physiology*, 9(JUN), 1-10. <https://doi.org/10.3389/fphys.2018.00610>
- Falbriard, M., Meyer, F., Mariani, B., Millet, G. P., & Aminian, K. (2020). Drift-Free Foot Orientation Estimation in Running Using Wearable IMU. *Frontiers in Bioengineering and Biotechnology*, 8(February), 65. <https://doi.org/10.3389/fbioe.2020.00065>
- Fan, J. L., & Kayser, B. (2016). Fatigue and Exhaustion in Hypoxia: The Role of Cerebral Oxygenation. In *High Altitude Medicine and Biology*. <https://doi.org/10.1089/ham.2016.0034>
- Farley, C. T., & González, O. (1996). Leg stiffness and stride frequency in human running. *Journal of Biomechanics*, 29(2), 181-186. [https://doi.org/10.1016/0021-9290\(95\)00029-1](https://doi.org/10.1016/0021-9290(95)00029-1)
- Fasel, B., Duc, C., Dadashi, F., Bardyn, E., Savary, M., Farine, P. A., & Aminian, K. (2017). A wrist sensor and algorithm to determine instantaneous walking cadence and speed in daily life walking. *Medical and Biological Engineering and Computing*, 55(10), 1773-1785. <https://doi.org/10.1007/s11517-017-1621-2>
- Fasel, B., Sporri, J., Chardonens, J., Kroll, J., Muller, E., & Aminian, K. (2018). Joint Inertial Sensor Orientation Drift Reduction for Highly Dynamic Movements. *IEEE Journal of Biomedical and Health Informatics*, 22(1), 77-86. <https://doi.org/10.1109/JBHI.2017.2659758>
- Fasel, B., Spörri, J., Kröll, J., Müller, E., & Aminian, K. (2019). A magnet-based timing system to detect gate crossings in Alpine ski racing. *Sensors (Switzerland)*. <https://doi.org/10.3390/s19040940>
- Favre, J., Aissaoui, R., Jolles, B. M., de Guise, J. A., & Aminian, K. (2009). Functional calibration procedure for 3D knee joint angle description using inertial sensors. *Journal of Biomechanics*, 42(14), 2330-2335. <https://doi.org/10.1016/j.jbiomech.2009.06.025>
- Favre, J., Jolles, B. M., Aissaoui, R., & Aminian, K. (2008). Ambulatory measurement of 3D knee joint angle. *Journal of Biomechanics*, 41(5), 1029-1035. <https://doi.org/10.1016/j.jbiomech.2007.12.003>
- Favre, J., Jolles, B. M., Siegrist, O., & Aminian, K. (2006). Quaternion-based fusion of gyroscopes and accelerometers to improve 3D angle measurement. *Electronics Letters*, 42(11), 612-614. <https://doi.org/10.1049/el:20060124>
- Fellin, R. E., Rose, W. C., Royer, T. D., & Davis, I. S. (2010). Comparison of methods for kinematic identification of footstrike and toe-off during overground and treadmill running. *Journal of Science and Medicine in Sport*, 13(6), 646-650. <https://doi.org/10.1016/j.jsams.2010.03.006>
- Fenn, W. O. (1930). Frictional and kinetic factors in the work of sprint running. *American Journal of Physiology-Legacy Content*, 92(3), 583-611.

Chapter 9. General Discussion

- Fenn, Wallace O. (1930). Work Against Gravity and Work Due To Velocity Changes in Running. *American Journal of Physiology-Legacy Content*, 93(2), 433-462. <https://doi.org/10.1152/ajplegacy.1930.93.2.433>
- Ferber, R., & Macdonald, S. (2015). Running Mechanics and Gait Analysis. *Medicine & Science in Sports & Exercise*, 47(11), 2485. <https://doi.org/10.1249/01.mss.0000472950.28201.3d>
- Ferraris, F., Grimaldi, U., & Parvis, M. (1955). Procedure for effortless in-field calibration of three-axial rate gyro and accelerometers. *Sens. Mater.*, 7(5), 331-330.
- Ferraris, F., Grimaldi, U., & Parvis, M. (1995). Procedure for effortless in-field calibration of three-axis rate gyros and accelerometers. *Sensors and Materials*, 7(5), 311-330. <https://doi.org/0914-4935>
- Folland, J. P., Allen, S. J., Black, M. I., Handsaker, J. C., & Forrester, S. E. (2017). Running Technique is an Important Component of Running Economy and Performance. *Medicine and Science in Sports and Exercise*, 49(7), 1412-1423.
- Forrester, S. E., & Townend, J. (2015). The effect of running velocity on footstrike angle - A curve-clustering approach. *Gait and Posture*, 41(1), 26-32. <https://doi.org/10.1016/j.gaitpost.2014.08.004>
- Fourchet, F., Millet, G. P., Tomazin, K., Guex, K., Nosaka, K., Edouard, P., Degache, F., & Millet, G. Y. (2012). Effects of a 5-h hilly running on ankle plantar and dorsal flexor force and fatigability. *European Journal of Applied Physiology*. <https://doi.org/10.1007/s00421-011-2220-9>
- Foxlin, E. (2005). Pedestrian tracking with shoe-mounted inertial sensors. *IEEE Computer Graphics and Applications*, 25(6), 38-46. <https://doi.org/10.1109/MCG.2005.140>
- Galper, D. I., Trivedi, M. H., Barlow, C. E., Dunn, A. L., & Kampert, J. B. (2006). Inverse association between physical inactivity and mental health in men and women. *Medicine and Science in Sports and Exercise*, 38(1), 173-178. <https://doi.org/10.1249/01.mss.0000180883.32116.28>
- García-López, J., Peleteiro, J., Rodríguez-Marroyo, J. A., Morante, J. C., Herrero, J. A., & Villa, J. G. (2005). The validation of a new method that measures contact and flight times during vertical jump. *International Journal of Sports Medicine*, 26(4), 294-302. <https://doi.org/10.1055/s-2004-820962>
- García-Pinillos, F., Latorre-Román, P., Ramirez-Campillo, R., & Roche-Seruendo, L. E. (2019). Agreement between spatiotemporal parameters from a photoelectric system with different filter settings and high-speed video analysis during running on a treadmill at comfortable velocity. *Journal of Biomechanics*, 93, 213-219. <https://doi.org/10.1016/j.jbiomech.2019.06.017>
- Gardiner, E. N. (Edward N. (2002). *Athletics in the ancient world*. Courier Corporation.

- Garofolini, A., Taylor, S., & Lepine, J. (2019). Evaluating dynamic error of a treadmill and the effect on measured kinetic gait parameters: Implications and possible solutions. *Journal of Biomechanics*, 82, 156-163. <https://doi.org/10.1016/j.jbiomech.2018.10.025>
- Geyer, H., Seyfarth, A., & Blickhan, R. (2006). Compliant leg behaviour explains basic dynamics of walking and running. *Proceedings of the Royal Society B: Biological Sciences*, 273(1603), 2861-2867. <https://doi.org/10.1098/rspb.2006.3637>
- Giandolini, M., Gimenez, P., Temesi, J., Arnal, P. J., Martin, V., Rupp, T., Morin, J.-B., Samozino, P., & Millet, G. Y. (2016). Effect of the Fatigue Induced by a 110-km Ultramarathon on Tibial Impact Acceleration and Lower Leg Kinematics. *PloS One*, 11(3), e0151687. <https://doi.org/10.1371/journal.pone.0151687>
- Giandolini, M., Poupard, T., Gimenez, P., Horvais, N., Millet, G. Y., Morin, J.-B., & Samozino, P. (2014). A simple field method to identify foot strike pattern during running. *Journal of Biomechanics*, 47(7), 1588-1593. <https://doi.org/10.1016/j.jbiomech.2014.03.002>
- Giandolini, M., Vernillo, G., Samozino, P., Horvais, N., Edwards, W. B., Morin, J.-B., & Millet, G. Y. (2016). Fatigue associated with prolonged graded running. In *European Journal of Applied Physiology*. <https://doi.org/10.1007/s00421-016-3437-4>
- Gietzelt, M., Wolf, K. H., Marschollek, M., & Haux, R. (2013). Performance comparison of accelerometer calibration algorithms based on 3D-ellipsoid fitting methods. *Computer Methods and Programs in Biomedicine*. <https://doi.org/10.1016/j.cmpb.2013.03.006>
- Girard, O., Millet, G. P., Slawinski, J., Racinais, S., & Micallef, J. P. (2013). Changes in running mechanics and spring-mass behaviour during a 5-km time trial. *International Journal of Sports Medicine*. <https://doi.org/10.1055/s-0032-1329958>
- Girard, Olivier, Racinais, S., Kelly, L., Millet, G. P., & Brocherie, F. (2011). Repeated sprinting on natural grass impairs vertical stiffness but does not alter plantar loading in soccer players. *European Journal of Applied Physiology*, 111(10), 2547-2555. <https://doi.org/10.1007/s00421-011-1884-5>
- Goss, D. L., & Gross, M. T. (2012). Relationships among self-reported shoe type, footstrike pattern, and injury incidence. *US Army Med Dep J*, December, 25–30.
- Gottschall, J. S., & Kram, R. (2005). Ground reaction forces during downhill and uphill running. *Journal of Biomechanics*, 38(3), 445-452. <https://doi.org/10.1016/j.jbiomech.2004.04.023>
- Graurock, D., Schauer, T., & Seel, T. (2016). Automatic pairing of inertial sensors to lower limb segments - A plug-and-play approach. *Current Directions in Biomedical Engineering*, 2(1), 715-718. <https://doi.org/10.1515/cdbme-2016-0155>
- Gruber, A. H., Boyer, K. A., Derrick, T. R., & Hamill, J. (2014). Impact shock frequency components and attenuation in rearfoot and forefoot running. *Journal of Sport and Health Science*, 3(2), 113-121. <https://doi.org/10.1016/j.jshs.2014.03.004>

Chapter 9. General Discussion

- Gruber, A. H., Umberger, B. R., Braun, B., & Hamill, J. (2013). Economy and rate of carbohydrate oxidation during running with rearfoot and forefoot strike patterns. *Journal of Applied Physiology (Bethesda, Md. : 1985)*, 115(May 2013), 194-201. <https://doi.org/10.1152/japplphysiol.01437.2012>
- Gurchiek, R. D., McGinnis, R. S., Needle, A. R., McBride, J. M., & van Werkhoven, H. (2017). The use of a single inertial sensor to estimate 3-dimensional ground reaction force during accelerative running tasks. *Journal of Biomechanics*, 61, 263-268. <https://doi.org/10.1016/j.jbiomech.2017.07.035>
- Gurchiek, R. D., McGinnis, R. S., Needle, A. R., McBride, J. M., & van Werkhoven, H. (2018). An adaptive filtering algorithm to estimate sprint velocity using a single inertial sensor. *Sports Engineering*, 21(4), 389-399. <https://doi.org/10.1007/s12283-018-0285-y>
- Gurchiek, R. D., Rupasinghe Arachchige Don, H. S., Pelawa Watagoda, L. C. R., McGinnis, R. S., Van Werkhoven, H., Needle, A. R., McBride, J. M., & Arnholt, A. T. (2019). Sprint assessment using machine learning and a wearable accelerometer. *Journal of Applied Biomechanics*. <https://doi.org/10.1123/jab.2018-0107>
- Halilaj, E., Rajagopal, A., Fiterau, M., Hicks, J. L., Hastie, T. J., & Delp, S. L. (2018). Machine learning in human movement biomechanics: Best practices, common pitfalls, and new opportunities. *Journal of Biomechanics*, 81, 1-11. <https://doi.org/10.1016/j.jbiomech.2018.09.009>
- Hamill, J., Bates, B. T., Knutzen, K. M., & Sawhill, J. A. (1983). Variations in ground reaction force parameters at different running speeds. *Human Movement Science*, 2(1-2), 47-56. [https://doi.org/10.1016/0167-9457\(83\)90005-2](https://doi.org/10.1016/0167-9457(83)90005-2)
- Hamill, Joseph, & Gruber, A. H. (2017). Is changing footstrike pattern beneficial to runners? In *Journal of Sport and Health Science* (Vol. 6, Issue 2, pp. 146-153). Elsevier B.V. <https://doi.org/10.1016/j.jshs.2017.02.004>
- Hamner, S. R., Seth, A., & Delp, S. L. (2010). Muscle contributions to propulsion and support during running. *Journal of Biomechanics*, 43(14), 2709-2716. <https://doi.org/10.1016/j.jbiomech.2010.06.025>
- Handsaker, J. C., Forrester, S. E., Folland, J. P., Black, M. I., & Allen, S. J. (2016). A kinematic algorithm to identify gait events during running at different speeds and with different footstrike types. *Journal of Biomechanics*, 49(16), 4128-4133. <https://doi.org/10.1016/j.jbiomech.2016.10.013>
- Hanley, B., Bissas, A., Merlino, S., & Gruber, A. H. (2019). Most marathon runners at the 2017 IAAF World Championships were rearfoot strikers, and most did not change footstrike pattern. *Journal of Biomechanics*, 92, 54-60. <https://doi.org/10.1016/j.jbiomech.2019.05.024>

- Hanon, C., & Gajer, B. (2009). Velocity and stride parameters of world-class 400-meter athletes compared with less experienced runners. *Journal of Strength and Conditioning Research*, 23(2), 524-531. <https://doi.org/10.1519/JSC.0b013e318194e071>
- Hasegawa, H., Yamauchi, T., & Kraemer, W. J. (2007). Foot Strike Patterns of Runners at the 15-km Point During an Elite-Level Half Marathon. *The Journal of Strength and Conditioning Research*, 21(3), 888. <https://doi.org/10.1519/R-22096.1>
- Hatala, K. G., Dingwall, H. L., Wunderlich, R. E., & Richmond, B. G. (2013). Variation in Foot Strike Patterns during Running among Habitually Barefoot Populations. *PLoS ONE*, 8(1), 4-9. <https://doi.org/10.1371/journal.pone.0052548>
- Hauswirth, C., Le Meur, Y., Couturier, A., Bernard, T., & Brisswalter, J. (2009). Accuracy and repeatability of the polar RS800sd to evaluate stride rate and running speed. *International Journal of Sports Medicine*, 30(5), 354-359. <https://doi.org/10.1055/s-0028-1105936>
- Heinrich, B. (2009). *Why we run: a natural history*. Harper Collins.
- Herren, R., Sparti, A., Aminian, K., & Schutz, Y. (1999). The prediction of speed and incline in outdoor running in humans using accelerometry. *Medicine and Science in Sports and Exercise*, 31(7), 1053-1059. <https://doi.org/10.1097/00005768-199907000-00020>
- Higginson, B. K. (2009). Methods of running gait analysis. *Current Sports Medicine Reports*, 8(3), 136-141. <https://doi.org/10.1249/JSR.0b013e3181a6187a>
- Hillstrom, H. J., Song, J., Kraszewski, A. P., Hafer, J. F., Mootanah, R., Dufour, A. B., Chow, B. S., & Deland, J. T. (2013). Foot type biomechanics part 1: Structure and function of the asymptomatic foot. *Gait and Posture*, 37(3), 445-451. <https://doi.org/10.1016/j.gaitpost.2012.09.007>
- Hinrichs, R. N. (2016). Upper Extremity Function in Running. II: Angular Momentum Considerations. *International Journal of Sport Biomechanics*, 3(3), 242-263. <https://doi.org/10.1123/ijsb.3.3.242>
- Hinrichs, R. N., Cavanagh, P. R., & Williams, K. R. (2016). Upper Extremity Function in Running. I: Center of Mass and Propulsion Considerations. *International Journal of Sport Biomechanics*, 3(3), 222-241. <https://doi.org/10.1123/ijsb.3.3.222>
- Ho, C.-S., Chang, C.-Y., & Lin, K.-C. (2019). The wearable devices application for evaluation of 110 meter high hurdle race. *Journal of Human Sport and Exercise*, 15(1). <https://doi.org/10.14198/jhse.2020.151.04>
- Hobara, H., Inoue, K., Gomi, K., Sakamoto, M., Muraoka, T., Iso, S., & Kanosue, K. (2010). Continuous change in spring-mass characteristics during a 400 m sprint. *Journal of Science and Medicine in Sport*. <https://doi.org/10.1016/j.jsams.2009.02.002>

- Hoffman, M. D., Ong, J. C., & Wang, G. (2010). Historical analysis of participation in 161km ultramarathons in North America. In *International Journal of the History of Sport*. <https://doi.org/10.1080/09523367.2010.494385>
- Högberg, P. (1952). Length of stride, stride frequency, “flight” period and maximum distance between the feet during running with different speeds. *Arbeitsphysiologie*, 14(6), 431-436. <https://doi.org/10.1007/BF00934422>
- Hong, Y., Wang, L., Li, J. X., & Zhou, J. H. (2012). Comparison of plantar loads during treadmill and overground running. *Journal of Science and Medicine in Sport*, 15(6), 554-560. <https://doi.org/10.1016/j.jsams.2012.01.004>
- Horvais, N., & Samozino, P. (2013). Effect of midsole geometry on foot-strike pattern and running kinematics. *Footwear Science*, 5(2), 81-89. <https://doi.org/10.1080/19424280.2013.767863>
- Hreljac, A. (2004). Impact and Overuse Injuries in Runners. *Medicine and Science in Sports and Exercise*, 36(5), 845-849. <https://doi.org/10.1249/01.MSS.0000126803.66636.DD>
- Hu, J. S., Sun, K. C., & Cheng, C. Y. (2013). A kinematic human-walking model for the normal-gait-speed estimation using tri-axial acceleration signals at waist location. *IEEE Transactions on Biomedical Engineering*, 60(8), 2271-2279. <https://doi.org/10.1109/TBME.2013.2252345>
- Iskra, J., & Coh, M. (2011). Biomechanical studies on running the 400 M hurdles. *Human Movement*, 12(4), 315-323. <https://doi.org/10.2478/v10038-011-0035-5>
- Iskra, J., Przednowek, K., Krzeszowski, T., Wiktorowicz, K., & Pietrzak, M. (2017). Kinematic analysis of the upper limbs in stepping over the hurdle the use of IMU-based motion capture. *IcSPORTS 2017 - Proceedings of the 5th International Congress on Sport Sciences Research and Technology Support*, 102-106. <https://doi.org/10.5220/0006503101020106>
- Iversen, J. R., & McMahon, T. A. (1992). Running on an incline. *Journal of Biomechanical Engineering*, 114(4), 435-441. <https://doi.org/10.1115/1.2894092>
- Jain, A., Nandakumar, K., & Ross, A. (2005). Score normalization in multimodal biometric systems. *Pattern Recognition*, 38(12), 2270-2285. <https://doi.org/10.1016/j.patcog.2005.01.012>
- Japkowicz, N. (2000). The Class Imbalance Problem: Significance and Strategies. *Proceedings of the 2000 International Conference on Artificial Intelligence*, 111-117. <https://doi.org/10.1.1.35.1693>
- John, G. H., Kohavi, R., & Pfleger, K. (1994). Irrelevant Features and the Subset Selection Problem. In *Machine Learning Proceedings 1994* (pp. 121-129). Morgan Kaufmann Publishers. <https://doi.org/10.1016/b978-1-55860-335-6.50023-4>

- Kasmer, M. E., Liu, X., Roberts, K. G., & Valadao, J. M. (2013). Foot-strike pattern and performance in a marathon. *International Journal of Sports Physiology and Performance*, 8(3), 286. <https://doi.org/10.1016/bs.mcb.2015.01.016>. Observing
- Keele, K. D. (1983). Leonardo Da Vinci's Elements of the Science of Man. In *New York: Academic Press*. <https://doi.org/10.1016/c2013-0-10957-9>
- Kerhervé, H. A., Millet, G. Y., & Solomon, C. (2015). The dynamics of speed selection and psycho-physiological load during a mountain ultramarathon. *PLoS ONE*. <https://doi.org/10.1371/journal.pone.0145482>
- King, D. L., McCartney, M., & Trihy, E. (2019). Initial contact and toe off event identification for rearfoot and non-rearfoot strike pattern treadmill running at different speeds. *Journal of Biomechanics*, 90, 119-122. <https://doi.org/10.1016/j.jbiomech.2019.04.023>
- Kiselyov, K., & Muallem, S. (2008). Mitochondrial Ca²⁺ homeostasis in lysosomal storage diseases. *Cell Calcium*, 44(1), 103-111. <https://doi.org/10.1016/j.ceca.2007.12.005>
- Kohavi, R., & John, G. H. (1997). Wrappers for feature subset selection. *Artificial Intelligence*, 97(1-2), 273-324. [https://doi.org/10.1016/s0004-3702\(97\)00043-x](https://doi.org/10.1016/s0004-3702(97)00043-x)
- Koska, D., Gaudel, J., Hein, T., & Maiwald, C. (2018). Validation of an inertial measurement unit for the quantification of rearfoot kinematics during running. *Gait and Posture*, 64(December 2017), 135-140. <https://doi.org/10.1016/j.gaitpost.2018.06.007>
- Kucherenko, T., Beskow, J., & Kjellström, H. (2018). *A Neural Network Approach to Missing Marker Reconstruction in Human Motion Capture*. <http://arxiv.org/abs/1803.02665>
- Kugler, F., & Janshen, L. (2010). Body position determines propulsive forces in accelerated running. *Journal of Biomechanics*, 43(2), 343-348. <https://doi.org/10.1016/j.jbiomech.2009.07.041>
- Kulmala, J. P., Kosonen, J., Nurminen, J., & Avela, J. (2018). Running in highly cushioned shoes increases leg stiffness and amplifies impact loading. *Scientific Reports*, 8(1). <https://doi.org/10.1038/s41598-018-35980-6>
- Kunze, K., Lukowicz, P., Junker, H., & Tröster, G. (2005). Where am I: Recognizing on-body positions of wearable sensors. *Lecture Notes in Computer Science*, 3479, 264-275. https://doi.org/10.1007/11426646_25
- Kyröläinen, H., Avela, J., & Komi, P. V. (2005). Changes in muscle activity with increasing running speed. *Journal of Sports Sciences*, 23(10), 1101-1109. <https://doi.org/10.1080/02640410400021575>
- Kyrolainen, H., Pullinen, T., Candau, R., Avela, J., Huttunen, P., & Komi, P. V. (2000). Effects of marathon running on running economy and kinematics. *European Journal of Applied Physiology*, 82(4), 297-304. <https://doi.org/10.1007/s004210000219>

Chapter 9. General Discussion

- Lafortune, M. (1988). Biomechanical analysis of 110 m hurdles. *Track and Field News*, 105, 3355-3365.
- Lambert, M. I., Dugas, J. P., Kirkman, M. C., Mokone, G. G., & Waldeck, M. R. (2004). Changes in running speeds in a 100 km ultramarathon race. *Journal of Sports Science and Medicine*.
- Larson, P. (2014). Comparison of foot strike patterns of barefoot and minimally shod runners in a recreational road race. *Journal of Sport and Health Science*, 3(2), 137-142. <https://doi.org/10.1016/j.jshs.2014.03.003>
- Larson, P., Higgins, E., Kaminski, J., Decker, T., Preble, J., Lyons, D., McIntyre, K., & Normile, A. (2011). Foot strike patterns of recreational and sub-elite runners in a long-distance road race. *Journal of Sports Sciences*, 29(15), 1665-1673. <https://doi.org/10.1080/02640414.2011.610347>
- Lavcanska, V., Taylor, N. F., & Schache, A. G. (2005). Familiarization to treadmill running in young unimpaired adults. *Human Movement Science*, 24(4), 544-557. <https://doi.org/10.1016/j.humov.2005.08.001>
- Lazzer, S., Salvadego, D., Taboga, P., Rejc, E., Giovanelli, N., & Di Prampero, P. E. (2015). Effects of the Etna uphill ultramarathon on energy cost and mechanics of running. *International Journal of Sports Physiology and Performance*. <https://doi.org/10.1123/ijsp.2014-0057>
- Lebleu, J., Gosseye, T., Detrembleur, C., Mahaudens, P., Cartiaux, O., & Penta, M. (2020). Lower limb kinematics using inertial sensors during locomotion: Accuracy and reproducibility of joint angle calculations with different sensor-to-segment calibrations. *Sensors (Switzerland)*, 20(3), 1-17. <https://doi.org/10.3390/s20030715>
- Lee, D. chul, Brellenthin, A. G., Thompson, P. D., Sui, X., Lee, I. M., & Lavie, C. J. (2017). Running as a Key Lifestyle Medicine for Longevity. *Progress in Cardiovascular Diseases*, 60(1), 45-55. <https://doi.org/10.1016/j.pcad.2017.03.005>
- Lee, J. B., Mellifont, R. B., & Burkett, B. J. (2010). The use of a single inertial sensor to identify stride, step, and stance durations of running gait. *Journal of Science and Medicine in Sport*, 13(2), 270-273. <https://doi.org/10.1016/j.jsams.2009.01.005>
- Lee, Y. S., Ho, C. S., Shih, Y., Chang, S. Y., Róbert, F. J., & Shiang, T. Y. (2015). Assessment of walking, running, and jumping movement features by using the inertial measurement unit. *Gait and Posture*, 41(4), 877-881. <https://doi.org/10.1016/j.gaitpost.2015.03.007>
- Leedy, M. G. (2000). Commitment to distance running: Coping mechanism or addiction? *Journal of Sport Behavior*.
- Leitch, J., Stebbins, J., Paolini, G., & Zavatsky, A. B. (2011). Identifying gait events without a force plate during running: A comparison of methods. *Gait and Posture*, 33(1), 130-132. <https://doi.org/10.1016/j.gaitpost.2010.06.009>

- Lieberman, D. E., Venkadesan, M., Werbel, W. A., Daoud, A. I., Dandrea, S., Davis, I. S., Mangeni, R. O., Pitsiladis, Y., D'Andrea, S., Davis, I. S., Mang'eni, R. O., & Pitsiladis, Y. (2010). Foot strike patterns and collision forces in habitually barefoot versus shod runners. *Nature*, 463(7280), 531-535. <https://doi.org/10.1038/nature08723>
- Lieberman, D. E., Warrener, A. G., Wang, J., & Castillo, E. R. (2015). Effects of stride frequency and foot position at landing on braking force, hip torque, impact peak force and the metabolic cost of running in humans. *Journal of Experimental Biology*, 218(21), 3406-3414. <https://doi.org/10.1242/jeb.125500>
- Ling, H., Hardy, J., & Zetterberg, H. (2015). Neurological consequences of traumatic brain injuries in sports. In *Molecular and Cellular Neuroscience*. <https://doi.org/10.1016/j.mcn.2015.03.012>
- Lopes, A. D., Hespanhol, L. C., Yeung, S. S., & Pena Costa, L. O. (2012). What are the Main Running Related Musculoskeletal Injuries. *Sports Medicine*, 42(10), 892-905. <https://doi.org/10.2165/11631170-000000000-00000>
- Lorenz, D. S., & Pontillo, M. (2012). Is There Evidence to Support a Forefoot Strike Pattern in Barefoot Runners? A Review. *Sports Health*, 4(6), 480-484. <https://doi.org/10.1177/1941738112448055>
- Luhtanen, P., & Komi, P. V. (1978). Mechanical factors influencing running speed. *Biomechanics*, VI(B2), 22-28.
- Lynch, S. L., & Hoch, A. Z. (2010). The female runner: Gender specifics. *Clinics in Sports Medicine*, 29(3), 477-498. <https://doi.org/10.1016/j.csm.2010.03.003>
- Macadam, P., Cronin, J., Neville, J., & Diewald, S. (2019). Quantification of the validity and reliability of sprint performance metrics computed using inertial sensors: A systematic review. In *Gait and Posture*. <https://doi.org/10.1016/j.gaitpost.2019.07.123>
- Macera, C. A., Pate, R. R., Powell, K. E., Jackson, K. L., Kendrick, J. S., & Craven, T. E. (1989). Predicting lower-extremity injuries among habitual runners. *Archives of Internal Medicine*, 149(11), 2565-2568. <https://doi.org/10.1001/archinte.1989.00390110117026>
- Madgwick, S. O. H., Harrison, A. J. L., & Vaidyanathan, R. (2011). Estimation of IMU and MARG orientation using a gradient descent algorithm. *IEEE International Conference on Rehabilitation Robotics*, 1-7. <https://doi.org/10.1109/ICORR.2011.5975346>
- Mann, R., Malisoux, L., Urhausen, A., Meijer, K., & Theisen, D. (2016). Plantar pressure measurements and running-related injury: A systematic review of methods and possible associations. In *Gait and Posture* (Vol. 47, pp. 1-9). <https://doi.org/10.1016/j.gaitpost.2016.03.016>
- Mannini, A., Sabatini, A. M., & Intille, S. S. (2015). Accelerometry-based recognition of the placement sites of a wearable sensor. *Pervasive and Mobile Computing*, 21, 62-74. <https://doi.org/10.1016/j.pmcj.2015.06.003>

Chapter 9. General Discussion

- Marcora, S. (2009). Perception of effort during exercise is independent of afferent feedback from skeletal muscles, heart, and lungs. In *Journal of Applied Physiology*. <https://doi.org/10.1152/jappphysiol.90378.2008>
- Marey, É.-J. (1873). *La machine animale*. Bailliere. <https://books.google.com/books?hl=en&lr=&id=TFvExvyZekUC&pgis=1>
- Mariani, B., Hoskovec, C., Rochat, S., Büla, C., Penders, J., & Aminian, K. (2010). 3D gait assessment in young and elderly subjects using foot-worn inertial sensors. *Journal of Biomechanics*, 43(15), 2999-3006. <https://doi.org/10.1016/j.jbiomech.2010.07.003>
- Mariani, B., Rochat, S., Büla, C. J., & Aminian, K. (2012). Heel and toe clearance estimation for gait analysis using wireless inertial sensors. *IEEE Transactions on Biomedical Engineering*, 59(12 PART2), 3162-3168. <https://doi.org/10.1109/TBME.2012.2216263>
- Mariani, B., Rouhani, H., Crevoisier, X., & Aminian, K. (2013). Quantitative estimation of foot-flat and stance phase of gait using foot-worn inertial sensors. *Gait and Posture*, 37(2), 229-234. <https://doi.org/10.1016/j.gaitpost.2012.07.012>
- Martin, P. E., Sanderson, D. J., & Umberger, B. . (2008). Factors Affecting Preferred Rates of Movement in Cyclic Activities. In *Biomechanics in Sport* (pp. 142-160). <https://doi.org/10.1002/9780470693797.ch7>
- Martin, V., Kerhervé, H., Messonnier, L. A., Banfi, J. C., Geyssant, A., Bonnefoy, R., Féasson, L., & Millet, G. Y. (2010). Central and peripheral contributions to neuromuscular fatigue induced by a 24-h treadmill run. *Journal of Applied Physiology*. <https://doi.org/10.1152/jappphysiol.01202.2009>
- Maurer, C., Federolf, P., von Tscharn, V., Stirling, L., & Nigg, B. M. (2012). Discrimination of gender-, speed-, and shoe-dependent movement patterns in runners using full-body kinematics. *Gait and Posture*, 36(1), 40-45. <https://doi.org/10.1016/j.gaitpost.2011.12.023>
- McClay, I., & Manal, K. (1998). A comparison of three-dimensional lower extremity kinematics during running between excessive pronators and normals. *Clinical Biomechanics*, 13(3), 195-203. [https://doi.org/10.1016/S0268-0033\(97\)00029-6](https://doi.org/10.1016/S0268-0033(97)00029-6)
- McGhee, R. B., & Jain, A. K. (1972). Some properties of regularly realizable gait matrices. *Mathematical Biosciences*, 13(1-2), 179-193. [https://doi.org/10.1016/0025-5564\(72\)90033-8](https://doi.org/10.1016/0025-5564(72)90033-8)
- McGrath, D., Greene, B. R., O'Donovan, K. J., & Caulfield, B. (2012). Gyroscope-based assessment of temporal gait parameters during treadmill walking and running. *Sports Engineering*, 15(4), 207-213. <https://doi.org/10.1007/s12283-012-0093-8>
- McKenzie, D. C., Clement, D. B., & Taunton, J. E. (1985). Running Shoes, Orthotics, and Injuries. In *Sports Medicine: An International Journal of Applied Medicine and Science in Sport and Exercise* (Vol. 2, Issue 5, pp. 334-347). <https://doi.org/10.2165/00007256-198502050-00003>

- McClean, B. (1994). The biomechanics of hurdling : Force plate analysis to assess hurdling technique. *Nsa*, 9(4), 55-58.
- McMahon, T. A., & Cheng, G. C. (1990). The mechanics of running: How does stiffness couple with speed? *Journal of Biomechanics*, 23(SUPPL. 1), 65-78. [https://doi.org/10.1016/0021-9290\(90\)90042-2](https://doi.org/10.1016/0021-9290(90)90042-2)
- Mei, Q., Gu, Y., Xiang, L., Baker, J. S., & Fernandez, J. (2019). Foot pronation contributes to altered lower extremity loading after long distance running. *Frontiers in Physiology*, 10(MAY), 1-12. <https://doi.org/10.3389/fphys.2019.00573>
- Mercer, J. A., Bates, B. T., Dufek, J. S., & Hreljac, A. (2003). Characteristics of shock attenuation during fatigued running. *Journal of Sports Sciences*, 21(11), 911-919. <https://doi.org/10.1080/0264041031000140383>
- Mercer, J. A., Devita, P., Derrick, T. R., & Bates, B. T. (2003). Individual effects of stride length and frequency on shock attenuation during running. *Medicine and Science in Sports and Exercise*, 35(2), 307-313. <https://doi.org/10.1249/01.MSS.0000048837.81430.E7>
- Mercer, J. A., Vance, J., Hreljac, A., & Hamill, J. (2002). Relationship between shock attenuation and stride length during running at different velocities. *European Journal of Applied Physiology*, 87(4-5), 403-408. <https://doi.org/10.1007/s00421-002-0646-9>
- Mero, A., Komi, P. V., & Gregor, R. J. (1992). Biomechanics of Sprint Running : A Review Biomechanics of Sprint Running. *Sports Medicine*, 6(13), 376-392.
- Mertens, J. C., Boschmann, A., Schmidt, M., & Plessl, C. (2018). Sprint diagnostic with GPS and inertial sensor fusion. *Sports Engineering*. <https://doi.org/10.1007/s12283-018-0291-0>
- Meyer, C., Mohr, M., Falbriard, M., Nigg, S. R., & Nigg, B. M. (2018). Influence of footwear comfort on the variability of running kinematics†. *Footwear Science*, 10(1), 29-38. <https://doi.org/10.1080/19424280.2017.1388296>
- Meyer, F., Falbriard, M., Aminian, K., & Millet, G. P. (2018). How accurate is visual determination of foot strike pattern and pronation assessment. *Gait and Posture*. <https://doi.org/10.1016/j.gaitpost.2017.12.012>
- Miller, R. H., & Hamill, J. (2015). Optimal footfall patterns for cost minimization in running. *Journal of Biomechanics*, 48(11), 2858-2864. <https://doi.org/10.1016/j.jbiomech.2015.04.019>
- Millet, G. P., & Millet, G. Y. (2012). Ultramarathon is an outstanding model for the study of adaptive responses to extreme load and stress. In *BMC Medicine*. <https://doi.org/10.1186/1741-7015-10-77>
- Millet, G. Y., Banfi, J. C., Kerherve, H., Morin, J. B., Vincent, L., Estrade, C., Geyssant, A., & Feasson, L. (2011). Physiological and biological factors associated with a 24 h treadmill ultra-marathon performance. *Scandinavian Journal of Medicine and Science in Sports*. <https://doi.org/10.1111/j.1600-0838.2009.01001.x>

- Millet, Guillaume Y., Morin, J. B., Degache, E., Edouard, P., Feasson, L., Verney, J., & Oullion, R. (2009). Running from Paris to Beijing: Biomechanical and physiological consequences. *European Journal of Applied Physiology*. <https://doi.org/10.1007/s00421-009-1194-3>
- Milner, C. E., & Paquette, M. R. (2015). A kinematic method to detect foot contact during running for all foot strike patterns. *Journal of Biomechanics*, 48(12), 3502-3505. <https://doi.org/10.1016/j.jbiomech.2015.07.036>
- Mitschke, C., Kiesewetter, P., & Milani, T. L. (2018). The effect of the accelerometer operating range on biomechanical parameters: Stride length, velocity, and peak tibial acceleration during running. *Sensors (Switzerland)*, 18(1). <https://doi.org/10.3390/s18010130>
- Mitschke, C., Zaumseil, E., & Milani, T. L. (2017). The influence of inertial sensor sampling frequency on the accuracy of measurement parameters in rearfoot running. *Computer Methods in Biomechanics and Biomedical Engineering*, 20(14), 1502-1511. <https://doi.org/10.1080/10255842.2017.1382482>
- Miyazaki, S. (1997). Long-term unrestrained measurement of stride length and walking velocity utilizing a piezoelectric gyroscope. In *IEEE Transactions on Biomedical Engineering* (Vol. 44, Issue 8, pp. 753-759). <https://doi.org/10.1109/10.605434>
- Mizrahi, J., & Susak, Z. (1982). In-vivo elastic and damping response of the human leg to impact forces. In *Journal of Biomechanical Engineering* (Vol. 104, Issue 1, pp. 63-66). <https://doi.org/10.1115/1.3138305>
- Mizrahi, Joseph, Verbitsky, O., Isakov, E., & Daily, D. (2000). Effect of fatigue on leg kinematics and impact acceleration in long distance running. *Human Movement Science*, 19(2), 139-151. [https://doi.org/10.1016/S0167-9457\(00\)00013-0](https://doi.org/10.1016/S0167-9457(00)00013-0)
- Mo, S., & Chow, D. H. K. (2018). Accuracy of three methods in gait event detection during overground running. *Gait and Posture*, 59(June 2017), 93-98. <https://doi.org/10.1016/j.gaitpost.2017.10.009>
- Monaghan, G. M., Hsu, W. H., Lewis, C. L., Saltzman, E., Hamill, J., & Holt, K. G. (2014). Forefoot angle at initial contact determines the amplitude of forefoot and rearfoot eversion during running. *Clinical Biomechanics*, 29(8), 936-942. <https://doi.org/10.1016/j.clinbiomech.2014.06.011>
- Moore, I. S. (2016). Is there an economical running technique? A review of modifiable biomechanical factors affecting running economy. *Sports Medicine*, 46(6), 793-807. <https://doi.org/10.1007/s40279-016-0474-4>
- Morgan, W. P. (1979). Negative addiction in runners. *Physician and Sportsmedicine*. <https://doi.org/10.1080/00913847.1979.11948436>
- Morin, J. B., Dalleau, G., Kyröläinen, H., Jeannin, T., & Belli, A. (2005). A Simple Method for Measuring Stiffness During Running. *Journal of applied biomechanics*, 21(2), 167-180.

- Morin, J. B., Samozino, P., & Millet, G. Y. (2011). Changes in running kinematics, kinetics, and spring-mass behavior over a 24-h run. *Medicine and Science in Sports and Exercise*, 43(5), 829-836. <https://doi.org/10.1249/MSS.0b013e3181fec518>
- Morin, J. B., Tomazin, K., Edouard, P., & Millet, G. Y. (2011). Changes in running mechanics and spring-mass behavior induced by a mountain ultra-marathon race. *Journal of Biomechanics*, 44(6), 1104-1107. <https://doi.org/10.1016/j.jbiomech.2011.01.028>
- Morin, J. B., Jeannin, T., Chevallier, B., & Belli, A. (2006). Spring-mass model characteristics during sprint running: Correlation with performance and fatigue-induced changes. *International Journal of Sports Medicine*, 27(2), 158-165. <https://doi.org/10.1055/s-2005-837569>
- Muniz-Pardos, B., Sutehall, S., Gellaerts, J., Falbriard, M., Mariani, B., Bosch, A., Asrat, M., Schaible, J., & Pitsiladis, Y. P. (2018). Integration of Wearable Sensors into the Evaluation of Running Economy and Foot Mechanics in Elite Runners. *Current Sports Medicine Reports*, 17(12), 480-488. <https://doi.org/10.1249/JSR.0000000000000550>
- Muñoz-Jimenez, M., Latorre-Román, P. A., Soto-Hermoso, V. M., & García-Pinillos, F. (2015). Influence of shod/unshod condition and running speed on foot-strike patterns, inversion/eversion, and vertical foot rotation in endurance runners. *Journal of Sports Sciences*, 33(19), 2035-2042. <https://doi.org/10.1080/02640414.2015.1026377>
- Munro, C. F., Miller, D. I., & Fuglevand, A. J. (1987). Ground reaction forces in running: A reexamination. *Journal of Biomechanics*, 20(2), 147-155. [https://doi.org/10.1016/0021-9290\(87\)90306-X](https://doi.org/10.1016/0021-9290(87)90306-X)
- Nagel, A., Fernholz, F., Kibele, C., & Rosenbaum, D. (2008). Long distance running increases plantar pressures beneath the metatarsal heads. A barefoot walking investigation of 200 marathon runners. *Gait and Posture*. <https://doi.org/10.1016/j.gaitpost.2006.12.012>
- Nedergaard, N. J., Verheul, J., Drust, B., Etchells, T., Lisboa, P., Robinson, M. A., & Vanrenterghem, J. (2018). The feasibility of predicting ground reaction forces during running from a trunk accelerometry driven mass-spring-damper model. *PeerJ*, 2018(12), 1-17. <https://doi.org/10.7717/peerj.6105>
- Neugebauer, J. M., Hawkins, D. A., & Beckett, L. (2012). Estimating Youth Locomotion Ground Reaction Forces Using an Accelerometer-Based Activity Monitor. *PLoS ONE*, 7(10). <https://doi.org/10.1371/journal.pone.0048182>
- Nicol, C., Komi, P. V., & Marconnet, P. (1991a). Effects of marathon fatigue on running kinematics and economy. *Scandinavian Journal of Medicine & Science in Sports*, 1(4), 195-204. <https://doi.org/10.1111/j.1600-0838.1991.tb00296.x>
- Nicol, C., Komi, P. V., & Marconnet, P. (1991b). Fatigue effects of marathon running on neuromuscular performance: I. Changes in muscle force and stiffness characteristics. *Scandinavian Journal of Medicine & Science in Sports*, 1(1), 10-17. <https://doi.org/10.1111/j.1600-0838.1991.tb00265.x>

Chapter 9. General Discussion

- Nigg, B. M., Cole, G. K., & Nachbauer, W. (1993). Effects of arch height of the foot on angular motion of the lower extremities in running. *Journal of Biomechanics*, 26(8), 909-916. [https://doi.org/10.1016/0021-9290\(93\)90053-H](https://doi.org/10.1016/0021-9290(93)90053-H)
- Nigg, B. M., Mohr, M. M., & Nigg, S. R. (2017). Muscle tuning and preferred movement path - a paradigm shift. *Current Issues in Sport Science (CISS)*, 2, 1-12. https://doi.org/10.15203/ciss_2017.007
- Nigg, Benno, Behling, A. V., & Hamill, J. (2019). Foot pronation. *Footwear Science*, 11(3), 131-134. <https://doi.org/10.1080/19424280.2019.1673489>
- Nigg, BM. (1983). External force measurements with sport shoes and playing surfaces. *Biomechanical Aspects of Sport Shoes and Playing Surfaces. University of Calgary, Canada*, 11.
- Nilsson, J., Thorstensson, A., & Halbertsma, J. (1985). Changes in leg movements and muscle activity with speed of locomotion and mode of progression in humans. *Acta Physiologica Scandinavica*, 123(4), 457-475. <https://doi.org/10.1111/j.1748-1716.1985.tb07612.x>
- Noehren, B., Hamill, J., & Davis, I. (2013). Prospective evidence for a hip etiology in patello-femoral pain. *Medicine and Science in Sports and Exercise*.
- Norris, M., Anderson, R., & Kenny, I. C. (2013). Method analysis of accelerometers and gyroscopes in running gait: A systematic review. *Proceedings of the Institution of Mechanical Engineers, Part P: Journal of Sports Engineering and Technology*, 228(1), 3-15. <https://doi.org/10.1177/1754337113502472>
- Norris, Michelle, Kenny, I. C., & Anderson, R. (2016). Comparison of accelerometry stride time calculation methods. *Journal of Biomechanics*, 49(13), 3031-3034. <https://doi.org/10.1016/j.jbiomech.2016.05.029>
- Novacheck, T. F. (1998). The biomechanics of running. *Gait and Posture*, 7(1), 77-95. [https://doi.org/10.1016/S0966-6362\(97\)00038-6](https://doi.org/10.1016/S0966-6362(97)00038-6)
- Nummela, A., Keränen, T., & Mikkelsen, L. O. (2007). Factors related to top running speed and economy. *International Journal of Sports Medicine*, 28(8), 655-661. <https://doi.org/10.1055/s-2007-964896>
- Nummela, A., Vuorimaa, T., & Rusko, H. (1992). Changes in force production, blood lactate and emg activity in the 400-m sprint. *Journal of Sports Sciences*, 10(3), 217-228. <https://doi.org/10.1080/02640419208729920>
- Ogueta-Alday, A., Morante, J. C., Rodríguez-Marroyo, J. A., & García-López, J. (2013). Validation of a new method to measure contact and flight times during treadmill running. *Journal of Strength and Conditioning Research*, 27(5), 1455-1462. <https://doi.org/10.1519/JSC.0b013e318269f760>

- Otsuka, M., & Isaka, T. (2019). Intra-athlete and inter-group comparisons: Running pace and step characteristics of elite athletes in the 400-m hurdles. *PLoS ONE*, 14(3). <https://doi.org/10.1371/journal.pone.0204185>
- Pageaux, B. (2014). The psychobiological model of endurance performance: an effort-based decision-making theory to explain self-paced endurance performance. In *Sports medicine (Auckland, N.Z.)*. <https://doi.org/10.1007/s40279-014-0198-2>
- Pappas, P., Paradisis, G., Tsolakis, C., Smirniotou, A., & Morin, J. B. (2014). Reliabilities of leg and vertical stiffness during treadmill running. *Sports Biomechanics*, 13(4), 391-399. <https://doi.org/10.1080/14763141.2014.981853>
- Paquette, M. R., & Melcher, D. A. (2017). Impact of a long run on injury-related biomechanics with relation to weekly mileage in trained male runners. *Journal of Applied Biomechanics*, 33(3), 216-221. <https://doi.org/10.1123/jab.2016-0170>
- Park, S. K., & Suh, Y. S. (2010). A zero velocity detection algorithm using inertial sensors for pedestrian navigation systems. *Sensors (Switzerland)*, 10(10), 9163-9178. <https://doi.org/10.3390/s101009163>
- Payne, A. H. (1983). Foot to ground contact forces of elite runners. *Biomechanics VII-B*, 746-753.
- Perl, D. P., Daoud, A. I., & Lieberman, D. E. (2012). Effects of footwear and strike type on running economy. *Medicine and Science in Sports and Exercise*, 44(7), 1335-1343. <https://doi.org/10.1249/MSS.0b013e318247989e>
- Perry, S. D., & LaFortune, M. A. (1995). Influences of inversion/eversion of the foot upon impact loading during locomotion. *Clinical Biomechanics*, 10(5), 253-257. [https://doi.org/10.1016/0268-0033\(95\)00006-7](https://doi.org/10.1016/0268-0033(95)00006-7)
- Pes, B. (2020). Learning from high-dimensional biomedical datasets: The issue of class imbalance. *IEEE Access*, 8, 13527-13540. <https://doi.org/10.1109/ACCESS.2020.2966296>
- Peters, A., Galna, B., Sangeux, M., Morris, M., & Baker, R. (2010). Quantification of soft tissue artifact in lower limb human motion analysis: a systematic review. *Gait and Posture*, 31(1), 1-8. <https://doi.org/10.1016/j.gaitpost.2009.09.004>
- Phillips, J., Hendricks, C., & Phillips, J. (2015). *Factors contributing to running injuries . A narrative review A narrative review. July.*
- Provot, T., Chiementin, X., Bolaers, F., & Murer, S. (2019). Effect of running speed on temporal and frequency indicators from wearable MEMS accelerometers. *Sports Biomechanics*, 00(00), 1-13. <https://doi.org/10.1080/14763141.2019.1607894>
- Przednowek, K., Krzeszowski, T., Iskra, J., & Wiktorowicz, K. (2014). Markerless motion tracking in evaluation of hurdle clearance parameters. *IcSPORTS 2014 - Proceedings of the 2nd*

Chapter 9. General Discussion

- International Congress on Sports Sciences Research and Technology Support*, 129-136. <https://doi.org/10.5220/0005080601290136>
- Purcell, B., Channells, J., James, D., & Barrett, R. (2005). Use of accelerometers for detecting foot-ground contact time during running. *BioMEMS and Nanotechnology II*, 6036(JANUARY 2006), 603615. <https://doi.org/10.1117/12.638389>
- Rabita, G., Couturier, A., Dorel, S., Hausswirth, C., & Le Meur, Y. (2013). Changes in spring-mass behavior and muscle activity during an exhaustive run at VO₂max. *Journal of Biomechanics*. <https://doi.org/10.1016/j.jbiomech.2013.06.011>
- Rabita, G., Dorel, S., Slawinski, J., Sàez-de-Villarreal, E., Couturier, A., Samozino, P., & Morin, J. B. (2015). Sprint mechanics in world-class athletes: A new insight into the limits of human locomotion. *Scandinavian Journal of Medicine and Science in Sports*, 25(5), 583-594. <https://doi.org/10.1111/sms.12389>
- Raper, D. P., Witchalls, J., Philips, E. J., Knight, E., Drew, M. K., & Waddington, G. (2018). Use of a tibial accelerometer to measure ground reaction force in running: A reliability and validity comparison with force plates. *Journal of Science and Medicine in Sport*, 21(1), 84-88. <https://doi.org/10.1016/j.jsams.2017.06.010>
- Rawstorn, J. C., Maddison, R., Ali, A., Foskett, A., & Gant, N. (2014). Rapid directional change degrades GPS distance measurement validity during intermittent intensity running. *PLoS ONE*, 9(4), 1-6. <https://doi.org/10.1371/journal.pone.0093693>
- Reenalda, J., Maartens, E., Homan, L., & Buurke, J. H. (Jaap. (2016). Continuous three dimensional analysis of running mechanics during a marathon by means of inertial magnetic measurement units to objectify changes in running mechanics. *Journal of Biomechanics*, 49(14), 3362-3367. <https://doi.org/10.1016/j.jbiomech.2016.08.032>
- Reinschmidt, C., Van Den Bogert, A. J., Murphy, N., Lundberg, A., & Nigg, B. M. (1997). Tibio-calcaneal motion during running, measured with external and bone markers. *Clinical Biomechanics*, 12(1), 8-16. [https://doi.org/10.1016/S0268-0033\(96\)00046-0](https://doi.org/10.1016/S0268-0033(96)00046-0)
- Riley, P. O., Dicharry, J., Franz, J., Croce, U. Della, Wilder, R. P., & Kerrigan, D. C. (2008). A kinematics and kinetic comparison of overground and treadmill running. *Medicine and Science in Sports and Exercise*, 40(6), 1093-1100. <https://doi.org/10.1249/MSS.0b013e3181677530>
- Robberechts, P., Derie, R., Berghe, P. Van den, Gerlo, J., De Clercq, D., Segers, V., & Davis, J. (2019). *Predicting gait events from tibial acceleration in rearfoot running: a structured machine learning approach*. IC, 1-13. <http://arxiv.org/abs/1910.13372>
- Ruder, M., Jamison, S. T., Tenforde, A., Mulloy, F., & Davis, I. S. (2019). Relationship of Foot Strike Pattern and Landing Impacts during a Marathon. *Medicine and Science in Sports and Exercise*, 51(10), 2073-2079. <https://doi.org/10.1249/MSS.0000000000002032>

- Ryan, M., Elashi, M., Newsham-West, R., & Taunton, J. (2014). Examining injury risk and pain perception in runners using minimalist footwear. *British Journal of Sports Medicine*, 48(16), 1257-1262. <https://doi.org/10.1136/bjsports-2012-092061>
- Sabatini, A. M. (2005). Quaternion-based strap-down integration method for applications of inertial sensing to gait analysis. *Medical and Biological Engineering and Computing*, 43(1), 94-101. <https://doi.org/10.1007/BF02345128>
- Sabatini, A. M. (2006). Quaternion-based extended Kalman filter for determining orientation by inertial and magnetic sensing. *IEEE Transactions on Biomedical Engineering*, 53(7), 1346-1356. <https://doi.org/10.1109/TBME.2006.875664>
- Sabatini, A. M., Martelloni, C., Scapellato, S., & Cavallo, F. (2005). Assessment of walking features from foot inertial sensing. *IEEE Transactions on Biomedical Engineering*, 52(3), 486-494. <https://doi.org/10.1109/TBME.2004.840727>
- Saeedi, R., Purath, J., Venkatasubramanian, K., & Ghasemzadeh, H. (2014). Toward seamless wearable sensing: Automatic on-body sensor localization for physical activity monitoring. *2014 36th Annual International Conference of the IEEE Engineering in Medicine and Biology Society, EMBC 2014*, 5385-5388. <https://doi.org/10.1109/EMBC.2014.6944843>
- Saito, M., Kobayashi, K., Miyashita, M., & Hoshikawa, T. (1974). Temporal patterns in running. In *Biomechanics IV* (pp. 106-111). https://doi.org/10.1007/978-1-349-02612-8_15
- Salarian, A., Burkhard, P. R., Vingerhoets, F. J. G., Jolles, B. M., & Aminian, K. (2013). A novel approach to reducing number of sensing units for wearable gait analysis systems. *IEEE Transactions on Biomedical Engineering*, 60(1), 72-77. <https://doi.org/10.1109/TBME.2012.2223465>
- Salo, A., Grimshaw, P. N., & Marar, L. (1997). 3-D biomechanical analysis of sprint hurdles at different competitive levels. *Medicine and Science in Sports and Exercise*, 29(2), 231-237. <https://doi.org/10.1097/00005768-199702000-00011>
- Sardroodian, M., Madeleine, P., Voigt, M., & Hansen, E. A. (2015). Freely chosen stride frequencies during walking and running are not correlated with freely chosen pedalling frequency and are insensitive to strength training. *Gait and Posture*. <https://doi.org/10.1016/j.gaitpost.2015.04.003>
- Saugy, J., Place, N., Millet, G. Y., Degache, F., Schena, F., & Millet, G. P. (2013). Alterations of Neuromuscular Function after the World's Most Challenging Mountain Ultra-Marathon. *PLoS ONE*. <https://doi.org/10.1371/journal.pone.0065596>
- Savoldelli, A., Fornasiero, A., Trabucchi, P., Limonta, E., Torre, A. La, Degache, F., Pellegrini, B., Millet, G. P., Vernillo, G., & Schena, F. (2017). The energetics during the world's most challenging mountain Ultra-Marathon-A case study at the Tor des Geants®. *Frontiers in Physiology*. <https://doi.org/10.3389/fphys.2017.01003>

- Schache, A. G., Bennell, K. L., Blanch, P. D., & Wrigley, T. V. (1999). The coordinated movement of the lumbo-pelvic-hip complex during running: A literature review. In *Gait and Posture* (Vol. 10, Issue 1, pp. 30-47). [https://doi.org/10.1016/S0966-6362\(99\)00025-9](https://doi.org/10.1016/S0966-6362(99)00025-9)
- Scheerder, J., Breedveld, K., Borgers, J., & Vos, S. (2015). Who Is Doing a Run with the Running Boom? The Growth and Governance of One of Europe's Most Popular Sport Activities. In *Running across Europe: the rise and size of one of the largest sport markets* (pp. 1-21). Palgrave Macmillan.
- Schieb, D. A. (1986). Kinematic accommodation of novice treadmill runners. *Research Quarterly for Exercise and Sport*, 57(1), 1-7. <https://doi.org/10.1080/02701367.1986.10605381>
- Schmidt, M., Rheinländer, C., Nolte, K. F., Wille, S., Wehn, N., & Jaitner, T. (2016). IMU-based Determination of Stance Duration during Sprinting. *Procedia Engineering*, 147, 747-752. <https://doi.org/10.1016/j.proeng.2016.06.330>
- Schnohr, P., Marott, J. L., Lange, P., & Jensen, G. B. (2013). Longevity in male and female joggers: The Copenhagen City Heart Study. *American Journal of Epidemiology*, 177(7), 683-689. <https://doi.org/10.1093/aje/kws301>
- Schubert, A. G., Kempf, J., & Heiderscheit, B. C. (2014). Influence of Stride Frequency and Length on Running Mechanics: A Systematic Review. In *Sports Health*. <https://doi.org/10.1177/1941738113508544>
- Setuain, I., Lecumberri, P., Ahtiainen, J. P., Mero, A. A., Häkkinen, K., & Izquierdo, M. (2018). Sprint mechanics evaluation using inertial sensor-based technology: A laboratory validation study. *Scandinavian Journal of Medicine and Science in Sports*. <https://doi.org/10.1111/sms.12946>
- Sheerin, K. R., Reid, D., & Besier, T. F. (2019). The measurement of tibial acceleration in runners—A review of the factors that can affect tibial acceleration during running and evidence-based guidelines for its use. In *Gait and Posture* (Vol. 67, pp. 12-24). <https://doi.org/10.1016/j.gaitpost.2018.09.017>
- Shi, Y., Shi, Y., & Liu, J. (2011). A rotation based method for detecting on-body positions of mobile devices. *UbiComp'11 - Proceedings of the 2011 ACM Conference on Ubiquitous Computing*, 559-560. <https://doi.org/10.1145/2030112.2030212>
- Shiang, T. Y., Hsieh, T. Y., Lee, Y. S., Wu, C. C., Yu, M. C., Mei, C. H., & Tai, I. H. (2016). Determine the Foot Strike Pattern Using Inertial Sensors. *Journal of Sensors*, 2016. <https://doi.org/10.1155/2016/4759626>
- Shipway, R., & Holloway, I. (2010). Running free: Embracing a healthy lifestyle through distance running. *Perspectives in Public Health*, 130(6), 270-276. <https://doi.org/10.1177/1757913910379191>

- Simon, J., Doederlein, L., McIntosh, A. S., Metaxiotis, D., Bock, H. G., & Wolf, S. I. (2006). The Heidelberg foot measurement method: Development, description and assessment. *Gait and Posture*, 23(4), 411-424. <https://doi.org/10.1016/j.gaitpost.2005.07.003>
- Skog, I., Händel, P., Nilsson, J. O., & Rantakokko, J. (2010). Zero-velocity detection-An algorithm evaluation. *IEEE Transactions on Biomedical Engineering*, 57(11), 2657-2666. <https://doi.org/10.1109/TBME.2010.2060723>
- Smith, L., Preece, S., Mason, D., & Bramah, C. (2015). A comparison of kinematic algorithms to estimate gait events during overground running. *Gait and Posture*, 41(1), 39-43. <https://doi.org/10.1016/j.gaitpost.2014.08.009>
- Soltani, A., Dejnabadi, H., Savary, M., & Aminian, K. (2019). Real-world gait speed estimation using wrist sensor: A personalized approach. *IEEE Journal of Biomedical and Health Informatics*, 2194(c), 1-1. <https://doi.org/10.1109/jbhi.2019.2914940>
- Stacoff, A., Kaelin, X., Stuessi, E., & Segesser, B. (2016). The Torsion of the Foot in Running. *International Journal of Sport Biomechanics*, 5(4), 375-389. <https://doi.org/10.1123/ijsb.5.4.375>
- Strohrmann, C., Harms, H., Kappeler-setz, C., & Tr, G. (2012). *Monitoring Kinematic Changes With Fatigue in Running Using Body-Worn Sensors*. 16(5), 983-990.
- Strohrmann, C., Harms, H., Tr, G., Hensler, S., & Roland, M. (2011). Out of the Lab and Into the Woods : Kinematic Analysis in Running Using Wearable Sensors. *Proceedings of the 2011 ACM Conference on Ubiquitous Computing - UbiComp '11*, 119-122. <https://doi.org/10.1145/2030112.2030129>
- Sun, X., Lam, W.-K., Zhang, X., Wang, J., & Fu, W. (2020). Systematic Review of the Role of Footwear Constructions in Running Biomechanics: Implications for Running-Related Injury and Performance. *Journal of Sports Science and Medicine*, 19(1), 20-37. <http://www.jssm.org>
- Swain, D. P., & Franklin, B. A. (2006). Comparison of cardioprotective benefits of vigorous versus moderate intensity aerobic exercise. In *American Journal of Cardiology* (Vol. 97, Issue 1, pp. 141-147). <https://doi.org/10.1016/j.amjcard.2005.07.130>
- Taunton, J. E., Ryan, M. B., Clement, D. B., McKenzie, D. C., Lloyd-Smith, D. R., & Zumbo, B. D. (2002). A retrospective case-control analysis of 2002 running injuries. *British Journal of Sports Medicine*, 36(2), 95-101. <https://doi.org/10.1136/bjism.36.2.95>
- Teng, H. L., & Powers, C. M. (2014a). Influence of trunk posture on lower extremity energetics during running. *Medicine and Science in Sports and Exercise*, 47(3), 625-630. <https://doi.org/10.1249/MSS.0000000000000436>
- Teng, H. L., & Powers, C. M. (2014b). Sagittal plane trunk posture influences patellofemoral joint stress during running. *Journal of Orthopaedic and Sports Physical Therapy*, 44(10), 785-792. <https://doi.org/10.2519/jospt.2014.5249>

- Terrier, P., Ladetto, Q., Merminod, B., & Schutz, Y. (2000). High-precision satellite positioning system as a new tool to study the biomechanics of human locomotion. *Journal of Biomechanics*, 33(12), 1717-1722. [https://doi.org/10.1016/S0021-9290\(00\)00133-0](https://doi.org/10.1016/S0021-9290(00)00133-0)
- Thompson, M. A. (2017). Physiological and biomechanical mechanisms of distance specific human running performance. *Integrative and Comparative Biology*, 57(2), 293-300. <https://doi.org/10.1093/icb/ix069>
- Tian, F., Li, N., Zheng, Z., Huang, Q., Zhu, T., Li, Q., Wang, W., Tsai, T. Y., & Wang, S. (2020). The effects of marathon running on three-dimensional knee kinematics during walking and running in recreational runners. *Gait and Posture*, 75, 72-77. <https://doi.org/10.1016/j.gaitpost.2019.08.009>
- Tibshirani, R. (1996). Regression Shrinkage and Selection Via the Lasso. *Journal of the Royal Statistical Society: Series B (Methodological)*, 58(1), 267-288. <https://doi.org/10.1111/j.2517-6161.1996.tb02080.x>
- Tidow, G. (1991). Model technique analysis sheets for the hurdles. Part VII: High hurdles. *New Studies in Athletics*, 6(2), 51-66.
- Trudeau, M. B., Willwacher, S., Weir, G., Rohr, E., Ertel, C., Bruggemann, G. P., & Hamill, J. (2019). A novel method for estimating an individual's deviation from their habitual motion path when running. *Footwear Science*, 11(3), 135-145. <https://doi.org/10.1080/19424280.2019.1615004>
- Van bottenburg, M., Hover, P., & Scheerder, J. (2010). Don't miss the next boat. Chances and challenges of the second wave of running. *New Studies in Athletics*, 25(3/4), 125-143.
- van der Kruk, E., & Reijne, M. M. (2018). Accuracy of human motion capture systems for sport applications; state-of-the-art review. *European Journal of Sport Science*, 18(6), 806-819. <https://doi.org/10.1080/17461391.2018.1463397>
- Van Der Worp, M. P., Ten Haaf, D. S. M., Van Cingel, R., De Wijer, A., Nijhuis-Van Der Sanden, M. W. G., & Bart Staal, J. (2015). Injuries in runners; a systematic review on risk factors and sex differences. *PLoS ONE*, 10(2), 1-18. <https://doi.org/10.1371/journal.pone.0114937>
- Van Gent, R. N., Siem, D., Van Middeloop, M., Van Os, A. G., Bierma-Zeinstra, S. M. A., & Koes, B. W. (2007). Incidence and determinants of lower extremity running injuries in long distance runners: A systematic review. *Sport En Geneeskunde*, 40(4), 16-29. <https://doi.org/10.1136/bjsm.2006.033548>
- Van Hooren, B., Fuller, J. T., Buckley, J. D., Miller, J. R., Sewell, K., Rao, G., Barton, C., Bishop, C., & Willy, R. W. (2019). Is Motorized Treadmill Running Biomechanically Comparable to Overground Running? A Systematic Review and Meta-Analysis of Cross-Over Studies. *Sports Medicine*, 0123456789. <https://doi.org/10.1007/s40279-019-01237-z>

- Van Hulle, R., Schwartz, C., Denoël, V., Croisier, J. L., Forthomme, B., & Brûls, O. (2020). A foot/ground contact model for biomechanical inverse dynamics analysis. *Journal of Biomechanics*, 100, 109412. <https://doi.org/10.1016/j.jbiomech.2019.109412>
- Van Oeveren, B. T., De Ruiter, C. J., Hoozemans, M. J. M., Beek, P. J., & Van Dieën, J. H. (2019). Inter-individual differences in stride frequencies during running obtained from wearable data. *Journal of Sports Sciences*, 37(17), 1996-2006. <https://doi.org/10.1080/02640414.2019.1614137>
- van Werkhoven, H., Farina, K. A., & Langley, M. H. (2019). Using A Soft Conformable Foot Sensor to Measure Changes in Foot Strike Angle During Running. *Sports*, 7(8), 184. <https://doi.org/10.3390/sports7080184>
- Varley, M. C., Fairweather, I. H., & Aughey, R. J. (2012). Validity and reliability of GPS for measuring instantaneous velocity during acceleration, deceleration, and constant motion. *Journal of Sports Sciences*, 30(2), 121-127. <https://doi.org/10.1080/02640414.2011.627941>
- Vernillo, G., Doucende, G., Cassirame, J., & Mourot, L. (2019). Energetically optimal stride frequency is maintained with fatigue in trained ultramarathon runners. *Journal of Science and Medicine in Sport*, 22(9), 1054-1058. <https://doi.org/10.1016/j.jsams.2019.04.003>
- Vernillo, G., Giandolini, M., Edwards, W. B., Morin, J.-B., Samozino, P., Horvais, N., & Millet, G. Y. (2017). Biomechanics and Physiology of Uphill and Downhill Running. *Sports Medicine*, 47(4), 615-629. <https://doi.org/10.1007/s40279-016-0605-y>
- Vernillo, G., Millet, G. P., & Millet, G. Y. (2017). Does the running economy really increase after ultra-marathons? In *Frontiers in Physiology* (Vol. 8, Issue OCT). <https://doi.org/10.3389/fphys.2017.00783>
- Vernillo, G., Savoldelli, A., Skafidas, S., Zignoli, A., La Torre, A., Pellegrini, B., Giardini, G., Trabucchi, P., Millet, G. P., & Schena, F. (2016). An extreme mountain ultra-marathon decreases the cost of uphill walking and running. *Frontiers in Physiology*. <https://doi.org/10.3389/fphys.2016.00530>
- Vernillo, G., Savoldelli, A., Zignoli, A., Trabucchi, P., Pellegrini, B., Millet, G. P., & Schena, F. (2014). Influence of the world's most challenging mountain ultra-marathon on energy cost and running mechanics. *European Journal of Applied Physiology*. <https://doi.org/10.1007/s00421-014-2824-y>
- Viitasalo, J. T., Luhtanen, P., Mononen, H. V., Norvapalo, K., Paavolainen, L., & Salonen, M. (1997). Photocell contact mat: A new instrument to measure contact and flight times in running. *Journal of Applied Biomechanics*. <https://doi.org/10.1123/jab.13.2.254>
- Waegli, A., & Skalous, J. (2009). Optimization of two GPS/MEMS-IMU integration strategies with application to sports. *GPS Solutions*, 13(4), 315-326. <https://doi.org/10.1007/s10291-009-0124-5>

Chapter 9. General Discussion

- Walther, B. A., & Moore, J. L. (2005). The concepts of bias, precision and accuracy, and their use in testing the performance of species richness estimators, with a literature review of estimator performance. In *Ecography* (Vol. 28, Issue 6). <https://doi.org/10.1111/j.2005.0906-7590.04112.x>
- Warburton, D. E. R., Nicol, C. W., & Bredin, S. S. D. (2006). Health benefits of physical activity: The evidence. *Cmaj*, 174(6), 801-809. <https://doi.org/10.1503/cmaj.051351>
- Weenk, D., Van Beijnum, B. J. F., Baten, C. T., Hermens, H. J., & Veltink, P. H. (2013). Automatic identification of inertial sensor placement on human body segments during walking. *Journal of NeuroEngineering and Rehabilitation*, 10(1), 31. <https://doi.org/10.1186/1743-0003-10-31>
- Wehrlin, J. P., & Hallén, J. (2006). Linear decrease in VO₂max and performance with increasing altitude in endurance athletes. *European Journal of Applied Physiology*. <https://doi.org/10.1007/s00421-005-0081-9>
- Weyand, P. G., Kelly, M., Blackadar, T., Darley, J. C., Oliver, S. R., Ohlenbusch, N. E., Joffe, S. W., & Hoyt, R. W. (2001). Ambulatory estimates of maximal aerobic power from foot-ground contact times and heart rates in running humans. *Journal of Applied Physiology*, 91(1), 451-458. <https://doi.org/10.1152/jappl.2001.91.1.451>
- Weyand, P. G., Sandell, R. F., Prime, D. N. L., & Bundle, M. W. (2010). The biological limits to running speed are imposed from the ground up. *Journal of Applied Physiology (Bethesda, Md. : 1985)*, 108(4), 950-961. <https://doi.org/10.1152/japplphysiol.00947.2009>
- Weyand, P. G., Sternlight, D. B., Bellizzi, M. J., & Wright, S. (2000). Faster top running speeds are achieved with greater ground forces not more rapid leg movements. *Journal of Applied Physiology*, 89(5), 1991-1999.
- Willems, P. A., & Gosseye, T. P. (2013). Does an instrumented treadmill correctly measure the ground reaction forces? *Biology Open*, 2(12), 1421-1424. <https://doi.org/10.1242/bio.20136379>
- Williams, K. R., & Cavanagh, P. R. (1987). Relationship between distance running mechanics, running economy, and performance. *Journal of Applied Physiology*, 63(3), 1236-1245. <https://doi.org/10.1152/jappl.1987.63.3.1236>
- Williams, K.R. (2008). The Dynamics of Running. In *Biomechanics in Sport* (pp. 161-183). John Wiley & Sons. <https://doi.org/10.1002/9780470693797.ch8>
- Williams, Keith R. (1985). Biomechanics of running. *Exercise and Sport Sciences Reviews*, 13(1), 389-441. <https://doi.org/10.17832/isc.2013.23.1.4>
- Willson, J. D., & Kernozek, T. W. (1999). Plantar loading and cadence alterations with fatigue. *Medicine and Science in Sports and Exercise*, 31(12), 1828-1833. <https://doi.org/10.1097/00005768-199912000-00020>

- Winter, S. C., Gordon, S., Brice, S. M., Lindsay, D., & Barrs, S. (2020). A Multifactorial Approach to Overuse Running Injuries: A 1-Year Prospective Study. *Sports Health*, XX(X), 1-8. <https://doi.org/10.1177/1941738119888504>
- Winter, S., Gordon, S., & Watt, K. (2017). Effects of fatigue on kinematics and kinetics during overground running: A systematic review. In *Journal of Sports Medicine and Physical Fitness* (Vol. 57, Issue 6, pp. 887-899). <https://doi.org/10.23736/S0022-4707.16.06339-8>
- Witte, T. H., & Wilson, A. M. (2004). Accuracy of non-differential GPS for the determination of speed over ground. *Journal of Biomechanics*, 37(12), 1891-1898. <https://doi.org/10.1016/j.jbiomech.2004.02.031>
- Wixted, A. J., Billing, D. C., & James, D. A. (2010). Validation of trunk mounted inertial sensors for analysing running biomechanics under field conditions, using synchronously collected foot contact data. *Sports Engineering*, 12(4), 207-212. <https://doi.org/10.1007/s12283-010-0043-2>
- Wouda, F. J., Giuberti, M., Bellusci, G., Maartens, E., Reenalda, J., van Beijnum, B. J. F., & Veltink, P. H. (2018). Estimation of vertical ground reaction forces and sagittal knee kinematics during running using three inertial sensors. *Frontiers in Physiology*, 9(MAR). <https://doi.org/10.3389/fphys.2018.00218>
- Yang, S., Mohr, C., & Li, Q. (2011). Ambulatory running speed estimation using an inertial sensor. *Gait and Posture*, 34(4), 462-466. <https://doi.org/10.1016/j.gaitpost.2011.06.019>
- Yong, J. R., Silder, A., & Delp, S. L. (2014). Differences in muscle activity between natural forefoot and rearfoot strikers during running. *Journal of Biomechanics*, 47(15), 3593-3597. <https://doi.org/10.1016/j.jbiomech.2014.10.015>
- Yuan, Q., Asadi, E., Lu, Q., Yang, G., & Chen, I. M. (2019). Uncertainty-Based IMU Orientation Tracking Algorithm for Dynamic Motions. *IEEE/ASME Transactions on Mechatronics*, 24(2), 872-882. <https://doi.org/10.1109/TMECH.2019.2892069>
- Zadpoor, A. A., & Nikooyan, A. A. (2011). The relationship between lower-extremity stress fractures and the ground reaction force: A systematic review. *Clinical Biomechanics*, 26(1), 23-28. <https://doi.org/10.1016/j.clinbiomech.2010.08.005>
- Zhang, R., Yang, H., Höflinger, F., & Reindl, L. M. (2017). Adaptive Zero Velocity Update Based on Velocity Classification for Pedestrian Tracking. *IEEE Sensors Journal*, 17(7), 2137-2145. <https://doi.org/10.1109/JSEN.2017.2665678>
- Zhao, Y., Brahms, M., Gerhard, D., & Barden, J. (2016). Stance phase detection for walking and running using an IMU periodicity-based approach. *Advances in Intelligent Systems and Computing*, 392, 225-232. https://doi.org/10.1007/978-3-319-24560-7_29
- Zihajehzadeh, S., Loh, D., Lee, T. J., Hoskinson, R., & Park, E. J. (2015). A cascaded Kalman filter-based GPS/MEMS-IMU integration for sports applications. *Measurement: Journal*

of the International Measurement Confederation, 73, 200-210. <https://doi.org/10.1016/j.measurement.2015.05.023>

Zihajehzadeh, S., & Park, E. J. (2016). Regression model-based walking speed estimation using wrist-worn inertial sensor. *PLoS ONE*, 11(10), 1-16. <https://doi.org/10.1371/journal.pone.0165211>

Zijlstra, W., & Hof, A. L. (2003). Assessment of spatio-temporal gait parameters from trunk accelerations during human walking. *Gait and Posture*, 18(2), 1-10. [https://doi.org/10.1016/S0966-6362\(02\)00190-X](https://doi.org/10.1016/S0966-6362(02)00190-X)

Zimmermann, T., Taetz, B., & Bleser, G. (2018). IMU-to-segment assignment and orientation alignment for the lower body using deep learning. *Sensors (Switzerland)*, 18(1). <https://doi.org/10.3390/s18010302>

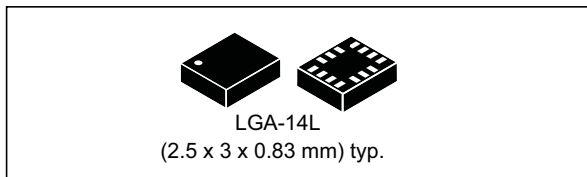
Zrenner, M., Gradl, S., Jensen, U., Ullrich, M., & Eskofier, B. M. (2018). Comparison of different algorithms for calculating velocity and stride length in running using inertial measurement units. *Sensors (Switzerland)*, 18(12). <https://doi.org/10.3390/s18124194>



Appendix

iNEMO inertial module: always-on 3D accelerometer and 3D gyroscope

Datasheet - production data



Features

- Power consumption: 0.85 mA in combo normal mode and 1.1 mA in combo high-performance mode up to 1.6 kHz.
- “Always-on” experience with low power consumption for both accelerometer and gyroscope
- Interface flexibility: selectable SPI (3/4-wire) or I²C with the main processor
- Auxiliary SPI (3-wire) to support OIS applications
- EIS/OIS support
- Accelerometer ODR up to 6.66 kHz
- Gyroscope ODR up to 3.33 kHz
- Smart FIFO
- $\pm 2/\pm 4/\pm 8/\pm 16$ g full scale
- $\pm 125/\pm 250/\pm 500/\pm 1000/\pm 2000$ dps full scale
- Analog supply voltage: 1.71 V to 3.6 V
- Independent IOs supply (1.62 V)
- Compact footprint, 2.5 mm x 3 mm x 0.83 mm
- SPI/I²C serial interface data synchronization feature
- Embedded temperature sensor
- ECOPACK[®], RoHS and “Green” compliant

Applications

- EIS and OIS for camera applications
- Collecting sensor data
- Motion tracking and gesture detection
- Pedometer, step detector and step counter
- Significant motion and tilt functions
- Indoor navigation
- IoT and connected devices
- Vibration monitoring and compensation

Description

The LSM6DS3H is a system-in-package featuring a 3D digital accelerometer and a 3D digital gyroscope performing at 1.1 mA (up to 1.6 kHz ODR) in high-performance mode and enabling always-on low-power features for an optimal motion experience for the consumer.

The LSM6DS3H supports main OS requirements, offering real, virtual and batch sensors with 4 kbyte FIFO + flexible 4 kbyte (FIFO or programmable) for dynamic data batching.

The LSM6DS3H gyroscope supports both OIS/EIS applications. The device can be connected to the camera module through a dedicated auxiliary SPI (Mode 3) while flexibility for the primary interface is available (I²C/SPI).

ST’s family of MEMS sensor modules leverages the robust and mature manufacturing processes already used for the production of micromachined accelerometers and gyroscopes.

The various sensing elements are manufactured using specialized micromachining processes, while the IC interfaces are developed using CMOS technology that allows the design of a dedicated circuit which is trimmed to better match the characteristics of the sensing element.

The LSM6DS3H has a full-scale acceleration range of $\pm 2/\pm 4/\pm 8/\pm 16$ g and an angular rate range of $\pm 125/\pm 250/\pm 500/\pm 1000/\pm 2000$ dps.

High robustness to mechanical shock makes the LSM6DS3H the preferred choice of system designers for the creation and manufacturing of reliable products.

The LSM6DS3H is available in a plastic land grid array (LGA) package.

Table 1. Device summary

Part number	Temp. range [°C]	Package	Packing
LSM6DS3H	-40 to +85	LGA-14L (2.5 x 3 x 0.83 mm)	Tray
LSM6DS3HTR	-40 to +85		Tape & Reel

4 Module specifications

4.1 Mechanical characteristics

@ Vdd = 1.8 V, T = 25 °C unless otherwise noted.

Table 3. Mechanical characteristics

Symbol	Parameter	Test conditions	Min.	Typ. ⁽¹⁾	Max.	Unit
LA_FS	Linear acceleration measurement range			±2		g
				±4		
				±8		
				±16		
G_FS	Angular rate measurement range			±125		dps
				±250		
				±500		
				±1000		
				±2000		
LA_So	Linear acceleration sensitivity ⁽²⁾	FS = ±2		0.061		mg/LSB
		FS = ±4		0.122		
		FS = ±8		0.244		
		FS = ±16		0.488		
G_So	Angular rate sensitivity ⁽³⁾	FS = ±125		4.375		mdps/LSB
		FS = ±250		8.75		
		FS = ±500		17.50		
		FS = ±1000		35		
		FS = ±2000		70		
LA_SoDr	Linear acceleration sensitivity change vs. temperature	from -40° to +85° delta from T=25°		±1		%
G_SoDr	Angular rate sensitivity change vs. temperature	from -40° to +85° delta from T=25°		±1.5		%
LA_TyOff	Linear acceleration typical zero-g level offset accuracy ⁽⁴⁾			±40		mg
G_TyOff	Angular rate typical zero-rate level ⁽⁴⁾			±10		dps
LA_OffDr	Linear acceleration zero-g level change vs. temperature			±0.5		mg/°C
G_OffDr	Angular rate typical zero-rate level change vs. temperature			±0.05		dps/°C

Table 3. Mechanical characteristics (continued)

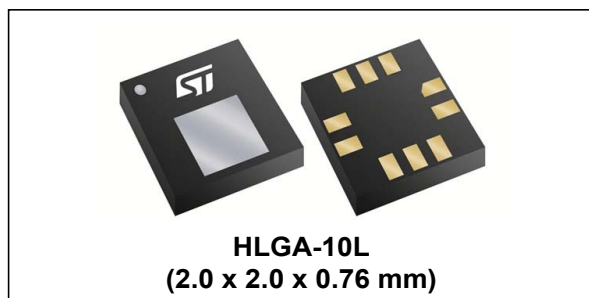
Symbol	Parameter	Test conditions	Min.	Typ. ⁽¹⁾	Max.	Unit
Rn	Rate noise density in high-performance mode ⁽⁵⁾			6		mdps/ $\sqrt{\text{Hz}}$
RnRMS	Gyroscope RMS noise in low-power mode ⁽⁶⁾			120		mdps
An	Acceleration noise density in high-performance mode ⁽⁷⁾	FS= $\pm 2\text{ g}$		90		$\mu\text{g}/\sqrt{\text{Hz}}$
		FS= $\pm 4\text{ g}$		90		$\mu\text{g}/\sqrt{\text{Hz}}$
		FS= $\pm 8\text{ g}$		110		$\mu\text{g}/\sqrt{\text{Hz}}$
		FS= $\pm 16\text{ g}$		180		$\mu\text{g}/\sqrt{\text{Hz}}$
RMS	Acceleration RMS noise in normal/low-power mode ⁽⁸⁾	FS= $\pm 2\text{ g}$		1.7		mg(RMS)
		FS= $\pm 4\text{ g}$		2.0		mg(RMS)
		FS= $\pm 8\text{ g}$		2.7		mg(RMS)
		FS= $\pm 16\text{ g}$		4.4		mg(RMS)
LA_ODR	Linear acceleration output data rate			12.5 26 52 104 208 416 833 1666 3332 6664		Hz
G_ODR	Angular rate output data rate			12.5 26 52 104 208 416 833 1666 3332 ⁽⁹⁾		
Vst	Linear acceleration self-test output change ⁽¹⁰⁾⁽¹¹⁾	FS = 2 g	90		1700	mg
	Angular rate self-test output change ⁽¹²⁾⁽¹³⁾	FS = 2000 dps	150		700	dps
Top	Operating temperature range		-40		+85	$^{\circ}\text{C}$

1. Typical specifications are not guaranteed.
2. Linear acceleration sensitivity after factory calibration test and trimming.
3. Angular rate sensitivity after factory calibration test and trimming.
4. Values after soldering.
5. RND (rate noise density) mode is independent of the ODR and FS setting.

6. Gyro noise RMS is independent of the ODR and FS setting.
7. Noise density in HP mode is the same for all ODRs.
8. Noise RMS in Normal/LP mode is the same for all the ODR RMS related to $BW = ODR / 2$ (for ODR /9, typ value can be calculated by $Typ * 0.6$)
9. To enable this ODR, refer to [CTRL4_C \(13h\)](#).
10. The sign of the linear acceleration self-test output change is defined by the STx_XL bits in [CTRL5_C \(14h\)](#), [Table 60](#) for all the axes.
11. The linear acceleration self-test output change is defined with the device in stationary condition as the absolute value of: $OUTPUT[LSb] \text{ (self-test enabled)} - OUTPUT[LSb] \text{ (self-test disabled)}$. $1LSb = 0.061 \text{ mg}$ at $\pm 2 \text{ g}$ full scale.
12. The sign of the angular rate self-test output change is defined by the STx_G bits in [CTRL5_C \(14h\)](#), [Table 59](#) for all the axes.
13. The angular rate self-test output change is defined with the device in stationary condition as the absolute value of: $OUTPUT[LSb] \text{ (self-test enabled)} - OUTPUT[LSb] \text{ (self-test disabled)}$. $1LSb = 70 \text{ mdps}$ at $\pm 2000 \text{ dps}$ full scale.

MEMS nano pressure sensor: 260-1260 hPa absolute digital output barometer

Datasheet - production data



Features

- 260 to 1260 hPa absolute pressure range
- Current consumption down to 3 μ A
- High overpressure capability: 20x full-scale
- Embedded temperature compensation
- 24-bit pressure data output
- 16-bit temperature data output
- ODR from 1 Hz to 75 Hz
- SPI and I²C interfaces
- Embedded FIFO
- Interrupt functions: Data Ready, FIFO flags, pressure thresholds
- Supply voltage: 1.7 to 3.6 V
- High shock survivability: 22,000 g
- Small and thin package
- ECOPACK[®] lead-free compliant

Applications

- Altimeters and barometers for portable devices
- GPS applications
- Weather station equipment
- Sport watches

Description

The LPS22HB is an ultra-compact piezoresistive absolute pressure sensor which functions as a digital output barometer. The device comprises a sensing element and an IC interface which communicates through I²C or SPI from the sensing element to the application.

The sensing element, which detects absolute pressure, consists of a suspended membrane manufactured using a dedicated process developed by ST.

The LPS22HB is available in a full-mold, holed LGA package (HLGA). It is guaranteed to operate over a temperature range extending from -40 °C to +85 °C. The package is holed to allow external pressure to reach the sensing element.

Table 1. Device summary

Order code	Temperature range [°C]	Package	Packing
LPS22HBTR	-40 to +85°C	HLGA-10L	Tape and reel

3 Mechanical and electrical specifications

3.1 Mechanical characteristics

VDD = 1.8 V, T = 25 °C, unless otherwise noted.

Table 3. Pressure and temperature sensor characteristics

Symbol	Parameter	Test condition	Min.	Typ. ⁽¹⁾	Max.	Unit
Pressure sensor characteristics						
PT _{op}	Operating temperature range		-40		+85	°C
PT _{full}	Full accuracy temperature range		0		+65	°C
P _{op}	Operating pressure range		260		1260	hPa
P _{bits}	Pressure output data			24		bits
P _{sens}	Pressure sensitivity			4096		LSB/hPa
P _{AccRel}	Relative accuracy over pressure	P = 800 - 1100 hPa T = 25 °C		±0.1		hPa
P _{AccT}	Absolute accuracy over temperature	P _{op} T = 0 to 65 °C After OPC ⁽²⁾		±0.1		hPa
		P _{op} T = 0 to 65 °C no OPC ⁽²⁾		±1		
P _{noise}	RMS pressure sensing noise ⁽³⁾	with embedded filtering		0.0075		hPa RMS
ODR _{Pres}	Pressure output data rate ⁽⁴⁾			1 10 25 50 75		Hz
Temperature sensor characteristics						
T _{op}	Operating temperature range		-40		+85	°C
T _{sens}	Temperature sensitivity			100		LSB/°C
T _{acc}	Temperature absolute accuracy	T = 0 to 65 °C		±1.5		°C
ODR _T	Output temperature data rate ⁽⁴⁾			1 10 25 50 75		Hz

1. Typical specifications are not guaranteed.

2. OPC: One-Point Calibration, see [RPDS_L \(18h\)](#), [RPDS_H \(19h\)](#).

3. Pressure noise RMS evaluated in a controlled environment, based on the average standard deviation of 50 measurements at highest ODR and with LC_EN bit = 0, EN_LPFP = 1, LPFP_CFG = 1.

4. Output data rate is configured acting on ODR[2:0] in [CTRL_REG1 \(10h\)](#).

Physilog® 4 Datasheet



Physilog® is a Swiss-made wearable standalone measurement unit containing inertial sensors.

The technology was born 10 years ago out of translational research collaborations between Lausanne's University Hospital (CHUV) and the Swiss Institute of Technology of Lausanne (EPFL). Physilog® provides objective and quantitative assessment of movement disorders and performance.

Physilog® 4, the latest Physilog® generation, was designed in 2013 by Gait Up. The Physilog® 4 Silver, comes with 10D sensing capabilities, USB charging and wireless functionalities. Physilog® 4 Gold has one more recording channel: either GPS, Bluetooth, Droplet or ECG module. In 2015, Physilog® sensors have been worn by more than 5000 subjects worldwide and have been validated for various applications in scientific publications.

SENSOR SPECIFICATIONS

Electrical characteristics

Internal Storage	4 Gb – Physilog® Silver: 9 days at 200Hz
Battery	Rechargeable Lithium Ion Polymer Battery life up to 23 hours*
Supply Voltage	DC min: 4.2V – max: 6V min: 125mA – max: 250mA
Port	Micro-USB for charging and data transfer
Operating Temperature	From -40°C to 45°C

* Depending on Physilog® model and configuration, see autonomy table below

Mechanical Characteristics

Dimensions	50 x 37 x 9.2 mm Anatomical curved shape
Weight	19 grams (including battery)
Button	Start/Stop membrane switch with dual-color LED
Material	ABS plastic (same as LEGO®)
Fixation	Double side Velcro or optional buckles with elastic straps

Gait Up S.A.

EPFL Innovation Park, Bâtiment C
CH-1015 Lausanne

» *tel.* +41 79 101 19 90

» *mail.* contact@gaitup.com

» *web.* www.gaitup.com

Physilog[®] 4 Silver Characteristics

Sensor Specifications	10 D Measurement			
	3D Accelerometer	3D Gyroscope	3D Magnetometer	Barometer
Measure	Linear acceleration	Angular Velocity	Magnetic field strength	Atmospheric pressure
Programmable range of measurement	±2g, ±4g, ±8g and ±16g	±250, ±500, ±1000, and ±2000°/sec	±1000 µT	10 mBar to 1200 mBar
Sampling rate	Programmable from 1 to 500 Hz (Magnetometer: max. 50Hz, Barometer: max. 100Hz)			
Wireless Synchronization	Radio frequency synchronization – as many Physilog [®] sensors as you wish			

Physilog[®] 4 sensors do not need yearly recalibration.

Physilog[®] 4 Gold options

In addition to the 10D sensing of the Physilog[®] 4 Silver, the Physilog[®] 4 Gold has one more channel which can be used for either GPS, Droplet or ECG option. A wireless version of the Physilog[®] 4 using Bluetooth exists for real time applications.

GPS module



A GPS module for outdoor localization can be added to the Physilog[®] 4. This option is available with or without an external antenna. The external antenna allows a more accurate and reliable localization. GPS data can be exported to csv using the Research ToolKit described below. The latitude, longitude, elevation and time of each measurement point are given in the csv file.

Antenna specifications:

- Size: 48x40x13mm
- Weight: <105g

Gait Up S.A.

EPFL Innovation Park, Bâtiment C
CH-1015 Lausanne

» tel. +41 79 101 19 90

» mail. contact@gaitup.com

» web. www.gaitup.com




High Quality Motion Sensor

Our latest generation Physilog® is a compact and versatile wearable device for sensing movement of any kind. Benefit from 18 years of R&D, collaboration and trust with top clinics, researchers and industrial partners, for applications in health monitoring, sports, entertainment and more. For applications in science: www.gaitup.com/science



Unique features

- ✓ Waterproof and dust resistant 
- ✓ Multi-standard wireless connectivity
- ✓ Long-term motion recording and on-board processing
- ✓ microUSB port for rapid file transfer and universal charging



Software

- > Free SDKs for accessing raw data and 3D angles
- > Free companion App to sync, check battery, and program sensors
- > Free MATLAB/Python/C/C++ routines to sync, stream, read, plot
- > Professional applications for Gait and Running
- > On-demand custom algorithm libraries and OEM/licencing

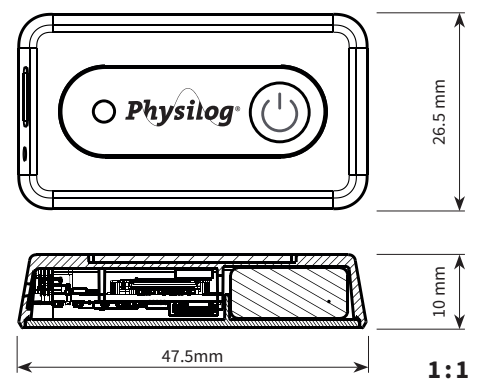
Specifications

Component	Manufacturer	Remarks
Inertial Sensors	STMicroelectronics	3D Accelerometer up to 16g 3D Gyroscope up to 2000°/s
Ambient Sensor	STMicroelectronics	Barometric altitude from 260 to 1260 hPa Temperature sensor accuracy of +/-1.5°C
Radio Chip	Nordic Semiconductors	Multi-standard: Bluetooth Low Energy (BLE), Ant+, and Near field communication (NFC)
Internal Memory	Apacer	Class 10 microSD Card, 8Gb
Microcontroller	Nordic Semiconductors	ARM® Cortex® M4 with floating-point for on-board processing
Micro-USB interface	Amphenol FCI & Microchip	Waterproof IP64, with dedicated chip for fast data transfer. High-speed USB 2.0
Battery	Renata	Lithium Ion Polymer Accumulators 3.7V 140mAh
Plastic Enclosure	ABS Polylac® PA-757	Biocompatible with bi-color LED and 8mm button
Operating Temperature		From -20° to 45° C
Assembly	Locatis Electronics SA (CH)	Weight 11 gramms Dimensions 26,5x47,5x10 mm

Accessories

- > Rubber clip (for shoe laces/belt)
- > Elastic Velcro® straps
- > Bio-compatible patches (for skin)
- > Transport case
- > microUSB <-> USB cables
- > External sync. with lab systems

Size



Certifications

Medical CE class 1 pending, ISO 13485 certified
(IEC 60950, IP64 RT&TE, FCC, IC)





Curriculum Vitae

Falbriard Mathieu

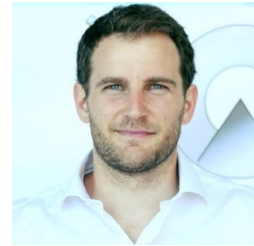
Chemin de la Joliette 3, 1006 Lausanne

Date of birth: September 25th, 1989

Nationality: Swiss

Phone: +41 78 638 58 53

E-Mail: mathieu.falbriard@epfl.ch



Education

- **EPFL (Lausanne), PhD in Electrical Engineering:** 2015 - present
Laboratory of Movement Analysis and Measurement (LMAM)
Supervisor: Prof. Kamiar Aminian
Thesis: *"Assessment of Real-World Running With Lab-Validated Algorithms Based on Foot-Worn Inertial Sensors"*
 - Supervised 13 semester projects and 1 master thesis project
 - Teaching assistant for "Analysis and Modeling of Locomotion" and "Sensors in Medical Instrumentation"
- **EPFL (Lausanne), MSc in Communication Systems:** 2013 - 2015
Master thesis in the industry (Gait Up S.A., Switzerland) supervised by Dr. Benoît Mariani: *"Run Up foot strike analyzer: Field testing and R&D"*
- **EPFL (Lausanne), BSc in Communication Systems:** 2010 - 2013
One year exchange at Iowa State University, USA: 2012 – 2013
Specialization in Mathematics
- **EPFL (Lausanne), Special Mathematics Course** 2009 - 2010
- **CEJEF DivTech (Porrentruy), Professional Maturity** 2008 - 2009
- **CEJEF DivTech (Porrentruy), CFC in Computer Science:** 2005 - 2008
Republic and Canton of the Jura Award for the best overall grade
Sport-Art-Sudy program in Ice Hockey

Professional experience

- Back-end developer at Artionet Web Agency S.A. Summer 2013
- E-commerce web developer at Hockey Expert S.A. 2011 - 2012

Activities and Interests

- President of the Lausanne University Club (LUC) Rugby 2017 - present
- President of the Ass. de Développement et Promotion du Rugby au Jura 2019 - present
- Rugby, ice hockey, surfing, and boxing

Languages

- French: native language
- English: fluent (speaking, reading, writing)
- German: intermediate (speaking, reading, writing)

Journal publications

- Meyer, F., **Falbriard, M.**, Aminian, K., & Millet, G. P. (2018). How accurate is visual determination of foot strike pattern and pronation assessment. *Gait & posture*, 60, 200-202.
- Falbriard, M.**, Meyer, F., Mariani, B., Millet, G. P., & Aminian, K. (2018). Accurate estimation of running temporal parameters using foot-worn inertial sensors. *Frontiers in physiology*, 9, 610.
- Meyer, C., Mohr, M., **Falbriard, M.**, Nigg, S. R., & Nigg, B. M. (2018). Influence of footwear comfort on the variability of running kinematics. *Footwear Science*, 10(1), 29-38.
- Muniz-Pardos, B., Sutehall, S., Gellaerts, J., **Falbriard, M.**, Mariani, B., Bosch, A., ... & Pitsiladis, Y. P. (2018). Integration of wearable sensors into the evaluation of running economy and foot mechanics in elite runners. *Current sports medicine reports*, 17(12), 480-488.
- Degache, F., Serain, E., Vernillo, G., Meyer, F., **Falbriard, M.**, Savoldelli, A., ... & Millet, G. P. (2019). Postural control follows a bi-phasic alteration pattern during mountain ultra-marathon. *Frontiers in physiology*, 9, 1971.
- Falbriard, M.**, Mohr, M., & Aminian, K. (2020). Hurdle Clearance Detection and Spatiotemporal Analysis in 400 Meters Hurdles Races Using Shoe-Mounted Magnetic and Inertial Sensors. *Sensors*, 20(2), 354.
- Jeker, D., **Falbriard, M.**, Vernillo, G., Meyer, F., Savoldelli, A., Degache, F., ... & Millet, G. P. (2020). Changes in spatio-temporal gait parameters and vertical speed during an extreme mountain ultra-marathon. *European Journal of Sport Science*, (just-accepted), 1-12.
- Falbriard, M.**, Meyer, F., Mariani, B., Millet, G. P., & Aminian, K. (2020). Drift-Free Foot Orientation Estimation in Running Using Wearable IMU. *Frontiers in Bioengineering and Biotechnology*, 8, 65.

Conference papers

- Falbriard, M.**, Anker, R., and Mariani, B. (2015). *Translating movement data in performance or disability metrics using barcode and signature*. 33rd International Conference on Biomechanics in Sports, Poitiers, France, June 29 - July 3, 2015.
- Falbriard, M.**, Meyer, F., Mariani, B., Millet, G.P., and Aminian, K. (2016). *Objective Running Analysis Using Foot-worn Inertial Sensors*. CTI-Micro/Nano event, Basel, Switzerland, June 30, 2016.
- Falbriard, M.**, Fasel, B., Spörri, J., and Aminian, K. (2016). *A ski racer's turn cycle structure depends on slope inclination, speed and gate off-set*. 7th International Congress on Science and Skiing (ICSS), St. Christoph am Arlberg, Austria, December 10 - 15, 2016.
- Fasel, B., Spörri, J., Gilgien, M., Gerber, N., and **Falbriard, M.**, et al. (2016). *IMU and GNSS-based turn switch detection in alpine ski racing*. 7th International Congress on Science and Skiing (ICSS), St. Christoph am Arlberg, Austria, December 10 - 15, 2016.
- Bauer, C. M., **Falbriard, M.**, and Aminian K. (2017). *Hurdle detection and leading leg identification using foot-worn inertial sensors in 400m hurdles races*. 9th annual conference of the Swiss Society of Sport Science, Zurich, Switzerland, February 9 - 10, 2017.
- Falbriard, M.**, Meyer, F., Millet, G. P., and Aminian, K. (2017). *Foot-worn inertial sensors assessment of the temporal events and contact time during running*. 9th annual conference of the Swiss Society of Sport Science, Zurich, Switzerland, February 9 - 10, 2017.
- Meyer, F., **Falbriard, M.**, Aminian, K., and Millet, G.P. (2017). *How accurate is visual determination of foot strike pattern and pronation assessment*. 22nd European College of Sport Science (ECSS), Ruhr, 2017.

- Falbriard, M.**, Meyer, F., Mariani, B., Millet, G. P., and Aminian, K. (2017). *Contact time and foot strike angles estimation using foot worn inertial sensors in running*. 35th International Conference on Biomechanics in Sports, Cologne, Germany, June 14 – 18, 2017.
- Falbriard, M.**, Mohr, M., and Aminian K. (2019). *Hurdle Crossing Detection Methods Using Foot-Worn Inertial and Magnetic Sensors in 400 meters Races*. 27th Congress of the International Society of Biomechanics, Calgary, Canada, July 31 – August 4, 2019.